TECHNISCHE UNIVERSITÄT MÜNCHEN

Lehrstuhl für Experimentelle Genetik

Homotypic chondro-osseous differentiation, metastasis and osteotropism in Ewing Tumors

Kristina von Heyking

Vollständiger Abdruck der von der Fakultät Wissenschaftszentrum Weihenstephan für Ernährung, Landnutzung und Umwelt der Technischen Universität München zur Erlangung des akademischen Grades eines

Doktors der Naturwissenschaften

genehmigten Dissertation.

Vorsitzender: Univ.-Prof. Dr. S. Scherer
Prüfer der Dissertation:

1. Univ.-Prof. Dr. M. Hrabé de Angelis
2. Univ.-Prof. Dr. S. Burdach
3. Univ.-Prof. Dr. B. Küster

Die Dissertation wurde am 13.11.2012 bei der Technischen Universität München eingereicht und durch die Fakultät Wissenschaftszentrum Weihenstephan für Ernährung, Landnutzung und Umwelt am 25.02.2013 angenommen.

meinem Verlobten und meinen Eltern

Table of contents

1. Introduction

1.1. Bone – structure, development and regulation

Bones are organs, which are made of osseous tissues as well as bone marrow, cartilage, blood vessels, epithelium and nerves. They support and protect the different organs of the body, perform hematopoiesis and store minerals, like calcium or magnesium [1,2]. Additionally, bones are important for movement and sound transduction. Due to changes in physical load and damage caused by recurrent micro-fractures, living bone is constantly being remodeled [2,3]. In adults bone remodeling proceeds at about 10 % per year, whereas the state of the bones is always close to equilibrium between bone formation and bone resorption [4].

Osseous tissues are mineralized connective tissues and form the rigid, but slightly flexible, part of the bones. The specific properties of the osseous tissues are based on the characteristics of the calcified bone matrix, which consists to 35 % of organic and to 65 % of inorganic components [1]. The organic components include collagen type I (up to 90 %), but also other bone proteins like osteocalcin (BGLAP), osteopontin (OPN) and alkaline phosphatase (ALP) [4]. Hydroxyapatite is the largest part of the inorganic components, besides citrate- and carbonate ions as well as magnesium and sodium [1]. Osseous tissue is not a uniformly solid material, but can grade into two groups due to its different porosity. The hard outer layer of bones consists of compact (cortical) bone tissue, which accounts for 80 % of the total bone mass of an adult skeleton. It is rich in blood vessels and consists of a solid, hard mass with a porosity of only 5 – 30 %. The particular characteristics of this tissue are the osteon and the Haversian canals. Trabecular (cancellous) bone tissue is found in the interior of the bones and is composed of a three-dimensional scaffold of pillars and beams, which provide room for hematopoietic and fat tissues as well as for blood vessels. Its porosity ranges from 30 – 90 % [1,4]. Due to their form, four types of bones can be identified consisting of compact and trabecular tissues in various relations: long, short, flat and irregular bones [2].

The formation of bone tissue during fetal development of the mammalian skeletal system is accomplished by two different processes, namely intramembranous and endochondral ossification. Intramembranous ossification leads to the formation of the flat bones of the skull, but also of the mandible, maxilla and clavicles and is also important for the natural healing of bone fractures. During intramembranous ossification, bone tissue is formed directly by mesenchymal stem cells (MSCs), which

first differentiate into osteoprogenitors [5]. This lineage commitment is regulated by different transcription factors and their co-regulators, such as runt-related transcription factor 2 (RUNX2), sry-box 9 (SOX9) and the morphogens transforming growth factor, beta 1 (TGFβ), bone morphogenic protein (BMP) as well as parathyroid hormone-like hormone (PTHrP) [5–7]. After an extensive proliferation phase, osteogenic cells aggregate near or around blood vessels forming so called bone spicules and differentiate into mature osteoblasts [1,5]. The expression of osteoblast-related genes is induced by cell-matrix and cell-cell interactions and leads to the formation of the osteoid, a non-calcified extracellular matrix consisting of proteoglycans, glycoproteins and collagen type I [7,8]. In the presence of ALP, secreted from osteoblasts, hydroxyapatite precipitates and the osteoid becomes mineralized. Thus, the majority of osteoblasts (approximately 85 %) undergo apoptosis, while the rest differentiates into osteocytes [5]. The last two steps of the intramembranous ossification are the formation of the trabeculae, which surround the osteocytes, and the development of the periosteum around the trabeculae by differentiating MSCs [1].

Endochondral ossification, on the other hand, is an essential process during the formation of most of the other bone tissues, for example long bones and vertebrae. The special characteristic of endochondral ossification is the use of the hyaline cartilage "skeleton" of the fetus as a model upon which the bones will form. Thus, formation of the cartilage intermediate by chondrogenesis is the earliest step of skeletal development via endochondral ossification [9]. Chondrogenesis, which is similar to osteoblastogenesis, can be divided into 4 steps beginning with mesenchymal cell recruitment, proliferation and condensation, which is regulated by mesenchymal-epithelial cell interactions [10,11]. To ensure correct limb patterning, undifferentiated mesenchymal cells express different fibroblast growth factors (FGFs), BMPs, homeobox genes (*HOXA*, *HOXD*) and Wnt pathway genes (*WNT2A*, *WNT2C*) during cell recruitment and proliferation [12–15]. The initiation of condensation is among other things associated with increased hyaluronidase activity and TGFβ expression [9]. The next step includes the differentiation of chondroprogenitors into chondrocytes and is required for subsequent stages of skeletogenesis. This phase is regulated by the transcription factor SOX9, which induces the expression of different cartilage-specific matrix proteins, like collagen, type II, alpha 1 (COL2A1) [16–18]. After a proliferative phase among other things stimulated by PTHrP [19], mature chondrocytes terminal differentiated into the hypertrophic phase. This last step is regulated by RUNX2 and characterized by the expression of collagen, type X, alpha 1 (COL10A1), vascular endothelial growth factor (VEGF) and ALP [9,20,21]. After formation of the hyaline cartilage “skeleton”, endochondral ossification is initiated. The first modifications occur

in the diaphysis, the primary center of ossification. There, ALP induces the calcification of the matrix, thus promoting apoptosis of the hypertrophic chondrocytes, which in turn forms cavities within the bone. Subsequently, VEGF-stimulated blood vessels can invade and transport hematopoietic cells, osteoprogenitor cells and other cells inside the cavity [1,21]. The progenitor cells differentiate into mature osteoblasts, which first secrete osteoid and then initiate the mineralization of the matrix, as previously described for intramembranous ossification. At a later time dependent on the respective bone, ossification is also detectable in the secondary center of ossification, the epiphysis [1].

Bone resorption is mediated by osteoclasts, which reside in a small cavity called Howship's lacunae on the surface of the bone tissues [1]. Attachment to the bone matrix in the sealing zone is facilitated by the integrin αvβ3 and OPN, which are expressed from osteoclasts [22]. To digest the mineralized bone matrix and the organic components, the osteoclasts secrete a carbonic anhydrase and several hydrolytic enzymes through the ruffled boarder [1].

To maintain the balance between bone development and bone resorption, in general two cell types are necessary: osteoblasts and osteoclasts. These osteogenic cells can communicate with each other through cell-cell interactions, diffusible paracrine factors and cell-bone matrix interactions. Due to osteoblast-osteoclast communication bone remodeling can be separated into three phases: initiation, transition and termination of bone remodeling [23]. The initiation phase starts in response to external stimuli, like bone micro-fractures, loss of mechanical loading or low blood calcium. Both micro-fractures and loss of mechanical loading can be sensed by osteocytes leading to apoptosis and the simultaneous release of chemokines [24–26]. This promotes the expression of chemokine, cc motif, ligand 2 (CCL2) from osteoblasts and of chemokine, cxc motif, ligand 12 (CXCL12) produced by bone vascular endothelial and bone marrow stromal cells to activate the maturation of osteoclast precursors via chemokine, cxc motif, receptor 4 (CXCR4) binding [27,28]. Additionally, tumor necrosis factor receptor/ligand superfamily, member 11 (RANK/RANKL) interactions are essential for the differentiation of osteoclasts [23,29,30]. Several soluble factors can further enhance osteoclastogenesis, on the one hand through RANKL induction in osteoblasts (PTHrP) and on the other hand through the secretion of osteoclast survival factors (colony-stimulating factor (M-CSF) and interleukins (IL6 and IL11)) [3,23]. The stimulation of osteoblast precursor maturation through osteoclasts is characteristic for the transition phase. Osteoblastogenesis is induced by the release of TGFβ, BMPs and Ca^{2+} from bone matrix and through an bidirectional signaling mechanism between the

ephrin receptors EPHB2 on osteoclasts and EPHB4 on the surface of osteoblasts [31]. Finally, bone-resorbing osteoclasts undergo apoptosis [23] and thus the termination phase is initiated. During this phase the activity of osteoclasts is suppressed by the expression of osteoprotegerin (OPG) from osteoblasts, which is regulated through Wnt/β-catenin signaling pathway, NOTCH-pathway and the expression of the transcription factor early B-cell factor 2 (EBF2) [32–35]. Simultaneously, osteocytes secrete sclerostin, which suppresses osteoblastic bone formation [36].

In summary, bone is a very complex organ. The development, resorption and regulation involve many aspects and mechanisms, which can mutate or be influenced by tumor cells resulting in a pathogenic phenotype.

1.2. Cancer to bone

Mutated or abnormal growth of bone tissues can be either benign or malignant, depending on whether the tumor can spread, destroy bone and whether it is a threat to life or not. Malignant tumors (cancer) can be divided into primary tumors, which begin in bone tissues, and secondary tumors, which metastasize into the bone from other parts of the body. The most common primary bone cancers are osteosarcomas, chondrosarcomas and Ewing tumors (ETs) [37]. With an incidence of much less than 1 % of all cancers, primary bone tumors are quite rare. However, they account for about 5 % of all cancers observed in children. Additionally some of the most frequent epithelial tumors including breast, lung and prostate cancer metastasize into bone tissues. The most common symptom of cancer into bone is pain, but hypercalcaemia, swelling and pathological bone fractures are devastating consequences of bone tumors, as well [38]. The treatment of primary bone cancer is dependent among other things on tumor entity, stage and localization of the cancer, but usually includes surgery, chemo- and radiation therapy, which are used alone or in combination. In localized bone tumors, the 5 year survival is about 40 % for males and about 50 % for females, while the presence of metastases significantly reduces overall survival, especially after metastasis into bone [39]. Thus, it is very important to obtain more information about the underlying molecular mechanisms to improve the treatment of bone cancer patients. For that reason, this doctoral thesis analyzes the mechanisms leading to metastasis, bone invasiveness and osteolysis using the example of Ewing tumors as the most malignant primary bone tumor characterized by early metastasis in 25 % of cases.

1.3. Ewing tumors (ETs)

The Ewing sarcoma family of Tumors (ESFTs) consist of a group of cancers including common Ewing tumor (ET), peripheral neuroepithelioma, peripheral primitive neuroectodermal tumor (PNET) and Askin tumor (PNET of the chest wall), which all derive from the same type of stem cells [40,41]. This doctoral study is focused on ETs, the second most common malignancy of bone and soft-tissues in children and adolescents after osteosarcoma that accounts for 10 – 15 % of all primary bone tumors [40]. It usually occurs in the second decade of life with an incidence of 3.3 in 1 x 10^6 under the age of 15 [42,43] and slightly more males than females are affected (ratio 1.5:1) [40]. Interestingly, the incidence of ETs is ten times higher in Caucasians compared to individuals of African and Asian ancestry indicating that genetic predisposition may play a role in this malignancy [40–42]. The most common primary sites of this highly malignant tumor are the long bones of the extremities usually involving the diaphysis (58 %), followed by the pelvis (20 %) and the axial skeleton and ribs (13 %) [40,41]. Even though most ETs arise in bone tissues, about 15 % of primarily ETs are found in diverse extra-osseous parts of the body [44]. Although prognosis for patients with localized disease has markedly improved in past decades (5 year survival is about 70 %), metastatic disease – present in about 25 % of ET patients at diagnosis – is usually associated with fatal outcome [42,45–51]. Primary metastases frequently arise in lungs and/or bone tissues and especially the development of metastases in bones is a catastrophic event in the clinical course of ET patients (5 year survival is less than 10 %) [42,49–52].

ETs were originally described by the American pathologist James Ewing in 1921 as “diffuse endothelioma of bone" [53] due to its unclear histogenesis. Although it could be shown, that ETs display mesenchymal, neuroectodermal as well as endothelial features, its precise cell of origin remains elusive until today [54–57]. Recent work has suggested that MSCs may originate from the neuroepithelium, potentially explaining the observed neuroectodermal and endothelial features of ETs [58,59]. Furthermore, it is known that human bone marrow MSCs can migrate to all body compartments during embryonic development [44], which is important in respect to the distribution of primary ETs in the body [40,44]. Thus, MSCs of hematopoietic or neuroectodermal origin are strong candidates for the cell of ET origin, possibly in transition from an undifferentiated state to a more differentiated phenotype back to the endothelial, neuroectodermal or to the chondro-osseous lineage. In general, ETs are defined on histopathological level by small round cells stained blue on routine hematoxylin and eosin (H&E) staining. Because different other tumor entities including leukemia, medulloblastoma and

neuroblastoma look very similar under the microscope, ETs are hardly distinguishable from other small-round-blue-cell tumors on the histological level. For that reason, tumor samples need to be analyzed with additional histological markers including CD99 antigen, X chromosome (CD99, [58]), friend leukemia virus integration 1 (FLI1, [60]) and caveolin 1 (CAV1, [61]). However, these marker genes are not really specific enough for an exact classification, which is why it is indispensable to examine the molecular background of the tumor sample to clearly identify ETs. This is possible, because as an unifying hallmark, all ETs are genetically defined by non-random gene rearrangements that fuse *EWS* (*Ewing sarcoma breakpoint region 1*), located on chromosome 22q12, and a member of the *ETS* (*e-twenty-six*) gene family of transcription factors [40,62]. The most common chromosomal translocation include the *FLI1* gene (*friend leukemia virus integration 1*) on chromosome 11, which is involved in about 85 % of cases, followed by the *ERG* (*v-ets avian erythroblastosis virus e26 oncogene homolog*) gene in 5 - 10 % of cases [40,41,62]. Within the t(11;22) translocation, different chromosome breakpoint sites are possibly resulting in a large number of *EWS-FLI1* fusion combinations. In approximately 60 % of cases, the first seven *EWS* exons joined to exon 6 to 9 of *FLI1*, termed EWS-FLI1 type 1 [40,58]. The oncogenic fusion protein EWS-ETS functions on the one hand as an aberrant transcription factor, via the N-terminal EWS domain and the conserved ets DNA binding domain of members of the ETS family. On the other hand it is a potent repressor even in post-transcriptional processes that determines the complex and highly malignant phenotype of ETs [62–64]. To better understand the effect of EWS-FLI1, the 68 kDa large fusion protein was artificially expressed in human primary fibroblasts, murine and human MSCs and different tumor cell lines including neuroblastoma and rhabdomyosarcoma cell lines [63,65,66]. Interestingly, expression of EWS-FLI1 in nearly all cell lines other than MSCs resulted in cell death supporting the hypothesis of MSCs as the cell of origin in ETs. Although expression of EWS-FLI1 results in ET-specific gene expression and further causes changes in the differentiation characteristics of neuroblastoma and rhabdomyosarcoma cells, the cell lines do not fully transform into ETs [63,65,67]. This indicates that additional factors and mechanisms seem to be necessary to generate highly malignant tumor cells, which exhibit features similar to those of ETs. One possible alternative mechanism includes the inactivation of frequent tumor suppressor genes, such as p53 or p16, which are able to induce tolerance to EWS-FLI1 in primary cells [62,68,69]. Although, these mutations are associated with worse clinical outcome, the inactivation of p53 and other tumor suppressor genes is rare in ETs (10 – 20 %) indicating that additional mechanisms are essential to develop ETs of a specific progenitor cell [62].

Nevertheless, EWS-FLI1 seems to be an important candidate for targeted therapy, because of its unique expression in the cells of the tumor and its great influence on the oncogenic phenotype of this tumor entity. However, no therapeutic applications based on the EWS-FLI1 fusion protein reached the clinical trial status so far due to the lack of enzymatic activity, inherent bioavailability and administrative problems, like *in vivo* application [70]. Since overall survival of patients with metastatic disease, especially after the development of bone metastases is still insufficient, there is an urgent need to get more information about the underlying molecular mechanisms of this tumor to develop new therapeutic treatment modalities. Due to the characteristics of ETs including primary and metastatic tumor growth in bone tissues, this malignancy may serve well to analyze tumor growth in bone and possibly might be a good model system to learn more about cancers to bone in general, too. In a previous microarray analysis, Staege *et al.* identified 37 genes, which were overexpressed or even specifically expressed in primary ETs compared to normal tissue and which are potential new target genes [55]. Among them are also the bone-associated genes *chondromodulin 1* (*CHM1*), *dickkopf 2* (*DKK2*) and *integral membrane protein 2A* (*ITM2A*), which are interesting genes for further investigation in the context of bone tumors.

1.4. Dickkopf 2

1.4.1. Current knowledge on DKK2

The dickkopf family is an evolutionarily ancient gene family consisting of four main members in vertebrates (DKK1 - 4) and a unique DKK3-related protein soggy (sgy; also called dickkopf-like protein 1 (DKKl1)) [71,72]. The main human *DKK* genes, with the exception of *DKK3*, are located within the well-characterized chromosome paralogy group (4/5/8/10; *DKK2* 4q25), that were duplicated early in the evolutionarily process of vertebrates [71]. Due to this observation, DKK3 seems to be a divergent member of the dickkopf family, which is also confirmed by different other criteria including the low DNA similarity between *DKK3* and the other 3 family members *DKK1*, *2* and *4* [71,73]. DKKs are secreted glycoproteins of 255 – 350 amino acids (aa) and a calculated molecular weight between 24 and 29 kDa for DKK1, 2 and 4 and 38 kDa for DKK3 [71]. All family members possess an N-terminal signal sequence and share 2 conserved cysteine-rich domains (Cys), whereas the sequence similarity outside of these domains is very low between the different DKKs [72,73]. Each of the two cysteine-rich domains display a characteristic spacing of cysteines and other conserved aa and are separated by a

linker region of 50 – 55 aa (12 aa for DKK3) [71,72]. The N-terminal cysteine-rich domain (Dkk_N; formerly known as Cys1) is unique to the members of the dickkopf family, while the C-terminal cysteine-rich domain (Cys2) shares a sequence homology of 10 cysteine residues to that of the colipase fold [74]. The colipase fold, originally described in a co-enzyme required for the optimal activity of pancreatic lipases [75], is found in a variety of different proteins including toxins and protease inhibitors [71]. The non-catalytic colipase fold is important for the interaction of proteins with the membrane and thus essential for the biological activity of DKKs mediated through interactions with the Wnt/β-catenin signaling pathway. Furthermore, DKKs contain various dibasic cleavage sites, which may be substrates for furin-type proteases and may explain the significant amounts of smaller molecular weight observed in sodium dodecyl sulfate-polyacrylamide gel electrophoresis (SDS-PAGE) compared to the calculated molecular weight [71].

Expression of DKKs could be observed in a wide range of tissues including heart, brain, skeletal muscle and lung, as well as in different bone-associated cells like osteoblasts or chondrocytes [72,76]. Thus it is not surprising, that DKKs play an important role in different processes of embryonic development, including anterior-posterior axial patterning, limb development, somitogenesis and eye formation [71]. But also in the adult, DKKs are implicated in various processes, like bone development and bone disease, cancer and Alzheimer's disease [71,77–79]. Interestingly, all functions mentioned above are mediated through one pathway: Wnt/β-catenin signaling. However, it cannot be ruled out that DKKs may influence signal cascades independent of their ability to affect this essential pathway [71].

With regard to DKK2, its precise cellular function remains elusive so far, because secreted DKK2 can either function as a Wnt agonist or antagonist, depending on the cellular context and the expressed amount of its binding partner low density lipoprotein receptor-related protein 6 (LRP6) and its cofactor Kremen 2 (KRM2) [80–84]. In the context of the Wnt/β-catenin pathway, DKK2 may promote osteoclastogenesis by enhancing the expression of the osteoclast differentiation factors, RANKL and M-CSF, while concurrently decreasing the mRNA levels of the decoy receptor of RANKL, OPG [85]. Additionally, DKK2 also seems to play a role in osteoblast proliferation and the initiation of osteoblastogenesis, which may be explained by the different influence of DKK2 on Wnt/β-catenin signaling [85,86]. Furthermore, Li *et al.* demonstrated that DKK2 regulates terminal osteoblast differentiation into mineralized matrices through both canonical Wnt antagonism-dependent and -independent mechanisms, which was confirmed by others [86–88]. Due to its function as a NOTCH signaling target, DKK2

seems to be a key player in stem cell signaling networks that again, at least in part, is mediated via the Wnt pathway [89]. As published previously, expression of DKK2 is deregulated in different tumor entities, like gastrointestinal, colorectal or renal cancer as well as leukemia influencing proliferation, apoptosis and anchorage-independent tumor growth [90–95]. Interestingly, in most of these malignancies DKK2 functions as a Wnt antagonist and is epigenetically silenced. To analyze DKK2 silencing in more detail, viable and fertile DKK2 mouse mutants were established. These mice are blind, supporting the role of DKK2 in eye development via the regulation of the corneal versus epidermal fate of the ocular surface epithelium [71,96]. Furthermore, DKK2$^{-/-}$ mice show low bone mineral density and osteopenia due to major effects on matrix mineralization. The osteoid surface is increased in these animals, without a significant change in the amount of osteoclasts indicating that DKK2 involves terminal osteoblast differentiation [87]. Based on these observations, DKK2 is an important candidate for the regulation of the chondrogenic/osteogenic differentiation potential of ETs as well as for ET proliferation, invasion and osteotropism.

1.4.2. Wnt/β-catenin signaling pathway

Different pathways are triggered by Wnt proteins, which employ Wnt receptors of the frizzled seven transmembrane class. The most frequent one is the canonical or Wnt/β-catenin signaling pathway, which is influenced by members of the dickkopf family [71,97]. The other pathways are non-canonical and less important, for example the planar cell polarity pathway (PCP) and the Wnt/Ca^{2+} cascade [98,99]. As previously described, the Wnt/β-catenin signaling pathway is critically involved in cell-cell communication in embryonic and adult development regulating among other things antero-posterior axial patterning, cell fate, limb development as well as bone formation [71,100–103]. Furthermore, this highly conserved pathway is the second most common mutated pathway in cancer after mitogen-activated protein kinase (MAPK) signaling pathway [104–107].

In the majority of normal cells, the Wnt/β-catenin signaling pathway is inactive. In the absence of the activating Wnt proteins, the destruction complex, including the proteins axin, APC gene (APC), glycogen synthase kinase 3 beta (GSK3β), casein kinase 1 alpha-1 (CK1α) and β-catenin, can form. In this complex β-catenin is phosphorylated on multiple serine/threonine residues by several kinases, mainly GSK3β, but also CK1α (Ser45) and targeted to ubiquitination by beta-transducin repeat-containing protein (βTrCP) [101,108]. Thus, β-catenin is recognized and degraded by the

proteasomal machinery, why it cannot accumulate in the nucleus and activate gene expression. Due to binding of the transcription factor/lymphoid enhancer-binding factor 1 (TCF/LEF) to Groucho and specific repressor sequences on the DNA, gene expression is inhibited in this inactive state. In the active phase of the pathway, secreted Wnt proteins bind to frizzled (Fz) and its co-receptor LRP5/LRP6, which is subsequently phosphorylated by CK1α. Following dimerization of Fz and LPR5/LRP6, the cytoplasmic phosphoprotein disheveled (Dvl) is recruited, posttranslationally modified and can bind to Fz and axin. Moreover, axin can bind to the phosphorylated co-receptor LRP5/LRP6 leading to degradation of the destruction complex and accumulation of β-catenin in the cytoplasm and later on in the nucleus [108]. In the nucleus, β-catenin associates with the TCF/LEF family of transcription factors to regulate the expression of canonical Wnt target genes such as *cyclin D1* (*CCND1*), *ephrin receptor B2* (*EPHB2*) or *v-myc avian myelocytomatosis viral oncogene homolog* (*c-MYC* [108–112]).

Activity of the Wnt/β-catenin signaling pathway is inhibited by several mechanisms including inactivation of Wnts (Wnt inhibitory factor (WIF), secreted frizzled-related proteins (sFRP) and WNT5A), mutation of important pathway proteins (axin and APC) or deregulation of Wnt agonists or antagonists such as DKKs [113].

1.5. BRICHOS family proteins

1.5.1. BRICHOS domain

The BRICHOS family consists of about 12 protein families linked to diverse major diseases such as dementia (ITM2A-C), respiratory disease (pulmonary surfactant protein C precursor (proSP-C)) and cancer (CHM1, ITM2A, carbonic anhydrase XI (CA11) and gastrokine (GKN1+2)) as well as tenomodulin (TNMD), which is closely related to CHM1 [114–116]. All members of the BRICHOS family have four domains: hydrophobic (transmembrane region), linker, BRICHOS and C-terminal region [114]. The only evolutionally conserved region is the 100 aa BRICHOS domain (51 – 83 % identity between all BRICHOS protein families) including a pair of conserved cysteine residues that probably form a disulphide bridge. The function of the BRICHOS domain has not yet been sufficiently resolved, but there is some evidence that this domain might have a chaperon-like activity possibly preventing proteins from amyloid formation [114–116].

The two BRICHOS-domain containing proteins CHM1 and ITM2A are examined in more detail due to their up-regulation in ETs compared to normal tissue [55].

1.5.2. Current knowledge on CHM1

Chondromodulin 1 (*CHM1*, previously known as *leukocyte cell-derived chemotaxin 1* (*LECT1*)) is located on chromosome 13 (7 exons) and belongs to the BRICHOS family as described above [114,117]. The 334 aa precursor protein is probably cleaved by furin proteases at the predicted cleavage sites into two isoforms, on the one hand into the single-pass transmembrane protein chondrosufactant protein (CH-SP) and on the other hand into the 120 aa mature CHM1 glycoprotein in the C-terminal region [118,119]. The precursor as well as the CH-SP protein has a short half-life indicating that they do not have a function [118]. Following glycosylation of the N-terminus of the mature protein, CHM1 is rapidly secreted [118,120]. Additionally, Azizan *et al.* observed another un-glycosylated form of the 25 kDa CHM1 protein in the cartilage (9 kDa), which was cleaved by an extracellular processing event and may able to diffuse more rapidly through the matrix [118].

CHM1 is almost solely expressed in the cartilage, more precisely in the interterritorial matrix of the cartilage, and to a lesser extend in other avascular tissues such as eyes and cardiac valves [119,121,122]. Furthermore it was published, that this glycoprotein is highly detectable in chondrocytes of the resting, proliferating and early hypertrophic phase, but not in osteoblasts and chondrocytes of the late hypertrophic phase and the calcified zone [119,122,123]. An important role of CHM1 is the strong anti-angiogenic function of this secreted protein, which maintained the avascular phenotype of different tissues, although various angiogenetic factors are expressed, for example FGF2 and VEGF in the cartilage [119,121–124]. Moreover, avascularity and the resulting hypoxia are important for inducing chondrogenesis, another important function of CHM1 [125]. As described previously, this cartilage-specific protein is a key factor in chondrocyte proliferation and development and simultaneously inhibited terminal chondrocyte hypertrophy and endochondral ossification [123,125]. Furthermore, CHM1 seems to influence cell-cycle progression via the inhibitor p21 and synthesis of proteoglycan in chondrocytes [125,126]. In an animal model, it was shown that the viable and fertile $CHM1^{-/-}$ mice exhibit no differences in chondrogenesis and endochondral bone formation during embryogenesis. However, the mutant mice showed a significant increase in angiogenesis, VEGF expression, bone mineral density and reduced bone resorption compared to bone formation in the context of fracture repair [121,127,128].

This indicates that CHM1 seems to be critical under stress conditions such as bone repair or malignancy in bones, as demonstrated in chondrosarcoma and adenocarcinoma [126,128,129]. Due to these findings, CHM1 seems to be important in angiogenesis and the osteogenic behavior of ETs, especially in chondrogenic differentiation and osteotropism.

1.5.3. Current knowledge on ITM2A

The ITM2 family consists of three members (ITM2A, B and C), which have about 40 % protein homology especially in the C-terminal part [130]. The *ITM2A* gene (also called *E25A*) was mapped on chromosome X (6 exons) and codes for a type II transmembrane protein of 263 aa and a molecular weight of 29 kDa [131,132]. It belongs to the BRICHOS family and different isoforms are detectable due to posttranslational processing and modification [130,133]. As previously described, ITM2A is predominantly located intracellular on large cytoplasmic vesicles and the Golgi apparatus and only to a lesser extend (about 4 %) on the cell surface [134].

Unlike the other two ITM2 family members, expression of ITM2A is limited to specific osteogenic and chondrogenic tissues. As shown by Deleersnijder *et al*., ITM2A can be specifically identified in the outer perichondrial rim of the postnatal mandibular condyle indicating a specific expression of this gene in resting and proliferating chondrocytes of the early phases of chondrogenesis [132,133,135]. In contrast, the deeper layer of the condyles, containing more differentiated chondroblasts and chondrocytes, exhibit no ITM2A expression. Furthermore, ITM2A is strongly expressed in mature osteoblasts [132]. This indicates that ITM2A plays an important role in osteogenesis and the early phases of chondrogenesis by simultaneously suppressing the transition to hypertrophic cells [130–133]. Moreover, myogenic differentiation as well as T-cell selection seems to be influenced by ITM2A, too [134,136]. Until now, little is known in the context of pathological implications of ITM2A, although there is some evidence that ITM2A influences dementia and tumor growth, in the latter case for example in alveolar rhabdomyosarcoma [114,137]. Even though no ITM2A$^{-/-}$ mouse model was established so far, to the best of the author's knowledge, current findings clearly demonstrated the influence of ITM2A on osteogenic and especially chondrogenic differentiation implicating *ITM2A* as an interesting gene in the pathophysiological context of ETs.

1.6. Aim of this study and overview of the experimental approach

The aim of this doctoral thesis was to illuminate the role of the bone-associated genes *CHM1*, *DKK2* and *ITM2A* in ET pathology, especially in respect to differentiation, metastasis and the osteogenic behavior of this malignancy. For that reason, dependence on CHM1, DKK2 and ITM2A upon the specific ET oncogenic fusion protein EWS-FLI1 was first analyzed after RNAi-mediated EWS-FLI1 knock-down in different established ET cell lines using qRT-PCR. To assess the potential influence of the bone-associated genes on ET pathology, each of these genes were transiently and constitutively suppressed in three ET cell lines, more precisely in A673, SK-N-MC and TC-71. Subsequently, the effect of gene knock-down on ET phenotype and tumorigenicity was examined by the use of several *in vitro* and *in vivo* assays. Microarray analyses were performed to identify downstream target genes of CHM1, DKK2 and ITM2A and to get more information about the underlying molecular mechanisms leading to the phenotype observed. Following evaluation of the microarray data, using among others gene set enrichment analysis (GSEA), further *in vitro* experiments were used to verify the findings. As the current knowledge about *CHM1*, *DKK2* and *ITM2A* indicate that these genes might play a role in the differentiation potential of cells suitable *in vitro* assays and Western blot analyses were performed to confirm this hypothesis. Furthermore, the involvement of the three bone-associated genes in bone invasiveness and osteolysis was analyzed in stable shRNA infectants in different ET cell lines using qRT-PCR as well as an orthotopic bone xenotransplantation model. Afterwards, immunohistological analyses were performed on murine organs to further examine the *in vivo* results and to better quantify bone invasiveness and osteolysis. With regard to DKK2, different analyses on mRNA and protein level were used to identify the effect of this gene on Wnt/β-catenin signaling pathway in ETs. Furthermore, clinical implications of DKK2 were analyzed in a pilot screening of human ET patients.

In summary, this work explores candidate ET target genes for target-orientated therapeutic strategies. Additionally, this study may contribute to the elucidation of the complex mechanisms resulting in cancer to bone and osteolysis, possibly transferable to other bone-associated tumor entities.

2. Materials

2.1. List of manufacturers

Manufacturers	Locations
Abcam	Cambridge, UK
Abbott	Wiesbaden, Germany
Abnova	Taipei, Taiwan
AEG	Nürnberg, Germany
Affimetrix	High Wycombe, UK
Ambion	Austin, TX, USA
Amersham Biosciences	Piscataway, NJ, USA
Applied Biosystems	Darmstadt, Germany
ATCC	Rockyville, MD, USA
B. Braun Biotech Int.	Melsungen, Germany
BD Biosciences Europe	Heidelberg, Germany
Becton Dickinson (BD)	Heidelberg, Germany
Berthold detection systems	Pforzheim, Germany
Biochrom	Berlin, Germany
Biometra	Göttingen, Germany
BioRad	Richmond, CA, USA
Biozym	Hess. Olendorf, Germany
Brand	Wertheim, Germany
Calbiochem	Darmstadt, Germany
Carestream Health, Inc.	Stuttgart, Germany
Cell Signaling Technology	Frankfurt a. M., Germany
Charles River Laboratories	Wilmington, MA, USA
Clontech-Takara Bio Europe	Saint-Germain-en-Laye, France
DSMZ	Braunschweig, Germany
Eppendorf	Hamburg, Germany
Eurofins MWG GmbH	Ebersberg, Germany
Falcon	Oxnard, CA, USA
Feather	Osaka, Japan
Fermentas	St. Leon-Rot, Germany

GE Healthcare	Uppsala, Sweden
Genomed	St. Louis, MO, USA
Genzyme	Neu-Isenburg, Germany
GFL	Segnitz, Germany
Gibco	Darmstadt, Germany
GLW	Würzburg, Germany
Greiner Bio one	Nürtingen, Germany
Hamilton	Bonaduz, Switzerland
Heidolph Instruments	Schwabach, Germany
Heraeus	Hanau, Germany
Invitrogen	Karlsruhe, Germany
Jackson ImmunoResearch Laboratories	Baltimore, MD, USA
Kern	Balingen-Frommern, Germany
Köttermann	Uetze/Hänigsen
Laborservice	Harthausen, Germany
Leica	Wetzlar, Germany
LMS	Brigachtal, Germany
Lonza	Basel, Switzerland
Macherey-Nagel	Düren, Germany
Memmert	Schwabach, Germany
Merck	Darmstadt, Germany
Metabion	Martinsried, Germany
Millipore	Billerica, MA, USA
Molecular BioProducts, MbP	San Diego, CA, USA
Nalgene	Rochester, NY, USA
Nikon	Düsseldorf, Germany
Nunc	Naperville, IL, USA
PAA	Cölbe, Germany
Pechiney Plastic Packaging	Menasha, WI, USA
Peqlab	Erlangen, Germany
Peske OHG	München, Germany
Philips	Hamburg, Germany
Promega	Madison, WI, USA

Qiagen	Chatsworth, CA, USA
R&D Systems	Minneapolis, MN, USA
Ratiopharm	Ulm, Germany
Roche	Mannheim, Germany
Roche/ACEA Biosciences	San Diego, CA, USA
(Carl) Roth	Karlsruhe, Germany
Santa Cruz Biotechnology	Heidelberg, Germany
Sartorius	Göttingen, Germany
Scientific Industries	Bohemia, NY, USA
Scotsman	Milan, Italy
Sempermed	Wien, Austria
Sequiserve	Vaterstetten, Germany
Sigma	St. Louis, MO, USA
Siemens	München, Germany
Stratagene	Cedar Creek, TX, USA
Syngene	Cambridge, UK
Systec	Wettenberg, Germany
Taylor-Wharton	Husum, Germany
Techlab	Braunschweig, Germany
Thermo Scientific	Braunschweig, Germany
TKA GmbH	Niederelbert, Germany
TPP	Trasadingen, Switzerland
Thermo Fisher Scientific	Ulm, Germany
Whatman	Dassel, Germany
Zeiss	Jena, Germany

2.2. General material

Materials	**Manufacturers**
Combs (Western blot)	Peqlab
Cryovials	Nunc
Culture dishes (Nunclon^{TM} surface 100 mm)	Nunc
Cuvettes	Roth
E-plates (96-well)	Roche

Filters for cells, Cell Strainer	Falcon
Filters for solutions (0.2 µm and 0.45 µm)	Sartorius
Flasks for cell culture (25cm^2, 75 cm^2 and 175 cm^2)	TPP
Flasks for cell culture (75 cm^2 and 175 cm^2)	Falcon
Gloves (nitrile, latex)	Sempermed
Hybond-P PVDF membrane	GE Healthcare
Hypodermic needle (23 G, 30 G)	B. Braun
Parafilm	Pechiney Plastic Packaging
Pasteur pipettes	Peske OHG
Petri dishes	Falcon
Pipettes (2, 5, 10 and 25 ml)	Falcon
Pipette tips (10, 200 and 1000 µl)	MbP
Pipette tips (10, 200 and 1000 µl with a filter)	Biozym
Plates for cell culture (6-well, 24-well and 96-well)	TPP
Plates for invasion-assay (24-well)	Becton Dickinson
Plates for qRT-PCR (96-well)	Applied Biosystems
Scalpels (Nr. 12, 15, 20)	Feather
Syringes (27 G x 318'', 0.45 mm x 10 mm)	BD Biosciences
Syringes (GC, 1710LT)	Laborservice
Syringes (Hamilton 100 µl, 250 µl)	Techlab
Syringes (Omnifix-F, 9161406V)	B. Braun
Tubes for cell culture (polystyrene, 15 ml)	Falcon
Tubes for cell culture (polypropylene, 15 ml and 50 ml)	Falcon
Tubes for molecular biology, Safelock (1.5 ml and 2 ml)	Eppendorf
Tubes for FACS™ (5 ml)	Falcon
Whatman paper	Whatman

2.3. Instruments and equipment

Type of device		**Manufacturer**
Airflow		Köttermann
Autoclave	2540EL	Systec
Autoclave	V95	Systec

Bacteria shaker	Certomat BS-T	Sartorius
Centrifuge	Multifuge 3 S-R	Heraeus
Centrifuge	Biofuge fresco	Heraeus
Controlled-freezing box		Nalgene
Drying cabinet		Memmert
Electroporator	Gene Pulser Xcell™	BioRad
Electrophoresis chamber		BioRad
ELISA Reader	Multiskan Ascent	Thermo Scientific
Flow cytometer	FACSCalibur™	Becton Dickinson
Freezer (-80 °C)	Hera freeze	Heraeus
Freezer (-20 °C)	cool vario	Siemens
Fridge (+4 °C)	cool vario	Siemens
Gel documentation	Gene Genius	Syngene
Ice machine	AF 100	Scotsman
Incubator	B20	Heraeus
Incubator	Hera cell 150	Heraeus
Liquid Nitrogen Tank	L-240 K series	Taylor-Wharton
Luminometer	Sirius Luminometer	Berthold detection systems
Multichannel pipette	(10-100 µl)	Eppendorf
Heating block	Thermomixer Comfort	Eppendorf
Hemocytometer	Neubauer	Brand
Microliter syringe	710NR	Hamilton
Micropipettes	(0.5-10 µl, 10-100 µl, 20-200 µl, 100-1000 µl)	Eppendorf
Microscope (fluorescence)	AxioVert 100	Zeiss
Microscope	DMIL	Leica
Microwave oven		Siemens, AEG
Mini centrifuge	MCF-2360	LMS
PCR cycler	iCycler	BioRad
Pipetting assistant	Easypet	Eppendorf
Power supplier	Standard Power Pack P25	Biometra
qRT- PCR cycler	7300 Real-Time PCR	Applied Biosystems
Rotator		GLW
Scales	770	Kern

Scales	EW3000-2M	Kern
Semi-Dry Transfer Apparatus	Fastblot	Biometra
SDS-PAGE chamber	Minigel-Twin	Biometra
Shaker	Polymax 2040	Heidolph Instruments
Spectrophotometer	GeneQuant II	Amersham Biosciences
Sterile Bench		Heraeus
Water bath		GFL
Western blot documentation	Gel Logic 1500 imaging sytem	Carestream Health, Inc.
Vortexer	Vortex-Genie 2	Scientific Industries
Water purification system	TKA GenPure	TKA GmbH

2.4. Chemical and biological reagents

Reagents	**Manufacturer**
30% Acrylamide	Sigma
Agar	Sigma
Agarose	Invitrogen
Ampicillin	Merck
AmpliTaq DNA Polymerase	Invitrogen
Ammonium persulfate (APS)	Sigma
β-Mercaptoethanol	Sigma
BCP (1-bromo-3-chloropropane)	Sigma
BenchMark™ Prestained Protein Ladder	Invitrogen
BHA (butylated hydroxyanisole)	Sigma
Blue Juice Gel Loading Buffer	Invitrogen
Bradford reagent	BioRad
Bromphenol blue	Sigma
Calcein AM	Merck
DEPC (diethyl pyrocarbonate)	Sigma
Deoxycholic acid	Roth
1kb DNA Ladder	Invitrogen
dNTPs	Roche
DMEM medium	Invitrogen

DMSO (dimethyl sulfoxide)	Merck
DTT (DL-Dithiothreitol)	Sigma
EDTA (ethylenediaminetetraacetate)	Merck
EtBr (Ethidium bromide)	BioRad
Ethanol	Merck
FBS (fetal bovine serum)	Biochrom
37% Formaldehyde	Merck
Gentamycin	Biochrom
Glycerol	Merck
Glycine	Merck
G418	PAA
HBSS (Hank's buffered salt solution)	Invitrogen
HCl (hydrochloric acid)	Merck
HEPES	Sigma
HiPerFect Transfection Reagent	Qiagen
Human IgG	Genzyme
IMDM medium	Invitrogen
Isoflurane	Abbott
Isopropanol	Sigma
KCl (potassium chloride)	Merck
L-glutamine	Invitrogen
Matrigel matrix	BD Biosciences
Maxima™ Probe / ROX qPCR Master Mix (2 x)	Fermentas
McCoys5A medium	Biochrom
Methanol	Roth
Methylcellulose	R&D Systems
$MgCl_2$ (magnesium chloride)	Invitrogen
NaCl (sodium chloride)	Merck
Na_2HPO_4 (sodium phosphate dibasic)	Merck
NaH_2PO_4 (sodium phosphate monobasic)	Merck
NaN_3 (sodium azide)	Merck
NaOH (sodium hydroxide)	Merck
Novaminsulfon	ratiopharm
PBS 10 x (phosphate buffered saline)	Invitrogen

PCR Buffer (10 x)	Invitrogen
Peptone	Invitrogen
Penicillin / streptomycin	Invitrogen
PFA (paraformaldehyde)	Merck
Polyacrylamide (30% Acrylamide / Bis)	Merck
Polybrene (hexadimethrine bromide)	Sigma
Propidium iodide	Sigma
Protease Inhibitor cocktail tablets	Roche
Proteinase K	Sigma
Puromycin	PAA
Ready-Load 1 Kb DNA Ladder	Invitrogen
RNase A (Ribonuclease A)	Roche
RPMI 1640 medium	Invitrogen
SDS	Sigma
Skim milk powder	Merck
Sodium chloride	Merck
SYBR Green Master Mix	Applied Biosystems
TEMED (N,N,N′,N′-Tetramethylethan-1,2-diamin)	Sigma
Tris	Merck
Triton X-100	Sigma
Trypan blue	Sigma
Trypsin / EDTA	Invitrogen
Tween 20	Sigma

2.5. Commercial reagent kits

Name	**Manufacturer**
Affymetrix GeneChip Whole Transcript Sense Target Labeling Kit	Affimetrix
Annexin V-PE Apoptose Detection Kit I	BD Biosciences
Angiogenesis System: Endothelial Cell Invasion	BD Biosciences
Cell Invasion Assay	BD Biosciences
Cell proliferation ELISA BrdU Kit	Roche
DNeasy® Blood & Tissue Kit	Qiagen
ECL-Plus Western Blot Detection System	GE Healthcare

High-Capacity cDNA Reverse Transcription Kit	Applied Biosystems
Human Methylcellulose Base Media	R&D Systems
JETSTAR 2.0 Plasmid Maxiprep Kit	Genomed
Ne-Per® Nuclear and Cytoplasmic Extraction Reagents	Thermo
NucleoSpin® Plasmid Kit	Macherey-Nagel
MycoAlert Mycoplasma Detection Kit	Lonza
QIAEX II Gel Extraction Kit	Qiagen
QIAquick PCR Purification Kit	Qiagen
RNeasy® Mini Kit	Qiagen
StemPro® Chondrogenesis Differentiation Kit	Gibco
StemPro® Osteogenesis Differentiation Kit	Gibco
StrataPrep® DNA Gel Extraction Kit	Stratagene
TRI Reagent RNA Isolation Kit	Ambion
TaqMan® Gene Expression Assays	Applied Biosystems

2.6. Media, buffers and solutions

Table 1: Cell culture media and universal solutions

Name	Ingredients
Standard tumor medium	500 ml RPMI 1640 or DMEM 10% FBS, 2 mM L-glutamine, 100 µg/ml gentamycin
4% formaldehyde	4% Formalin, 55 mM Na_2HPO_4, 12 mM $NaH_2PO_4 \cdot 2\ H_2O$
4% paraformaldehyde	4% PFA in 1 x PBS, adjusted to pH 7.4 with NaOH
FACS staining buffer	2% FBS, 0.05% NaN_3 dissolved in 1 x PBS

Table 2: Buffer and gel for DNA / RNA electrophoresis

Name	Ingredients
TAE running buffer	50 x TAE: 2 M Tris, 10% EDTA (0.5 M), 5.71% HCl
Electrophoresis gel	200 ml TAE buffer (1 x), 0.7-3% agarose, 3 µl EtBr

Table 3: Buffers and solutions for cell cycle analysis

Name	Ingredients
Sample buffer	0.1% Glucose (w/v) in 1 x PBS, 0.22 µm filtration, stored at 4°C
PI staining solution	50 µg / ml Propidium iodide and 100 U / ml RNase A in sample buffer

Table 4: Buffers and gels for Western blot analysis

Name	Ingredients
Laemmli buffer (3 x)	188 mM Tris/HCl pH 6.8, 3% SDS, 45% Glycerol, 0.05% Bromphenol blue, 7.5% ß-Mercaptoethanol
SDS running buffer (1 x)	25 mM Tris, 200 mM Glycine, 0.1% (w/v) SDS
Separating buffer (4 x)	1.5 M Tris, 0.4% SDS, adjusted to pH 8.8 with HCl
Separating gel (8-12.5%)	(10%): 3.33 ml 30% Acrylamide / Bis, 2.5 ml Separating Buffer (4 x), 4.17 ml water, 50 µl APS (10%), 20 µl TEMED
Stacking buffer (4 x)	0.5 M Tris, 0.4% SDS, adjusted to pH 6.8 with HCl
Stacking gel (4.5%)	750 µl 30% Acrylamide / Bis, 1.25 ml Stacking Buffer (4 x), 3 ml water, 50 µl APS (10%), 20 µl TEMED
Transfer buffer (5 x)	25 mM Tris pH 8.3, 192 mM Gylcine
TBS (10 x)	0.5 M Tris-HCl pH 7.4, 1.5 M NaCl
TBS-T	1 x TBS including 0.05% (v/v) Tween 20

2.7. Antibodies

Table 5: Antibodies for Western blot

Antibody	Source	Dilution	Product No.	Manufacturer
anti-β-catenin	mouse	1:1000	#610154	BD Biosciences
anti-DKK2	rabbit	1:100	PAB3570	Abnova
anti-GAP43	rabbit	1:1000	ab7462	Abcam
anti-Histone H3	Rabbit	1:5000	ab1791	Abcam

anti-HPRT (FL-218)	rabbit	1:500	sc-20975	Santa Cruz
anti-Kremen1	mouse	1:500	ab57872	Abcam
anti-Kremen2	mouse	1:500	ab68906	Abcam
anti-Lamin A+C	mouse	1:80	ab5090	Abcam
anti-LRP6 (C-10)	mouse	1:500	sc-25317	Santa Cruz
anti-mouse IgG HRP	goat	1:1000	sc-2060	Santa Cruz
anti-rabbit IgG HRP	bovine	1:1000	sc-2370	Santa Cruz

Table 6: Antibodies for immunofluorescence and immunohistochemistry

Antibody	Source	Dilution / Amount	Product No.	Manufacturer
anti-β-catenin	mouse	1:100	610154	BD Biosciences
anti-Caspase 3	rabbit	1:200	9664	Cell Signaling Technology
anti-DKK2	rabbit	1:50	PAB3570	Abnova
anti-GFAP	mouse	1:100	556330	BD Biosciences
anti-mouse IgG+IgM F(ab`)$_2$-FITC	goat	1:100	115-096-068	Jackson ImmunoResearch

Table 7: Antibodies for flow cytometry

Antibody	Conjugation	Dilution	Product No.	Manufacturer
CD29	APC	1:20	559883	BD Biosciences
CD49a	PE	1:20	559596	BD Biosciences
CD49b	FITC	1:20	555498	BD Biosciences
CD49c	PE	1:20	556025	BD Biosciences
CD49d	APC	1:20	559881	BD Biosciences
CD49e	PE	1:20	555617	BD Biosciences
CD49f	PE	1:20	555736	BD Biosciences
Isotype mouse IgG	FITC	1:20	345815	Becton Dickinson
Isotype mouse IgG	PE	1:20	345816	Becton Dickinson
Isotype mouse IgG	APC	1:20	345818	Becton Dickinson
Isotype rat IgG2b, κ	PE	1:20	553989	BD Biosciences

2.8. Small interfering RNAs

Small interfering RNAs (siRNAs) were obtained from Qiagen, except EWS-FLI1_1 and EWS-FLI1_2 siRNAs [138], which were synthesized by Eurofins MWG GmbH.

Table 8: Small interfering RNA used for transient transfection

siRNA Name	Target Sequence (5'-3')
Control (non-silencing) siRNA	5´-AAT TCT CCG AAC GTG TCA CGT-3`
CHM1_1 siRNA	5'-CAC GAA GGA ATC TGT TGT ATA-3'
CHM1_4 siRNA	5'-CCA GAA CTT TAG TAT ATG CAA-3'
DKK2_1 siRNA	5'-ATG GGA TTT GCT ATC ATA ATA -3'
DKK2_8 siRNA	5'-AGG GCC TGT CTT GCA AAG TAT-3'
EWS-FLI1_1 siRNA	5'-GCT ACG GGC AGC AGA ACC CTT-3'
EWS-FLI1_2 siRNA	5´-GCA GAA CCC TTC TTA TGA CTT-3'
ITM2A_5 siRNA	5'-AAC TCA GAT ACT GAC CGG CAA-3'
ITM2A_7 siRNA	5'-CAA ACT TAT GTG GTT CGA GAA-3'
MMP1_7 siRNA	5'-AAG CTA ACC TTT GAT GCT ATA-3'
MMP1_12 siRNA	5'-ATG ATG AAT ATA AAC GAT CTA-3'
MMP7_3 siRNA	5'-TGG ACG GAT GGT AGC AGT CTA-3'
MMP7_6 siRNA	5'-TGC AGT GAT GTA TCC AAC CTA-3'
MMP9_3 siRNA	5'-CAC GCA CGA CGT CTT CCA GTA-3'
MMP9_6 siRNA	5'-ACG GCT TGC CCT GGT GCA GTA-3'

2.9. Oligonucleotides for retroviral gene transfer

All oligonucleotides were obtained from Metabion International AG.

Table 9: Oligonucleotides used for retroviral gene transfer

Name	Sequence (5'-3')
CHM1-for	5'-GAT CCG CGA AGG AAT CTG TTG TAT ATT CAA GAG ATA TAC AAC AGA TTC CTT CGC TTT TTT CTA GAG-3'
CHM1-rev	5'-AAT TCT CTA GAA AAA AGC GAA GGA ATC TGT TGT ATA TCT CTT GAA TAT ACA ACA GAT TCC TTC GCG-3'
control-for	5'-GAT CCG TTC TCC GAA CGT GTC ACG TTT CAA GAG AAC GTG ACA CGT TCG GAG AAC TTT TTT CTA GAG-3'
control-rev	5'-AAT TCT CTA GAA AAA AGT TCT CCG AAC GTG TCA CGT TCT CTT GAA ACG TGA CAC GTT CGG AGA ACG-3'

DKK2-for	5'-GAT CCG GGG ATT TGC TAT CAT AAT ATT CAA GAG ATA TTA TGA TAG CAA ATC CCC TTT TTT CTA GAG-3'
DKK2-rev	5'-AAT TCT CTA GAA AAA AGG GGA TTT GCT ATC ATA ATA TCT CTT GAA TAT TAT GAT AGC AAA TCC CCG-3'
ITM2A-for	5'-GAT CCG GCA TGA ATA TAT CAC CTA ATT CAA GAG ATT AGG TGA TAT ATT CAT GCC TTT TTT CTA GAG-3'
ITM2A-rev	5'-AAT TCT CTA GAA AAA AGG CAT GAA TAT ATC ACC TAA TCT CTT GAA TTA GGT GAT ATA TTC ATG CCG-3'

2.10. Primers for PCR and qRT-PCR

The concentration of primers was 900 and 250 nM, respectively.

Table 10: Primers for PCR and qRT-PCR

Name	Sequence (5'-3')
ACTB for	5`-GGC ATC GTG ATG GAC TCC G-3`
ACTB rev	5`-GCT GGA AGG TGG ACA GCG A-3`
EWS-FLI1 for	5'-TAG TTA CCC ACC CAA ACT GGA T-3'
EWS-FLI1 rev	5'-GGG CCG TTG CTC TGT ATT CTT AC-3'
pSIREN for	5`-GGG CAG GAA GAG GGC CTA T-3`
pSIREN rev	5`-GAG ACG TGC TAC TTC CAT TTG TC-3`

2.11. Gene expression assays for qRT-PCR

2.11.1. TaqMan Gene Expression Assays

All TaqMan Gene Expression Assays were obtained from Applied Biosystems.

Table 11: TaqMan Gene Expression Assays

Gene	Assay ID
ABCG2	Hs00184979_m1
BCL2L1	Hs00236329_m1
BGLAP	Hs01587814_g1
CCND1	Hs00765553_m1
CD44	Hs01075861_m1
CDH1	Hs01023894_m1

CHM1	Hs00993254_m1
COL1A1	Hs00164004_m1
COL10A1	Hs00166657_m1
CXCR4	Hs00237052_m1
DKK2	Hs00205294_m1
EPHB2	Hs00362096_m1
GAPDH	Hs99999905_m1
GAP43	Hs00176645_m1
GFAP	Hs00157674_m1
HIF1α	Hs00153153_m1
ICAM1	Hs00164932_m1
ID2	Hs04187239_m1
IFITM1	Hs01652522_g1
IL6	Hs00985639_m1
ISG15 (G1P2)	Hs00192713_m1
ITM2A	Hs04176575_m1
JAG1	Hs01070032_m1
JUN	Hs01103582_s1
LEF1	Hs01547250_m1
MCL1	Hs01050896_m1
M-CSF	Hs00174164_m1
MMP1	Hs00899658_m1
MMP7	Hs01042796_m1
MMP9	Hs00234579_m1
NANOG	Hs02387400_g1
NGFR	Hs00609977_m1
NOTCH	Hs01062014_m1
OPG	Hs00900358_m1
OPN (SPP1)	Hs00959010_m1
PROM1	Hs01009250_m1
PTHrP	Hs00174969_m1
RANKL	Hs00243522_m1
RUNX2	Hs00231692_m1

SLIT2	Hs00191193_m1
SOX9	Hs00165814_m1
TGFβ	Hs00998133_m1
VEGF	Hs00176573_m1

2.11.2. QuantiTect® Primer Assays

All SYBR Green-based detection qRT-PCR primers were obtained from Qiagen (QuantiTect®Primer Assay).

Table 15: Primers for qRT-PCR (SYBR Green-based detection)

Gene	Assay ID
β-actin	QT00095431
ID2	QT00210637

2.12. Expression vector

Expression vector were obtained from Clontech-Takara Bio Europe.

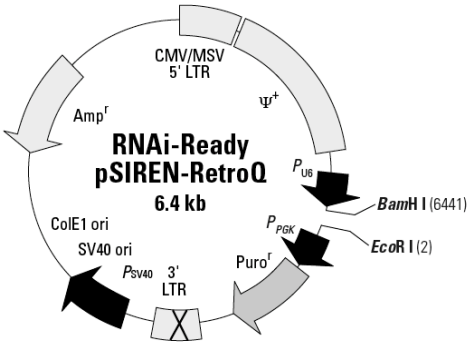

Figure 1: RNAi-Ready pSIREN-RetroQ vector
RNAi-Ready pSIREN-RetroQ vector produced by Clontech-Takara Bio Europe.

2.13. Human cell lines, mouse strains and bacterial strain

2.13.1. Human cell lines

Human cell lines were purchased from the German Collection of Microorganisms and Cell Cultures (DSMZ), except A673 ET cell line, which was purchased from ATCC (LGC Standards). ET cell line VH64 was kindly provided by Dr. Marc Hotfilder (Münster University, Germany). Human SB-KMS-KS1, previously known as SBSR-AKS, and SB-KMS-MJ1 ET cell lines were generated in the laboratory. Osteosarcoma cell lines were kindly provided by Dr. Jan Smida and Prof. Dr. Michaela Nathrath (Helmholtz Center Munich, Neuherberg, Germany). Retrovirus packaging cell line PT67 was obtained from Clontech-Takara Bio Europe.

Table 12: Description of utilized human cell lines

Cell Line	Description
A673	ET cell line (type 1 translocation), established from the primary tumor of a 15-year-old girl [139], p53 mutation
cALL2	human B cell precursor leukemia, established from the peripheral blood of a 15-year-old Caucasian girl with acute lymphoblastic leukemia (cALL); MHH-cALL2 [140]
CHP126	neuroblastoma cell line, established from a large retroperitoneal tumor of a 14-month-old girl (with neuroblastoma stage III) [141]
HOS	osteosarcoma cell line, established from the bone of a 13-year-old Caucasian girl [142]
HOS-58	osteosarcoma cell line, established from the leg of a 21-year old man [143]
MG-63	osteosarcoma cell line, established from the bone of a 14-year-old Caucasian boy
MHH-ES1	ET cell line (type 2 translocation), established from the ascites of a 12-year-old Turkish boy with a tumor of the left pelvis and additional peritoneal metastases
MHH-NB11	neuroblastoma cell line, established from an adrenal metastasis of a 4-year-old Caucasian boy
MNNG	osteosarcoma cell line, derived from HOS by transformation with 0.01 mcg/ml MNNG (a carcinogenic nitrosamine), full name

	MNNG/HOS Cl #5 [R-1059-D] [144,145]
Nalm6	human B cell precursor leukemia, established from the peripheral blood of a 19-year-old man with acute lymphoblastic leukemia (ALL) in relapse
RD-ES	ET cell line (type 2 translocation), established from the primary tumor localizised in the humerus of a 19-year-old Caucasian man
SaOS	osteosarcoma cell line, established from the bone of a 11-year-old Caucasian girl [146,147]
SB-KMS-MJ1	ET cell line (type 1 translocation), established from a bone metastasis of the left groin of a 24–year-old Caucasian woman
SB-KMS-KS1	ET cell line (type 1 translocation), established from an extraosseous inguinal metastasis of a 17-year old girl (new nomenclature, originally designated as SBSR-AKS)
SH-SY5Y	neuroblastoma cell line, established from a bone marrow biopsy of a 4-year-old girl with metastatic neuroblastoma
SJSA01	osteosarcoma cell line, established in 1982 from the primary tumor of a 19-year-old black man diagnosed with primitive multipotential sarcoma of the femur (new nomenclature, originally designated as OsA-CL) [148,149]
SIMA	neuroblastoma cell line, established from the adrenal tumor tissue resected after treatment from a 20-month-old boy of European origin with neuroblastoma (stage III) in 1991
SK-ES1	ET cell line (type 2 translocation), established from an 18-year-old man
SK-N-MC	ET cell line (type 1 translocation), established from the supraorbital metastases of a 14-year-old girl (Askin's tumor, related to ET)
TC-71	ET cell line (type 1 translocation), established in 1981 from a biopsy of recurrent tumor at the primary of a 22-year-old man with metastatic ET (humerus)
U2OS	osteosarcoma cell line, established from the bone of a 15-year-old Caucasian girl
VH64	ET cell line (type 2 translocation), established from an extraosseous

	lung metastasis [150]
ZK-58	osteosarcoma cell line, established from the leg of a 21-year-old man
697	human B cell precursor leukemia, established from bone marrow of a 12-year-old boy with ALL in relapse

2.13.2. Mouse strains

Two different immune deficient mouse strains were used in this doctoral thesis.

Table 13: Description of utilized mouse strains

Mouse strain	Characteristics	Origin
BALB/c $Rag2^{-/-}\gamma c^{-/-}$	Absence of all T-lymphocyte, B-lymphocyte and NK cell function	Central Institute for Experimental Animals (Kawasaki, Japan)
NOD.CB17-*Prkdc*^{scid}/NcrCrl	Impaired B- and T-cell lymphocyte development, deficient NK cell function	Charles River Laboratories International, Inc. (Wilmington, MA, USA)

The *Recombination activating gene 2* (*Rag2*)-*gamma(c)* knock-out ($Rag2^{-/-}\gamma c^{-/-}$) mouse is a mutated mouse strain, which was generated by back-crossing of two immunocompromised mouse models, the *gamma(c)* knock-out and the *Rag2* knock-out mice. The homozygous *gamma(c)* knock-out mice lack the *gamma(c)* receptor gene, why the development of lymphocytes is severely compromised. As a consequence, natural killer (NK) cell population is severely depleted in these mice, but they do have a small number of T- and B-lymphocytes. To further completely eliminate the T and B cell population in that animal model, the *gamma(c)* knock-out mouse was back-crossed onto the *Rag2* knock-out mouse. Homozygous Rag2 knock-out mice lack several exons of the *Rag2* gene, resulting in the inability to initiate V(D)J rearrangement. Therefore, these *Rag2* knock-out mice are incapable of generating any T- and B-lymphocytes [151]. As a result, the back-crossed $Rag2^{-/-}\gamma c^{-/-}$ mice were absent regarding T-lymphocyte, B-lymphocyte and NK cell functions. Thus, this immunodeficient animal model can be used in studies addressing vaccine development, transplantation paradigms or, as in this study, cancer biology.

The NOD.CB17-*Prkdc*^{scid}/NcrCrl immunodeficient mice are very useful in tumor biology and xenograft research. The SCID mutation has been transferred onto a non-obese diabetic background. Animals homozygous for the SCID mutation have impaired T and B cell lymphocyte development. The NOD background additionally results in deficient NK cell function.

2.13.3. Bacterial strain

The following bacterial strain was used for plasmid enrichment to generate stable knock-down cells by retroviral gene transfer.

Table 14: Description of utilized bacterial strain

***E. coli* strain**	**Genotype Description**	**Origin**
One Shot® TOP10 Chemically Competent	F- *mcr*A ∆(*mrr-hsd*RMS-*mcr*BC) φ80*lac*Z∆M15 ∆*lac*X74 *rec*A1 *ara*D139 ∆(*ara-leu*)7697 *gal*U *gal*K *rps*L (StrR) *end*A1 *nup*G	Invitrogen

3. Methods

3.1. Cell culture

ET and adherent neuroblastoma cell lines as well as the osteosarcoma cell lines MNNG, MG-63, SJSA01 and ZK-58 were cultured in RPMI 1640 (Invitrogen) containing 10 % fetal bovine serum (FBS) (Biochrom), 2 mM L-glutamine and 100 µg/ml gentamycin (both Invitrogen) at 37 °C in 5 % CO_2 in plastic flasks in a humidified atmosphere. Depending on the number of cells needed for analysis, cell lines were grown in middle-sized culture flasks (75 cm^2 adherence surface) containing 20 ml medium or in large-sized flask (175 cm^2 adherence surface) with 30 ml of medium. Approximately every 3 - 4 days the medium was removed and cells were split 1:2 to 1:10. For this purpose, cells were washed once with 1 x PBS and incubated 5 min with 2 ml and 3 ml 1 x trypsin at 37 °C (5 % CO_2) to remove the adherent cells from the plastic flasks. Detached cells were re-suspended in fresh RPMI standard tumor medium, centrifuged at 1200 rpm for 7 min and spread in new culture flasks.

The other adherent osteosarcoma cell lines HOS, HOS-58, SaOS and U2OS were cultured in different media (DMEM, IMDM and McCoys5A) all containing 10 % fetal bovine serum (FBS) (Biochrom), 2 mM L-glutamine (Invitrogen) and 100 µg/ml gentamycin (Invitrogen) at 37 °C in 5 % CO_2 in a humidified atmosphere.

The neuroblastoma cell line CHP126, which grow in suspension, were cultured in a middle-sized culture flask with 30 ml RPMI medium in a humidified atmosphere at 37 °C (5 % CO_2). Approximately every 4 days, cells were split 1:1 to 1:5 and cultured in an appropriate volume of fresh medium.

The retrovirus packaging cell line PT67 was grown at 37 °C in 8 % CO_2 in middle-sized culture flasks in a humidified atmosphere in DMEM (Invitrogen) containing 10 % fetal bovine serum (FBS) (Biochrom), 1 % glutamine and 100 µg/ml gentamycin (both Invitrogen).

For long-term storage in liquid nitrogen (-192 °C) cells were re-suspended at a concentration of 1 x 10^6 to 1 x 10^7 per 1 ml FBS / 10 % DMSO and 1 ml aliquots of the cell suspension were transferred into cryovials. The cryovials were placed into controlled freezing boxes, stored 12 - 18 h at -80 °C and were then transferred into the liquid nitrogen freezer for further storage.

To re-culture the cryopreserved cells, vials were removed from liquid nitrogen and thawed at room temperature until the cell suspension started to defrost. In order to remove toxic DMSO the cell suspension was transferred into a 50 ml Falcon tube

carrying 10 ml of fresh standard medium, and cells were pelletized at 1200 rpm for 7 min in a centrifuge. Subsequently, the pellet was re-suspended in 20 ml fresh medium and the suspension was transferred into a middle-sized culture flask and stored in an incubator at 37 °C (5 % CO_2) in a humidified atmosphere.

For most analyses cell counts were determined with a Neubauer hemocytometer. Cell viability was assessed by trypan blue (Sigma) exclusion method.

Cultured cells were checked routinely for purity (EWS-FLI1 translocation product, surface antigen or HLA-phenotype) and mycoplasma contamination using MycoAlert™ Mycoplasma Detection Kit according to manufacturer's instructions (Lonza).

3.2. RNA isolation

3.2.1. RNA isolation using RNeasy Mini Kit

To analyze gene expression by quantitative Real Time PCR cellular RNA, larger than 200 bases, was isolated using the RNeasy® Mini Kit according to manufacturer's instructions (Qiagen Handbook 04/2006). Briefly, up to 1 x 10^7 cells were re-suspended in 350 µl of RLT buffer (containing 10 µl ß-mercaptoethanol per 1 ml RLT) and mixed with an equal amount of 70 % ethanol. After vortexing for 20 s, the lysate was transferred onto RNeasy® column and centrifuged 1 min at 10000 rpm to enable binding of the RNA to the silica-gel membrane within the RNeasy® column. The membrane was washed three times with two different wash buffers (1 x RW1 buffer and 2 x RPE buffer) with a final centrifugation step at 12000 rpm for 2 min to dry the membrane. Elution of RNA was carried out for up to 5 min on ice with 40 µl RNase-free water. RNA concentration was determined photometrically at 260 nm and isolated RNA was then either used for cDNA synthesis (see 3.3) or stored at -80 °C for later analysis.

3.2.2. RNA isolation using TRI Reagent RNA Isolation Kit

Isolation of RNA from frozen tissues was done using TRI Reagent RNA Isolation Kit according to manufacturer's protocol (Ambion Manual Version 0610). Briefly, at least 0.125 cm^3 of frozen tissue was physically crushed, re-suspended in 1 - 2 ml TRI Reagent and homogenized with a 19-gauge needle. After incubation for 5 min at RT, 100 µl BCP (1-bromo-3-chloropropane) per 1 ml TRI Reagent was added and samples were vigorously vortexed for 20 s, followed by a centrifugation step at 4000 rpm for 60 min at 4 °C. The aqueous RNA phase was transferred into a new reaction tube and

RNA was precipitated by adding 500 µl isopropanol per 1 ml TRI Reagent. After vortexing for 20 s, the sample was again centrifuged at 4000 rpm for 30 min at 4 °C. Subsequently, the RNA pellet was washed with 1 ml 75 % ethanol and centrifuged at 4000 rpm for 10 min at 4 °C. After removal of ethanol the pellet was air-dried for 5 - 10 min and isolated RNA was dissolved in 50 - 100 µl RNase-free water. RNA concentration was determined photometrically at 260 nm and RNA was stored at -80 °C for later analysis.

RNA isolation with TRI Reagent RNA Isolation Kit was also used to isolate total RNA from cultured cells, since RNA isolation by RNeasy Mini Kit is not sufficient for the isolation of RNA molecules smaller than 200 bases due to given high salt conditions (see 3.2.1).

3.3. cDNA synthesis

To examine gene expression by quantitative Real Time PCR, isolated RNA has to be reverse transcribed into complementary DNA (cDNA) using the High-Capacity cDNA Reverse Transcription Kit. According to manufacturer's instructions (Applied Biosystems Insert P/N 4375222 REV A) 15 µl of 2 x RT master mix containing 0.8 µl 25 x dNTPs (100 mM), 1 µl MultiScribe™ Reverse Transcriptase (RT), 2 µl 10 x RT Random Primers, 2 µl 10 x RT Buffer and 9.2 µl nuclease-free water were mixed with 5 µl RNA solution (containing 1 µg purified RNA). The cDNA was synthesized under the following thermal cycling conditions: 10 min 25 °C; 120 min 37 °C; 5 min 85 °C; ∞ 4 °C. Synthesized cDNA was either instantly used for examination of gene expression by quantitative Real Time PCR (see 3.4) or stored at -20 °C.

To check the quality of the generated cDNA, especially from *ex vivo* tumor probes, β-actin PCR was performed using 5 µl 10 x Rxn Buffer, 1.5 µl MgCl, 1 µl dNTPs, 0.5 µl β-actin primer (forward and reverse, see Table 10), 0.3 µl AmpliTaq DNA Polymerase and 1 µl cDNA in a final volume of 50 µl per reaction. Following cycler conditions were used: 2 min 94 °C; [30 s 94 °C; 30 s 59 °C; 45 s 72 °C] 35 x; 7 min 72 °C; ∞ 4 °C. Separation of PCR products was done in 1 % agarose gel by electrophoresis.

3.4. Quantitative Real-Time PCR (qRT-PCR)

3.4.1. Standard qRT-PCR

Quantification of synthesized cDNA by qRT-PCR is a useful tool to examine differential gene expression as the amount of cDNA corresponds to the amount of cellular mRNA. This method allows a sequence specific quantification, as a fluorescent reporter-containing probe specifically hybridizes with its corresponding sequence inside the gene of interest, and its fluorescence can only be detected after breakdown of the sample by the exonuclease activity of the Taq polymerase that specifically amplifies the target sequence due to gene specific primers. qRT-PCR was performed using Maxima™ Probe/ROX qPCR Master Mix (2x) (containing Hot Start Taq DNA Polymerase, PCR buffer and dNTPs) and specific TaqMan® Gene Expression Assays (Applied Biosystems), which consist of two unlabeled PCR primers and a FAM™ dye-labeled TaqMan® MGB probe. Analyses were performed in 96-well plates and the reaction mix was prepared according to the manufacturer's instructions (Fermentas PureExtreme™ Insert) as follows: 10 µl of Maxima™ Probe/ROX qPCR Master Mix (2 x), 1 µl TaqMan® Gene Expression Assays (see Table 11), 0.5 µl cDNA template and 8.5 µl RNase-free water. The final concentration of primers and probe were 0.9 and 0.25 µM respectively. Gene expression profiles were normalized to the mRNA levels of the housekeeping gene *glyceraldehyde 3-phosphate dehydrogenase* (*GAPDH*) and calculated using the 2^{-ddCt} method. The mean value and standard deviations of duplicates are displayed graphically using Microsoft Excel, as well as standard error of the mean of at least two independent experiments. Using the conventional t-test carried out determination of the statistical significance. Fluorescence was detected and measured in an AB 7300 Real-Time PCR system using a three-step cycling protocol: 1 s 50 °C; 10 min 95 °C; [15 s 95 °C; 1 min 60 °C] 40 x (Applied Biosystems).

3.4.2. qRT-PCR using SYBR Green

SYBR Green is a highly specific dsDNA binding fluorescent dye that enables detection of all amplified PCR products without requiring specific dye-labeled probes (SYBR Green-based detection). According to the manufacturer's instructions, SYBR Green-based qRT-PCR was performed by use of POWER SYBR™ GREEN PCR Master Mix (Applied Biosystems) containing SYBR Green I dye, AmpliTaq Gold® DNA Polymerase, PCR buffer and dNTPs. Gene specific primers (0.4 µM each) and 0.5 µl cDNA template were added to 12.5 µl Master Mix and adjusted to a final volume of 25 µl with RNase-free water. Gene expression profiles were normalized to the mRNA levels of the

housekeeping gene *β-actin* (*ACTB*) and calculated using the 2^{-ddCt} method. The mean value and standard deviations of duplicates are displayed graphically using Microsoft Excel, as well as standard error of the mean of two and more independent experiments. Determination of the statistical significance was carried out by using the conventional t-test. Fluorescence was again detected and measured with an AB 7300 Real-Time PCR System (Applied Biosystems; see 3.4.1).

3.4.3. Detection of EWS-FLI1

There are no inventoried TaqMan® Gene Expression Assays for the detection of EWS-FLI1 mRNA levels available. For that reason, primers detecting EWS (sense) and FLI1 (antisense) of the oncogenic fusion protein were designed (see Table 15). The master mix was prepared as followed: 10 µl of Maxima™ Probe/ROX qPCR Master Mix (2 x), 0.6 µl of each primer (0.3 µM) and 0.4 µl of FAM probe (0.2 µM) to 7.6 µl RNase-free water. To a final volume of 19.5 µl Master Mix per 96-well 0.5 µl of cDNA template was added. Gene expression profiles were normalized to GAPDH mRNA levels and calculated using the 2^{-ddCt} method. Fluorescence was detected and measured with an AB 7300 Real-Time PCR System (Applied Biosystems; see 3.4.1).

Table 15: Gene expression assay to detect EWS-FLI1 mRNA by qRT-PCR.

sense primer	5'-TAG TTA CCC ACC CAA ACT GGA T-3'
antisense primer	5'-GGG CCG TTG CTC TGT ATT CTT AC-3'
FAM probe	5'-FAM-CAG CTA CGG GCA GCA GAA CCC TTC TT-TAMRA -3'

3.5. Transient RNA interference (RNAi)

For transient protein knock-down, cells were transfected with small interfering RNA (siRNA) using the HiPerFect Transfection Reagent according to standard procedures for large-scale transfection in 100 mm dishes (Qiagen Handbook 05/2008). Briefly, 1 - 3 x 10^6 cells were plated into 100 mm culture dishes at a final volume of 12 ml medium containing 5 nM siRNA (see Table 8) and 36 µl transfection reagent. After incubation for 48 - 72 h at 37 °C (5 % CO_2) in a humidified atmosphere, RNA was isolated (see 3.2), reverese transcribed into cDNA (see 3.3) and transient gene knock-down was examined by qRT-PCR (see 3.4) in comparison to cells transfected with control siRNA (neg.control). To exclude unspecific down-regulation of the gene investigated, different siRNAs were analyzed. Furthermore, to exclude induction of an interferon (IFN)

response, mRNA levels of the IFN responsive genes (*ubiquitin-like modifier ISG15* (*ISG15)* and *interferon-induced transmembrane protein 1* (*IFITM1)*) were monitored by the use of specific gene expression assays (see Table 11). If mRNA expression of one of these genes was induced more than twofold after siRNA treatment, the respective siRNA was not used for further experiments [152,153].

3.6. Retrovirus-mediated stable RNA interference

According to manufacturer's protocol, synthetic oligonucleotides corresponding to siRNA sequences with best knock-down efficiency were cloned into the pSIREN-RetroQ retroviral vector to generate cell lines with constitutive protein knock-down (Clontech Manual Version No. PR631543). The synthetic oligonucleotides (see Table 9) were annealed to generate double strand (ds) oligonucleotides and ligated into pSIREN-RetroQ retroviral vector. The small hairpin RNA (shRNA) constructs were transformed into chemically competent TOP10 *E. coli* bacteria and plasmid DNA was purified using NucleoSpin® Plasmid Kit according to manufacturer's instructions (Macherey-Nagel Manual 03/2005/ Rev 02). After sequencing, the correct constructs were transfected by electroporation (capacitance of 960 µF and 270 V / 0.4 cm) into RetroPack PT67 packaging cells and viral supernatant were isolated 48 h after transfection. Viral supernatant can immediately used to induce stable protein knock-down or stored at -80 °C.

To generate stably transfected ET cell lines, 1 x 10^5 cells/well were seeded into six well culture plates and incubated 12 - 18 h at 37 °C (5 % CO_2) in a humidified atmosphere. After addition of 1 ml viral supernatant and 4 µg/ml polybrene, cells were again incubated for 24 - 48 h under normal culture conditions. Selection of infectants with constitutive protein knock-down was made using 2 µg puromycin per ml RPMI medium. To analyze stable gene knock-down compared to shRNA control (pSIREN^{negsiRNA}), RNA was isolated, reverse transcribed into cDNA and gene expression was examined by qRT-PCR (see 3.2, 3.3 and 3.4). As described above, mRNA levels of the IFN responsive genes *ISG15* and *IFITM1* were monitored to exclude down-regulation or induction of genes due to an IFN response.

3.7. Isolation of genomic DNA (gDNA)

To examine genomic integration of retroviral vector constructs, total DNA from cultured cells was isolated using the DNeasy® Blood & Tissue Kit according to manufacturer's

protocol (Qiagen Handbook 07/2006). Briefly, 1 - 5 x 10^6 cells were re-suspended in 200 µl 1 x PBS containing 20 µl proteinase K and transferred onto a DNA-binding membrane within the DNeasy® column. After direct cell lysis with specific buffers and selective binding of DNA to the membrane, samples were washed and DNA was eluted in 100 µl sterile water. DNA concentration was determined photometrically at 260 nm.

To amplify integrated pSIREN-RetroQ vector-derived DNA using PCR analysis following primers (see Table 10) and cycler conditions were used: 5 min 94 °C; [30 s 94 °C; 30 s 58 °C; 15 s 72 °C] 40 x; 7 min 72 °C; ∞ 4 °C. PCR was performed using 5 µl 10 x Rxn Buffer, 1.5 µl MgCl, 1 µl dNTPs, 0.5 µl pSIREN primer (forward and reverse), 0.3 µl AmpliTaq DNA Polymerase and 2 µl gDNA in a final volume of 50 µl per reaction. Separation of DNA fragments occurred in 1 % agarose gel by electrophoresis.

3.8. Proliferation assay

3.8.1. xCELLigence proliferation assay

Cell proliferation of A673 and SK-N-MC cells was measured with an impedance-based instrument system (xCELLigence, Roche/ACEA Biosciences) enabling label-free real time cell analysis as previously described [153]. Briefly, 1 - 3 x 10^4 cells were seeded into 96-well E-plates with 200 µl media containing 10 % FBS and allowed to grow up to 72 - 100 h. Cellular impedance was measured periodically every 4 h across interdigitated gold micro-electrodes on the bottom of tissue culture E-plates. The presence of the cells on top of the electrodes will affect the local ionic environment at the electrode/solution interface, leading to an increase in the electrode impedance, which is displayed as cell index (CI) values. The more cells are attached on the electrodes, the larger the increases in electrode impedance.

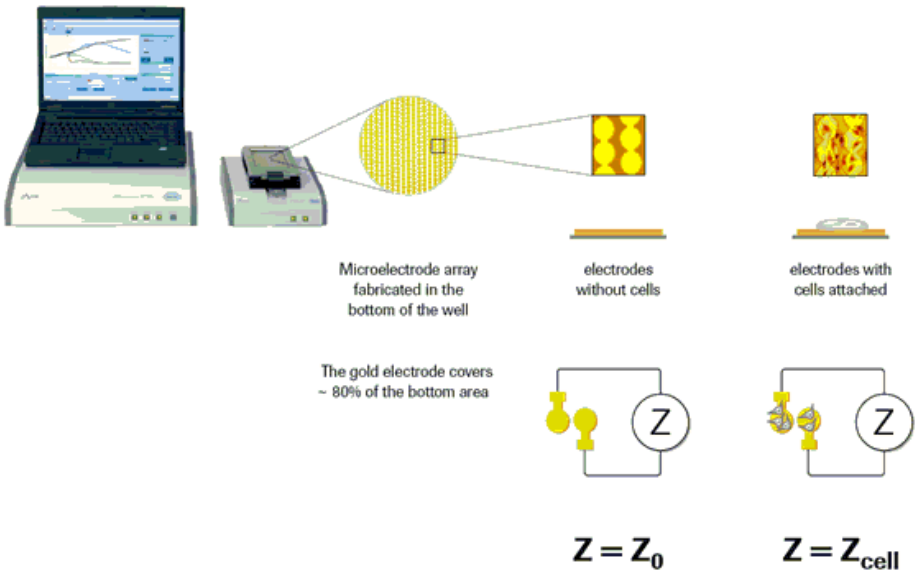

Figure 2: Diagramm of xCELLigence technology
Indication of source (http://www.roche-applied-sciences.com/sis/xcelligence.index.jsp?id=xcect_010000)

3.8.2. BrdU incorporation assay

Cell proliferation of TC-71 cells was quantified using Cell Proliferation ELISA, BrdU (Colorimetric) Kit according to manufacturer`s instructions (Roche Instruction Manual 08/2007), because cell attachment was not strong enough to use xCELLigence proliferation assay. Briefly, 2 x 10^3 cells per 96-well were seeded in hexaplicates or octaplicates at a final volume of 100 µl and incubated at 37 °C (5 % CO_2) in a humidified atmosphere. Subsequently, 20 µl/well of BrdU (5-bromo-2'-deoxyuridine) labeling solution was added to the cells at defined time points (0 h, 24 h, 48 h, 72 h) and cells were re-incubated for another 14 h in the presence of BrdU, which gets incorporated in the DNA of proliferating cells. Labeling medium of semi-adherent TC-71 cells was then removed by flicking off, after a centrifugation step of 1200 rpm for 10 min. Cells were then dried with a hair dryer for 15 min and stored at 4 °C until analysis within the next 1 - 4 days.

For analysis cells were lysed and incubated with a specific peroxidase conjugated anti-BrdU-antibody to detect incorporated BrdU. Reaction product was quantified by measuring the absorbance (450 nm) using a Multiscan Ascent ELISA reader. The mean value and standard error of the mean are displayed graphically using Microsoft Excel. Determination of the statistical significance was carried out by using the conventional t-test. The absorbance values directly correlate with the amount of DNA synthesis and hereby to the proliferation rate of cells.

3.9. Apoptosis and necrosis assay

Apoptotic cells were analyzed using Annexin V-PE Apoptosis Detection Kit I according to manufacturer`s instructions (BD Biosciences Pharmingen™ Insert rev. 006). Annexin V is a phospholipid-binding protein with a high affinity to phosphatidylserin (PS), a membrane protein that gets exclusively exposed to the outer leaflet of the plasma membrane during early stages of apoptosis. To differentiate between viable cells with an intact plasma membrane and nonviable, necrotic cells that lost membrane integrity 7-Amino-Actinomycin D (7-AAD) was used. Combination of these two markers allowed discrimination between viable cells (Annexin V-PE and 7-AAD negative), early apoptosis (Annexin V-PE positive, 7-AAD negative), and end stage apoptosis (Annexin V-PE and 7-AAD positive).

For analysis cells were counted and washed twice with 1 x PBS. Subsequently, 1 x 10^5 cells were re-suspended in 100 µl of 1 x binding buffer and stained with 2 µl of Annexin V-PE and 7-AAD. After 30 min of incubation at room temperature (RT) 400 µl of 1 x binding buffer were added, and samples were analyzed within 1 h by flow cytometry using a FACSCalibur™ Flow cytometer. To set up the correct forward scatter (FSC) and sideward scatter (SSC) for the cell population as well as the correct parameters for detecting fluorescence an unstained sample as well as samples with Annexin V-PE and 7-AAD alone were included.

3.10. Cell cycle analysis

Cell cycle analysis was performed by flow cytometry using propidium iodide (PI), a DNA intercalating agent. Since PI intercalates into double-stranded nucleic acids and emits a fluorescence signal after excitation by a 488 nm laser, fluorescence intensity of the stained cells correlate with the amount of DNA they contain. This allows differentiation between phases of cell cycle, as the fluorescence of cells in the G_2/M phase is twice as high as that of cells in the G_0/G_1 phase through DNA duplication during intermediate S phase.

To analyze cell cycle progression, 2 x 10^6 cells per sample were washed twice with pre-cooled sample buffer (see Table 3) and centrifuge at 1200 rpm for 10 min (4 °C). Subsequently, cells were fixated by drop-wise addition of 1 ml ice-cold 70 % ethanol while vortexing. After incubation for 18 - 24 h at 4 °C cells were centrifuged and re-suspended in 1 ml staining buffer containing RNase A and PI to remove any RNA, followed by incubation for 30 - 60 min at RT (under agitation). Cell cycle analysis was then measured with a FACSCalibur™ Flow cytometer.

3.11. Flow cytometry

To analyze expression of cell surface antigens/proteins using flow cytometry, cells were trypsinized, counted and washed twice with 1 x PBS. Afterwards, 5 x 10^5 cells/ sample were re-suspended in 40 µl staining buffer with 100 µg/ml human IgG (10 µl) and incubated for 20 min on ice to block unspecific binding sites. After a centrifugation step at 1500 rpm for 5 min (4 °C), cells were washed once with 200 µl pre-cooled staining buffer and then incubated in 100 µl staining buffer with 5 µl Fluorophore-labeled specific antibody (see Table 7). To find the right settings for the cell population, one unstained sample and one sample stained with the isotype controls for every fluorophore investigated was used for setting up the correct FSC and SSC as well as the parameters for detecting fluorescence. All samples were incubated on ice (shielded from light) for 30 min, followed by two washing steps with staining buffer, before the samples were re-suspended in 200 µl 1 x PBS and measured with a FACSCalibur™ Flow cytometer. At least 20000 events/sample were recorded. In case the samples could not be analyzed within two hours, they were fixed by re-suspending them in 200 µl 1 x PBS / 1 % paraformaldehyde and stored at 4 °C. Before measurement, samples were washed twice with 1 x PBS and measured in 1 x PBS with a FACSCalibur™ Flow cytometer.

3.12. Western blot analysis

Examination of protein expression was performed by Western blot analyses, in which proteins are separated, depending on their molecular weight by gel electrophoresis, transferred onto a membrane, and afterwards identified with specific antibodies.

For this purpose either whole protein lysates or separated cytoplasmic and nuclear extracts from cultured cells were generated. Procedures were essentially done as described previously [152]. Cells were first trypsinized, counted and washed twice with 1 x PBS. For whole protein lysates, 2 - 4 x 10^6 cells were re-suspended in 200 µl 3 x Laemmli-buffer, which contains 30 µl ß-mercaptoethanol per 1 ml 3 x Laemmli. Following an incubation step at 55 °C for 10 min to denature proteins, cell lysates were homogenized through a 23-gauge needle and then centrifuged for 5 min at 14000 rpm. Aliquots of the supernatants were stored at -20 °C or immediately processed for SDS-PAGE. To separate cytoplasmic and nuclear extracts from cultured cells the NE-PER® Nuclear and Cytoplasmic Extraction Reagents Kit (Thermo) was used according to the manufacturer's instructions. Briefly, 2 x 10^6 cells were re-suspended in 200 µl ice-cold CER I buffer containing proteinase inhibitors and incubated on ice for 10 min. To cause

cell membrane disruption and release of cytoplasmic contents 5.5 µl ice-cold CER II buffer was added. After recovering the intact nuclei from the cytoplasmic extract by centrifugation for 5 min at maximum speed, the nuclei are lysed with 100 µl ice-cold NER buffer (containing proteinase inhibitors) for a total of 40 min. Aliquots of the cytoplasmic and nucleic extracts were stored at -80 °C until use.

Dependent on the molecular weight of the protein to be separated 8 - 12.5 % polyacrylamide gels were used (see Table 4). After samples were boiled at 55 °C for 10 min, 10 - 30 µl of denatured and reduced protein lysates were transferred to the SDS-PAGE and electrophoresis was carried out at 70 - 90 V for 2.5 - 3.5 h. Molecular weight of the separated proteins was determined by comparison with a prestained molecular weight standard.

For detection by specific antibodies, proteins had to be transferred onto a membrane by applying an electrical field. Therefore, the gel and a methanol-activated Hybond-P PVDF membrane were sandwiched between Whatman filter papers (soaked in 1 x transfer buffer; see Table 4), and transfer was done under semi-dry conditions at 0.8 mA/cm^2 for 2.5 h in a blotting device. Unspecific binding sites were blocked by immersing the membrane in 5 % skim milk / 0.05 % Tween 20 for 1 h at RT or overnight at 4 °C.

The membrane was then incubated with primary antibody (see Table 5), targeting the protein of interest, for appropriate time. Antibodies were diluted according to the manufacturer's instructions in 5 % skim milk / 0.05 % Tween 20. Subsequently, the membrane was washed 3 x (5 min per wash) in 1 x TBS-T, incubated for 1 - 2 h with horseradish peroxidase (HRP) coupled secondary antibody in 5 % skim milk / 0.05 % Tween 20 and washed again as before plus once in 1 x TBS for 5 - 10 min.

According to the manufacturer's protocol, antibody-antigen complexes were detected using the ECL-Plus Western Blotting Detection System (GE Healthcare Booklet RPN2132PL Rev D 2006), which is based on the oxidation of a Luminogen by HRP and peroxide, resulting in a chemoluminescent signal detectable by a CCD camera. Signals of antibody-antigen complexes were detected with the Gel Logic 1500 imaging system and analyzed with Kodak Molecular Imaging Software (Version 5.0).

To reactivate dried PVDF membrane, membrane was incubated in methanol (~1 min), washed once with $H_2O_{dest.}$ and 1 x TBS-T (~5 min) and blocked for 1 h in 5 % skim milk / 0.05 % Tween 20.

3.13. Immunofluorescence (IF)

IF was carried out as previously described [152,154]. Briefly, cells were fixated in 4 % paraformaldehyde and washed two times with 1 x PBS. To perforate cell membranes, cells were incubated for 30 min with 0.1 % Triton X-100. After incubation for 30 min with 100 µg human IgG to block unspecific binding sites, cells were stained with a specific antibody for 12 - 18 h at 4°C (see Table 6). Following multiple washing steps with 1 x PBS, samples were incubated with an adequate secondary antibody for 1 - 2 h at RT in the dark. Subsequently, cells were again washed 3 x in 1 x PBS, dried and analyzed by fluorescence microscopy using a Nikon Eclipse TS 100 with an attached Nikon Coolpix 5400 camera.

3.14. Colony forming assay

Procedures were described previously [152]. To analyze contact-independent growth capacity, 5 x 10^3 cells were re-suspended in 300 µl cell resuspension solution and seeded in duplicate into a 35 mm plate containing 1.5 ml methylcellulose-based media (R&D Systems) according to the manufacturer's instructions and cultured for 10 - 14 days at 37 °C / 5 % CO_2 in a humidified atmosphere.

3.15. Invasion assay

To study cell invasion, the *BioCoat™ Angiogenesis System: Endothelial Cell invasion* was used (BD Biosciences) according to the manufacturer's instructions as previously described [153]. Briefly, the plate was first removed from -20 °C storage and allowed to adjust to RT. Pre-warmed RPMI medium without any supplements was added into the insert wells and allowed the rehydration of the Matrigel for 1 h at 37 °C (5 % CO_2). After careful removal of the medium, 5 x 10^4 cells, re-suspended in 250 µl RPMI medium without FBS, were added to each insert well. As a chemoattractant, 700 µl media containing 10 % FBS was added to each of the bottom wells. After incubation for 48 h at 37 °C (5 % CO_2) in a humidified atmosphere, invasive cells at the bottom side of the membranes were stained with Calcein AM solution at a concentration of 4 µg/ml. Therefore, the insert plate was transferred into a second BD Falcon 24-well plate containing 0.5 ml/well of 4 µg/ml Calcein AM in pre-warmed HBSS (Hank's buffered salt solution) with 0.15 % DMSO and incubated for 90 min at 37 °C (5 % CO_2). Cells were imaged by fluorescence microscopy using a Zeiss AxioVert 100 with attached AxioCam MRm and the visualizing program AxioVision Rel. 4.7 (Carl Zeiss).

Photographed invasive cells were then counted using the image processing package Fiji.

3.16. Differentiation assays

3.16.1. Endothelial tube formation assay

Endothelial differentiation was analyzed using Matrigel matrix assay according to the manufacturer's instruction (BD Biosciences Manual SPC-356234 Rev 5.0) as previously described [152,155]. Briefly, cells were seeded at 4 - 7 x 10^4 cells per well onto 75 µl Matrigel at a final volume of 100 µl in a 96-well plate and incubated for 24 - 48 h at 37 °C (5 % CO_2) in a humidified atmosphere. Following a washing step with 1 x PBS, cells were stained with 1 µg/ml Calcein AM Fluorescent Dye for 30 min in the dark and cellular tube formation was examined by fluorescence microscopy using a Nikon Eclipse TS 100 with an attached Nikon Coolpix 5400 camera.

3.16.2. Neuronal differentiation assay

For neuron/astrocyte-like cell differentiation, 7 x 10^4 cells were seeded at a final volume of 3 ml DMEM medium into six-well plates and incubated for 24 h at 37 °C (8 % CO_2) in a humidified atmosphere. To induce neuronal differentiation, cells were treated for 6 days with 0.1 mM BHA (butylated hydroxyanisole) in the presence of 2 % DMSO [152,156]. The differentiated cells were identified either with immunofluorescence against glial fibrillary acid protein (GFAP, see Table 6 and 3.13) and/or with an antibody against the neuronal marker growth-associated protein 43 (GAP43, see Table 5) using Western blot analysis (see 3.12).

3.16.3. Chondrogenic differentiation assay

To test chondrogenic cell differentiation potential, cells were cultured in specific differentiation media (STEMPRO® Chondrogenesis Differentiation Kit, GIBCO, Invitrogen) according to the manufacturer's instructions. Briefly, cells were trypsinized, counted and washed twice with 1 x PBS. Pellets were re-suspended in an appropriate volume of pre-warmed DMEM medium containing 10 % FBS (Biochrom), 2 mM glutamine and 5 µg/ml gentamycin (both Invitrogen) to a final cell concentration of 1.6 x 10^7 cells. To generate micromass cultures, cells were seeded in 5 µl cell droplets in the

center of 6-well plate wells and cultured for 5 - 15 min under high humidity conditions, before pre-warmed chondrogenic differentiation media was carefully added. Samples were incubated for up to two weeks at 37 °C (5 % CO_2) in a humidified atmosphere, while differentiation media was changed every 2 - 3 days. To validate differentiation efficacy, expression of the well-known chondrogenic marker genes, *sry-box 9* (*SOX9*), an early transcription factor of chondrogenesis and *Collagen type X alpha 1* (*COL10A1*), which is used to identify terminally differentiated hypertrophic chondrocytes [157], was monitored by qRT-PCR (see 3.4).

3.16.4. Osteogenic differentiation assay

Osteogenic cell differentiation capacity was examined using STEMPRO® Osteogenesis Differentiation Kit (GIBCO, Invitrogen) according to the manufacturer's instructions. Briefly, cells were trypsinized, counted and washed twice with 1 x PBS and pellets were re-suspended in an appropriate volume of pre-warmed DMEM medium containing 10 % FBS (Biochrom), 2 mM glutamine and 5 µg/ml gentamycin (both Invitrogen). 1 x 10^4 cells were seeded into each well of a 6-well plate and cells were incubated for a minimum of 2 h up to 24 h at 37 °C (5 % CO_2) in a humidified atmosphere. Subsequently, DMEM media was replaced with pre-warmed osteogenic differentiation media and samples were further incubated for up to three weeks. Approximately every 3 - 4 days, cells were split and differentiation media was changed. At the molecular level, osteogenic differentiation was controlled by the expression of the early osteogenic marker gene *Collagen type I alpha 1* (*COL1A1*) and *Osteopontin* (*OPN*), which is expressed later in the differentiation process [157] using qRT-PCR (see 3.4).

3.17. *In vivo* experiments

To analyze local or invasive tumor growth *in vivo,* 1.5 - 3 x 10^6 ET cells and derivatives were detached with 2 - 3 ml 1 x trypsin, washed twice with 1 x PBS and re-suspended in a final volume of 0.2 ml.

To investigate local tumor growth cells were injected subcutaneously into the inguinal region of immune deficient $Rag2^{-/-}\gamma c^{-/-}$ or NOD/scid mice (see Table 13; [152,158]) using a 26-gauge needle attached to a 1 ml syringe and tumor size was determined. Mice bearing a tumor > 10 mm in diameter (determined with a caliper) were considered

as positive and sacrificed. Tumors were excised for immunohistochemistry (see 3.18) and RNA was prepared for gene expression analysis *ex vivo* (see 3.2.2 and 3.4).

To analyze *in vivo* invasive growth, ET cells and derivatives were injected in a volume of 0.2 ml into the tail vein of immunodeficient $Rag2^{-/-}\gamma c^{-/-}$ mice using a 30-gauge needle. Mice were euthanized after four to five weeks and metastatic spread was examined in individual organs. Affected murine organs were excised and fixated with 4 % formaldehyde for immunohistochemistry (see 3.18) [152,153]. Furthermore, all apparent metastases within an organ were counted.

To examine colonization, invasion into bone tissues and osteolysis, mice were anesthetized with 500 mg/ml Novaminsulfon (Ratiopharm) and isoflurane (Abbott). A 30-gauge needle was introduced through the proximal tibia plateau and 2 x 10^5 ET cells and derivatives in a volume of 20 µl were injected into the medullary cavity [159]. Tumors and affected tissues were recovered and processed for histological analysis. Intra-tibial tumor formation was monitored by X-ray radiography.

3.18. Immunohistochemistry (IHC) of murine samples

Histological analyses were performed in cooperation with Prof. Dr. Irene Esposito and Dr. Julia Calzada-Wack (Institute of Pathology, Klinikum rechts der Isar, TU München, Germany; and Institute of Pathology, Helmholtz Center Munich, Neuherberg, Germany). Tumor samples and affected murine organs were fixed in 4 % formaldehyde and embedded in paraffin. 3 – 5 µm thick sections from all tissues were cut and stained with hematoxylin and eosin (H&E), as previously described [152,153]. To analyze apoptosis, samples were stained with Cleaved Caspase 3 antibody (see Table 6). Van Gieson staining was used to better demonstrate bone architecture. Osteoclasts were detected by tartrate-resistant acid phosphatase staining (TRAP) and the amount of TRAP-positive cells was counted in up to 20 segments to generate the average number of osteoclasts per mm^2. All sections were reviewed and interpreted by two pathologists (Prof. Dr. Irene Esposito and Dr. Julia Calzada-Wack).

3.19. Study population and immunohistochemistry (IHC) of human samples

The pilot study consists of 19 human ET samples prior to treatment with confirmed histological diagnosis (reference pathology), which were obtained from Dr. Daniel Baumhoer of the Bone Tumor Reference Center at the Institute of Pathology of the

University of Basel (University Hospital Basel, Switzerland). Pertinent clinical data of patients with respect to overall survival and tumor localization were compiled from the Institute of Pathology of the University of Basel. Informed consent was obtained from all patients and/or their legal guardians.

IHC was performed in cooperation with Prof. Dr. Irene Esposito and Dr. Katja Steiger (Institute of Pathology, Klinikum rechts der Isar, TU München, Germany; and Institute of Pathology, Helmholtz Center Munich, Neuherberg, Germany). IHC analyses of human clinical samples were done on formalin-fixed, paraffin-embedded, pre-chemotherapy primary tumors. All samples were kindly provided by Dr. Daniel Baumhoer (University Hospital Basel, Switzerland) and were collected at the Department of Pathology of the Technische Universität München for immediate IHC staining. For IHC, 4 µm sections were cut and stained manually with bright DAB (KPL immunologic, Gaithersburg, USA). The following primary antibody was used: polyclonal rabbit anti-DKK2 (1:100; PAB3570; Abnova). DKK2 immunoreactivity was scored according to signal intensity and localization observed with grade 0 = no immunoreactivity; grade 1 = low intensity, membranous; grade 2 = low intensity, cytoplasmic and grade 3 = moderate intensity, cytoplasmic, as previously described [160]. All sections were reviewed and interpreted by two pathologists (Prof. Dr. Irene Esposito and Dr. Katja Steiger).

3.20. Microarray analysis

Changes in gene expression profiles upon protein knock-down by RNA interference (see 3.5) were analyzed by microarray technology. Experiments were essentially done as previously described [152,153] in cooperation with Olivia Prazeres da Costa, M. Sc. (Expression Core Facility at the Institute for Medical Microbiology, Immunology and Hygiene of the TU München, Germany). After transient siRNA transfection of A673 and SK-N-MC (see 3.5), RNA was isolated with TRI Reagent RNA Isolation Kit (see 3.2.2), quantified spectro-photometrically and RNA quality was analyzed by 0.7 % agarose gel electrophoresis. Total RNA (200 ng) was amplified and labeled using Affymetrix GeneChip Whole Transcript Sense Target Labeling Kit according to manufacturer's protocol. cRNA was hybridized to Affymetrix Human Gene 1.0 ST arrays and microarray data were subsequently analyzed using different control tools to ensure representative, high quality data (detailed procedure is available at www.affymetrix.com). The whole data set is available at the Gene Expression Omnibus (GSE36100; [161]).

Data analyzes occurred using Affimetrix software “Microarray Suite 5.0”, independent one-sample t-test [162] and Genesis software package [163]. For the identification of differentially expressed genes significance analysis of microarrays (SAM) was used [164]. Transcripts were functionally assigned using GO-annotations (http://www.cgap.nci.nih.gov). Gene set enrichment analysis (GSEA) and pathway analyzes were performed with the GSEA tool (http://www.broad.mit.edu/gsea) [165].

3.21. Statistical analysis

Data are mean ± SEM as indicated. Differences were analyzed by unpaired two-tailed student’s t-test as indicated using Excel (Microsoft), or Prism 5 (GraphPad Software); p values < 0.05 were considered statistically significant.

4. Results

4.1. Overexpression of bone-associated genes in Ewing tumors (ETs)

To identify an ET-specific gene expression profile, 11 ET samples were analyzed in a previous study in comparison to 133 normal tissues (NT) of diverse origin using high-density DNA microarrays (EOS-Hu01) containing 35356 oligonucleotide probe sets to a query of 25194 gene clusters. This analysis revealed a specific expression signature of 38 probe sets corresponding to 37 genes that are strongly up-regulated or even specifically expressed in ETs compared to normal body atlas (NBA) [55]. Among them are five genes, namely *chondromodulin 1* (*CHM1*; previously known as *LECT1*), *dickkopf 2* (*Dickkopf, Xenopus, Homolog 2; DKK2*), *cytochrome p450, subfamily xxvib, polypeptide 1* (*CYP26B1*); *integral membrane protein 2A* (*ITM2A*) and *growth/differentiation factor 10* (*GDF10*), which are all known to be associated with bone development, formation and bone re-organization. Based on the microarray expression data, three groups of up-regulated genes could be distinguished, at which *CHM1* belongs to the group of genes with exclusive expression in ETs that are not expressed at detectable levels in any normal tissue. *CYP26B1* belongs to the second group, because it is expressed in ETs and at a lower level in many or all other tissues. The other three bone-associated genes *DKK2*, *ITM2A* and *GDF10* were expressed in ETs and a restricted number of normal tissues and can therefore be assigned to the third group. A short summary of the relevant microarray results is given in Table 16.

Table 16: Summary of bone-associated genes up-regulated in ETs

No.	GeneBank Accession No.	Name*	UniGene*	% ET**	% NBA**
5	AF050147	*LECT1*	Hs.421391	100.00	0.00
18	BE047680	*DKK2*	Hs.211869	81.82	12.78
19	AF252297	*CYP26B1*	Hs.91546	100.00	69.17
24	AA356764	*ITM2A*	Hs.17109	90.91	45.11
38	D49493	*GDF10*	Hs.2171	45.45	1.50

Extract of the summary of the microarray results published by Staege *et al.* showing the data of the five bone-associated genes out of 38 up-regulated probe sets in ETs compared to NBA [55]. * Names and UniGene numbers are according to build No. 172, released on 2004-07-17; ** Percentage of samples in the data set with intensity values of > 60.

Due to their high expression in a wide range of different ET samples (> 80 %) and simultaneously their low expression levels in only a few tissues of the NBA (< 46 %) the following genes have been carefully selected for further investigation: *CHM1*, *DKK2* and *ITM2A*. The expression profile of these three genes in ETs compared to normal and fetal tissue is shown in Figure 3.

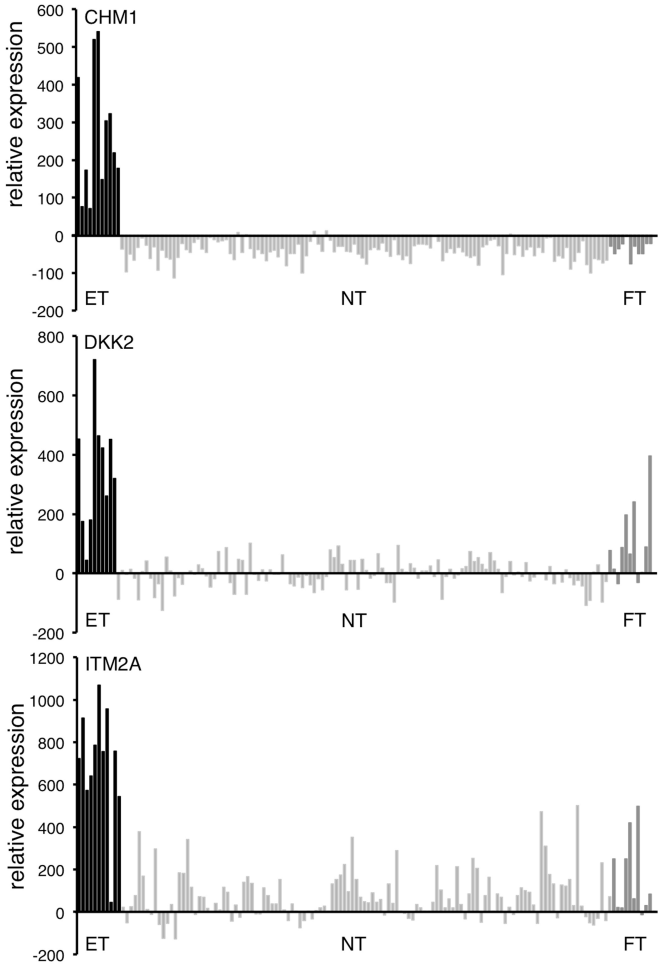

Figure 3: Bone-associated gene expression in ETs compared to normal tissue
Microarray data that show the expression profile of CHM1, DKK2 and ITM2A on mRNA level in primary ET samples (black bars) compared to normal body tissue (NT; light grey bars) and fetal tissue (FT; dark grey bars) [55].

ETs are small-round-cell tumors that stain blue on routine H&E stained sections and can be easily confused with other pediatric tumors on the histological level. To examine, whether the selected genes are exclusively overexpressed in ETs compared to other pediatric small-round-blue-cell tumors, the mRNA expression levels of CHM1, DKK2 and ITM2A were analyzed in 857 different normal tissues (GSE3526, GSE7307, [166]) compared to 154 different ET (GSE34620, GSE12102, [167,168]), 519 leukemia (GSE10609, GSE7440, GSE11877, [169–173]), 119 medulloblastoma (GSE10327,

[174]) and 169 neuroblastoma (GSE16237, GSE13136, [175,176]) samples, using a comparative study of the amc onco-genomics software tool (www.amc.com). As shown in Figure 4, CHM1 and DKK2 exhibited only a high mRNA expression level in ETs, while ITM2A was additionally overexpressed in some ALL samples.

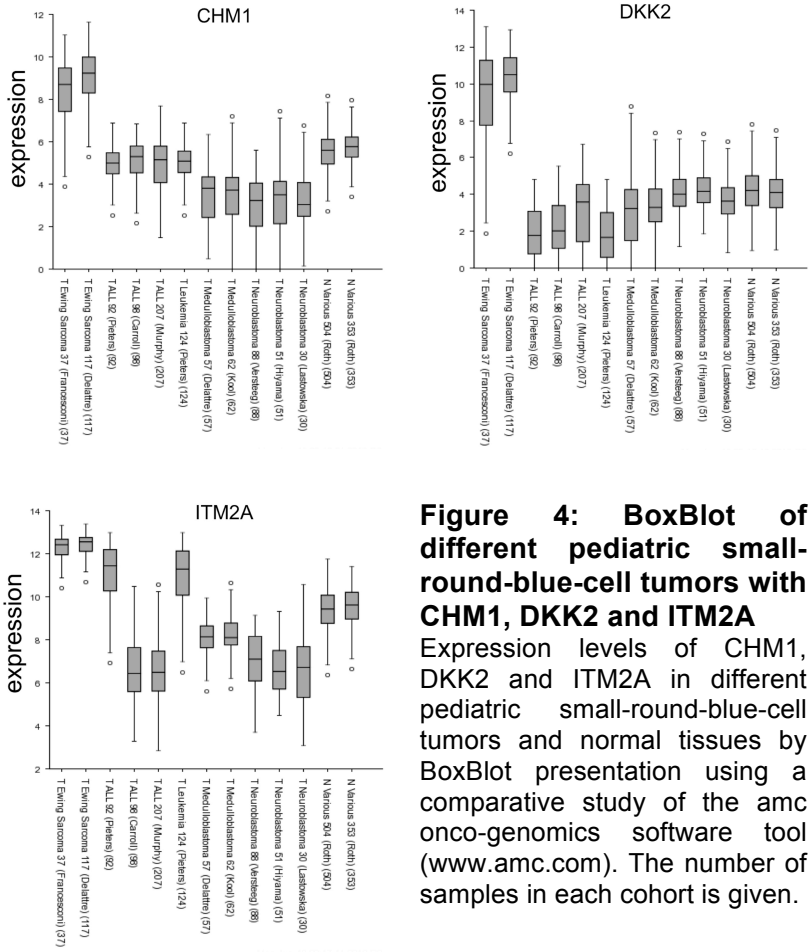

Figure 4: BoxBlot of different pediatric small-round-blue-cell tumors with CHM1, DKK2 and ITM2A
Expression levels of CHM1, DKK2 and ITM2A in different pediatric small-round-blue-cell tumors and normal tissues by BoxBlot presentation using a comparative study of the amc onco-genomics software tool (www.amc.com). The number of samples in each cohort is given.

To verify the observed expression profile for the cell lines used in this study, mRNA levels of nine different ET cell lines, four neuroblastoma and three ALL cell lines were quantified (see 3.4). Furthermore, to analyze whether CHM1, DKK2 and ITM2A play a role in other bone-associated tumors, various ET cell lines were tested against a series of different osteosarcoma cell lines, the most frequently observed bone tumor in children. As shown in Figure 5, qRT-PCR using specific gene expression assays for *CHM1*, *DKK2* and *ITM2A* (see Table 11) revealed a high mRNA expression of all three genes in ETs; especially for DKK2, which is unexceptionally expressed in all ET cell lines investigated. In the case of CHM1 and ITM2A, mRNA levels were not detected in all ET cell lines, for example not in VH-64 and SB-KMS-MJ1, which were established from bone metastases. Furthermore, as can be seen in Figure 5, CHM1 and ITM2A

were almost exclusively expressed in ETs, whereas DKK2 mRNA levels were additionally detectable in osteosarcomas, another bone-associated pediatric tumor, but not in ALLs or neuroblastomas, a histological mimic (small-round-blue cells) of ETs.

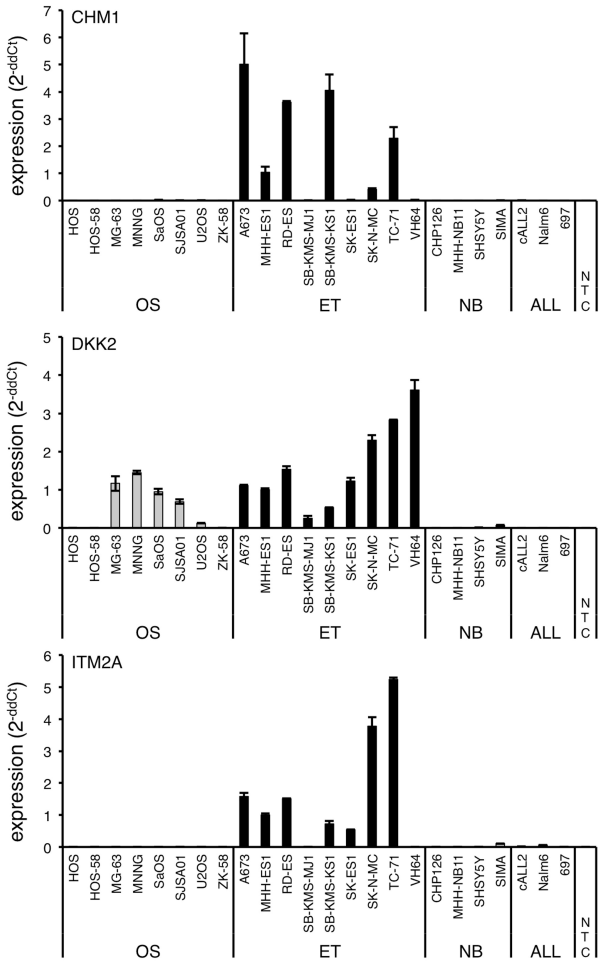

Figure 5: Gene expression in different ET cell lines compared to other pediatric tumor cell lines
Expression of CHM1, DKK2 and ITM2A on mRNA level in nine different ET cell lines (black bars) in comparison to eight osteosarcoma cell lines (OS; light grey bars), four neuroblastoma cell lines (NB; light grey bars) and three ALL cell lines (light grey bars) analyzed by qRT-PCR. NTC: non template control (H_2O). Data are mean ± SEM.

High expression of specific genes in ETs compared to NBA indicates that expression of these genes is dependent on the oncogenic fusion protein EWS-ETS, which is unexceptionally expressed in all ETs. To investigate whether *CHM1*, *DKK2* or *ITM2A* expression is induced by this transcription factor, the most frequent translocation product EWS-FLI1 was transiently knocked down in four different ET cell lines (A673, SK-N-MC, SB-KMS-KS1 and TC-71; see 3.5), which all show a high mRNA expression of the genes of interest (see Figure 5). 48 h after transient transfection with specifically designed EWS-FLI1 siRNAs [138], RNA was isolated and knock-down efficiency was

determined by qRT-PCR using specific gene expression assays for *EWS-FLI1*, *CHM1*, *DKK2* and *ITM2A* (see Table 11 and 3.4). As shown in Figure 6, EWS-FLI1_1 siRNA only suppressed EWS-FLI1 expression in A673 and SK-N-MC cells, while EWS-FLI1_2 siRNA treatment reduced EWS-FLI1 mRNA levels down to 20 – 40 % of normal values in all ET cell lines compared to control siRNA (neg.control) transfected cells. Moreover, knock-down of EWS-FLI1 with EWS-FLI1_2 siRNA reduced CHM1 mRNA expression down to 50 – 65 % compared to control cells. In contrast, transient knock-down of EWS-FLI1 by specific siRNAs did only affect DKK2 expression in A673 cells (not significant), but not in three other ET cell lines, indicating DKK2 expression in ET to be independent of EWS-FLI1. The same seems true for the regulation of ITM2A expression.

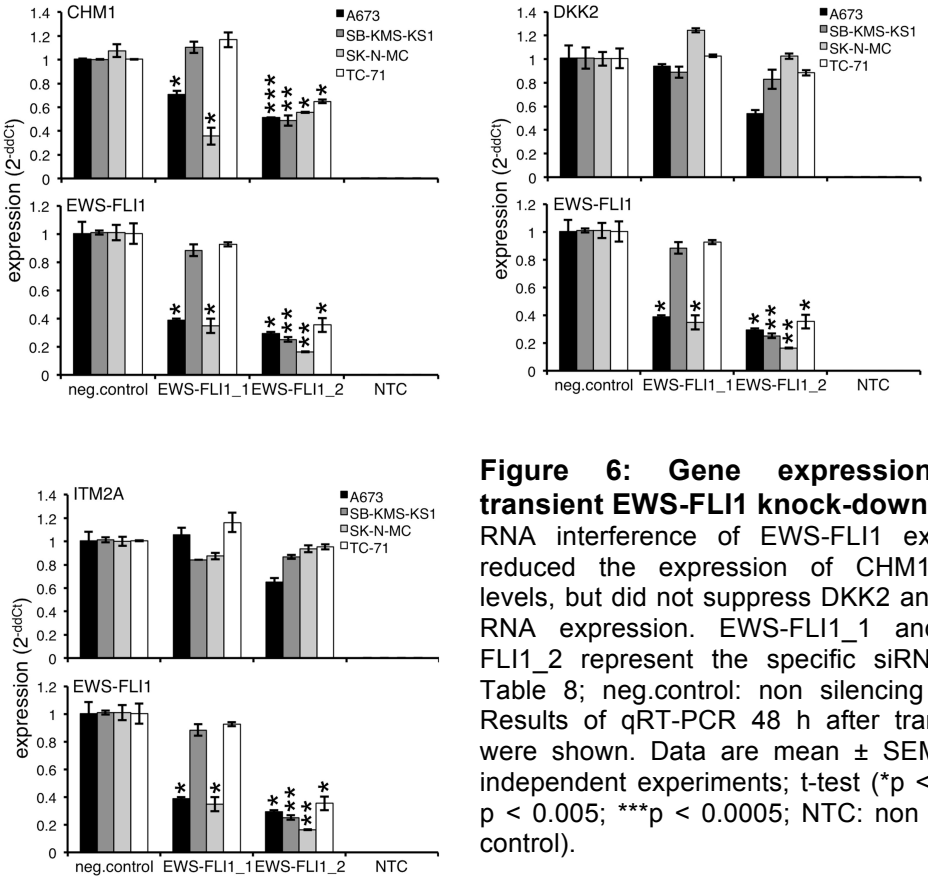

Figure 6: Gene expression after transient EWS-FLI1 knock-down
RNA interference of EWS-FLI1 expression reduced the expression of CHM1 mRNA levels, but did not suppress DKK2 and ITM2A RNA expression. EWS-FLI1_1 and EWS-FLI1_2 represent the specific siRNAs (see Table 8; neg.control: non silencing siRNA). Results of qRT-PCR 48 h after transfection were shown. Data are mean ± SEM of two independent experiments; t-test (*p < 0.05; ** p < 0.005; ***p < 0.0005; NTC: non template control).

4.2. The role of DKK2 in ET pathogenesis

To analyze the impact of DKK2 overexpression on the phenotype of ETs in several *in vitro* and *in vivo* assays, DKK2 was transiently and constitutively down-regulated in different ET cell lines (A673, SK-N-MC and TC-71). Two different siRNAs (DKK2_1 and DKK2_8) were tested in three ET cell lines by transient RNA interference (see 3.5). 72 h after transfection, RNA was isolated and qRT-PCR analyzes were performed to measure DKK2 mRNA expression (see 3.4 and Table 11). To exclude a target-mediated induction of unspecific interferon responses, mRNA expression of IFN responsive genes *ISG15* and *IFITM1* was determined by qRT-PCR, as well. As shown in Figure 7, transient transfection with DKK2_1 siRNA reduced DKK2 mRNA levels down to 60 % in A673 cells, 50 % in TC-71 cells and up to 30 % off in SK-N-MC cells. DKK2_8 siRNA treatment resulted in a down-regulation of DKK2 expression up to 20 - 35 % in A673 and SK-N-MC cells. Because DKK2 mRNA levels were clearly reduced by both siRNAs, DKK2_1 as well as DKK2_8 were used in further transient transfection experiments to exclude off-target effects.

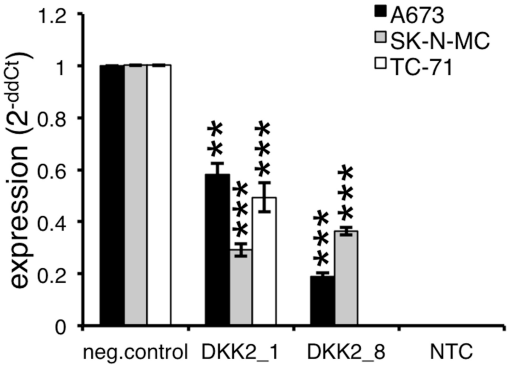

Figure 7: DKK2 expression after transient gene knock-down using qRT-PCR
Expression of DKK2 72 h after transient transfection with DKK2_1 and DKK2_8 siRNAs compared to corresponding controls, transfected with non-silencing siRNA (neg.control). Data are mean ± SEM of three independent experiments; t-test (**p < 0.005; ***p < 0.0005; NTC: non template control).

To generate ET cell lines with constitutive DKK2 knock-down, oligonucleotides encoding the target sequence of DKK2_1 siRNA were cloned into the pSIREN RetroQ vector (see 3.6). This method enabled a stable DKK2 knock-down, mediated by permanent expression of shRNAs, which induce Dicer-dependent cleavage of endogenous DKK2 mRNA. Retroviral gene transfer of the pSIREN^{DKK2} construct into three different ET cell lines resulted in a suppression of DKK2 mRNA levels down to 10 – 35 % compared to control cells, constitutively transfected with pSIREN^{negsiRNA} (see Figure 8).

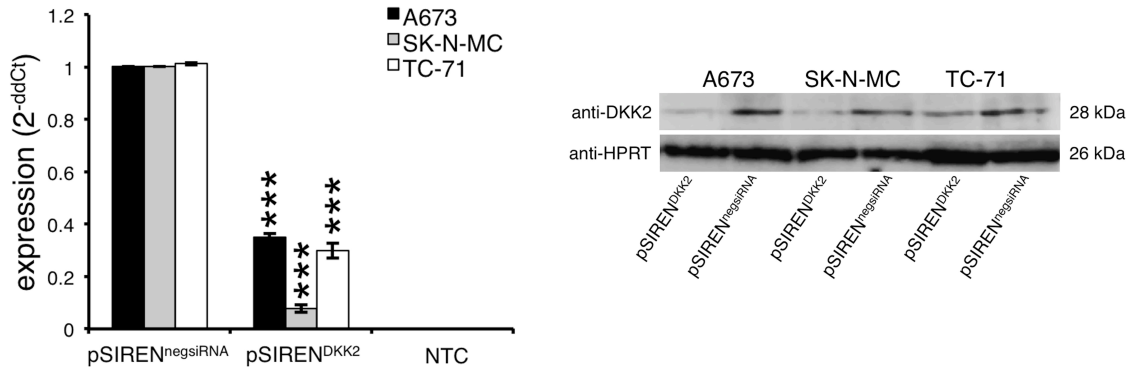

Figure 8: Quantification of DKK2 levels after constitutive DKK2 knock-down

Left panel: Constitutive suppression of DKK2 mRNA expression after infection of ET cells with DKK2 specific shRNA constructs as measured by qRT-PCR ($pSIREN^{DKK2}$, control: $pSIREN^{negsiRNA}$). Data are mean ± SEM of more than 20 independent experiments; t-test (***p < 0.0005; NTC: non template control). **Right panel:** Detection of DKK2 protein levels after constitutive DKK2 knock-down in three ET cell lines using Western blot analysis. Antibody against hypoxanthine guanine phosphoribosyltransferase (HPRT) was used as loading control.

4.2.1. DKK2 increases tumor growth and metastasis *in vitro* and *in vivo*

To examine whether DKK2 knock-down influences the phenotype of ET cells, different *in vitro* and *in vivo* assays were performed with the transiently and constitutively transfected ET cell lines A673, SK-N-MC and TC-71. Using an xCELLigence instrument, the effect of DKK2 knock-down on the proliferation of A673 and SK-N-MC cells was first analyzed (see 3.8.1). The proliferation of TC-71 cells was examined using BrdU incorporation assay (see 3.8.2), due to the semi-adherent growth behavior of these cell line.

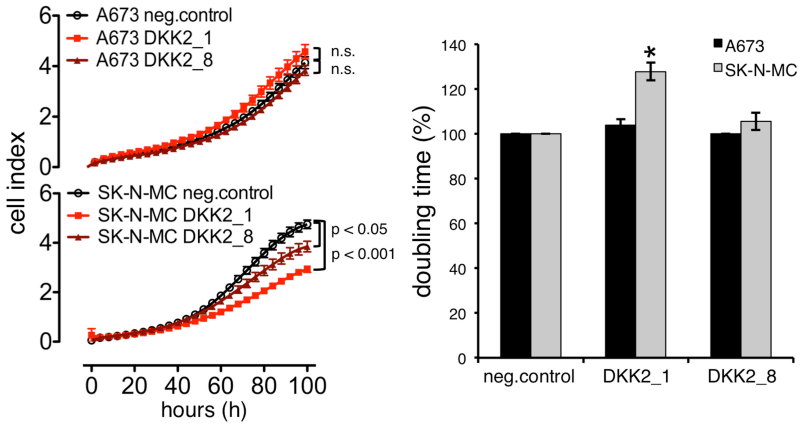

Figure 9: Proliferation assay of siRNA treated ET cell lines

Left panel: Analysis of proliferation of transiently infected ET cell lines with xCELLigence. Cellular impedance was measured every 4 h (relative cell index). Data are mean ± SEM (hexaplicates/group); t-test (p: p-value; n.s.: not significant). **Right panel:** Doubling time of A673 and SK-N-MC cells transiently infected with DKK2_1 and DKK2_8 siRNAs. Data are mean ± SEM of two independent experiments/cell line (hexaplicates/group); t-test (*p < 0.05).

Although transient DKK2 suppression had only a clear effect on the proliferation potential in SK-N-MC cells (see Figure 9), constitutive down regulation of DKK2 revealed a significant inhibition of proliferation in all ET cell lines investigated, as shown in Figure 10. In particular, the doubling time of SK-N-MC and TC-71 cells was significantly increased up to 6-fold after DKK2 suppression.

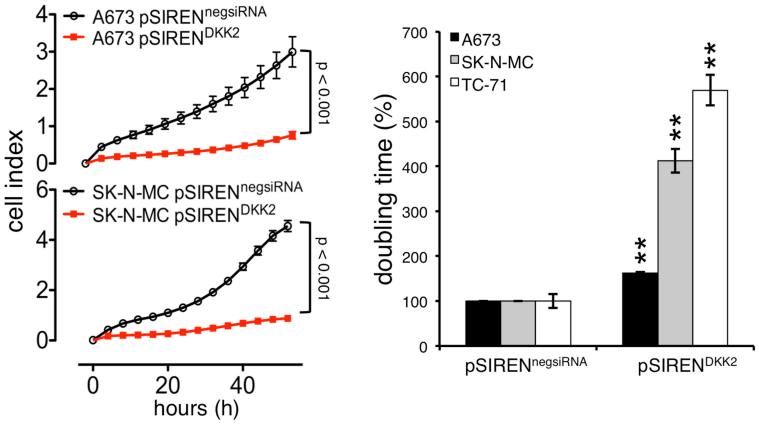

Figure 10: Proliferation assay of ET cell lines with constitutive DKK2 knock-down
Left panel: Analysis of proliferation of constitutively infected ET cell lines with xCELLigence. Cellular impedance was measured every 4 h (relative cell index). Data are mean ± SEM (hexaplicates/group); t-test (p: p-value). **Right panel:** Doubling time of constitutive A673, SK-N-MC and TC-71 DKK2 shRNA infectants and respective controls. Data are mean ± SEM of two independent experiments/cell line (hexaplicates/group); t-test (**p < 0.005).

To test whether DKK2 influences cell cycle progression, stably infected A673, SK-N-MC and TC-71 cells with reduced DKK2 expression were analyzed by flow cytometry using propidium iodide (PI), a DNA intercalating agent (see 3.10). Although proliferation of ET cells was significantly suppressed after DKK2 knock-down, no clear effect on cell cycle progression could be detected (see Figure 11). However, the rate of dead cells after DKK2 knock-down seems to be slightly higher compared to pSIREN^{negsiRNA} control cells.

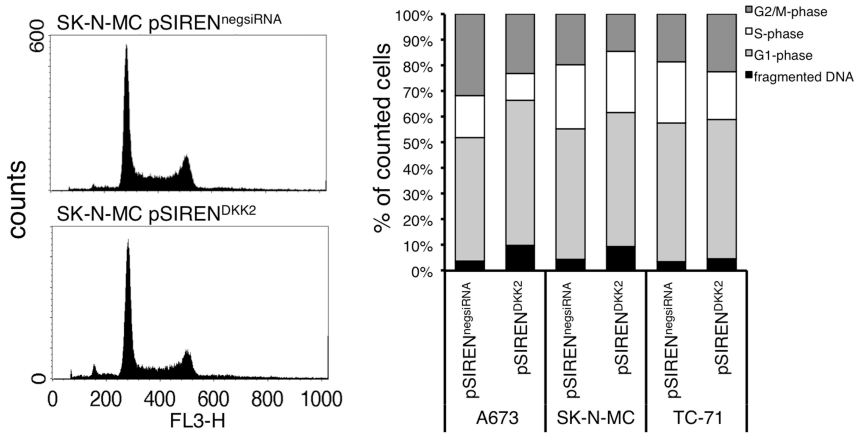

Figure 11: Cell cycle analysis of DKK2 knock-down and control cells
Left panel: Example of cell cycle progression in SK-N-MC pSIREN^{DKK2} and pSIREN^{negsiRNA} cells. **Right panel:** Summary of two independent cell cycle distribution analyses of DKK2 shRNA infectants in A673, SK-N-MC and TC-71 cells by propidium iodine staining and flow cytometry.

Contact-independent growth capacity of tumor cells *in vitro* can give a hint to the degree of malignancy of these cells *in vivo*. To determine the effect of pSIREN^{DKK2} cells on contact-independent growth capacity of ET cells *in vitro*, colony formation assays using methylcellulose-based media were performed (see 3.14). After incubation for 14 days at 37 °C (5 % CO_2) in a humidified atmosphere, culture dishes were photographed and colonies were counted using the image processing package Fiji. As shown in Figure 12, constitutive DKK2 knock-down clearly reduced colony formation in all three ET cell lines in a dose dependent manner (see Figure 8).

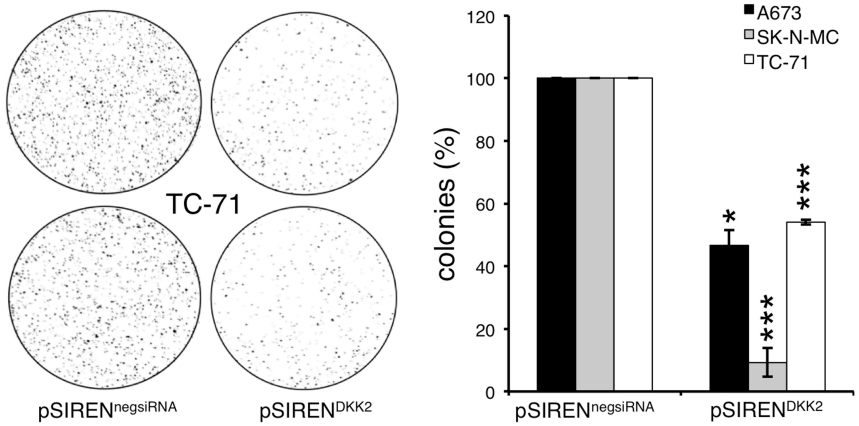

Figure 12: Colony forming assay of pSIREN^{DKK2}-infected and control cells
Analysis of anchorage-independent colony formation in methylcellulose of ET cell lines with stable DKK2 knock-down (pSIREN^{DKK2}) and respective controls (pSIREN^{negsiRNA}). **Left panel:** Macrographs show a representative experiment with TC-71. **Right panel:** Number of counted colonies using Fiji. Data are mean ± SEM of three independent experiments (duplicates/group); t-test (*$p < 0.05$; ***$p < 0.0005$).

To further examine whether the suppression of DKK2 in ETs affects tumorigenicity in *vivo*, stable pSIREN^{DKK2} A673 and SK-N-MC cells and respective controls were injected subcutaneously into the inguinal region of immunodeficient mice and tumor growth was analyzed (see 3.17). As expected, DKK2 knock-down clearly delayed local tumor growth in both ET cell lines (see Figure 13). The inhibition seemed to be dose dependent on the DKK2 expression level, since in SK-N-MC cells with stronger DKK2 suppression, determined *ex vivo* after tumor growth by qRT-PCR, revealed the most prominent delay in local tumor growth.

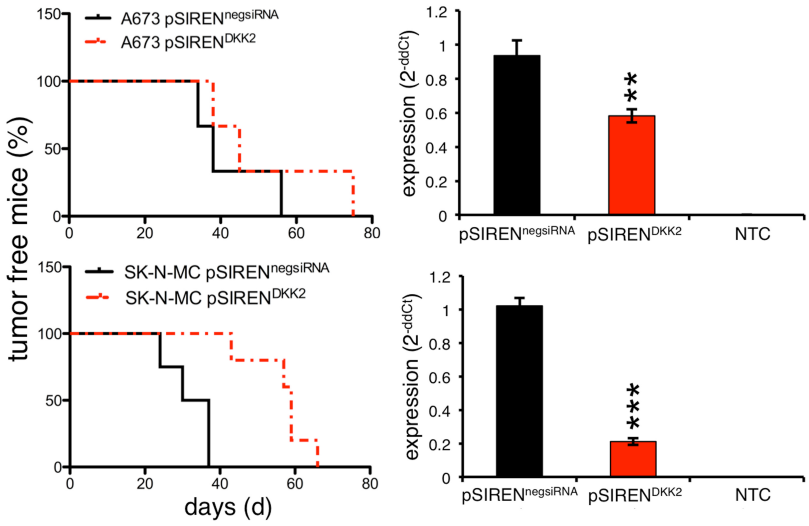

Figure 13: Kaplan-Meier blot of local tumor growth
Left panel: Evaluation of tumorigenicity of constitutive A673 and SK-N-MC DKK2 shRNA infectants in immunodeficient mice (3 - 5 mice/group). Mice with an average tumor size > 10 mm in diameter were considered as positive and sacrificed. **Right panel:** Quantification of DKK2 mRNA levels of tumor samples post *ex vivo* using qRT-PCR (**p < 0.005; ***p < 0.0005).

Furthermore, to investigate the influence of DKK2 knock-down on the metastatic behavior of ET cells, A673 or SK-N-MC cells with constitutive DKK2 knock-down and respective controls were injected into the tail veins of immune deficient Rag2$^{-/-}\gamma c^{-/-}$ mice (see 3.17). As shown in Figure 14, suppression of DKK2 significantly reduced the number of lung and liver metastases in both ET cell lines. While A673 as well as SK-N-MC control infectants (pSIREN^{negsiRNA}) colonized into the liver, A673 pSIREN^{negsiRNA} cells additionally exhibited lots of lung metastases. In contrast, pSIREN^{DKK2} infectants showed a clearly decreased amount of liver metastases and A673 cells with stable DKK2 knock-down almost completely lost their ability to metastasize into lungs. SK-N-MC pSIREN^{DKK2} infectants did not affect lung tissues as well as the respective controls. Additionally, some control infectants developed metastases in the kidney and the ovary (3/8). Surprisingly, no bone metastases were detected, even though ETs are known bone tumors. Taken together, pSIREN^{DKK2} infectants revealed a strong reduction of

overall metastatic potential by up to 94.7 % (see Table 17), suggesting a critical role of DKK2 in ET growth and metastasis.

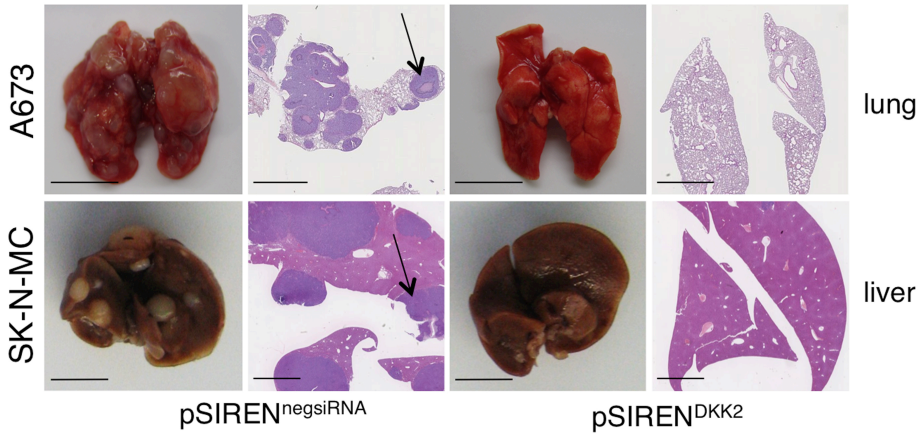

Figure 14: Affected organs after intravenous injection of pSIREN^{DKK2} and pSIREN^{negsiRNA} cells
Analysis of metastatic potential of A673 and SK-N-MC cells with stable DKK2 knock-down and controls (pSIREN^{negsiRNA}; 4 mice/group). All macroscopically visible metastases in lungs, livers, kidneys and ovaries were confirmed by histology. The left panels demonstrate lung and liver with extend metastasis (arrow) and the right panels depict lung and liver without metastasis after pSIREN^{DKK2} injection (H&E; scale bar upper panel: 5 mm or 2 mm; lower panel: 1 cm or 5 mm).

Table 17: Number of apparent metastases after DKK2 knock-down

	average number of apparent metastases per mouse			
	A673		SK-N-MC	
	pSIREN^{negsiRNA}	pSIREN^{DKK2}	pSIREN^{negsiRNA}	pSIREN^{DKK2}
liver	3	1	33	2
lung	95	3	0	0
kidney	0	0	2	0
ovary	1	0	0	0
summary	99	4	35	2

Analysis of metastatic potential of A673 and SK-N-MC cells with stable DKK2 knock-down and controls (pSIREN^{negsiRNA}; 4 mice/group). All macroscopically visible metastases in lungs, livers, kidneys and ovaries were counted and an average number of apparent metastases per mouse is shown. Decimal numbers will be rounded up.

4.2.2. DKK2 knock-down inhibits invasiveness regulated by MMP1 *in vitro*

To identify possible DKK2 downstream targets that are presumably involved in metastasis, DKK2 was transiently down-regulated in A673 and SK-N-MC cells (see Figure 7) and their expression pattern was compared to pSIREN^{negsiRNA} cells in a microarray analysis on human Gene ST arrays (Affymetrix, GSE36100). Considering a

minimum linear fold change > ±1.5 281 differentially regulated genes of which 207 genes were down-regulated after DKK2 knock-down were identified (see Figure 15).

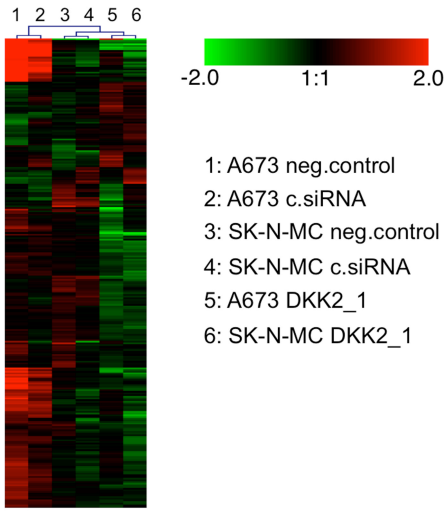

Figure 15: Microarray data of transiently DKK2 siRNA transfected cells
Microarray data of selected genes after transient DKK2 knock-down (GSE36100) in A673 and SK-N-MC cells. Each column represents one individual array. Panel shows the first most significant genes of the SAM analysis identified by a fold change > ±1.5 and a t-test p-value > 0.05 (c.siRNA: control siRNA).

Differential expression of five of these genes, which all have been reported to be involved in cellular invasiveness and migration, was confirmed by qRT-PCR in ET cells after constitutive DKK2 knock-down (see Figure 8 and Figure 16). The only up-regulated gene of these five genes is the key cell-cell adhesion molecule *E-Cadherin* (*CDH1*), which is a well-established antagonist of invasion and metastasis [177–179]. The four down-regulated genes are the integral cell membrane glycoprotein *CD44*, which has a postulated role in matrix adhesion and migration [180–182], the *cellular adhesion molecule 1* (*ICAM1*), which is important for endothelial transmigration into tissues [183–185], and the matrix metalloproteinases *MMP1* and *MMP7*, both of which are zinc-dependent endopeptidases with crucial roles in migration and invasion [186–191].

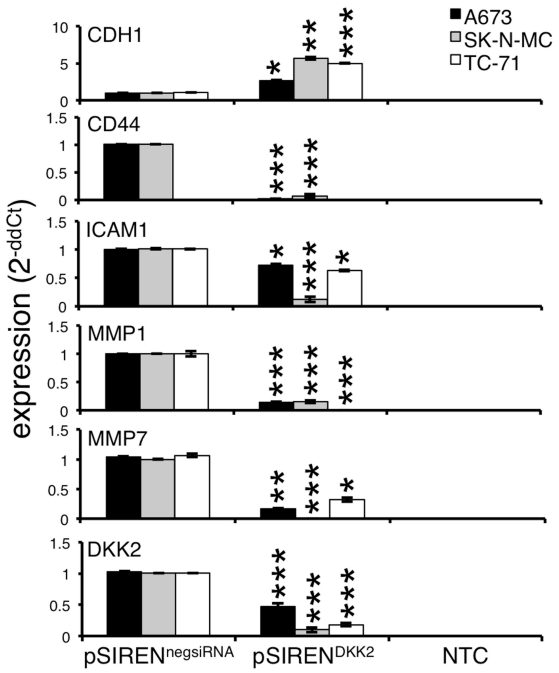

Figure 16: Verification of microarray data by qRT-PCR
Confirmation of the array results for selected genes presumably influencing invasiveness with constitutive DKK2 knock-down infectants using qRT-PCR. *CDH1*: *E-Cadherin*; *CD44*: *CD44 antigen*; *ICAM1*: *intercellular adhesion molecule 1*; *MMP1*: *matrix metalloproteinase 1*; *MMP7*: *matrix metalloproteinase 7*; *DKK2*: *dickkopf 2*; NTC: non template control. Data are mean ± SEM of three independent experiments; t-test (*p < 0.05; **p < 0.005; ***p < 0.0005).

To further elucidate the basis of the observed metastatic phenotype of ET cells after DKK2 knock-down, *in vitro* analyses of invasive growth were performed. In this context, stably DKK2 silenced ET cells showed significantly reduced invasiveness when subjected to Matrigel-covered transwell assays (BioCoat^{TM} Angiogenesis System) (see 3.15 and Figure 17). As previously reported MMPs seems to be important for ET invasiveness [153]. Therefore, the invasiveness of A673 and SK-N-MC cells after treatment with 3 nM or 6 nM Batimastat (BB-94), a specific MMP inhibitor, was examined. As expected, treatment with BB-94 prominently reduced the amount of tumor cells crossing the Matrigel (see Figure 17). To get more information about the precise mechanism, MMP1 or MMP7, each with two different specific siRNAs, were transiently knocked down (see supplementary Figure 58). As shown in Figure 17, only knock-down of MMP1, but not of MMP7, reduced invasiveness of ET cells, suggesting that the reduced invasive potential of DKK2 silenced ET cells is mediated - at least in part - via MMP1.

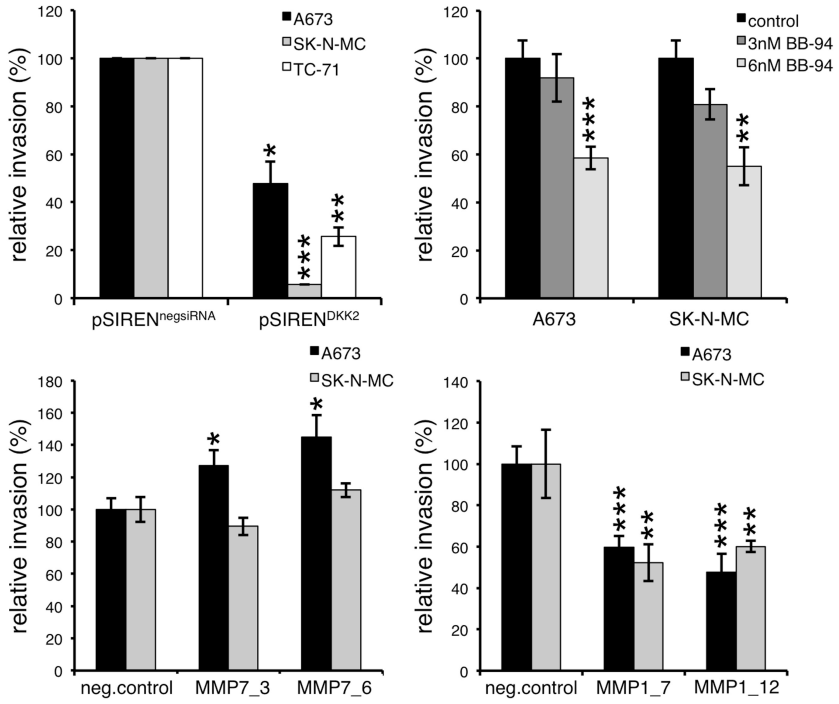

Figure 17: Analyses of invasion of ET cell lines through Matrigel
Upper left panel: Analysis of invasiveness of ET cell lines through Matrigel after transfection with specific DKK2 shRNA constructs. Data are mean ± SEM of two independent experiments; t-test. **Upper right panel:** Analysis of invasiveness of A673 and SK-N-MC cell lines treated with 3 or 6 nM of the MMP-inhibitor Batimastat (BB-94) or vehicle. Data are mean ± SEM of two independent experiments; t-test. **Lower panel:** Invasiveness of A673 and SK-N-MC cells after transfection with two specific MMP1 (**right**) or MMP7 (**left**) siRNAs 48 h before seeding. Data are mean ± SEM; t-test (*$p < 0.05$; **$p < 0.005$; ***$p < 0.0005$).

To analyze their contribution to cell invasion and migration, the expression of a series of integrin and adhesion molecules were tested in different ET cell lines after constitutive DKK2 knock-down using flow-cytometric analysis (see 3.11 and Table 7), but no influence of DKK2 was found (see Table 18).

Table 18: Flow-cytometric analysis of integrin and adhesion molecule expression after DKK2 knock-down

Integrin / adhesion molecule		A673		SK-N-MC		TC-71	
		pSIREN^{negsiRNA}	pSIREN^{DKK2}	pSIREN^{negsiRNA}	pSIREN^{DKK2}	pSIREN^{negsiRNA}	pSIREN^{DKK2}
CD29	**β1**	++	++	++	++	++	++
CD49a	**α1**	(+)	(+)	-	-	(+)	(+)
CD49b	**α2**	(+)	(+)	-	-	(+)	(+)
CD49c	**α3**	-	-	-	-	-	-
CD49d	**α4**	-	-	-	-	+	+
CD49e	**α5**	++	++	++	++	++	++
CD49f	**α6**	+	+	-	-	(+)	(+)

Expression of a series of integrin and adhesion molecules in different ET cell lines after constitutive DKK2 suppression using flow-cytometric analysis. Semi-quantitative evaluation: – = no, (+) = faint, + = moderate, and ++ strong expression.

4.2.3. DKK2 seems to be a Wnt agonist in ETs

Members of the dickkopf family are secreted proteins that typically antagonize Wnt/β-catenin signaling. While DKK1 acts as a pure inhibitor of Wnt/β-catenin signaling, DKK2 can either function as a Wnt agonist or antagonist, depending on the cellular context [71], whereas the role in ETs has still not been resolved. Interestingly, three of the genes identified by previous microarray analysis, which are involved in invasiveness and metastasis, are well known Wnt target genes, too. As previously described, expression of CDH1 is down-regulated [192,193] and expression of CD44 and MMP7 is up-regulated after activation of the Wnt/β-catenin pathway [194–196]. Suppression of DKK2 significantly enhanced the expression level of CDH1 and suppressed the mRNA levels of the other two genes in different ET cell lines, as shown in this study (see Figure 16). The observed expression profile point out that DKK2 may activate this important pathway. To further examine these findings, expression of five additional Wnt target genes were analyzed in stably pSIREN^{DKK2}- and pSIREN^{negsiRNA}-infected A673, SK-N-MC and TC-71 cells. *Cyclin D1* (*CCND1* [109,110]), *ephrin receptor EphB2* (*EPHB2* [111]), *inhibitor of dna binding 2* (*ID2,* [197,198]) as well as *jun proto-oncogene* (*c-JUN,* [199]) and *lymphoid enhancer-binding factor 1* (*LEF1,* [200,201]) are all Wnt target genes, which are up-regulated after pathway activation. As shown in Figure 18, expression levels of all genes investigated were suppressed after DKK2 knock-down, supporting the assumption of the agonistic function of DKK2.

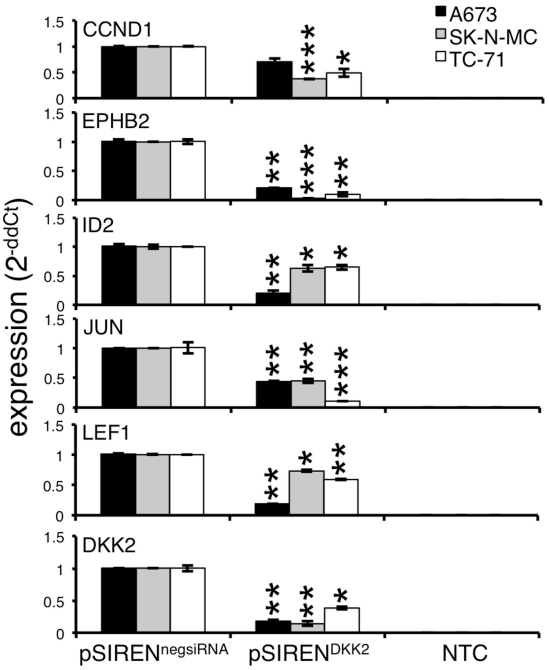

Figure 18: Expression of Wnt target genes after DKK2 knock-down
Expression of the Wnt target genes *CCND1*: *cyclin D1, EPHB2*: *ephrin receptor B2*; *ID2: inhibitor of dna binding 2*; *JUN*: *jun proto-oncogene*; *LEF1*: *lymphoid enhancer-binding factor 1* after DKK2 knock-down using qRT-PCR. DKK2 expression levels as control. NTC: non template control. Data are mean ± SEM of three independent experiments; t-test (*p < 0.05; **p < 0.005; ***p < 0.0005).

As summarized in a review by Christof Niehrs [71], the precise cellular function of secreted DKK2 in respect to Wnt/β-catenin signaling is depending on the cellular context and the expressed amount of its binding partner low density lipoprotein receptor-related protein 6 (LRP6) [71,80,81] and its cofactor Kremen 2 (KRM2) [82,83]. DKK2 can bind to LRP6, if this protein is present in sufficient quantities, and induces a conformation where the auto-inhibition of the extracellular domain of LRP6 is blocked, leading to receptor activation. However, in the presence of KRM2, the receptor complex (DKK2-LRP6-KRM2) may be internalized by endocytosis and thus Wnt/β-catenin signaling is inhibited [71]. Whole cell lysates of different ET cell lines constitutively transfected with pSIREN^{DKK2} or pSIREN^{negsiRNA} were prepared for Western blot analysis and proteins were separated using 10 % SDS-PAGE (see 3.12). Specific antibodies against LRP6, KRM1 and KRM2 were used to identify available protein levels on PVDF membranes (see Table 5), to obtain more information on the function of DKK2. As shown in Figure 19, pSIREN^{negsiRNA}-transfected ET cell lines expressed high LRP6 protein levels, while DKK2 knock-down decreased the amount of LRP6 in A673, SK-N-MC and TC-71. In contrast, expression of KRM1 and KRM2 revealed no differences between DKK2 knock-down and control cells (see Figure 19). Importantly, protein expression of KRM2 in ET cell lines was very low, which emphasizes the agonistic role of DKK2 in Wnt signaling.

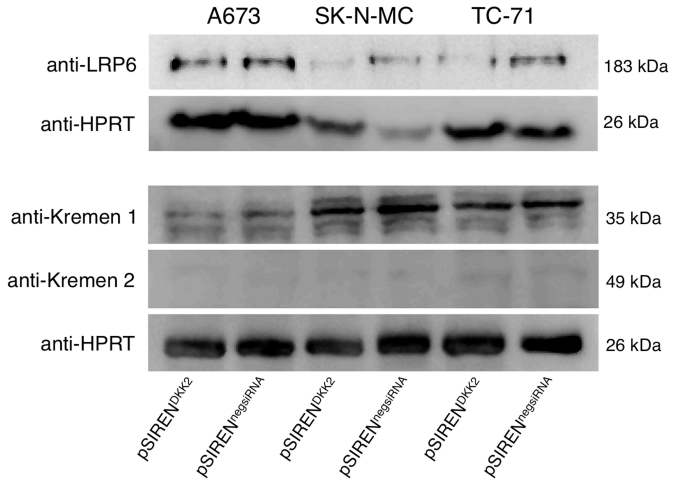

Figure 19: Analysis of LRP6 and KRM1/2 upon DKK2 suppression in ET cell lines
Protein expression of LRP6, KRM1 and KRM2 was examined in different ET cell lines by Western blot analysis after DKK2 knock-down and in respective controls. HPRT was used as loading control.

Considering that DKK2 activates Wnt/β-catenin signaling, protein levels of β-catenin should be higher in pSIREN^{negsiRNA}-transfected ET cell lines compared to cells stably transfected with DKK2 shRNA. The reason for that is that β-catenin would not be degraded but accumulates in the cytoplasma and would then be transported into the nucleus. β-catenin localization was first tested in whole cells by immunofluorescence using specific antibodies (see 3.13 and Table 6). Due to the low magnification, localization of β-catenin was only detectable in the cytoplasma, as exemplarily shown for SK-N-MC cells in Figure 20. But as expected, suppression of DKK2 slightly diminished β-catenin levels in the cytoplasma (see Figure 20).

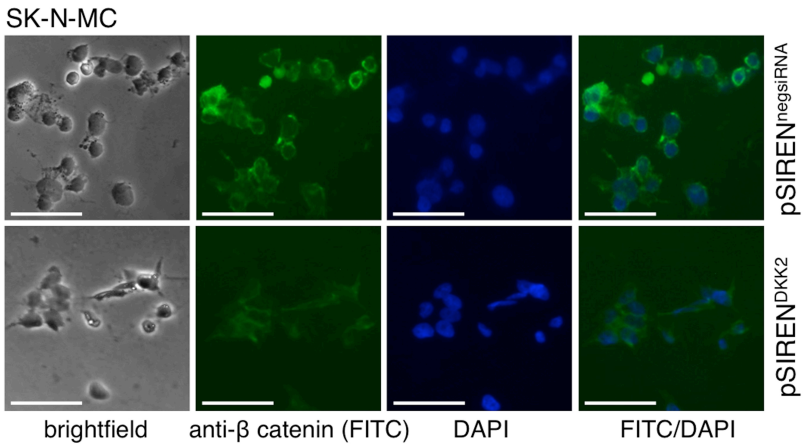

Figure 20: Detection of β-catenin in ET cell lines by IF
Phase contrast and fluorescence microscopy (FITC, DAPI and overlay FITC/DAPI) of stably transfected pSIREN^{DKK2} and pSIREN^{negsiRNA} SK-N-MC cells incubated with a specific anti-β-catenin antibody using IF. Similar results were obtained for A673 and TC-71 (scale bar 0.5 mm).

To get more information about the β-catenin levels in the nucleus, nuclear extracts from different ET cell lines with constitutive DKK2 knock-down and respective controls were analyzed by Western blot analysis (see 3.12 and Table 5). The amount of β-catenin was reduced after DKK2 knock-down not only in the cytoplasma, but also in the nucleus, as can be seen in Figure 21.

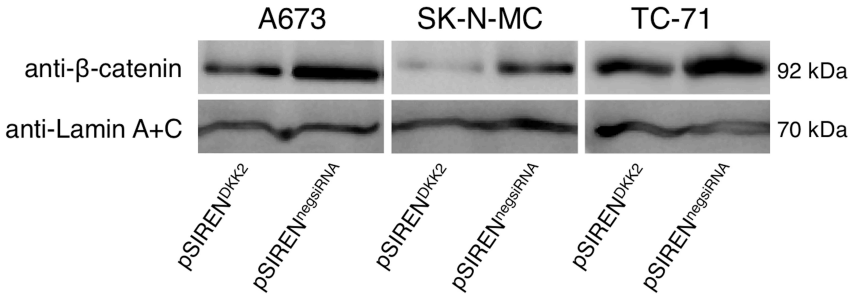

Figure 21: Detection of β-catenin in the nucleus of different ET cell lines after DKK2 knock-down
Detection of β-catenin in the nuclear extract of A673, SK-N-MC and TC-71 cells stably transfected with DKK2 shRNA and respective controls by Western blot analysis. Anti-Lamin A+C was used as loading control.

In summary, the available results allow the conclusion, that DKK2 is an agonist of Wnt/β-catenin signaling and probably activates the pathway via an interaction of DKK2 and LRP6 in the absence of KRM2.

4.2.4. DKK2 down-regulation increases apoptosis *in vitro* and *in vivo*

Subsequent gene set enrichment analysis (GSEA) of our microarray data identified 75 differentially regulated gene sets (NES < -1.54 or NES > 1.30), that belong to one of the three ontologies: molecular function, cellular component or biological processes (C5: GO gene sets, v3.0; [202]).

Set-to-set analysis of leading edge top ranked down-regulated gene sets (C5_all, v3.0) revealed a strong over-representation of gene sets involved in anti-apoptotic pathways (see Figure 22).

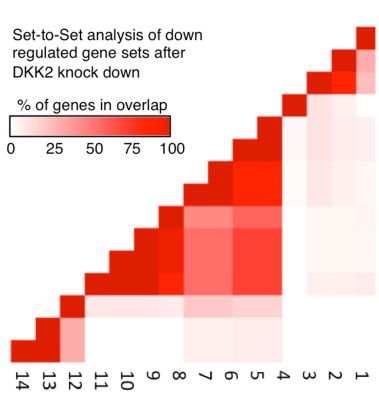

	pathway name	NES	p
1	mitotic cell cycle checkpoint	-1.70	0.01
2	DNA damage checkpoint	-1.60	0.02
3	DNA damage response signal transduction	-1.61	0.02
4	regulation of programmed cell death	-1.57	0.00
5	regulation of apoptosis	-1.56	0.00
6	apoptosis	-1.56	0.00
7	programmes cell death	-1.56	0.00
8	anti apoptosis	-1.58	0.01
9	negative regulation of apoptosis	-1.63	0.00
10	negative regulation of programmed cell death	-1.63	0.00
11	negative regulation of developmental process	-1.53	0.01
12	apoptotic program	-1.77	0.00
13	caspase activation	-1.57	0.04
14	positive regulation of caspase activity	-1.54	0.04

Figure 22: GSEA leading edge analysis of gene sets down-regulated after transient DKK2 knock-down
GSEA leading edge analysis of gene sets down-regulated after transient DKK2 knock-down (GSEA; C5_all, GO gene sets). Set-to-set analysis shows a correlation between DKK2 knock-down and down-regulation of anti-apoptotic genes (NES: normalized enrichment score; p: p-value).

To verify these findings, gene expression of two genes, which are part of the down-regulated gene sets, were analyzed in different ET cell lines with constitutive DKK2 knock-down by qRT-PCR (see 3.4). Both genes investigated belong to the BCL2-familiy (B-cell cll/lymphoma 2) of anti-apoptotic proteins: *bcl2-like 1* (*BCL2L1,* [203–205]) and *myeloid cell leukemia sequence 1* (*MCL1*, [206]). As expected, expression levels of the anti-apoptotic genes are significantly reduced after DKK2 knock-down when compared to control cells (pSIREN^{negsiRNA}; see Figure 23).

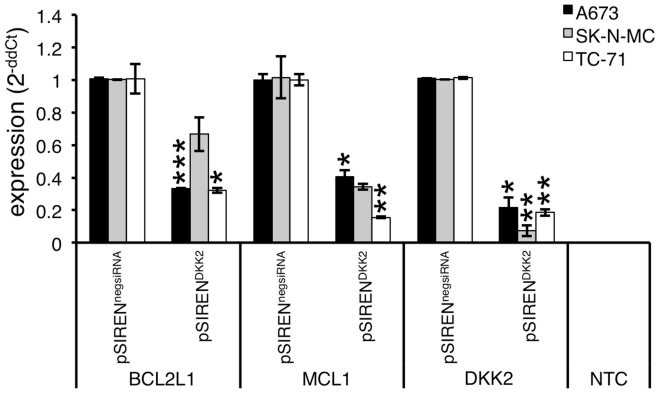

Figure 23: Expression of anti-apoptotic genes after DKK2 knock-down by qRT-PCR
qRT-PCR of ET cell lines with stable DKK2 knock-down (pSIREN^{DKK2}; control: pSIREN^{negsiRNA}). *BCL2L1: B-cell cll/lymphoma 2-like 1; MCL1: myeloid cell leukemia sequence 1; DKK2: dickkopf 2*; NTC: non template control. Data are mean ± SEM of two independent experiments; t-test (*p < 0.05; **p < 0.005; ***p < 0.0005).

In Figure 11, a slightly higher rate of dead cells after DKK2 knock-down (sub-G1 fraction) could be observed. To further examine this observation, the number of apoptotic and necrotic cells were determined using the Annexin V-PE Apoptosis Detection Kit I (see 3.9). While control cells had only between 2 and 5 % of apoptotic cells, constitutively transfected pSIREN^{DKK2} cells showed up to a 3.5-fold higher rate of apoptosis (10 - 20 % of apoptotic cells) especially in SK-N-MC and TC-71 cells (see Figure 24).

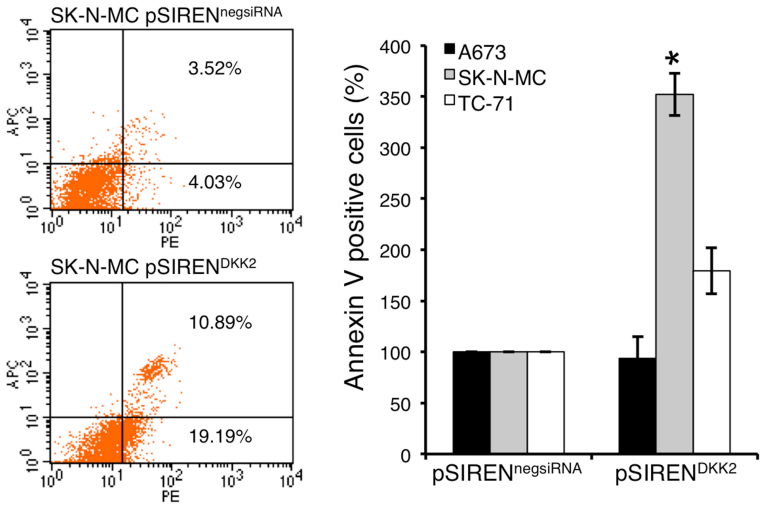

Figure 24: Annexin V detection assay with DKK2 knock-down and control cells
Results of flow-cytometric analysis of ET cell lines stably transfected with DKK2 shRNA and stained with anti-annexin-V-antibody (PE) and 7-AAD (APC). **Left panel**: Representative histogram of SK-N-MC derivatives. **Right panel**: Annexin V positive cells (%) in three ET cell lines after DKK2 knock-down and respective controls. Data are mean ± SEM of two independent experiments; t-test (*p < 0.05).

To analyze whether this effect is also detectable in *in vivo* tumor samples, various murine lung and liver metastases (see 4.2.1 and Figure 14) were stained with anti-cleaved Caspase 3 antibody to detect apoptosis (see Table 6). As demonstrated in Figure 25, knock-down of DKK2 clearly enhanced the amount of apoptotic cells, especially in samples injected with SK-N-MC pSIREN^{DKK2} cells, which is in line with the *in vitro* findings.

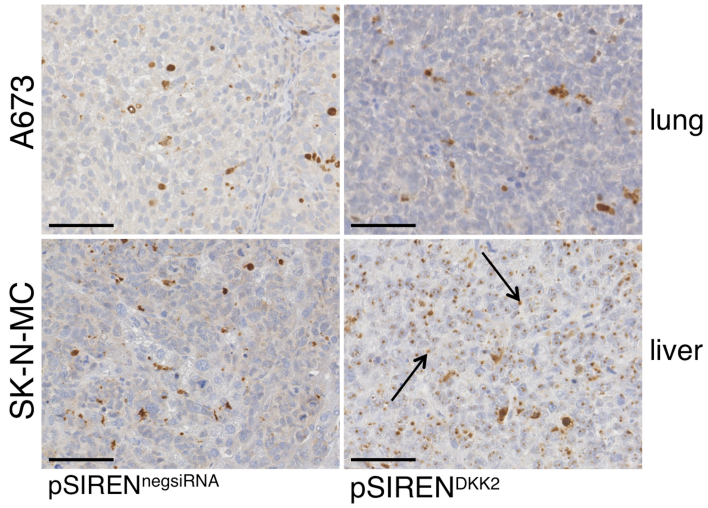

Figure 25: Cleaved Caspase 3 staining in murine tumor samples
Detection of apoptosis in murine lung and liver tumor samples after intravenous injection of different ET cell line derivatives (pSIREN^{negsiRNA} and pSIREN^{DKK2}) using anti-cleaved Caspase 3 antibody (scale bar 0.05 mm).

4.2.5. DKK2 knock-down increases neuronal differentiation *in vitro*

Moreover, the set-to-set analysis of the up-regulated gene sets (C5_all, v3.0) revealed a strong over-representation of gene sets involved in neuronal differentiation and development (see Figure 26).

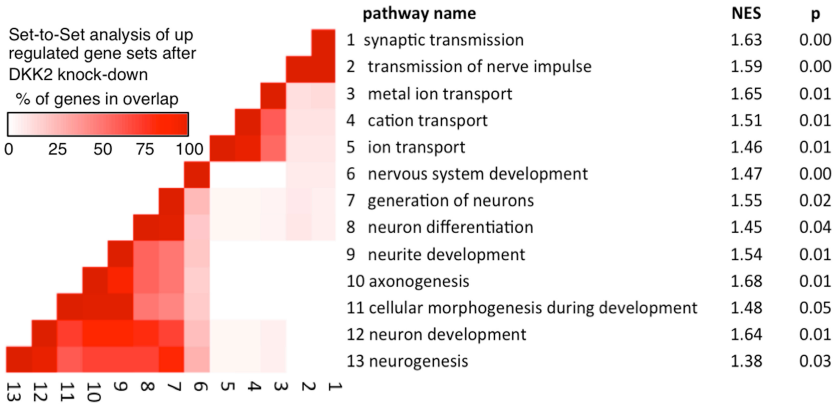

	pathway name	NES	p
1	synaptic transmission	1.63	0.00
2	transmission of nerve impulse	1.59	0.00
3	metal ion transport	1.65	0.01
4	cation transport	1.51	0.01
5	ion transport	1.46	0.01
6	nervous system development	1.47	0.00
7	generation of neurons	1.55	0.02
8	neuron differentiation	1.45	0.04
9	neurite development	1.54	0.01
10	axonogenesis	1.68	0.01
11	cellular morphogenesis during development	1.48	0.05
12	neuron development	1.64	0.01
13	neurogenesis	1.38	0.03

Figure 26: GSEA leading edge analysis of gene sets up-regulated after transient DKK2 knock-down
GSEA leading edge analysis of identified gene sets up-regulated by transient DKK2 knock-down (GSEA; C5_all, GO gene sets). Set-to-set analysis shows a correlation between DKK2 knock-down and up-regulation of neuronal differentiation genes (NES: normalized enrichment score; p: p-value).

To verify this prediction, expression of three leading edge genes, which are all involved in neurogenesis, were examined, namely *glial fibrillary acidic protein* (*GFAP,*

[207,208]), *nerve growth factor receptor* (*NGFR,* [209–211]) and *slit, drosophila, homolog of, 2* (*SLIT2,* [212–214]) using qRT-PCR. As can be seen in Figure 27, suppression of DKK2 significantly enhanced the expression levels of all three genes investigated in at least two ET cell lines.

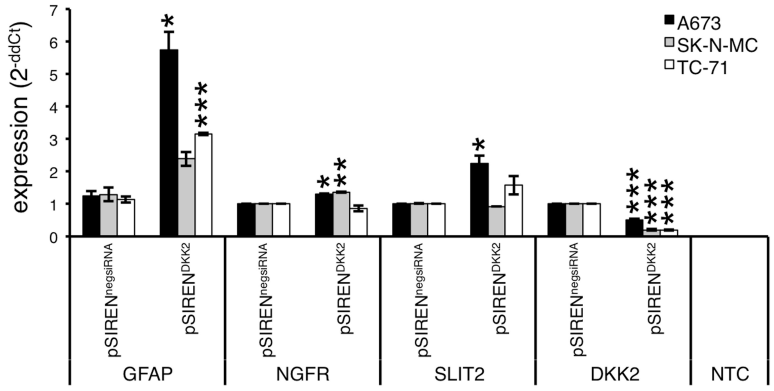

Figure 27: Expression of neurogenic genes in pSIREN^{DKK2} and pSIREN^{negsiRNA} cells
qRT-PCR of different neuronal marker genes after stable DKK2 knock-down. *GFAP*: *glial fibrillary acidic protein*; *NGFR*: *nerve growth factor receptor*; *SLIT2*: *SLIT, drosophila, homolog of, 2*; *DKK2*: *dickkopf 2*; NTC: non template control. Data are mean ± SEM of two independent experiments; t-test (*p < 0.05; **p < 0.005; ***p < 0.0005).

Subsequently, neurogenic differentiation with 0.1 mM BHA in 2 % DMSO [156] was induced in stable A673, SK-N-MC and TC-71 DKK2 shRNA infectants and respective controls. As shown in Figure 28 (left panel), ET cell lines were able to fully differentiate and express GFAP, a major intermediate filament protein of mature astrocytes [208], only after DKK2 suppression. Additionally, only the phenotype of pSIREN^{DKK2} transfected cells changed toward neuronal morphology upon BHA / DMSO treatment, as demonstrated by 1 – 2 times longer cell fibers. Similarly growth-associated protein 43 (GAP43), a protein exclusively expressed on the synaptosomal membrane of nerve tissues [215,216], is significantly higher expressed in ET cells after DKK2 knock-down (see Figure 28, right panel), indicating that DKK2 inhibits the neuronal differentiation potential of ET cells.

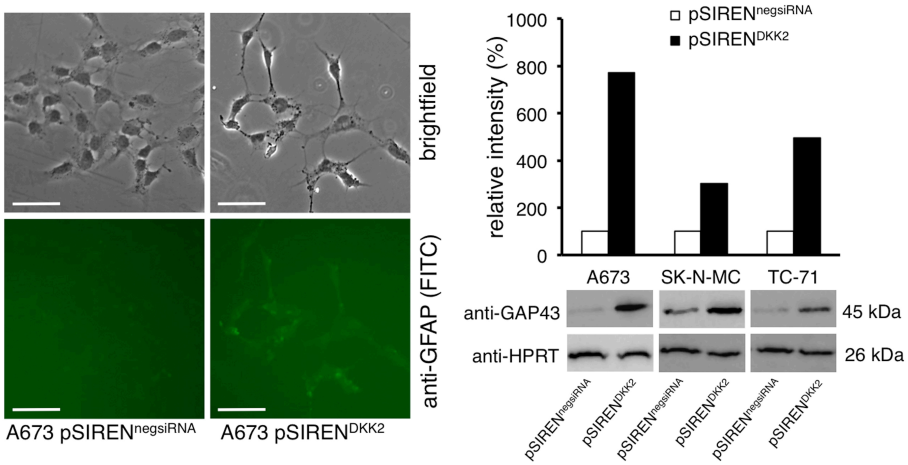

Figure 28: Quantification of neurogenic differentiation potential using IF and WB
Left panel: Analysis of neurogenic differentiation of stable A673 infectants pSIREN^{DKK2} and pSIREN^{negsiRNA} treated for 6 days with 0.1 mM BHA. Immunofluorescent staining of GFAP (GFAP: glial fibrillary acidic protein) is shown (scale bar 0.5 mm). Similar results have been obtained with SK-N-MC and TC-71 (data not shown). **Right panel:** Evaluation of the differentiation potential after neurogenic differentiation of ET cell lines constitutively transfected with DKK2 shRNA treated for 6 days with 0.1 mM BHA shown by Western blot analysis with anti-GAP43 antibody (GAP43: growth-associated protein 43) and corresponding densitometrie. HPRT was used as loading control.

4.2.6. DKK2 has no effect on angiogenesis *in vitro*

To further investigate whether DKK2 can influence the differentiation potential of ETs towards other tissues or lineages, several differentiation assays were performed. As Min *et al.* already demonstrated that DKK2 promotes angiogenesis [217], the endothelial differentiation capacity of ET cells was first examined in tube formation assays (see 3.16.1). Transiently and constitutively DKK2 or control siRNA / shRNA transfected SK-N-MC and RD-ES cells were seeded onto Matrigel matrix, containing laminin, collagen IV and different growth factors and the ability of ET cell lines to form tube-like structures was analyzed by fluorescence microscopy [155]. Control and DKK2 transfected SK-N-MC cells were unable to form tubes on Matrigel, as demonstrated in Figure 29. In contrast, RD-ES cells had the ability to form endothelial tubes, but there was no difference between cells with/without DKK2 knock-down (see Figure 29).

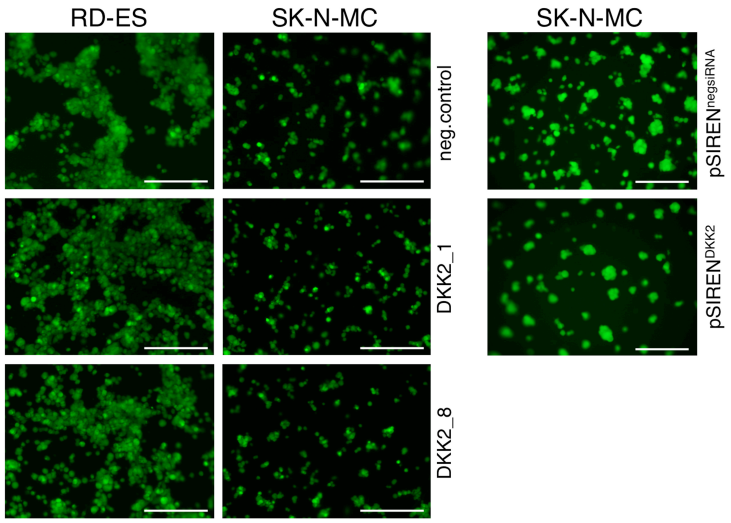

Figure 29: Tube formation assay of DKK2 suppressed ET cell lines
Left panel: To analyze endothelial differentiation potential of ET cells, transiently DKK2 transfected SK-N-MC and RD-ES cells were grown on Matrigel and stained with 4 µg/ml Calcein AM (scale bar 0.5 mm). **Right panel:** SK-N-MC cells with constitutive DKK2 knock-down were also analyzed by tube forming assay to learn more about the ability to differentiate into the endothelial lineage (scale bar 1 mm).

4.2.7. DKK2 enhances chondrogenic and osteogenic differentiation potential *in vitro*

Moreover, given that DKK2 is also implicated in terminal osteoblast differentiation [85,87] and osteoclastogenesis [77,85], the ability of ET cells to differentiate along bone lineages was subsequently analyzed. This might also be relevant for tumor pathology, since osteomimicry is an important factor for tumor localization in bone [188] and furthermore, 37 % of ET patients show increased intra-osseous density or diffuse sclerosis [218]. To further investigate these findings, three ET cell lines with constitutive DKK2 knock-down and respective controls were incubated with specific differentiation media containing among others dexamethasone and ascorbic acid in different concentrations for up to 21 days to induce chondrogenic or osteogenic differentiation (see 3.16.3 and 3.16.4). The differentiation potential of ET cell lines was determined by qRT-PCR using specific marker genes [157], namely the early chondrogenic marker gene *sry-box 9* (*SOX9,* [219]) and *collagen, type X, alpha-1* (*COL10A1*), which is used to identify terminally differentiated chondrocytes, for chondrogenic and *collagen, Type I, alpha-1* (*COL1A1*) and *secreted phosphoprotein 1* (*OPN,* [220]) for osteogenic differentiation. Interestingly, mRNA levels of all four marker genes investigated were significantly reduced after DKK2 knock-down already without specific differentiation media (see Figure 30). In agreement with these initial observations, induction of

chondrogenic and osteogenic differentiation with specific growth media was clearly impaired in DKK2 knock-down cells. Consistently, the expression increase of SOX9 and COL10A1 [157] after differentiation is reduced in DKK2 silenced cells for up to 22 % compared to control cells (see Figure 30). Similar results were obtained for osteogenic differentiation and the expression of the early and late osteogenic differentiation markers COL1A1 and OPN [157], respectively. As shown in the right panel of Figure 30, increase of the mRNA levels of COL1A1 (47 %) and OPN (72 %) was significantly higher in cells transfected with control shRNA, than in DKK2 knock-down cells (COL1A1: 29 % and OPN: 64 %).

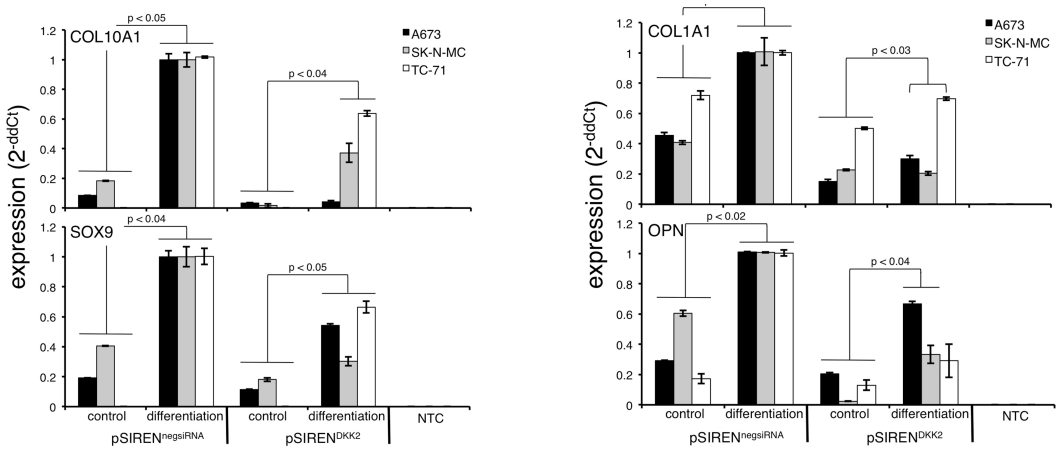

Figure 30: Chondrogenic and osteogenic differentiation assays with stably transfected DKK2 cells
Left panel: Chondrogenic differentiation of ET cell lines with specific shRNA constructs was shown by the expression of specific chondrogenic marker genes *COL10A1* (*collagen, type X, alpha-1*) and *Sox9* (*sry-box 9*) using qRT-PCR. Data are mean ± SEM of two independent experiments; t-test. **Right panel:** Analysis of osteogenic differentiation of ET shRNA infectants. Expression of the early (*COL1A1*: *collagen, type I, alpha-1*) and late (*OPN*: *secreted phosphoprotein 1, SPP1*) marker genes was shown by qRT-PCR. Data are mean ± SEM of two independent experiments; t-test (p: p-value).

4.2.8. DKK2 increases bone invasiveness and osteolysis *in vitro* and *in vivo*

As previously demonstrated in this study, DKK2 plays a role in chondrogenic and osteogenic differentiation, but it is still not known, if DKK2 is important for osteotropism as well as bone invasiveness and osteolysis. Therefore, the differential expression of key players associated with osteotropism was examined in stable DKK2 infectants using qRT-PCR. C*hemokine, cxc motif, receptor 4* (*CXCR4,* [221–223]), *parathyroid hormone-like hormone* (*PTHrP,* [224–227]), *RUNT-related transcription factor 2* (*RUNX2,* [228,229]) and *transforming growth factor beta-1* (*TGFβ,* [230,231]) were chosen for follow-up due to their involvement in preparing the pre-metastatic niche,

homing and invasion to bone as well as their role in local and metastatic tumor growth in bones [188]. Interestingly, the expression of these genes was significantly reduced in ET cells with constitutive DKK2 knock-down compared to controls (see Figure 31).

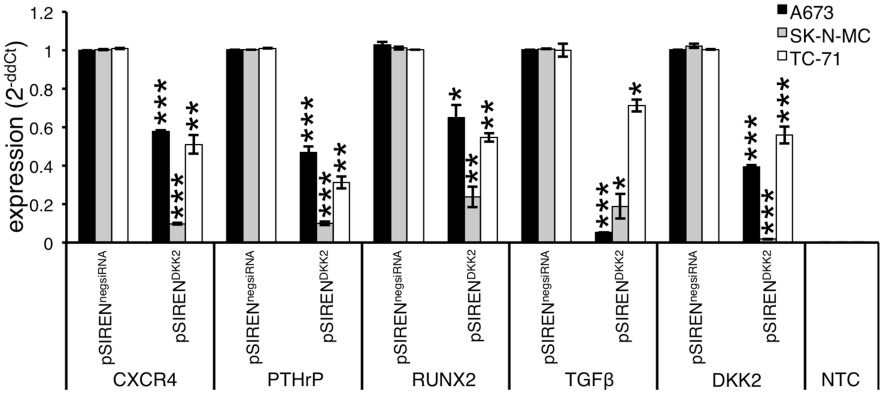

Figure 31: mRNA expression of key players associated with bone colonization in stable DKK2 infectants
qRT-PCR of ET cell lines with stable DKK2 knock-down and controls. *CXCR4*: *chemokine, cxc motif, receptor 4*; *PTHrP*: *parathytroid hormone-like hormone*, *PTHLH*; *RUNX2*: *runt-related transcription factor 2*; *TGFβ*: *transforming growth factor*, *beta-1*; *DKK2*: *dickkopf 2*. Data are mean ± SEM of three independent experiments; t-test (*p < 0.05; **p < 0.005; ***p < 0.0005).

Although osteosclerosis is of clinical relevance in ET pathology, osteolytic lesions are predominant in patients and interestingly, some genes important for homing and invasion to bone are known factors for osteolysis, as well. For example, the transcription factor RUNX2 and PTHrP have been implicated in promoting tumor osteolysis [188,225], as well as TGFβ [188], which is known to modulate different osteolytic factors, for example PTHrP [230] and tumor necrosis factor ligand superfamily, member 11 (RANKL). An increase in locally active RANKL, which favour osteolysis and is expressed even on ET cells [232], can be achieved directly by MMP7 [186] or indirectly by MMP1 [187], too. As shown in Figure 16 and Figure 31, DKK2 knock-down significantly decreased the expression levels of these matrix metalloproteinases and of the osteolytic genes described above. To further analyze these observations, gene expression of *RANKL*, its antagonist *tumor necrosis factor receptor superfamily, member 11B* (*osteoprotegerin*, *OPG*) and an important osteoclast survival factor *colony-stimulating factor, macrophage-specific* (*M-CSF*) were examined in A673, SK-N-MC and TC-71 cells with constitutive DKK2 knock-down and respective controls. Although three times more cDNA was necessary to detect any signals using qRT-PCR, it is obvious, that DKK2 knock-down significantly increased mRNA expression of OPG and at the same time decreased the amount of the two cytokines

RANKL and M-CSF, which are described to be essential and sufficient for osteoclastogenesis (see Figure 32) [5,23,30].

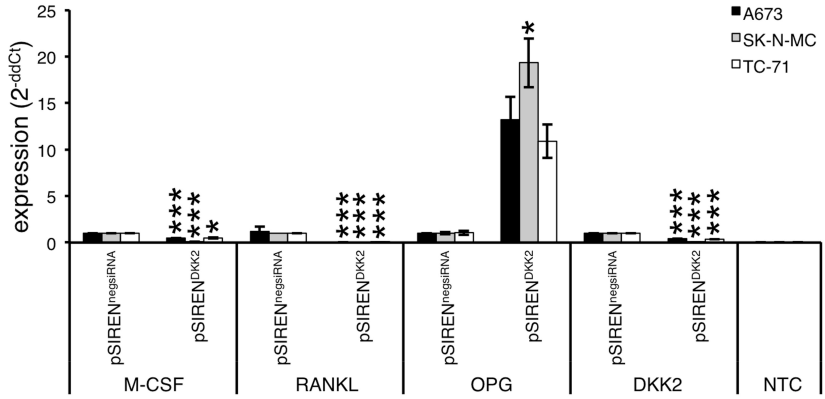

Figure 32: Expression levels of M-CSF, RANKL and OPG after DKK2 knock-down
mRNA expression of M-CSF and the antagonists OPG and RANKL in three different ET cell lines after constitutive suppression of DKK2 and respective controls. *M-CSF*: *colony-stimulating factor, macrophage-specific; RANKL: tumor necrosis factor ligand superfamily, member 11; OPG: tumor necrosis factor receptor superfamily, member 11B; DKK2*: *dickkopf 2*. NTC: non template control. Data are mean ± SEM of two independent experiments; t-test (*p < 0.05; ***p < 0.0005).

Since expression levels of OPG and RANKL are very low in ETs, four further genes important for osteolysis were analyzed by qRT-PCR in three ET cell lines stably transfected with pSIREN^{DKK2} and pSIREN^{negsiRNA}. As expected, DKK2 suppression clearly reduced the expression levels of the osteolytic genes *hypoxia-inducible factor 1, alpha subunit* (*HIF1α,* [188,233,234]), *interleukin 6* (*IL6,* [188,235]), *jagged 1* (*JAG1,* [235]) and *vascular endothelial growth factor receptor 1* (*VEGF, FLT1,* [188]) (see Figure 33).

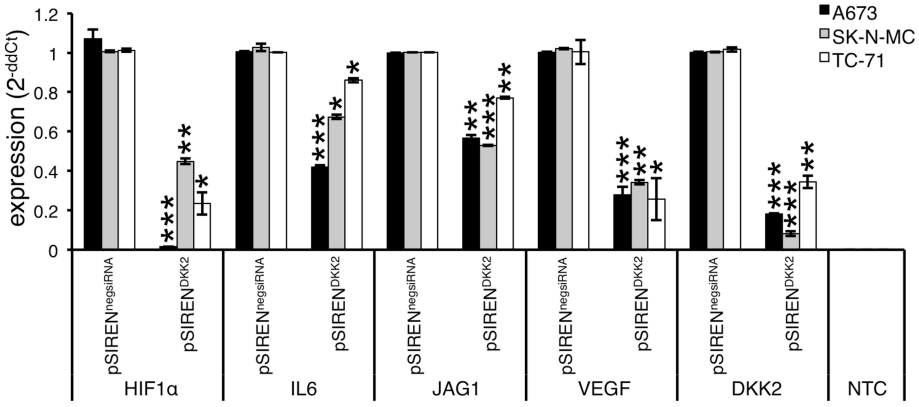

Figure 33: Osteolytic gene expression after DKK2 knock-down
Different ET cell lines with constitutive DKK2 knock-down and respective controls were analyzed by qRT-PCR. *HIF1α*: *genes hypoxia-inducible factor 1, alpha subunit*; *IL6*: *interleukin 6*; *JAG1*: *jagged 1*; *VEGF*: *vascular endothelial growth factor receptor 1*; *DKK2*: *dickkopf 2*. NTC: non template control. Data are mean ± SEM of two independent experiments; t-test (*p < 0.05; **p < 0.005; ***p < 0.0005).

Based on these *in vitro* results, further analyses were necessary to determine whether suppression of DKK2 has a role in the process of bone colonization, invasion and osteolysis *in vivo*, as well. To investigate this question, constitutively DKK2 silenced A673 cells were injected into the tibiae of immune deficient $Rag2^{-/-}\gamma c^{-/-}$ mice and bone infiltration and destruction was analyzed by X-ray radiography and histology (see 3.17). As shown in Figure 34, DKK2 knock-down significantly reduced bone infiltration and osteolysis *in vivo*. Only 25 % of the mice (2 / 8 mice) injected with A673 $pSIREN^{DKK2}$ cells exhibited an infiltration of tumor cells into bone (see right panel of Figure 34), whereas bone infiltration was observed in 87.5 % of the respective controls (7 / 8 mice). Moreover, only one mouse injected with DKK2 knock-down cells developed extensive osteolytic lesions (1 / 8 mice) compared to four mice injected with A673 $pSIREN^{negsiRNA}$ cells (4 / 8 mice).

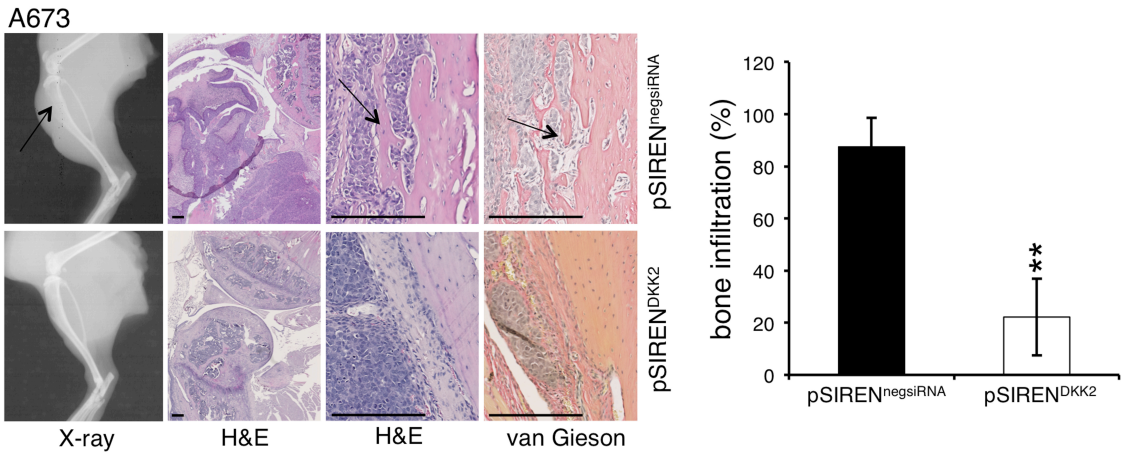

Figure 34: DKK2 knock-down suppressed bone invasiveness *in vivo*
Left panel: Analysis of bone invasiveness of constitutive A673 DKK2 shRNA infectants and negative controls in an orthotopic bone xenotransplantation model (8 mice/group). Affected bones were assessed by X-ray radiography and histology (H&E and van Gieson stains, scale bar 0.25 mm). A673 $pSIREN^{DKK2}$ cells caused significantly less tumor infiltration into bone when compared to A673 $pSIREN^{negsiRNA}$, where tumor cells destroy the cortical bone (arrows). **Right panel:** Percentage of mice exhibiting bone infiltration after intra-tibial injection. Data are mean ± SEM; t-test (**$p < 0.003$).

Furthermore, the $pSIREN^{DKK2}$-mediated lesions were smaller and less destructive than the lesions caused by control cells. To quantify osteolytic lesions, the amount of osteoclasts was detected by tartrate-resistant acid phosphatase staining (TRAP staining) in three different tumor samples per group (see 3.18). As can be seen in Figure 35, no clear differences were observed in the unaffected bone marrow. In contrast, the average number of osteoclasts was significantly decreased in A673 $pSIREN^{DKK2}$ tumor samples (0.35 osteoclasts / mm^2), compared to respective controls (1.42 osteoclasts / mm^2). Interestingly, the main part of the osteoclasts was not only

detected close to bone tissues as expected, but also on the whole outer rim of the tumors.

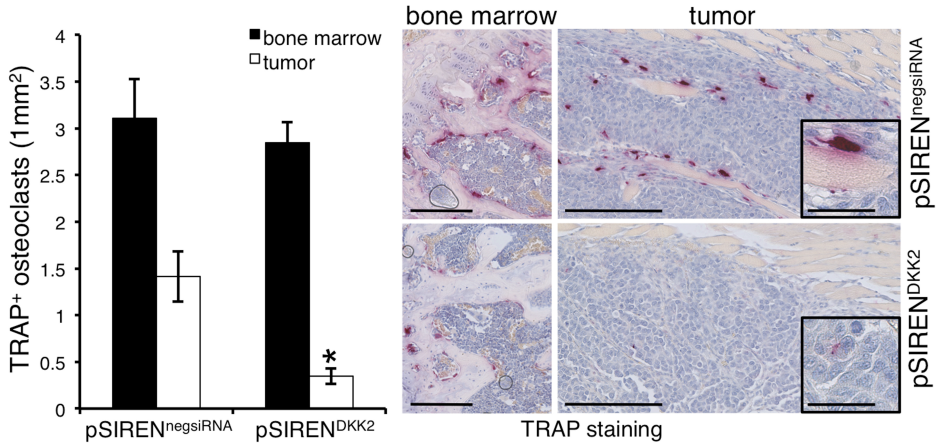

Figure 35: DKK2 knock-down clearly decreased the number of osteoclasts
Left panel: Quantitative summary of the average number of osteoclasts (mm^2) in unaffected bone marrow and tumor samples. Data are mean ± SEM of three independent samples (20 segments counted); t-test (*p < 0.01). **Right panel:** Analysis of osteolysis of constitutive A673 DKK2 shRNA infectants and negative controls in an orthotopic bone xenotransplantation model (8 mice/group). Affected bones were assessed by histology (TRAP staining, scale bar 0.25 mm or 0.05 mm). A673 $pSIREN^{DKK2}$ cells significantly suppressed osteolysis, which was detected by the reduced amount of osteoclasts in the tumor sample.

4.2.9. Clinical relevance of DKK2 in ETs

The current results indicate that DKK2 is an important player in ET malignancy, especially in ET metastasis, bone invasiveness and osteolysis. For this reason, it was interesting to analyze, whether the effect of DKK2 on the oncogenic phenotype of ETs is also detectable in human clinical samples. Therefore, expression of DKK2 was assessed in a pilot screening of 19 different ET samples prior to treatment using immunohistochemistry (see 3.19). As shown in Table 19, 17 of 19 patient samples (89.5 %) displayed detectable DKK2 protein levels, of which 11 exhibited a low immunoreactivity (intensity 1, 57.9 %) and 6 a moderate, and thus the highest, signal intensity (intensity 2, 31.6 %).

Due to the different DKK2 localization observed in samples with low signal intensity (cytoplasmic or membranous), four staining intensity grades were defined (see Figure 36). Interestingly, high immunoreactivity seemed to correlate on the one hand with a cytoplasmic protein localization of DKK2 in the tumor cells and on the other hand with enhanced bone infiltration, as shown in Table 19.

Table 19: Immunoreactivity and localization of DKK2 in human ET samples

sample number	intensity	DKK2 localization	tumor localization	infiltration
1	2	cytoplasmic/membranous	ilium	+
2	2	cytoplasmic/granular	ilium	+
3	2	cytoplasmic	fibula	+
4	2	cytoplasmic	tibia	n.d.
5	2	cytoplasmic	jawbone	+
6	2	cytoplasmic	ilium	+
7	1	cytoplasmic/membranous	ilium	+
8	1	cytoplasmic/granular	metatasale	+
9	1	cytoplasmic	fibula	+
10	1	cytoplasmic	ilium	+
11	1	cytoplasmic	orbita	+
12	1	cytoplasmic	femur	+
13	1	membranous	humerus	-
14	1	membranous	femur	+
15	1	membranous	humerus	+
16	1	membranous	humerus	n.d.
17	1	membranous	clavicula	-
18	0	-	rib	-
19	0	-	middle phalanx	-

Summary of signal intensity and localization of DKK2 expression in 19 different human ET samples from diverse origin is shown. Signal intensity is graded in "0" = no immunoreactivity; "1" = low signal intensity and "2" = moderate signal intensity. The final column summarizes the invasive behavior of the tumors investigated; "+" = infiltration of tumor cells into the bone, "-" = solide tumors without bone infiltration. n.d. = not unequivocally determinable.

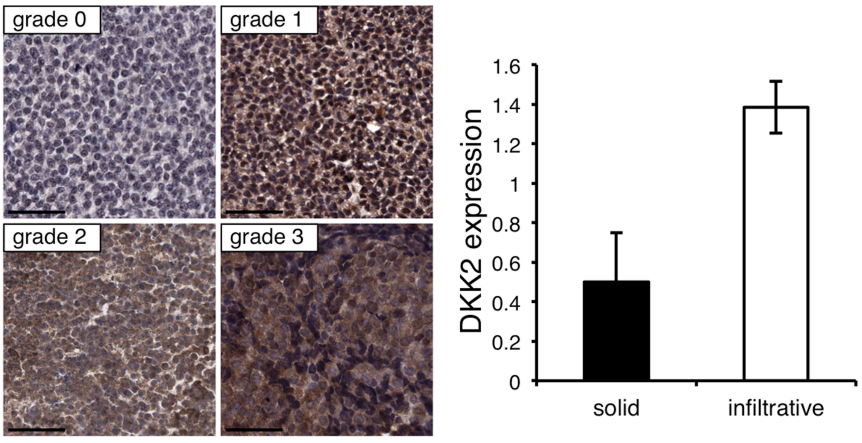

Figure 36: DKK2 expression in human ET patient samples
Left panel: DKK2 immunoreactivity (brown color) was scored according to DKK2 levels and localization observed with grade 0 = no immunoreactivity; grade 1 = low intensity, membranous; grade 2 = low intensity, cytoplasmic and grade 3 = moderate intensity, cytoplasmic (scale bars 0.05 mm). **Right panel:** Mean level of DKK2 expression in 19 different patients samples arranged according to the growth pattern (solid-circumscribed vs infiltrative). Data are mean ± SEM; t-test.

Subsequently, expression of DKK2 was correlated with the outcome of ET patients. For this purpose, DKK2 expression was classified in $DKK2^{high}$ samples consisting of infiltrative, moderate and low signal intensity (grade 1, 2 and 3) ETs and $DKK2^{low}$ samples, which include solid tumors with low or negative immunoreactivity (grade 0 and 1). Even though no significant statement could be made due to the small number of samples, overall survival in patients bearing ETs classified as $DKK2^{low}$ was enhanced compared to $DKK2^{high}$ cases, as demonstrated in Figure 37.

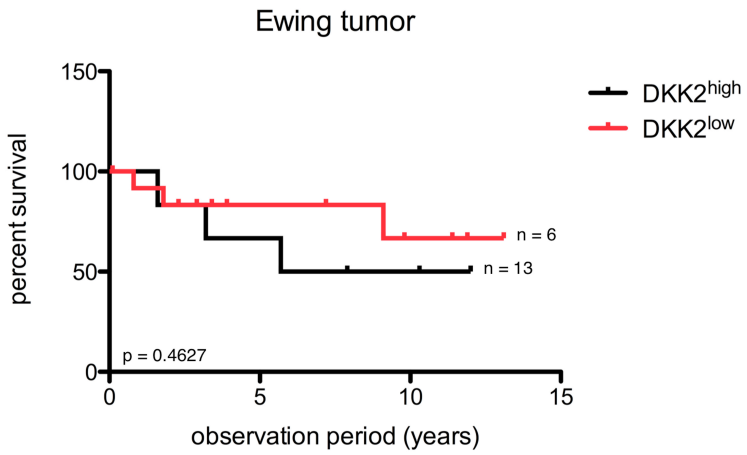

Figure 37: Overall survival in ET patients in respect to DKK2 expression
DKK2 expression seemed to correlate with overall survival (OS): Kaplan–Meier plot estimates for OS probability for DKK2 expression (n = 19 (n = 6 $DKK2^{low}$, n = 13 $DKK2^{high}$), p = 0.4627). Log-rank test (p: p-value).

4.3. The role of the BRICHOS-family genes, *CHM1* and *ITM2A*, in ET pathogenesis

Due to the complex biological mechanisms of tumor development, *DKK2* is probably not the only gene involved in the oncogenic behavior of ETs. Therefore, the influence of two other bone-associated, overexpressed genes, *chondromodulin 1* (*CHM1*) and *integral membrane protein 2A* (*ITM2A*), on ET pathogenesis was analyzed. For this purpose, CHM1 and ITM2A were transiently and constitutively down-regulated in three ET cell lines. For efficient transient gene knock-down, two different siRNAs (CHM1_1 and CHM1_4 or ITM2A_5 and ITM2A_7) were tested in the ET cell lines A673, SK-N-MC and TC-71 by RNA interference (see 3.5). Subsequently, CHM1 or ITM2A mRNA levels, as well as mRNA expression of IFN responsive genes *ISG15* and *IFITM1*, were determined 48 h after transfection by qRT-PCR (see 3.4 and Table 11). As shown in the left panel of Figure 38, transient transfection with CHM1_1 and CHM1_4 siRNAs reduced mRNA levels of CHM1 down to 25 – 53 % compared to cells transfected with non-silencing siRNA (neg.control). Gene expression of *ITM2A* was clearly down-regulated after transient transfection with ITM2A_5 and ITM2A_7 siRNAs, too (see right panel of Figure 38). Especially in SK-N-MC cells a significant reduction of ITM2A mRNA levels down to 7 – 12 % was observed (A673: 25 – 50 %; TC-71: 20 – 32 %). Because both CHM1 siRNAs and ITM2A siRNAs significantly suppressed gene expression, both siRNAs were used in further transient transfection experiments to exclude off-target effects.

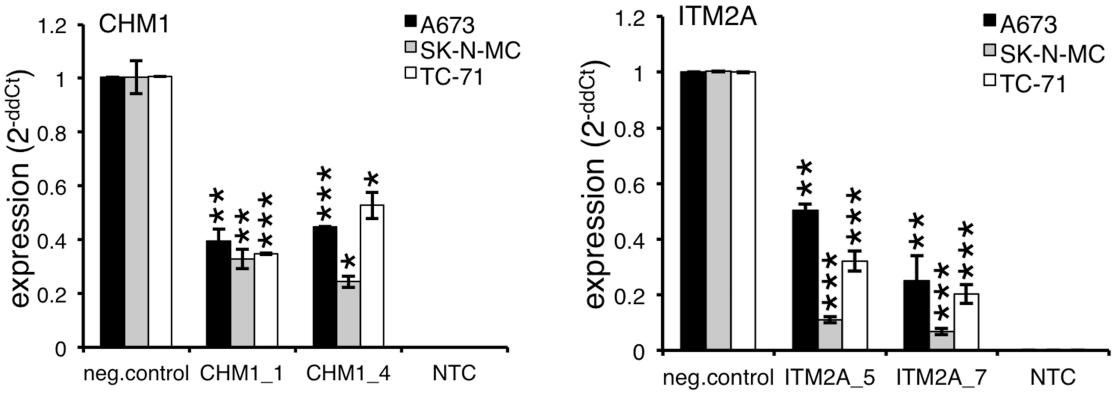

Figure 38: Transient gene knock-down in ET cell lines using RNA interference
Left panel: Transient CHM1 suppression in three ET cell lines with specific siRNAs (CHM1_1 and CHM1_4) using RNA interference. Knock-down efficacy was tested by qRT-PCR 48 h after transfection. Data are mean ± SEM of three independent experiments; t-test. **Right panel:** Quantification of ITM2A mRNA levels in different ET cell lines 48 h after transient transfection with ITM2A_5 and ITM2A_7 siRNAs compared to neg.control. Data are mean ± SEM of three independent experiments; t-test (*p < 0.05; **p < 0.005; ***p < 0.0005).

To generate ET cell lines with constitutive gene knock-down, the target sequence of the best CHM1 siRNA (CHM1_1), as well as the best ITM2A siRNA (ITM2A_7), were used to create oligonucleotides for retroviral gene transfer and were cloned into the pSIREN RetroQ vector (see 3.6). As shown in Figure 39, constitutive CHM1 knock-down ($pSIREN^{CHM1}$) resulted in a suppression of CHM1 mRNA levels down to 14 – 21 % compared to control cells, constitutively transfected with $pSIREN^{negsiRNA}$. ITM2A mRNA levels were significantly decreased after constitutive down-regulation of ITM2A ($pSIREN^{ITM2A}$) down to 17 – 32 % (see Figure 39).

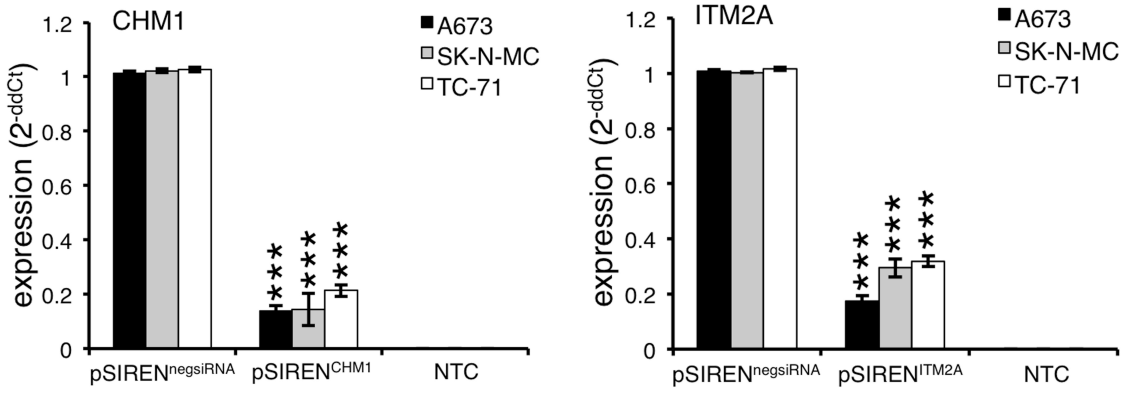

Figure 39: Quantification of CHM1 and ITM2A mRNA levels after constitutive gene knock-down
Left panel: Retroviral gene transfer of $pSIREN^{CHM1}$ construct into different ET cell lines. CHM1 mRNA levels were measured by qRT-PCR ($pSIREN^{CHM1}$, control: $pSIREN^{negsiRNA}$). Data are mean ± SEM of at least 15 independent experiments; t-test. **Right panel:** Quantification of ITM2A mRNA levels after constitutive ITM2A knock-down in A673, SK-N-MC and TC-71 cells compared to control cells. Data are mean ± SEM of at least 15 independent experiments; t-test. (***$p < 0.0005$).

4.3.1. Influence of BRICHOS genes on tumor growth and metastasis

To examine whether CHM1 or ITM2A knock-down influences the proliferative behavior of ET cells, constitutively CHM1 or ITM2A transfected A673 and SK-N-MC cells were analyzed using an xCELLigence instrument (see 3.8.1) or a BrdU incorporation assay (see 3.8.2) for $pSIREN^{CHM1}$-/$pSIREN^{ITM2A}$- and $pSIREN^{negsiRNA}$-transfected TC-71 cells. As shown in Figure 40, constitutive CHM1 knock-down clearly decreased proliferation in all ET cell lines investigated. In particular, the doubling time was significantly increased up to 4-fold (in TC-71 cells) after CHM1 knock-down.

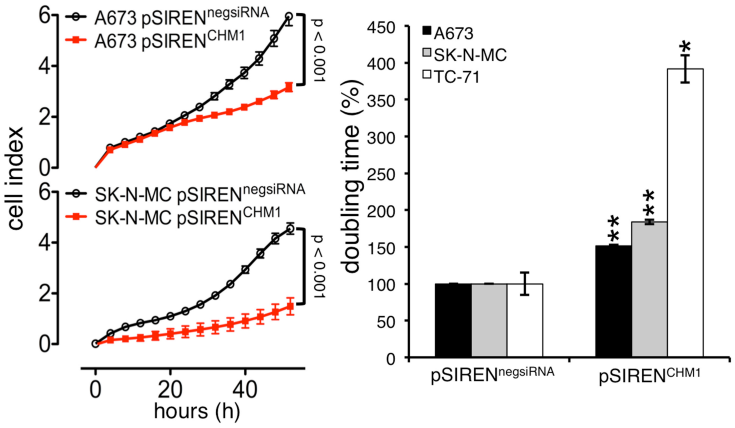

Figure 40: Proliferation assay of ET cell lines constitutively transfected with CHM1
Left panel: Analysis of proliferation of different ET cell line derivatives using xCELLigence. Cellular impedance was measured every 4 h (relative cell index). Data are mean ± SEM (hexaplicates/group); t-test (p: p-value). **Right panel:** Doubling time of ET cell lines with constitutive CHM1 knock-down and control cells. Data are mean ± SEM of two independent experiments/cell line (hexaplicates/group); t-test (*p < 0.05; **p < 0.005).

In contrast, stable suppression of ITM2A did not clearly affect the proliferative behavior and thus the doubling time of ET cell lines (see Figure 41). Only in A673 cells, ITM2A knock-down induced a slightly increased proliferation, as shown in Figure 41.

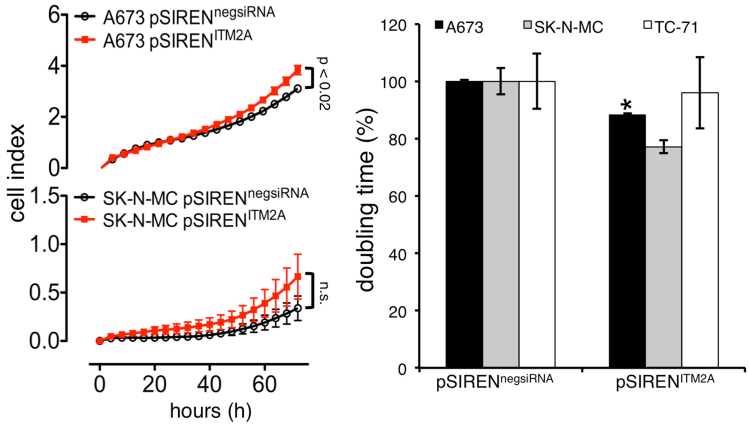

Figure 41: Proliferation assay of ET cell lines constitutively transfected with ITM2A
Left panel: Analysis of proliferation of constitutively ITM2A infected ET cell lines with xCELLigence. Cellular impedance was measured every 4 h (relative cell index). Data are mean ± SEM (hexaplicates/group); t-test (p: p-value; n.s.: not significant). **Right panel:** Doubling time of ET cell lines with stable ITM2A knock-down and control cells. Data are mean ± SEM of two independent experiments/cell line (hexaplicates/group); t-test (*p < 0.05).

To examine whether BRICHOS-family genes influence cell cycle progression, CHM1 or ITM2A were constitutively down-regulated in different ET cell lines, incubated with PI

overnight and analyzed by flow cytometry (see 3.10). As seen in Figure 42, neither CHM1 knock-down, nor ITM2A knock-down influenced the different replication phases.

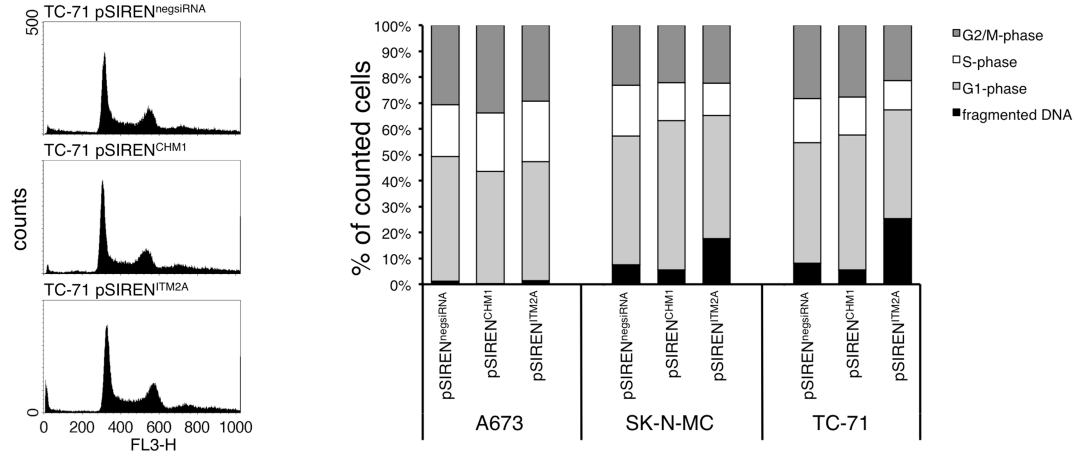

Figure 42: Cell cycle progression in ET cell lines with CHM1/ITM2A knock-down
Left panel: Representative example of cell cycle progression in TC-71 cells after stable CHM1 or ITM2A knock-down and respective controls. **Right panel:** Summary of two independent cell cycle distribution analyses of CHM1 and ITM2A shRNA infectants in A673, SK-N-MC and TC-71 cells by PI staining and flow cytometry.

Subsequently, the effect of CHM1 and ITM2A knock-down on *in vitro* contact-independent growth capacity was analyzed by colony formation assay using methylcellulose-based media (see 3.14). Three ET cell lines with constitutive CHM1 or ITM2A suppression were tested in duplicates and colonies were counted using the image-processing package Fiji after incubation for 14 days. As shown in Figure 43, constitutive CHM1, as well as ITM2A, knock-down significantly decreased contact-independent growth capacity in all three ET cell lines.

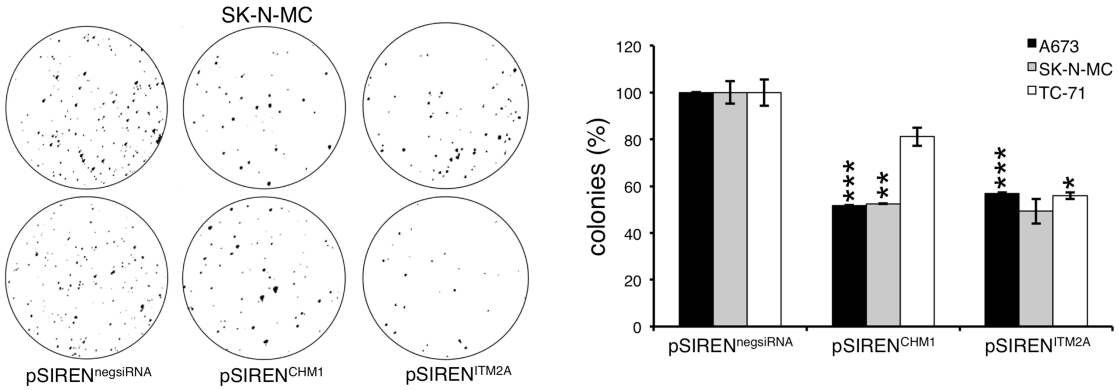

Figure 43: Colony formation assay after constitutive CHM1 or ITM2A knock-down
Analysis of anchorage-independent colony formation in methylcellulose of stable pSIREN^{CHM1}-, pSIREN^{ITM2A}- and pSIREN^{negsiRNA}-infected ET cell lines. **Left panel:** Macrographs show a representative experiment with SK-N-MC. **Right panel:** Number of counted colonies using Fiji. Data are mean ± SEM of three independent experiments (duplicates/group); t-test (*p < 0.05; **p < 0.005; ***p < 0.0005).

Based on these *in vitro* results further experiments were designed to examine whether the suppression of CHM1 or ITM2A affects tumorigenicity and metastasis *in vivo*. Different ET cell lines with constitutive CHM1 or ITM2A knock-down and respective controls were first injected subcutaneously into the inguinal region of immunodeficient $Rag2^{-/-}\gamma c^{-/-}$ mice and tumor growth was analyzed (see 3.17). As seen in Figure 44, CHM1 knock-down delayed local tumor growth in both ET cell lines, but not as strong as expected looking at the proliferative behavior of the cells (see Figure 40).

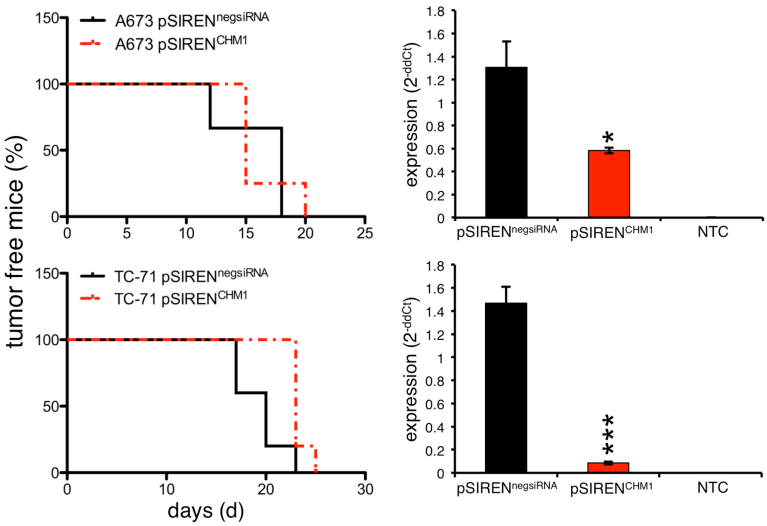

Figure 44: Kaplan-Meier plot of local tumor growth experiment with CHM1 knock-down
Left panel: Evaluation of tumorigenicity of constitutive A673 and TC-71 CHM1 shRNA infectants in immune deficient mice (3 - 5 mice/group). Mice with an average tumor size > 10 mm in diameter were considered as positive and sacrificed. Experiments with A673 cells were performed by Dr. Annette Fasan. **Right panel:** Quantification of CHM1 mRNA levels of tumor samples post *ex vivo* using qRT-PCR (*p < 0.05; ***p < 0.0005).

After ITM2A knock-down, local tumor growth was significantly increased compared to injection with $pSIREN^{negsiRNA}$ transfected A673 or SK-N-MC cells (see Figure 45). This observation is in line with the proliferative behavior of ET cell lines after ITM2A knock-down (see Figure 41), but nevertheless surprisingly, because ITM2A is up-regulated in ETs.

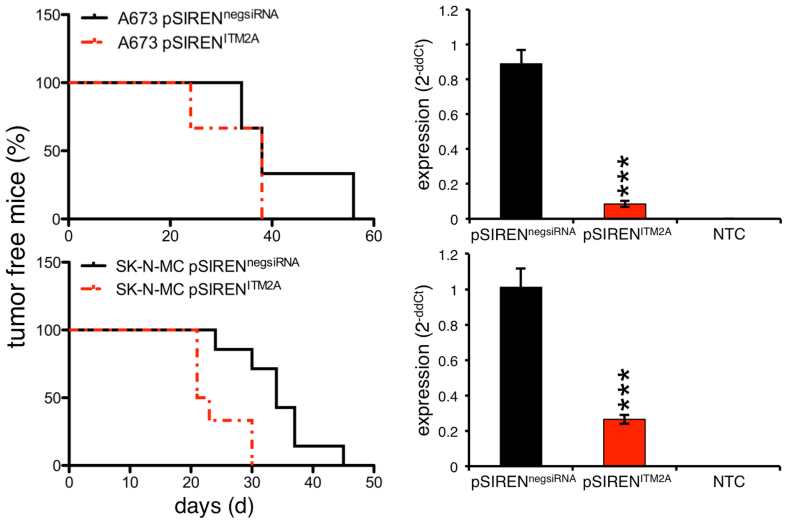

Figure 45: Kaplan-Meier plot of local tumor growth with ITM2A knock-down
Left panel: Evaluation of tumorigenicity of constitutive A673 and SK-N-MC ITM2A shRNA infectants in immunodeficient mice (3 - 5 mice/group). Mice with an average tumor size > 10 mm in diameter were considered as positive and sacrificed. **Right panel:** Quantification of ITM2A mRNA levels of tumor samples post *ex vivo* using qRT-PCR (***p < 0.0005).

As previously described in the doctoral thesis of Dr. Annette Fasan [236], CHM1 knock-down significantly reduce the amount of lung metastases compared to control cells in A673 cells. However, no differences could be observed in liver and kidney colonization. This result could be confirmed in a second cell line, even though CHM1 knock-down led to a small decrease in the amount of liver metastases in TC-71 cells (data not shown).

To examine the effects of ITM2A on ET metastasis, different ET cell lines constitutively transfected with ITM2A and nonsense shRNA were injected into the tail veins of Rag2$^{-/-}$ γc$^{-/-}$ mice to analyze metastasis (see 3.17). As shown in Figure 46, suppression of ITM2A in A673 cells clearly decreased the number of lung metastases, with a simultaneous enlargement of the metastatic area. This observation is in line with the *in vitro* results, because although knock-down of ITM2A significantly suppressed contact-independent colony formation compared to pSIREN^{negsiRNA} transfected cells (see Figure 43), the proliferation is increased after ITM2A suppression (see Figure 41). With regard to liver metastases, different ET cell lines showed different results. While ITM2A knock-down slightly increased the number of liver metastases in A673 cells, suppression of this gene significantly reduced the metastatic behavior in SK-N-MC cells (see Figure 46). Furthermore, suppression of neither CHM1 nor ITM2A exhibited bone metastases, similar to the respective controls (see Table 20).

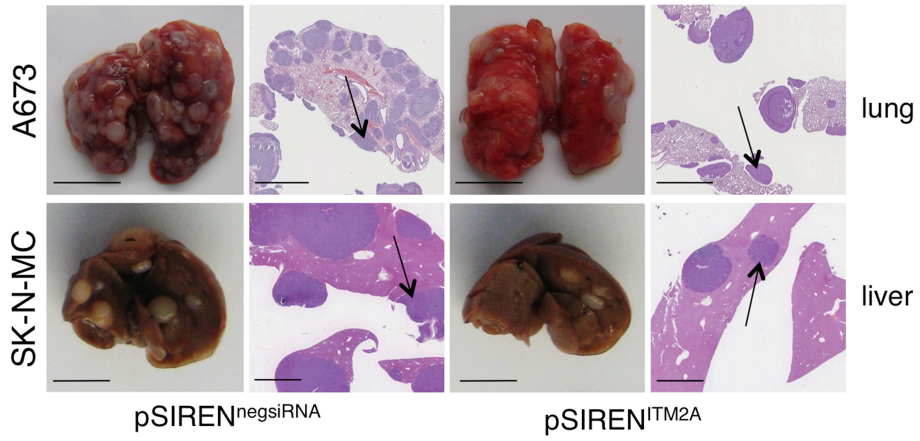

Figure 46: Analysis of affected organs after injection into the tail vein of Rag2$^{-/-}$ γc$^{-/-}$ mice after ITM2A knock-down
Analysis of metastatic potential of A673 and SK-N-MC cells with stable ITM2A knock-down and controls (pSIREN^{negsiRNA}; 4 mice/group). All macroscopically visible metastases in lungs, livers, kidneys and ovaries were confirmed by histology. The left panel demonstrates lung and liver with extend metastasis (arrow) and the right panel depicts lung and livers with metastasis after pSIREN^{ITM2A} injection (H&E; scale bar 5mm or 2mm).

Table 20: Number of apparent metastases after ITM2A knock-down

	average number of apparent metastases per mouse			
	A673		SK-N-MC	
	pSIREN^{negsiRNA}	pSIREN^{ITM2A}	pSIREN^{negsiRNA}	pSIREN^{ITM2A}
liver	3	4	33	6
lung	95	50	0	0
kidney	0	0	1	0
ovary	1	0	0	0
summary	99	54	34	6

Analysis of metastatic potential of A673 and SK-N-MC cells with stable ITM2A knock-down and controls (pSIREN^{negsiRNA}; 4 mice/group). All macroscopically visible metastases in lungs, livers, kidneys and ovaries were counted and an average number of apparent metastases per mouse is shown. Decimal numbers will be rounded up.

4.3.2. Invasiveness is regulated by MMPs after CHM1 or ITM2A knock-down

To better understand the metastatic behavior of ET cells after suppression of CHM1 or ITM2A, *in vitro* cell invasion was analyzed in different ET cell lines, stably transfected with pSIREN^{CHM1} or pSIREN^{ITM2A} and pSIREN^{negsiRNA}, using Matrigel-covered transwell assays (BioCoat^{TM} Angiogenesis System; see 3.15). As expected, CHM1 knock-down suppressed the invasive potential of all three ET cell lines; especially of SK-N-MC cells (see Figure 47). In contrast, down-regulation of ITM2A increased the number of

invasive cells in A673 and TC-71 cells, as shown in Figure 47. Only in SK-N-MC cells, ITM2A knock-down clearly decreased cell invasiveness through Matrigel. These *in vitro* results accurately represented the observed metastatic spread of ET cell lines after ITM2A knock-down into the liver, which might indicate, that Matrigel-covered transwell assay (BioCoat^{TM} Angiogenesis System) is only useful to predict the invasive potential resulting in liver metastases *in vitro*. A similar interpretation of the results after CHM1 or DKK2 knock-down seems possible.

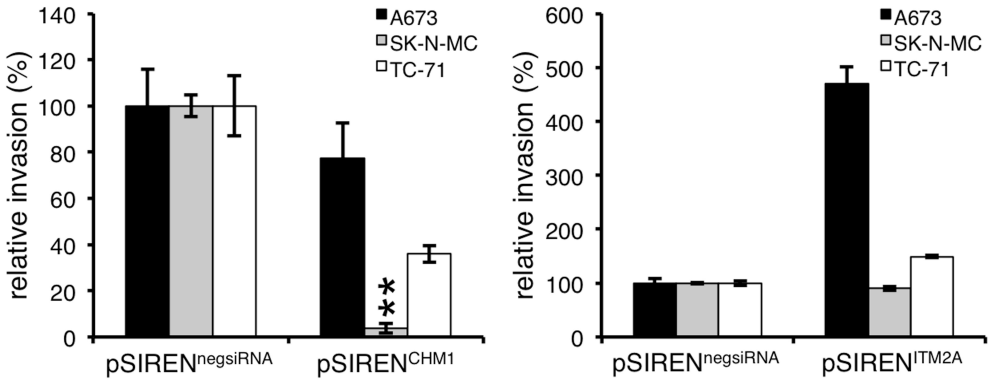

Figure 47: Analysis of invasiveness in ET cell lines through Matrigel after BRICHOS gene knock-down
Analysis of invasiveness of ET cell lines A673, SK-N-MC and TC-71 through Matrigel after transfection with specific CHM1 (**left panel**) or ITM2A (**right panel**) and nonsense shRNA constructs. Data are mean ± SEM of two independent experiments; t-test (**p < 0.005).

As previously demonstrated MMPs, especially MMP1, are important for ET invasiveness *in vitro* (see Figure 17 and [153,186–188]). To examine, if the reduced invasiveness after CHM1 or ITM2A knock-down is also influenced by MMPs, mRNA expression of MMP1, MMP7 and MMP9 was analyzed using qRT-PCR (see 3.4). As shown in Figure 48, only MMP9 was suppressed in all three ET cell lines after knock-down of CHM1 compared to pSIREN^{negsiRNA}. After suppression of ITM2A, expression levels of MMP1, MMP7 as well as MMP9 were reduced in A673 and TC-71 cells and increased in SK-N-MC cells (see Figure 48), which is in line with the results of the invasion assay (see Figure 47).

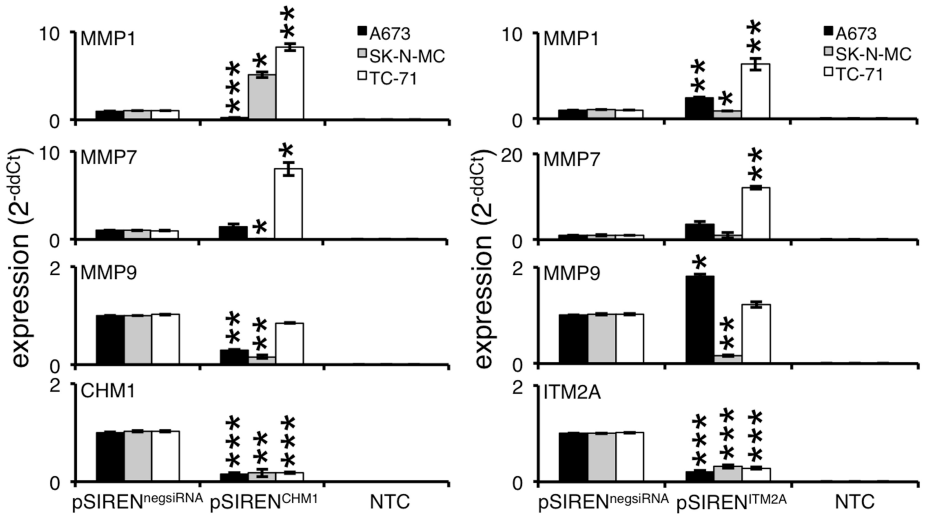

Figure 48: Expression levels of different MMPs after CHM1 or ITM2A knock-down
Detection of MMP mRNA expression levels in A673, SK-N-MC and TC-71 cells after constitutive CHM1 (**left panel**) or ITM2A (**right panel**) knock-down using qRT-PCR. *MMP1*: *matrix metalloproteinase 1*; *MMP7*: *matrix metalloproteinase 7*; *MMP9*: *matrix metalloproteinase* 9; *CHM1*: *chondromodulin 1*; *ITM2A*: *integral membrane protein 2A*. NTC: non template control. Data are mean ± SEM of two independent experiments; t-test (*p < 0.05; **p < 0.005; ***p < 0.0005).

To further investigate the role of MMP9 in ET invasion, A673 and SK-N-MC cells with transiently down-regulated MMP9 (MMP9_3 and MMP9_6 siRNAs; see supplementary Figure 58) and control siRNA were analyzed using Matrigel-covered transwell assays (BioCoat™ Angiogenesis System; see 3.15). As shown in Figure 49, MMP9 knock-down significantly reduced the invasive behavior of both ET cell lines. This observation indicates that MMP9 seems to be an important factor in the regulation of the invasive potential of ET cell lines after suppression of BRICHOS-family genes. Additionally in the case of ITM2A, MMP1 might influence invasiveness, too (see Figure 17, Figure 47 and Figure 48).

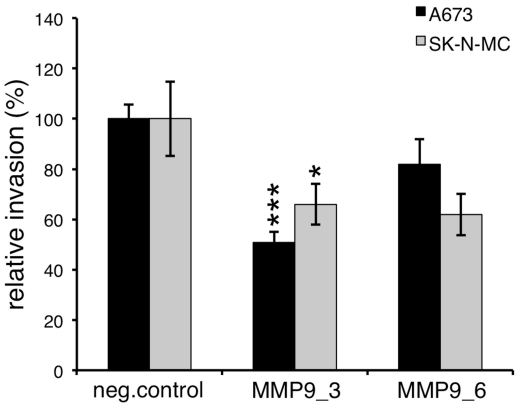

Figure 49: Invasion assay after transient MMP9 knock-down
Analysis of invasiveness of two different ET cell lines through Matrigel after transient knock-down of MMP9 (MMP9_3 and MMP9_6 siRNAs) and nonsense siRNA (neg.control). Data are mean ± SEM of two independent experiments; t-test (*p < 0.05; ***p < 0.0005).

To further analyze cell invasion and migration, expression of a series of integrin and adhesion molecules were tested in A673, SK-N-MC and TC-71 cells with constitutive CHM1 or ITM2A knock-down using flow-cytometric analysis (see 3.11 and Table 7). As demonstrated in Table 21, only CD49d expression was increased after CHM1 suppression.

Table 21: Flow-cytometric analysis of integrin and adhesion molecule expression after CHM1 knock-down

Integrin / adhesion molecule		A673		SK-N-MC		TC-71	
		pSIREN^{negsiRNA}	pSIREN^{CHM1}	pSIREN^{negsiRNA}	pSIREN^{CHM1}	pSIREN^{negsiRNA}	pSIREN^{CHM1}
CD29	**β1**	++	++	++	++	++	++
CD49a	**α1**	(+)	(+)	-	-	(+)	(+)
CD49b	**α2**	(+)	(+)	-	-	(+)	(+)
CD49c	**α3**	-	-	-	-	-	-
CD49d	**α4**	-	+	-	(+)	+	++
CD49e	**α5**	++	++	++	++	++	++
CD49f	**α6**	+	+	-	-	(+)	(+)

Expression of a series of integrin and adhesion molecules in different ET cell lines after constitutive CHM1 suppression using flow-cytometric analysis. Semi-quantitative evaluation: – = no, (+) = faint, + = moderate, and ++ strong expression.

After constitutive down-regulation of ITM2A no differences in integrin and adhesion molecule expression were observed compared to pSIREN^{negsiRNA} transfected cells (see Table 22).

Table 22: Flow-cytometric analysis of integrin and adhesion molecule expression after ITM2A knock-down

Integrin / adhesion molecule		A673		SK-N-MC		TC-71	
		pSIREN^{negsiRNA}	pSIREN^{ITM2A}	pSIREN^{negsiRNA}	pSIREN^{ITM2A}	pSIREN^{negsiRNA}	pSIREN^{ITM2A}
CD29	**β1**	++	++	++	++	++	++
CD49a	**α1**	(+)	(+)	-	-	(+)	(+)
CD49b	**α2**	(+)	(+)	-	-	(+)	(+)
CD49c	**α3**	-	-	-	-	-	-
CD49d	**α4**	-	-	-	-	+	+
CD49e	**α5**	++	++	++	++	++	++
CD49f	**α6**	+	+	-	-	(+)	(+)

Expression of a series of integrin and adhesion molecules in different ET cell lines after constitutive ITM2A suppression using flow-cytometric analysis. Semi-quantitative evaluation: – = no, (+) = faint, + = moderate, and ++ strong expression.

4.3.3. Knock-down of CHM1 and ITM2A increase bone invasiveness *in vitro* and *in vivo*

As previously demonstrated, the BRICHOS-family genes do not behave in the same manner in respect to general tumor growth, metastasis and invasiveness. Thus, the influence of the bone-associated genes *CHM1* and *ITM2A* on osteotropism was examined. Therefore, expression levels of previous genes associated with homing, invasion and colonization to bone (*CXCR4*, *PTHrP*, *RUNX2* and *TGFβ*; [188,221–230]) were analyzed in pSIREN^{CHM1}-, pSIREN^{ITM2A}- and pSIREN^{negsiRNA}-transfected ET cell lines using qRT-PCR. As demonstrated in the upper panel of Figure 50, suppression of CHM1 clearly reduced the expression levels of CXCR4 and RUNX2, but at the same time slightly increased the mRNA levels of TGFβ and PTHrP, whereas PTHrP-increase was especially observed in SK-N-MC cells. After ITM2A knock-down, the expression of all four genes was significantly reduced in SK-N-MC and TC-71 cells (see Figure 50). Only in A673 cells, down-regulation of ITM2A increased the mRNA expression levels of CXCR4 and PTHrP, as shown in the lower panel of Figure 50.

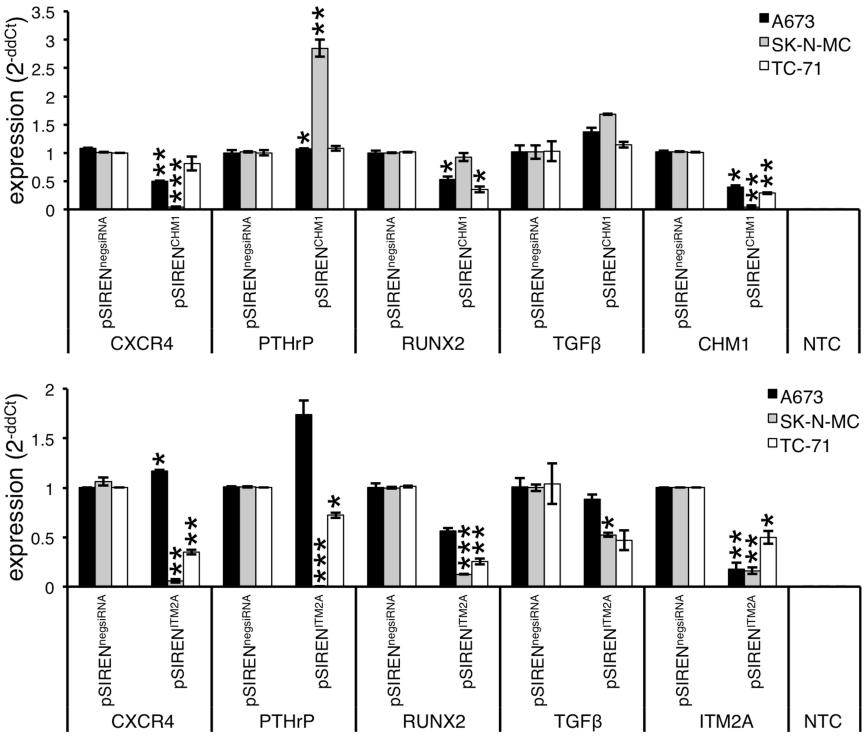

Figure 50: Expression of genes associated with bone colonization after CHM1 or ITM2A knock-down
qRT-PCR of ET cell lines constitutively transfected with pSIREN^{CHM1} or pSIREN^{ITM2A} and pSIREN^{negsiRNA}. *CXCR4*: *chemokine, cxc motif, receptor 4*; *PTHrP*: *parathytroid hormone-like hormone*, *PTHLH*; *RUNX2*: *runt-related transcription factor 2*; *TGFβ*: *transforming growth factor, beta-1*; *CHM1*: *chondromodulin 1*; *ITM2A*: *integral membrane protein 2A*. NTC: non template control. Data are mean ± SEM of three independent experiments; t-test (*p < 0.05; **p < 0.005; ***p < 0.0005).

Due to these ambiguous results, further *in vivo* analyses seemed necessary to determine the role of CHM1 and ITM2A in the process of colonization and invasion to bone, as well as osteolysis. Therefore, constitutively CHM1 or ITM2A transfected A673 cells were injected into the tibiae of immune deficient Rag2$^{-/-}\gamma c^{-/-}$ mice and bone infiltration and destruction was analyzed by X-ray radiography and histology (see 3.17). Interestingly, CHM1 as well as ITM2A knock-down showed no significant decrease in bone colonization and infiltration *in vivo*, compared to A673 pSIREN^{negsiRNA} cells, as demonstrated in Figure 51. In all three cases, bone infiltration was observed in about 80 % of the mice investigated (CHM1 and ITM2A: 4 / 5 mice; pSIREN^{negsiRNA}: 7 / 8 mice).

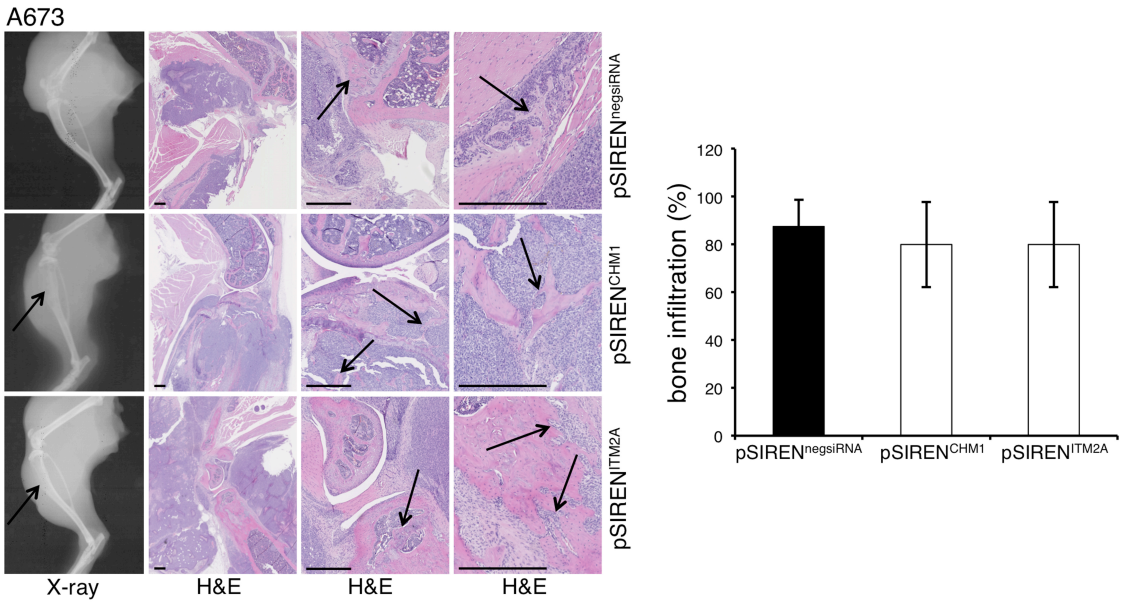

Figure 51: CHM1 or ITM2A knock-down increased bone invasiveness *in vivo*
Left panel: Analysis of bone invasiveness of constitutive A673 CHM1, ITM2A and nonsense shRNA infectants in an orthotopic bone xenotransplantation model (5 (CHM1 and ITM2A) and 8 (control) mice/group). Affected bones were assessed by X-ray radiography and histology (H&E, scale bar 0.5 mm). **Right panel:** Quantitative summary of mice exhibiting bone infiltration after intra-tibial injection (%). Data are mean ± SEM; t-test.

Furthermore, many mice developed severe osteolytic lesions, regardless of whether mice were injected with A673 pSIREN^{negsiRNA} (4 / 8 mice), pSIREN^{CHM1} (2 / 5 mice) or pSIREN^{ITM2A} (3 / 5 mice) cells. Suppression of CHM1 and ITM2A even enhanced the severity of the osteolytic lesions compared to respective controls, as demonstrated by the increased amount of osteoclasts in the tumor (see 3.18). As shown in Figure 52, the amount of osteoclasts was increased by up to 44.4 % after CHM1 (2.05 osteoclasts / mm^2) or up to 39.4 % after ITM2A (1.98 osteoclasts / mm^2) knock-down compared to A673 pSIREN^{negsiRNA} tumor samples (1.42 osteoclasts / mm^2). Interestingly, in tumors

injected with A673 pSIREN^{CHM1} and pSIREN^{ITM2A}, osteoclasts were found all over the tumor area with an accumulation close to the bone and the edge of the tumor comparable to control samples.

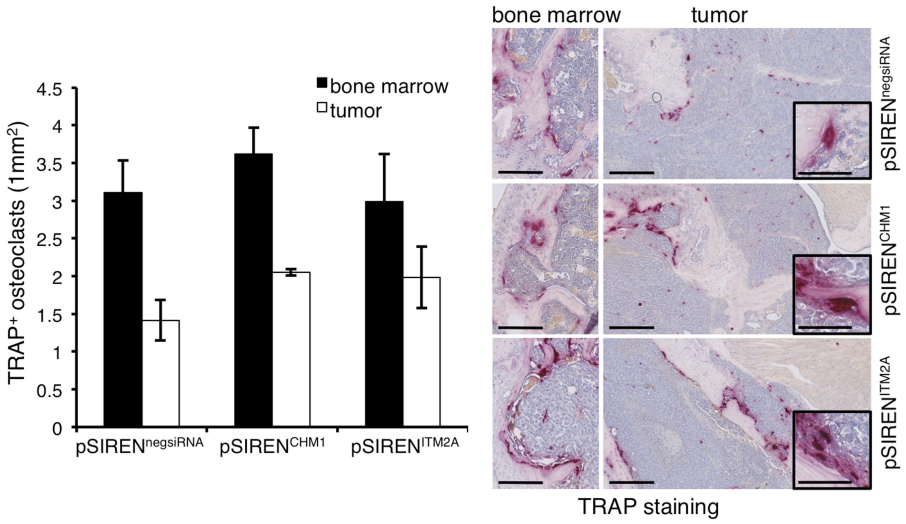

Figure 52: TRAP staining in tumor samples with CHM1 and ITM2A knock-down
Left panel: Quantitative summary of the average number of osteoclasts (mm^2) in unaffected bone marrow and tumor samples. Data are mean ± SEM of at least two independent samples (20 segments counted); t-test. **Right panel:** Analysis of osteolysis of A673 pSIREN^{CHM1} or pSIREN^{ITM2A} cells and negative controls in an orthotopic bone xenotransplantation model (5 - 8 mice/group). Affected bones were assessed by histology (TRAP staining, scale bar 0.25 mm or 0.05 mm). CHM1 and ITM2A knock-down significantly enhanced the amount of TRAP-positive osteoclasts in the tumor and thus increased the osteolytic phenotype.

Although, suppression of DKK2 and at least CHM1 show similar effects in ET phenotype, more precisely in ET growth and metastasis, the osteotropic behavior is completely different. Therefore, further analyses were necessary to get more information about the molecular mechanism of bone invasiveness and osteolysis in ETs, focusing on the role of the bone-associated genes *CHM1* and *ITM2A* compared to *DKK2*.

4.3.4. BRICHOS genes are involved in the chondro-osseous differentiation of ETs

One possible factor for the increased osteolysis after CHM1 and ITM2A knock-down might be a better localization to bone in combination with a change in the expression pattern of cancer cells, also known as osteomimicry. Therefore, three ET cell lines stably transfected with pSIREN^{CHM1}, pSIREN^{ITM2A} and pSIREN^{negsiRNA} were incubated with specific differentiation media to induce chondrogenic or osteogenic differentiation

(see 3.16.3 and 3.16.4). The differentiation potential was detected by qRT-PCR using specific marker genes [157]. As shown in Figure 53, expression of the chondrogenic marker genes *COL10A1* and *SOX9* was significantly increased after suppression of CHM1 and ITM2A compared to control cells, already without chondrogenic differentiation media. After incubation for 21 days, differentiation of pSIREN^{negsiRNA}-transfected cells into the chondrogenic lineage was successful, as demonstrated by the increased expression levels up to 79 % for COL10A1 and up to 62 % for SOX9 (see Figure 53). Although, the expression of these marker genes was generally higher in knock-down cells, the expression increase after incubation with specific media was significantly reduced after CHM1 and ITM2A silencing for up to 13 – 16 % (CHM1) and 3 – 5 % (ITM2A) compared to control cells (see Figure 53).

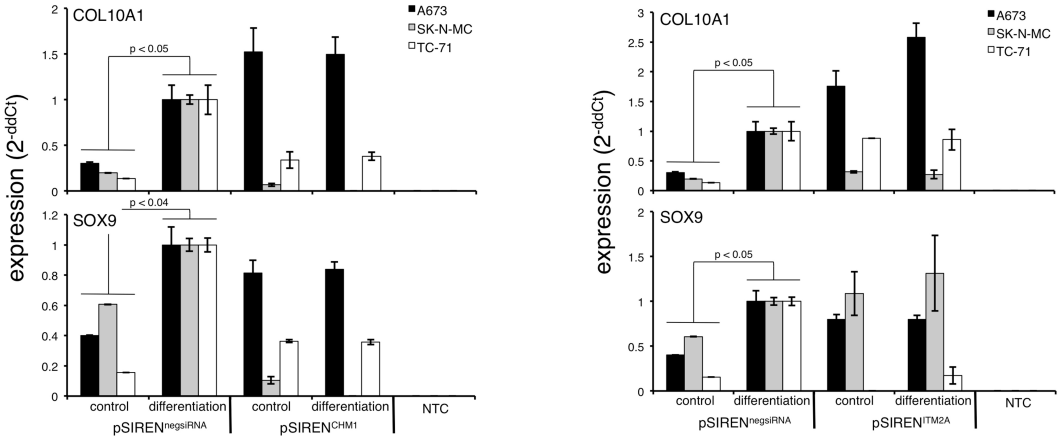

Figure 53: Expression of chondrogenic marker genes using qRT-PCR
Chondrogenic differentiation of ET cell lines with specific CHM1, ITM2A and nonsense shRNA constructs was shown by the expression of specific chondrogenic marker genes *COL10A1* (*collagen, type X, alpha-1*) and *Sox9* (*sry-box 9*) using qRT-PCR. Data are mean ± SEM of two independent experiments; t-test (p: p-value).

Similar to chondrogenic differentiation, expression levels of the osteogenic differentiation markers COL1A1 and OPN [157] were increased after BRICHOS-family gene knock-down under normal culture conditions, at least for A673 cells which were used in the *in vivo* experiment (see Figure 54). Interestingly, no differences were observed in the expression increase of the early marker gene *COL1A1* (42 - 47 %) after incubation for 14 days in osteogenic differentiation media. In contrast, increase of the mRNA levels of the late marker gene *OPN* was higher in cells transfected with control shRNA (75 %), than in CHM1 (53 %) or ITM2A (56 %) knock-down cells, as demonstrated in Figure 54. But due to the higher gene expression under normal conditions, ET cell lines with CHM1 or ITM2A knock-down seemed to be more differentiated than respective controls, especially in the chondrogenic lineage.

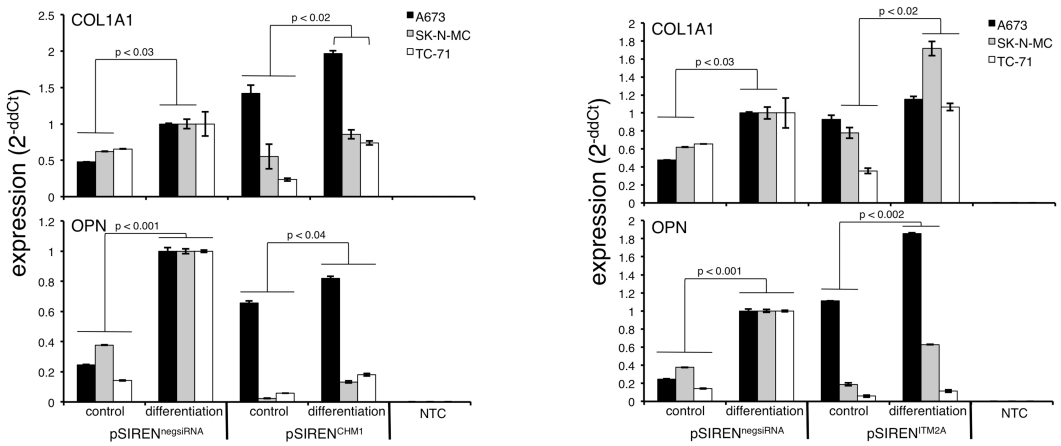

Figure 54: Expression of osteogenic marker genes using qRT-PCR
Analysis of osteogenic differentiation of ET shRNA infectants. Expression of the early (*COL1A1*: *collagen, type I, alpha-1*) and late (*OPN*: *secreted phosphoprotein 1, SPP1*) marker genes was shown by qRT-PCR. Data are mean ± SEM of two independent experiments; t-test (p: p-value).

Because suppression of CHM1 and ITM2A enhanced the differentiation status of ET cell lines, shown by increased expression of chondrogenic and osteogenic marker genes, BRICHOS-family genes might be important for the maintenance of an undifferentiated phenotype of tumor cells. To further examine this hypothesis, expression of different stem cell genes, namely *atp-binding cassette, subfamily g, member 2* (*ABCG2,* [237]), *homeobox transcription factor nanog* (*NANOG,* [238]) and *prominin 1* (*PROM1,* [239]), were analyzed in three ET cell lines with CHM1 or ITM2A knock-down and respective controls. As shown in Figure 55, knock-down of CHM1 and ITM2A decreased expression of at least two stem cell genes compared to pSIREN^{negsiRNA}-transfected cells.

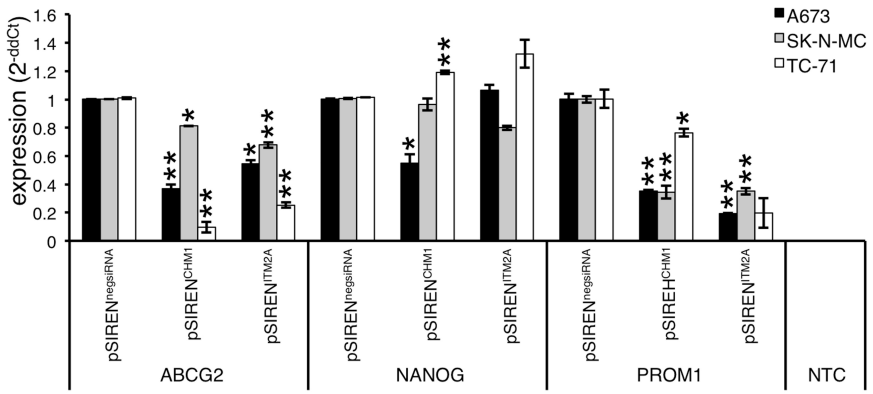

Figure 55: Expression of stem cell genes after CHM1 or ITM2A knock-down
mRNA levels of atp-binding cassette, subfamily g, member 2 (ABCG2), homeobox transcription factor nanog (NANOG) and prominin 1 (PROM1) in ET cell lines constitutively transfected with pSIREN^{CHM1}, pSIREN^{ITM2A} and pSIREN^{negsiRNA} were analyzed by qRT-PCR. NTC: non template control. Data are mean ± SEM of three independent experiments; t-test (*p < 0.05; **p < 0.005; ***p < 0.0005).

4.3.5. HIF1α, IL6, JAG1 and VEGF are important for osteolysis in ETs

Another obvious factor for the increased osteolytic phenotype of ET cell lines *in vivo* might be the different regulation of genes important for osteoclastogenesis and osteolysis by CHM1 and ITM2A. Although no significant differences so far were observed in the expression levels of genes associated with osteolysis (*RUNX2*, *PTHrP* and *TGFβ,* [224–226,229,230]) seven additional genes associated with the osteolytic phenotype (*M-CSF, RANKL, OPG, HIF1α, IL6, JAG1* and *VEGF*) were analyzed in pSIREN^{CHM1}-, pSIREN^{ITM2A}- and pSIREN^{negsiRNA}-transfected ET cell lines using qRT-PCR (see 3.4 and Table 11). Interestingly, the main components of osteoclast maturation (M-CSF, RANKL and OPG) exhibited a contradictorily expression pattern (see Figure 56). For example, knock-down of CHM1 significantly enhanced the expression of RANKL as well as the mRNA levels of its antagonist OPG. Furthermore, mRNA expression of M-CSF was enhanced in A673 cells but rather decreased in SK-N-MC cells after suppression of CHM1 and ITM2A.

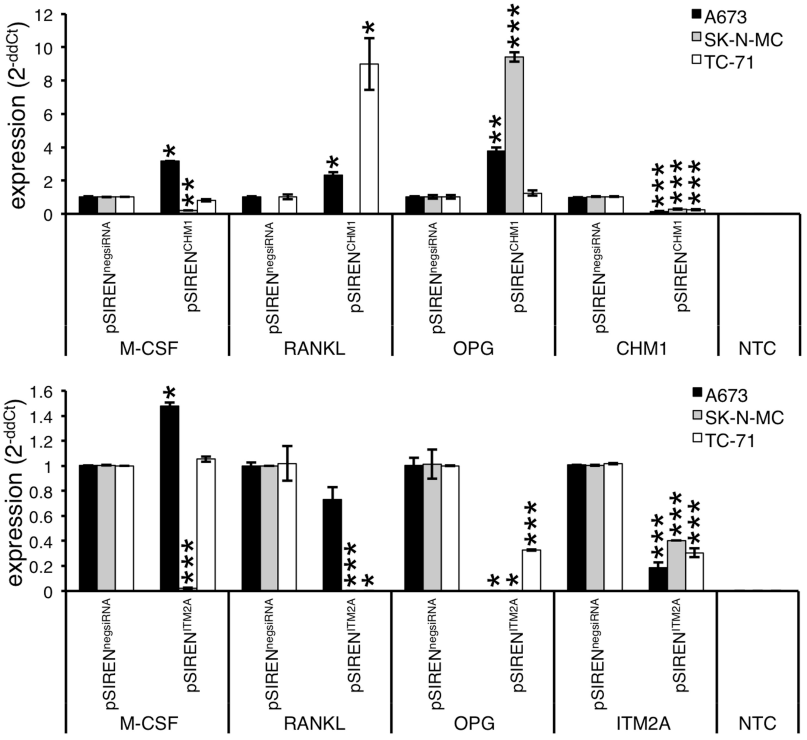

Figure 56: Expression of M-CSF, RANKL and OPG after CHM1 and ITM2A knock-down
Expression levels of M-CSF, RANKL and OPG in three different ET cell lines after constitutive suppression of CHM1 or ITM2A and respective controls. *M-CSF*: *colony-stimulating factor, macrophage-specific*; *RANKL: tumor necrosis factor ligand superfamily, member 11; OPG: tumor necrosis factor receptor superfamily, member 11B; CHM1: chondromodulin 1; ITM2A: integral membrane protein 2A.* NTC: non template control. Data are mean ± SEM of two independent experiments; t-test (*p < 0.05; **p < 0.005; ***p < 0.0005).

In contrast, CHM1 as well as ITM2A knock-down significantly increased the expression levels of the other osteolytic genes *HIF1α*, *IL6*, *JAG1* and *VEGF* [188,233–235] (see Figure 57), which could explain the severe osteolytic lesion observed *in vivo* (see Figure 51 and Figure 52).

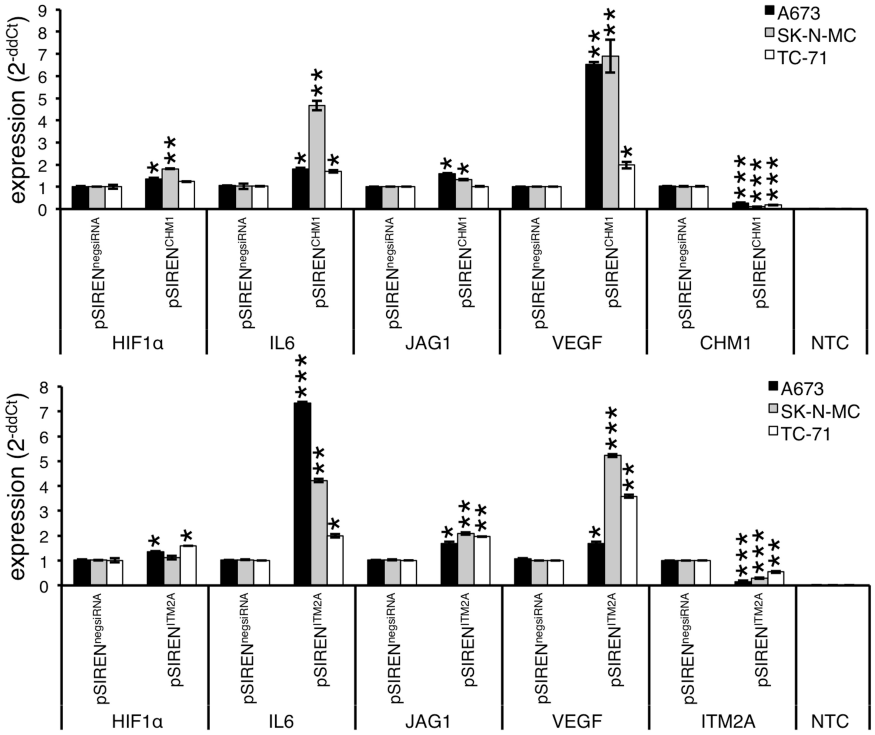

Figure 57: mRNA levels of osteolytic genes after CHM1 or ITM2A knock-down
Different ET cell lines with constitutive CHM1 or ITM2A knock-down and respective control were analyzed by qRT-PCR. *HIF1α*: *genes hypoxia-inducible factor 1, alpha subunit*; *IL6*: *interleukin 6*; *JAG1*: *jagged 1*; *VEGF*: *vascular endothelial growth factor receptor 1*; *CHM1*: *chondromodulin 1*; *ITM2A*: *integral membrane protein 2A*. NTC: non template control. Data are mean ± SEM of two independent experiments; t-test (*p < 0.05; **p < 0.005; ***p < 0.0005).

5. Discussion

5.1. Overexpression of bone-associated genes in Ewing tumors

ETs are primarily osteolytic bone tumors, mostly affecting children and young adolescence, characterized by early metastasis into lungs and bones [62]. Although prognosis of patients with localized disease has markedly improved in past decades, metastatic disease – present in about 25 % of ET patients at diagnosis – is usually associated with fatal outcome [42,45,47–49]. Especially the development of metastases in bones is a catastrophic event in the clinical course of ET patients [48,52]. To obtain more information about the fundamental molecular mechanisms of ET differentiation, invasion and bone localization, microarray data published by Staege *et al.* [55] were scanned for genes up-regulated in ETs compared to normal tissue, which may be important for bone development, formation and bone re-organization. Thereby, five bone-associated genes were identified (*CHM1*, *CYP26B1*, *DKK2*, *ITM2A* and *GDF10*). Due to high expression in a wide range of different ET samples (> 80 %) and simultaneously their low expression levels in only a few tissues of the NBA (< 46 %) *CHM1*, *DKK2* and *ITM2A* have been carefully selected for further investigation.

Because ETs are hardly distinguishable from other small-round-blue-cell tumors like leukemia, medulloblastoma and neuroblastoma, the author first analyzed, whether the selected genes are specifically overexpressed in ETs. For this purpose, mRNA expression of different small-round-blue-cell tumors (807 samples) and diverse ETs (154 samples) were examined using a comparative study of the amc onco-genomics software tool (www.amc.com). Furthermore, the results observed were confirmed for the cell lines investigated in this doctoral thesis using qRT-PCR. As demonstrated here, CHM1 and DKK2 are exclusively expressed in ET cell lines compared to other pediatric tumors of the same histological phenotype (see Figure 4 and Figure 5). This might be important, because there are only a few marker including CD99 antigen, X chromosome (CD99, [58]), friend leukemia virus integration 1 (FLI1, [60]) and caveolin 1 (CAV1, [61]), which are commonly expressed in ETs and differentiate them from other small-round-blue-cell tumors on the histological level. As shown by Staege *et al*. [55] and in this study, *CHM1* belongs to the group of genes with exclusive expression in almost all ETs that are not expressed at detectable levels in any normal tissue and therefore might be a good marker, too. Due to the results observed in this doctoral thesis, DKK2 might be used in routine pathology as an additional marker for ET diagnosis, based on its exclusive expression in ETs compared to other small-round-blue-cell tumors (see Figure 4 and Figure 5).

Since this study is focused on the question, which bone-associated genes, up-regulated in ETs, are involved in bone localization, invasion and metastasis, the expression levels of different ETs were analyzed compared to various samples of the most frequent pediatric bone tumor using qRT-PCR. Expression levels of CHM1, as well as ITM2A, are only enhanced in ETs, which was in part expected from the literature [240]. Interestingly, only DKK2 was additionally up-regulated in several osteosarcoma cell lines, supporting a specific role for DKK2 in bone localization and invasion (see Figure 5).

5.2. Influence of EWS-FLI1 in the regulation of bone-associated genes

Because ETs are genetically defined by chromosomal translocations that fuse the *EWS* gene and a member of the *ETS* family of transcription factors, an overexpression of particular genes may indicate that expression of these genes is dependent on the oncogenic fusion protein. Nevertheless, only 4 of 37 genes, which were found to be overexpressed in ETs by Staege *et al.* [55], are known EWS-FLI1 target genes, namely *cholecystokinin* (*CCK,* [241]), *cyclin D1* (*CCND1,* [242]), *enhancer of zeste, drosophila, homolog 2* (*EZH2,* [152,243,244]) and *six-transmembrane epithelial antigen of prostate* (*STEAP1*, [153]) Two out of the four genes (*CCK* and *CCND1*) are indirect targets and are involved in signaling pathways and gene regulation networks initiated by EWS-FLI1 [62], whereas *EZH2* and *STEAP1* might be direct targets of the oncogenic fusion protein [152,153]. Since no or only contradictory (*DKK2*) data about the EWS-FLI1 regulation of the bone-associated genes investigated are available in the literature, the influence of this transcription factor on *CHM1*, *DKK2* and *ITM2A* expression was examined in this doctoral thesis.

As can be seen in Figure 6, only *CHM1* is regulated by EWS-FLI1. Moreover, constitutive knock-down of CHM1 slightly decreased the expression of EWS-FLI1 in A673 and TC-71 cells, as well (see supplementary Figure 59), suggesting a mutual enhancement of the triggered effects. Interestingly, *CHM1* is the only one of the three genes, which is overexpressed in 100 % of ETs investigated by Staege *et al.*, just like *CCND1* and *EZH2* [55], two other known EWS-FLI1 target genes. Furthermore it was published, that CHM1 is also modulated by cell-specific epigenetic mechanisms [240,245,246] and post-translational modifications [118], as observed in chondrocytes or mesenchymal stem cells (MSCs). For instance, Aoyama *et al.* demonstrated, that expression of *CHM1* is regulated by binding of the transcription factor SP3 to the core promoter region, which is inhibited by methylation of CpG in the target genome

[240,245]. In addition, activity of SP3 is dependent on the acetylation status of associated histones, enhanced by E1A-binding protein 300 kDa (p300) and reduced by the transcriptional repressor YY1 [246].

With regard to DKK2, contradictory data are published. As reported by Miyagawa *et al*. [247], EWS-FLI1 might regulate *DKK2*. However, in line with the findings of Navarro *et al*. [248], the author demonstrated that DKK2 expression is independent of EWS-FLI1 (see Figure 6). Only in A673 cells a non-significant decrease in DKK2 mRNA levels was observed after transient suppression of EWS-FLI1. Microarray analysis with A673 cells performed by Navarro *et al*. also reiterates that the observed reduction of DKK2 expression is not significant [248]. Furthermore, DKK2 knock-down did not point out any differences on EWS-FLI1 expression levels compared to respective controls (see supplementary Figure 59). Variability of findings may depend on the cellular context as Miyagawa *et al.* used different ET cell lines than us and Navarro and colleagues [247,248]. Because EWS-FLI1 does not influence DKK2 mRNA levels, other mechanisms might be responsible for the regulation of DKK2. As demonstrated for different tumor entities, *DKK2* gene expression is regulated by epigenetic silencing via CpG island hypermetylation [90,92–95], which could also be important in ETs. In addition, there are also some genes implicated in the regulation of DKK2, for example the homeodomain transcription factors paired-like homeodomain transcription factor 2 (PITX2, [249,250]) and cut-like 1 (CUTL1, [251]) both known to play an important role in development and cell cycle progression.

Similarly to *DKK2*, *ITM2A* is not regulated by EWS-FLI1 and vice versa, as shown in Figure 6 and supplementary Figure 59. In rhabdomyosarcoma, gene expression of *ITM2A* is induced by the transcription factor paired box gene 3 (PAX3, [137]). As published by Schulte *et al.* [252], PAX3 may be present in most ETs indicating that this transcription factor might play a role in the regulation of ITM2A in ETs, too. Furthermore, van den Plas and Merregaert demonstrated that parathyroid hormone-like hormone (PTHrP) stimulates ITM2A expression, whether it has not yet been definitively resolved, whether the stimulatory effect is only important at late stages of the differentiation program or persists for longer periods [130]. In addition, analyses of the *ITM2A* promoter region revealed different potential binding sites for SP1, runt-related transcription factor 2 (RUNX2), sry-box 9 (SOX9) and cAMP response binding element (CREB) sequences [130,131,253].

5.3. Role of CHM1, DKK2 and ITM2A in ET pathogenesis

5.3.1. Influence on tumor growth and metastasis *in vitro* and *in vivo*

ETs are aggressive solid bone and soft tissue tumors, which metastasize to bone and lung tissues at a very early stage. Therefore, the author analyzed the role of CHM1, DKK2 and ITM2A in ET pathogenesis using different *in vitro* and *in vivo* assays. The *in vivo* assays were performed in NOD/scid or $Rag2^{-/-}\gamma c^{-/-}$ mice with a Balb/c background. These mice are immune deficient, but do not develop endogenous tumors enabling the analysis of tumor growth and metastasis of xenografted cancer cells [254,255].

First of all it was demonstrated, that CHM1 significantly induces proliferation *in vitro* and to a lesser extent *in vivo* in three different ET cell lines (see 4.3.1), but nevertheless this gene seems to have different effects dependent on the tumor entity. For example an overexpression of CHM1 significantly decreases DNA synthesis in HepG2 and HUVEC cells, but not in HeLa cells, as observed by Mera *et al*. [126]. Furthermore, CHM1 causes a clear suppression of tumor growth in athymic nude mice implanted with HepG2 or HT-29 as well as OUMS-27 cells [126,129]. In contrast, CHM1 enhances the proliferation of ETs in culture dishes and in $Rag2^{-/-}\gamma c^{-/-}$ mice, as demonstrated in Figure 40 and Figure 44. Interestingly, the CHM1-mediated effect on cell proliferation is clearly stronger *in vitro* than *in vivo*. Perhaps, this is because of the known function of CHM1 as an angiogenesis inhibitor [121–124,129], which could be demonstrated by the author in ETs, too (see supplementary Figure 60). Angiogenesis is a multistep process including degradation of the extracellular matrix, migration and proliferation of endothelial cells and, finally, tube formation, which is necessary to supply the tumor with sufficient nutrients [256–258]. Because the supply of cells plays only a limiting role in the *in vivo* assay, it might be possible, that the CHM1-mediated growth advantage is reduced by a poorer supplement of the tumor cells. This could explain the small differences observed *in vivo* after injection with $pSIREN^{CHM1}$- or $pSIREN^{negsiRNA}$-transfected cells. The effect of CHM1 on anchorage-independent colony formation seems also be dependent on the cell type. While overexpression of CHM1 reduces the number of colonies in HepG2 and HeLa cells, however without affecting the extracellular matrix-integrin complexes and their downstream molecules such as extracellular signal-regulated kinase (ERK), v-akt murine thymoma viral oncogene homolog 1 (AKT) and glycogen synthase kinase 3 beta (GSK3β) [126], the contrary effect is observed in chondrocytes [259,260] and ETs (see Figure 43). As shown in different other publications, CHM1 also significantly increases the proliferative behavior of chondrocytes and osteoblasts [119,259–261], which is similar to the effect observed by the author in respect to ETs (see Figure 40). This is quite interesting,

since ET cell lines are able to easily differentiate into the chondrogenic or osteogenic lineage, as demonstrated in this study (see Figure 53 and Figure 54). This may indicate, that ETs are possibly descending from a mesenchymal stem cell in transition to a more differentiated phenotype of the chondro-osseous lineage [53–57,62] and thus behave more like bone-associated cell types (for example chondrocytes and osteoblasts), than HUVECs or HepG2 cells [126]. Furthermore, CHM1 influences the metastatic behavior of ET cells *in vivo*. Especially the development of lung metastases was significantly decreased after injection with CHM1 knock-down cells, as demonstrated by Dr. Annette Fasan [236]. Surprisingly, no bone metastases could be observed after injection of A673, SK-N-MC or TC-71 cells into the tail veins of $Rag2^{-/-}\gamma c^{-/-}$ mice (see 4.3.1; [236]), although several publications demonstrated that this application method generates bone metastases after injection of ET cells [262–265]. But, there may be several reasons for these results: For example, the use of diverse mouse strains may explain the differences observed, more precise the absence of bone metastases in the experimental set-up used in this study. While the author worked with NOD/scid and $Rag2^{-/-}\gamma c^{-/-}$ mice (see Table 13), many other laboratories used athymic nude mice (Crl/nu/nu(CD1)BR; [263–265]) or another strain of NOD/scid mice (NOD/LtSz-$Prkdc^{scid}$/J; [262]). In addition, mice were pretreated in part with anti-asialo GM1 antiserum to deplete natural killer cells [263] or irradiated with a single dose of 3.5 Gray from a cobalt 60-unit 1 day before transplantation [262]. Although, the mouse strains investigated in this study are immune deficient and have only a very limited natural killer cell activity, maybe the tumor cells can easier metastasize into bone tissues due to the pretreatment. However, it should be noted, that the amount of bone metastases observed by other laboratories was very low indicating that the optimal experimental set-up has not been established so far. Nevertheless, intravenous injection is a useful tool to analyze the metastatic behavior of ET cells, with the exception of osteotropism.

With regard to DKK2, the oncogenic effect seems to be dependent on the tumor cells investigated, too. As shown in this study (see 4.2.1), DKK2 significantly increases cell proliferation, anchorage-independent growth and the oncogenic phenotype of ETs *in vivo*, which correlates with the *in vivo* findings of Miyagawa *et al.* observed in another ET cell line SK-ES1 [247]. However, overexpression of DKK2 decreases proliferation and colony formation in renal cell carcinoma (RCC) and colorectal cancer (CRC) cells *in vitro* [90,92]. In both tumor entities *DKK2* is epigenetically silenced by methylation and function in this cellular context as a Wnt antagonist [71,90,92]. In contrast, DKK2 is clearly overexpressed in ETs and seems to be a Wnt agonist, as demonstrated in this study (see 4.2.3). This could be the crucial point explaining the various effects of

DKK2, because a wide range of different Wnt target genes are involved in the regulation of cell proliferation, anchorage-independent colony formation and metastasis. Genes important for the proliferative behavior include, for example, *CCND1, lymphoid enhancer-binding factor 1* (*LEF1*) or *matrix metalloproteinase 7* (*MMP7*), which are all up-regulated after activation of the Wnt pathway [110,196,200,266]. Further studies have shown that the Wnt target genes *v-myc avian myelocytomatosis viral oncogene homolog* (*c-MYC*, [112,267]) and *insulin-like growth factor I* (*IGF1,* [268]) promote contact independent growth, while *E-cadherin* (*CDH1)*, which was down-regulated by the Wnt signaling pathway, reduces the ability of tumor cells to grow anchorage independent and to invade through Matrigel [269–272]. These findings are in line with the significantly decreased proliferative and metastatic behavior of ETs *in vitro* and *in vivo* after suppression of DKK2 observed in this study (see 4.2.1). Thus, it can be concluded, that a different regulation of the Wnt signaling pathway via DKK2, which seems to be dependent on the cellular context, might result in a different oncogenic phenotype.

While CHM1 and DKK2 are very important player in ET pathogenesis, the effect of ITM2A is not clear. Although, ITM2A significantly promotes anchorage-independent colony formation, the proliferative behavior of ETs *in vitro* as well as tumorigenicity *in vivo* is decreased by ITM2A (see 4.3.1). This is quite interesting, because ITM2A is highly overexpressed in ETs, which belong to the group of fast growing tumors. But ITM2A does not increase the proliferation rate in undifferentiated myoblast C2C12 cells, too, as published by van den Plas *et al.* [136]. Furthermore, the author demonstrated that ITM2A clearly increases the number of lung metastases, with a simultaneous reduction of the metastatic area (see Figure 46). This observation is in line with the *in vitro* results, because although ITM2A significantly increases contact-independent colony formation (see Figure 43), the proliferation rate is decreased by ITM2A (see Figure 41). Therefore, overexpression of ITM2A might be beneficial to ETs, however the proliferative behavior is reduced.

5.3.2. *In vitro* invasion of ETs is regulated by MMPs

Metastatic spread significantly reduces long term survival of patients, because of the existence of micrometastases, metastatic dormancy and in these context inadequate therapeutic approaches [49,50,177]. Research into the mechanisms of invasion and metastasis has accelerated dramatically over the past decade and different possible

mechanisms were identified [177]. As already mentioned, especially ETs are highly malignant tumors with early metastasis.

Therefore it is very interesting, that CHM1, DKK2 as well as ITM2A promote the invasive potential of ETs *in vivo*, especially metastasis into the lung (see 4.2.1 and 4.3.1). To get more information about the underlying molecular mechanisms of ET invasiveness, microarray analyses on human Gene ST arrays (Affymetrix), were performed to identify possible downstream targets that are presumably involved in metastasis. Although, no genes associated with the metastatic potential of tumor cells could be identified in the top 30 regulated genes in respect to CHM1 and ITM2A (data not shown), microarray results reveal some interesting genes for DKK2 (GSE36100).

One possible candidate is CDH1, a key cell-cell adhesion molecule, which is down-regulated by DKK2 and which has a strong anti-invasive and anti-metastatic role in tumor progression [177–179]. Possible functional implications include the sequestering of β-catenin in an CDH1-catenin adhesion complex, leading to inhibition of the canonical Wnt pathway [179,273]. Other genes associated with invasion and metastasis, are enhanced by DKK2 such as *CD44* - an integral cell membrane glycoprotein. As CD44 promotes cell proliferation, invasion and migration, it's up-regulation in ET cell lines may in part explain different other phenotypes observed in this study, too (see 4.2.1 and 4.2.2, [180–182]). The best-known CD44 ligand is hyaluronic acid [180]. However, Weber *et al.* demonstrated that secreted phosphoprotein 1 (OPN) is another potent ligand of CD44 [181]. OPN is secreted by tumor cells and promotes bone marrow cell recruitment and tumor formation in bones [188,274]. Moreover, CD44-OPN ligation may be exploited by tumor cells to enable OPN-mediated metastatic spread and hyaluronate-dependent growth in newly colonized tissues such as bones [181]. This could be important, because ETs are usually bone tumors. In addition, invasion of ET cells may also be promoted by the intercellular adhesion molecule 1 (ICAM1), which is important for the extravasation of circulating tumor cells during metastasis [183]. Finally, the matrix metalloproteinases MMP1 and MMP7, both of which are zinc-dependent endopeptidases with crucial roles in migration and invasion [186–191], are suppressed after DKK2 knock-down. Furthermore, Fuchs *et al.* could show that MMP1 seems to be directly activated by the ET-associated oncoproteins EWS-FLI1 and EWS-ER81 [275]. Of note, four of the five validated DKK2 target genes are associated with bone colonization, bone invasion and osseous differentiation, which is interesting in the pathophysiological context of ETs that frequently arise in and metastasize into bones.

As previously reported MMPs seem to be important for the invasive potential of different tumor cells [177,188] and in particular for ET invasiveness [153]. To further examine this observation, the invasive behavior of three pSIREN^{CHM1}-, pSIREN^{DKK2}- or pSIREN^{ITM2A}-transfected ET cell lines was analyzed compared to respective pSIREN^{negsiRNA}-transfected cells using Matrigel-covered transwell assays. Simultaneously, the author analyzed the invasiveness of ET cell lines after transient knock-down of different MMPs and the related mRNA expression pattern of MMP1, MMP7 and MMP9 after suppression of bone-associated genes. Interestingly, only MMP1 and MMP9 could influence the invasive potential in ETs (see Figure 17 and Figure 49).

As demonstrated in this study, CHM1 slightly promotes invasiveness when subjected to Matrigel-covered transwell assays, although the effect of CHM1 in respect to lung metastasis is much greater *in vivo*. Moreover, CHM1 enhances the expression levels of MMP9, but not of the other MMPs investigated, indicating an essential role of MMP9 in ET invasiveness (see Figure 47 and Figure 48). This observation is confirmed by different publications, as MMP9 is an important factor associated with invasion in many other tumor entities, like breast and prostate cancer [276–279]. Only long-term suppression of MMP9 in complimentary mouse models of pancreatic neuroendocrine carcinogenesis seems to increase invasion *in vivo* [280].

DKK2 clearly enhances the invasive behavior of ET cell lines, as well (see Figure 17). But in contrast to CHM1, DKK2 does not affect the expression of MMP9, but significantly enhances mRNA levels of MMP1. Thus MMP1 is responsible for the reduced invasiveness after DKK2 knock-down *in vitro*. Due to the greater influence of DKK2 on invasion *in vitro* and *in vivo*, the experimental data suggest, that MMP1 is a stronger regulator of ET invasiveness than MMP9. This suggestion is supported by Grunewald *et al*., because MMP1 is an important regulator in STEAP1-mediated tumor growth on Matrigel, too [153]. However, MMP1 (and MMP9) could not be the only relevant gene in ET invasion and metastasis, because in SK-N-MC cells the metastatic potential after DKK2 knock-down is reduced by up to 94 %, in comparison to 48 % after suppression of MMP1. For that reason, the other DKK2-dependent genes associated with invasion and metastasis, like *CDH1*, *CD44* and *ICAM1*, also seem to influence the metastatic potential in ETs (see Figure 16).

Regarding ITM2A, the number of invasive cells is suppressed in A673 and TC-71 cells, but increased in SK-N-MC cells (see Figure 47). Furthermore, ITM2A clearly decreases MMP1 and MMP9 mRNA expression in A673 and TC-71 cells and increases the expression levels in SK-N-MC cells, suggesting that MMP1 as well as MMP9 influence

ET invasion. These *in vitro* results accurately represent the metastatic spread of ET cell lines into the liver dependent on ITM2A expression (see Figure 46), which might indicate, that Matrigel-covered transwell assay (BioCoatTM Angiogenesis System) is only useful to predict the invasive potential resulting in liver metastases *in vitro*. The arguments in favor of that are very strong. Due to the structure of hepatic tissue, macromolecules like tumor cells don't have to overcome barriers such as membranes and basal laminas underneath the endothelium. The liver capillaries are instead surrounded by a discontinuous endothelium composed of liver sinusoidal endothelial cells (LSEC, [281]), which enable the tumor cells to be passively transported into the liver. Similarly to liver tissues, a structural barrier, comparable with a membrane, is also absent in the invasion assay used. This would also explain why influence of CHM1 on cell invasion is relatively low *in vitro*, while the effect *in vivo* is significantly higher in respect to lung metastases. However, CHM1 slightly promotes liver metastasis, which is in line with the *in vitro* results.

5.3.3. DKK2 seems to be a Wnt agonist

Wnt/β-catenin signaling pathway plays important roles in a wide range of developmental and physiological processes during embryogenesis and in adult organisms [71,100–103]. Furthermore, this pathway is closely linked to tumorigenesis [104–107], including colon cancer, malignant melanoma and prostate cancer, as well as ETs [84]. As previously reported, members of the dickkopf family typically antagonize Wnt/β-catenin signaling, by inhibiting the Wnt co-receptors LRP5 and LRP6 resulting in β-catenin degradation [71]. While DKK1 acts as a pure inhibitor of Wnt/β-catenin signaling, DKK2 can either function as a Wnt agonist or antagonist, depending on the cellular context [71,80,81], whereas the role in ETs has still not been resolved.

In this study, the author elucidated for the first time the function of DKK2 in the regulation of Wnt/β-catenin signaling in ETs, demonstrating that DKK2 seems to be a Wnt agonist. The expression analysis of different Wnt target genes using qRT-PCR demonstrated the enhancement of one (*CDH1*) and a significant suppression of seven different target genes (*CCND1*, *CD44*, *EPHB2*, *ID2*, *JUN*, *LEF1* and *MMP7* [109–111,192–201]) in three ET cell lines constitutively transfected with DKK2 shRNA (see Figure 16 and Figure 18). Additionally, four genes associated with homing and colonizing into bone as well as osteolysis are also known Wnt target genes, which are enhanced by DKK2 probably via activation of the Wnt/β-catenin signaling pathway, namely *IL6* [282], *JAG1* [283], *RUNX2* [284] and *VEGF* [285] (see Figure 31 and Figure

33). These experiments gave a first important hint about the agonistic role of DKK2 in Wnt signaling, but the molecular background so far remains elusive. To get an insight into the underlying mechanism, the author first focused on the Wnt co-receptor LRP6, because it was published, that DKK2 can activate canonical Wnt signaling pathway in the presence of high LRP6 protein concentrations [80–82]. Therefore, the amount of LRP6 in ET cell lines transfected with pSIREN^{DKK2} and pSIREN^{negsiRNA} was examined on protein level. Western blot analysis demonstrated that LRP6 is highly expressed in all ET cell lines investigated and, in addition, that DKK2 even seems to enhance the amount of this protein (see Figure 19). Further experiments are necessary to verify this observation and to get more information about the molecular mechanisms involved. With respect to DKK2-LRP6 interactions, it is yet known, that the extracellular domain of LRP6 seems to be autoinhibitory, because its depletion yields a constitutively active receptor [286,287]. Binding of the DKK2 colipase fold to LRP6 may induce a conformation where this autoinhibition is blocked, leading to receptor activation [80]. In contrast to DKK2, DKK1 binding to LRP6 via its colipase fold can't prevent this inhibitory effect, because of its DKK_N domain [81], why DKK1 can only act as a Wnt antagonist. In addition, Wu *et al*. demonstrated that DKK1 can inhibit Wnt activation via DKK2-LRP6 [288]. However, expression levels of DKK1 are very low in ETs, as shown in supplementary Figure 61. Thus, influence of DKK1 on DKK2-LRP6 mediated Wnt-activation can be neglected. But there is another factor, which can inhibit the receptor activation via DKK2-LRP6: the high affinity DKK receptor Kremen 2 (KRM2) [71,82,83,289]. In the presence of KRM2, DKK2 binds with its N-terminus (DKK_N) to KRM2 and the DKK2-LRP6 receptor complex may be internalized by endocytosis and thus activation of the Wnt signaling pathway is inhibited [82]. As demonstrated in this study, KRM2 is only expressed at very low protein concentration in ETs (see Figure 19). Thus DKK2 seems to be able to activate Wnt/β-catenin signaling, which was expected with regard to the Wnt target gene expression data. These results are also confirmed by the decreased amount of β-catenin observed in the cytoplasmic and the nucleic fraction of DKK2 knock-down cells (see Figure 20 and Figure 21). Because receptor activation of Wnt/β-catenin signaling first results in a cytoplasmatic stabilization and accumulation of β-catenin, which is then located into the nucleus and heterodimerizes with the TCF/LEF1 transcription complex to regulate target gene expression [35,108,290].

5.3.4. DKK2 knock-down increases apoptosis in ETs

As previously described, microarray analyses on human Gene ST arrays (Affymetrix) were performed to learn more about the downstream mechanisms of CHM1, DKK2 and ITM2A. In the first step, the top regulated genes were analyzed more closely, especially in respect to genes important for metastasis (see 4.2.2 and 5.3.2). Subsequently, gene set enrichment analysis (GSEA) was used to identify functional gene families, which are significantly influenced in their entirety after gene knock-down; even though the single genes are not under the top 30 regulated genes (see supplementary Figure 62).

Although, CHM1 and ITM2A exhibit no clearly regulated gene sets, which could explain the oncogenic phenotype of ETs (data not shown), set-to-set analysis of leading edge top ranked down-regulated gene sets (C5_all, v3.0) reveal a strong over-representation of gene sets involved in anti-apoptotic pathways after transient suppression of DKK2. The author could verify these findings in different ET cell lines with constitutive DKK2 knock-down analyzing gene expression of two genes, which were present in the down-regulated gene sets. Both genes investigated belong to the BCL2-familiy (B-cell cll/lymphoma 2) of anti-apoptotic proteins and were significantly suppressed after DKK2 knock-down (see Figure 23). The first one, bcl2-like 1 (BCL2L1), is the protein product of the larger mRNA of the *BCL-X* gene [205], which inhibits the release of apoptogenic cytochrome c through the mitochondrial channel VDAC by binding to it directly [204]. Furthermore, the NF-κB target gene *BCL2L1* blocks the pro-apoptotic activity of BH3 domain-only proteins, like bcl2-like 11 (BCL2L11) or bh3-interacting domain death agonist (BID) [203,291–293]. The second anti-apoptotic protein is myeloid cell leukemia sequence 1 (MCL1), which also seems to be regulated by mir-29 and the tumor suppressor protein SKP1-cullin-1-F-box complex that contains FBW7 as the F-box (SCF (FBW7)) [294,295]. MCL1 interacts with BCL2L11, BID and bcl2-associated x protein (BAX) to protect cells from apoptosis [296–298] and has an effect on cell cycle progression, too [295]. Thus, DKK2-mediated up-regulation of these anti-apoptotic genes is able to prevent cells from apoptosis leading to a further survival benefit of ETs. To analyze this observation in more detail, the author demonstrated in an *in vitro* assay, that DKK2 really reduces the number of apoptotic and necrotic cells using the Annexin V-PE Apoptosis Detection Kit I. Moreover, this observation could be confirmed in various murine lung and liver metastases *in vivo* by the detection of the cysteine-aspartic acid protease caspase 3, which is essential in the execution-phase of cell apoptosis. The results observed are not surprising, because it was previously reported, that members of the dickkopf family are involved in the regulation of apoptotic

cell death. In different studies, it could be shown, that both DKK1 and DKK3 are able to inhibit apoptosis by decreasing caspase activity and by suppression of BAX expression levels [299–301]. In contrast, Hirata *et al.* demonstrated that DKK2 inhibits renal cancer progression through apoptotic pathways [92]. However, DKK2 function as a Wnt antagonist in renal cancers [92], while in ETs DKK2 is a Wnt agonist as demonstrated in this study (see 4.2.3). Maybe the different role in Wnt signaling can explain the diverse phenotypes observed. This supposition is also confirmed by the fact, that some Wnt target genes up-regulated by DKK2 are also known to inhibit apoptosis, indicating that DKK2 suppresses cell death not only via the enhancement of defined anti-apoptotic genes. One of the Wnt target genes increased by DKK2 is *CD44* (see Figure 16 and 4.2.3), which inhibits apoptotic cell death possibly through MCL1 in different tumor entities, for example in colon carcinoma or CLL cells [182,302–304]. Furthermore, *ID2* [305], *LEF1* [306–308] and *VEGF* [309–311] are also genes activated by DKK2 via the Wnt/β-catenin signaling pathway and play an essential role in cell survival mechanisms (see Figure 18 and Figure 33). In contrast to the current data, Kang *et al.* demonstrated that CDH1 mediates suppression of anoikis through activation of v-erb-b2 avian erythroblastic leukemia viral oncogene homolog 4 (ERBB4) in ET cell lines grown in spheroid cultures [312]. CDH1 is down-regulated by DKK2 through activation of the Wnt/β-catenin signaling pathway (see Figure 16) and has a strong anti-invasive and anti-metastatic role in tumor progression [177–179]. Thus it was expected, that CDH1 rather induces detachment-induced cell death in ETs than suppresses anoikis, as observed in many other tumor cells [269–271,313]. Perhaps, the divergent phenotypes result from the different experimental set-up, because Kang *et al.* analyzed multicellular spheroids grown in suspension [312], while the author used adherent ET cell lines. Furthermore, the functional CDH1 downstream target ERBB4 is not enhanced in ETs after DKK2-mediated CDH1 up-regulation (data not shown, GSE36100) indicating a different mechanism for the increased expression of ERBB4, maybe due to the different experimental set-up used by Kang *et al*. [312].

5.3.5. Suppression of DKK2 influences neuronal differentiation *in vitro*

In addition to the clustering of the down-regulated gene sets (see Figure 22), set-to-set analysis of the up-regulated gene sets (C5_all, v3.0) revealed a strong over-representation of gene sets involved in neuronal differentiation and development after DKK2 knock-down (see Figure 26). At first, the author could confirm this prediction in three ET cell lines constitutively transfected with pSIREN^{DKK2} using qRT-PCR analysis, as shown in Figure 27. For this purpose, overexpression of three leading edge genes,

which are all involved in neurogenesis, were examined, namely *glial fibrillary acid protein* (*GFAP*)*, nerve growth factor receptor* (*NGFR*) and *slit, drosophila, homolog of, 2* (*SLIT2*). The first one is the intermediate-filament protein GFAP, which is exclusively expressed in neuronal tissues like immature oligodendrocytes and cells of the astroglial lineage [207,208] and thus function as a prototype antigen in nervous tissue identification [314]. NGFR is one of two receptor types of neurotrophins and is important for neuronal cell survival and differentiation [209–211,315]. The last gene investigated is *SLIT2*, which participates in the formation of the nervous and endocrine systems by protein-protein interactions [212–214] and further inhibits tumor growth and invasion [316,317]. To further verify the observed data on protein level, neuronal differentiation assay was performed using stably pSIREN^{negsiRNA}- and pSIREN^{DKK2}-transfected ET cell lines. As demonstrated in this study, only DKK2 knock-down cells are able to induce the typical neurogenic cell fibers and to fully differentiate into the neurogenic lineage as demonstrated by the expression of GFAP as well as growth-associated protein 43 (GAP43), a protein exclusively expressed on the synaptosomal membrane of nerve tissues [215,216] (see Figure 28). Interestingly, all genes involved in neurogenesis are not only regulated by DKK2, but are also known EZH2 target genes, as demonstrated in different tumor cells [317,318], even for ETs [152]. *EZH2* in turn is a direct target of EWS-FLI1, as shown by Richter *et al.* [152]. But as demonstrated in this study, *DKK2* is not regulated by EWS-FLI1 (see Figure 6), indicating an independent regulatory mechanism of neuronal genes indirectly by EWS-FLI1 via EZH2 and maybe directly by DKK2. Furthermore, it is possible, that DKK2 in addition regulate the differentiation potential of ETs indirectly via EWS-FLI1. The transcription factor RUNX2, which is enhanced by DKK2 (see Figure 31), bind to the oncogenic fusion protein EWS-FLI1 and blocks the differentiation potential of tumor cells, especially into osteoblasts [319]. This interaction maybe fostered by a DKK2-dependend RUNX2 suppression and thus promote the differentiation of ET cells, which could explain the increased neuronal differentiation of ET cells after DKK2 knock-down demonstrating that not only EWS-FLI1 driven histone methyltransferase EZH2 influences the differentiation potential of ETs [152]. Conversely, the DKK2 homolog and putative functional antagonist DKK1 seems to stimulate neurite outgrowth in ET cell lines, as demonstrated by Endo *et al.* [320].

5.3.6. Influence of bone-associated genes on angiogenesis

Angiogenesis is a critical factor for tumor growth and metastasis. Like normal tissues, tumor cells require nutrients and oxygen as well as an ability to evacuate metabolic

waste and carbon dioxide [177]. Above a tumor size of 1 – 2 mm in diameter passive diffusion from the preexisting vasculature fails to provide the necessary supply [177,256–258]. Therefore, the tumor and accessory cells like fibroblasts and macrophages secrete different factors that induce angiogenesis and to initiate the “angiogenic switch” [321]. The change from an avascular to a vascular phenotype is a multistep process including degradation of the extracellular matrix, migration and proliferation of endothelial cells and, finally, tube formation [177,256–258].

In previous studies it was demonstrated, that ITM2A [136] and DKK2 [217,299], as well as other members of the dickkopf family [322–324], promote tube formation in various tumor entities. Nevertheless, the author could not detect any differences in the angiogenic behavior of ET cell lines transfected with pSIREN^{negsiRNA} and pSIREN^{DKK2} or pSIREN^{ITM2A} (see Figure 29 and supplementary Figure 63), even though different DKK2 and ITM2A target genes are also known to influence angiogenesis, for example *MMP1* and *VEGF* [191,325]. This may have been due to the cell line investigated, which is hardly differentiable into the endothelial lineage. In contrast, CHM1 is a known angiogenesis inhibitor responsible for the avascular phenotype of cartilage [121–124,129]. Knock-down of CHM1 enables the endothelial differentiation of different cells, which could be also demonstrated by the author for ET cells in a tube formation assay (see supplementary Figure 60).

5.3.7. Regulation of chondrogenic and osteogenic differentiation *in vitro*

As demonstrated in this study, bone-associated genes regulate the neuronal and endothelial differentiation of ETs. Due to the known influence of CHM1 [125,127,261,326], DKK2 [76,85,87] and ITM2A [130,132,133,135] in chondro- and osteogenesis, it is quite interesting, whether the bone-associated genes investigated are important for the differentiation into bone lineages, too. Furthermore, the chondro-osseous differentiation potential of ET cells might also be relevant for tumor pathology, because osteomimicry is an essential factor for tumor localization in bone [188] and in addition, 37 % of ET patients show increased intra-osseous density or diffuse sclerosis [218]. To analyze this question, stably transfected A673, SK-N-MC and TC-71 cells were incubated with specific differentiation media for up to 21 days and differentiation was validated by the expression of known marker genes using qRT-PCR (see 3.16.3 and 3.16.4).

To check chondrogenic differentiation capacity in ET cell lines, two specific marker genes were chosen: *SOX9* and *collagen, type X, alpha 1* (*COL10A1)*. SOX9 is an early

transcription factor of chondrogenesis, which aggregates with various other proteins, like cAMP response element-binding protein 1 (CREB/p300, [327]) or c-musculo-aponeurotic fibrosarcoma (c-MAF, [328]), and activates the expression of different collagens (such as COL2A1 or COL10A1), aggrecan and cartilage link protein [157]. COL10A1 is expressed in the late differentiation phase and thus can be used to identify terminally differentiated hypertrophic chondrocytes [329,330]. As shown in Figure 30 and Figure 53, knock-down of different bone-associated genes significantly reduce the chondrogenic differentiation potential of all three ET cell lines up to 3 – 5 % (ITM2A) compared to control cells, although Boeuf *et al.* observed, that overexpression of ITM2A inhibits chondrogenic differentiation in MSCs [133]. This observation is in line with the current knowledge, that the genes investigated, especially ITM2A, are important for the initiation of chondrogenic differentiation, maturation and proliferation probably through the regulation of various target genes [76,125,135,136]. For example, the early phases of chondrogenesis are among other things associated with increased TGFβ [9] and PTHrP expression [19], while the hypertrophic phase is regulated by RUNX2 and characterized by the expression of COL10A1 (see 1.1). Interestingly, only expression of RUNX2 is clearly decreased after suppression of CHM1, DKK2 and ITM2A as demonstrated in this thesis (see Figure 31 and Figure 50). Furthermore, TGFβ and PTHrP are additionally down-regulated after DKK2 and to a lesser extend after ITM2A knock-down, but suppression of CHM1 does not affect the expression of TGFβ and even enhance the mRNA levels of PTHrP (see Figure 31 and Figure 50). Thus, chondrogenic differentiation capacity seems to be mainly regulated by RUNX2 and with respect to the early differentiation phases in part via TGFβ.

To quantify osteogenic differentiation potential of ETs, expression levels of COL1A1 and OPN were analyzed using qRT-PCR. *COL1A1* (*collagen, type I, alpha 1*) is activated by the transcription factor RUNX2 and belongs to the early markers of osteogenic differentiation [253,331]. In contrast, OPN is known to be expressed later in the differentiation phase [157]. This protein can bind to hydroxyapatite and is involved in the binding of osteoclasts to the surface of the mineralized bone matrix [22]. As demonstrated in this doctoral study, the early and late differentiation potential of ET cells is significantly enhanced by DKK2 (see Figure 30). This is in line with the findings of Li *et al*. that DKK2 promotes the expression of OPN in calvarial osteoblasts [87]. CHM1 and ITM2A only influences the osteogenic differentiation capacity of ET cell lines in the late phase, as measured by the reduced OPN enhancement after CHM1 and ITM2A knock-down (see Figure 54). Due to the lower RUNX2 expression after CHM1, DKK2 and ITM2A knock-down (see Figure 31 and Figure 50), the observed effect may be again mediated at least in part by RUNX2 since this protein promotes

chondrogenic as well as osteogenic differentiation and similarly suppression of RUNX2 abrogates cell differentiation potential [188,319,332].

Furthermore, it is very interesting, that expression of chondrogenic and osteogenic (especially in A673 cells) marker genes is significantly increased after suppression of CHM1 and ITM2A compared to control cells, already without specific differentiation media (see Figure 53 and Figure 54). In contrast, DKK2 knock-down significantly reduces the expression of known marker genes, as can be seen in Figure 30. The expression of genes normally restricted to genes within the bone is called osteomimicry and enables tumor cells to avoid detection by the immune system. Furthermore, the cells are able to attach to the bone surface and to better colonize and proliferate in the bone microenvironment as possibly mediated by DKK2 [333]. All characteristics mentioned may be important in the pathophysiological context of ETs, thus it is surprising that knock-down of genes up-regulated in ETs (*CHM1* and *ITM2A*) promote osteomimicry. The enhanced mRNA levels of COL1A1, COL10A1, OPN and SOX9 after CHM1 and ITM2A knock-down further indicate a more differentiated phenotype of the cells, compared to pSIREN^{negsiRNA}-transfected cells. Perhaps, the strongly differentiated phenotype of pSIREN^{CHM1}- and pSIREN^{ITM2A}-transfected ET cells even under normal culture conditions may additionally inhibit further differentiation into the chondrogenic and osteogenic lineage, as can be seen in Figure 53 and Figure 54. To further investigate this question, the author analyzed the expression of different stem cell genes, namely *atp-binding cassette, subfamily g, member 2* (*ABCG2)*, *homeobox transcription factor nanog* (*NANOG)* and *prominin 1* (*PROM1)*, in ET cell lines constitutively transfected with pSIREN^{CHM1}, pSIREN^{ITM2A} and pSIREN^{negsiRNA}. The first one, ABCG2 belongs to the ATP-binding cassette (ABC) superfamily of membrane transporter and is expressed in a wide variety of stem cells [237]. The membrane-associated transporter plays an important role in the multidrug resistance phenotype of many cancer cells by actively exporting a wide variety of drugs across the plasma membrane [334]. The transcription factor NANOG is able to maintain embryonic stem cell self-renewal and pluripotency [238]. The last gene investigated, *PROM1* (also known as AC133 antigen) was originally identified as a marker of hematopoietic stem cells [335,336]. It is a five-transmembrane glycoprotein, which is expressed in embryonic and adult stem cells as well as cancer stem cells and maintains stem cell properties by suppressing differentiation [239]. As demonstrated in Figure 55, CHM1 and ITM2A increase the expression of at least two stem cell genes indicating a critical role of these BRICHOS-genes in maintaining an undifferentiated phenotype of ETs.

ET cells of origin has not yet been satisfactorily resolved, but possibly ET cells descending from a mesenchymal stem cell in transition from an undifferentiated state to a more differentiated phenotype of the neuroectodermal, endothelial or, as hypothesized here, of the chondro-osseous lineage [53,56,57,62]. As so far demonstrated by the author, the bone-associated genes investigated are important for the suppression of the neuronal (*DKK2*; see 4.2.5) and endothelial (*CHM1*; see 5.3.6) differentiation capacity of ETs. Only knock-down of the up-regulated genes, *DKK2* as well as *EZH2*, can induce the neurogenic differentiation potential of A673, SK-N-MC and TC-71 cells (see Figure 28; [152]). Similarly, only suppression of CHM1 allows the differentiation of ET cells into the endothelial lineage (see supplementary Figure 60). In contrast, ET cell lines are able to fully differentiate along both bone lineages, even if suppression of CHM1 and ITM2A further enhance the chondrogenic and in part osteogenic phenotype of the tumor cells as demonstrated by the author (see 4.2.7). This may indicate, that ETs rather descending from a mesenchymal stem cell in transition to a more differentiated phenotype of the chondro-osseous lineage, than of the neuroectodermal or endothelial lineage.

5.3.8. Influence on bone localization and osteolysis *in vitro* and *in vivo*

As previously described, ETs frequently arise in and metastasize into bones and especially the development of metastases in bones is a catastrophic event in the clinical course of ET patients [48,52]. Even though many other cancers metastasize into bone, very little is known about the underlying molecular mechanisms that favor cancer cells osteotropism, meaning an extraordinary affinity for bone tissues. In recent years some genes were identified, that enabled bone metastasis of different tumor entities. Among them are *secreted phosphoprotein 1* (*OPN*; [337,338]) a potent ligand of CD44 [181], *cbp/p300-interacting transactivator, with glu/asp-rich c-terminal domain, 2* (*CITED2*; [339]), *hematopoietic cell E-selectin/L-selectin ligand glycoform of CD44* (*HCELL*, [340,341]), *cAMP response element-binding protein 1* (*CREB1*; [342]) and *secreted protein, acidic, cysteine-rich* (*SPARC*; [343]).

Since none of the studies have been carried out in ETs, the author analyzed the mRNA expression of various genes, which are known to be involved in preparing the pre-metastatic niche, homing and invasion to bone as well as in local and metastatic tumor growth in bones [188], in different ET cell lines constitutively transfected with pSIREN^{CHM}-, pSIREN^{DKK2}-, pSIREN^{ITM2A}- and pSIREN^{negsiRNA}. Among them are also some target genes of CITED2 (*TGFβ1*, *PTHrP;* [339,344]) and CREB1 (*PTHrP;* [342]),

as well as two additional genes important for osteotropism (*CXCR4* and *RUNX2*). CXCR4 (chemokine, cxc motif, receptor 4) is expressed on cancer cells and facilitates tumor cell homing into and colonization of bones through increased αvβ3 expression [188,345]. Furthermore, high CXCR4 expression seems associated with poor prognosis in ET patients [223]. The transcription factor RUNX2 affects cancer cell invasion, chondro-osseous differentiation and osteolysis [188,319,332] and can bind to the oncogenic fusion protein EWS-FLI1 [319]. As can be seen in Figure 50, suppression of CHM1 clearly reduces the expression of CXCR4 and RUNX2, but at the same time increases the mRNA levels of TGFβ and PTHrP. This might be important, because TGFβ has a central role in promoting bone metastasis and tumor expansion in bone, in part via regulation of PTHrP [188,230,231]. The tumor produced protein PTHrP can further promote osteotropism by enhancing the production of local factors in the bone marrow, such as chemokine, cc motif, ligand 2 (CCL2) either directly or indirectly through increased bone resorption [188,224,346]. In contrast, the expression of all four genes is significantly reduced in ET cells with constitutive DKK2 knock-down compared to control cells (see Figure 31). Interestingly, *CD44* and *OPN* as well as *MMP1*, *OPG* and *VEGF*, which are further target genes of CITED2, CREB1 and SPARC [342,343,347], are also suppressed by DKK2, as demonstrated in this study (see Figure 16, Figure 30 and 4.2.8). These results can give a first hint, that DKK2 is not only important for local tumor growth, metastasis and the differentiation potential of ETs, but also significantly influences the bone-associated phenotype of this tumor. Knock-down of ITM2A mostly decreases the expression levels of the genes investigated, too (see Figure 50). Only in A673 cells, expression of CXCR4 and PTHrP is enhanced after transfection with pSIREN^{ITM2A}. The previous results indicate that at least DKK2 and ITM2A promote the different aspects important for ET osteotropism *in vitro*, more precisely preparing the pre-metastatic niche, homing, colonization, invasion and metastasis into bone tissues.

To further examine this hypothesis, the author tried to analyze bone metastasis in A673 and TC-71 cells *in vivo*. Due to the absent bone metastases and the high amount of observed liver and lung metastases after intravenous inoculation (see Figure 14 and Table 17), the author injected different ET cell lines into the left cardiac ventricle of immune deficient mice to ensure that enough tumor cells reach the bone tissues before they are passively transported into the liver or actively into the lung. But again, no bone metastases could be detected (data not shown), even though Gonzalez *et al*. showed that EWS-FLI1-transfected murine C3H10T1/2 cells develop osteolytic lesions in different bone tissues after intra-cardiac injection [348]. However, Gonzalez *et al.* used a different mouse model and murine instead of human cells, which considerably limits

the problems caused by differences in the cell-cell communication of cells originated from different organisms. Even though it was not possible to generate bone metastases with the present mouse model, and thus clearly examine ET osteotropism *in vivo*, the author established an application model, which can be used to analyze the other aspects important for osteotropism, especially bone invasiveness and osteolysis. For this purpose, A673 cells constitutively transfected with pSIREN^{CHM1}-, pSIREN^{DKK2}-, pSIREN^{ITM2A}- and pSIREN^{negsiRNA} were injected into the medullary cavity of the right tibiae of immunodeficient Rag2$^{-/-}$γc$^{-/-}$ mice. As expected, knock-down of DKK2 significantly reduces the osteogenic behavior of A673 cells compared to respective controls. As can be seen in Figure 34, only 25 % of the mice injected with A673 pSIREN^{DKK2} cells exhibited an infiltration of tumor cells into bone, whereas bone infiltration could be observed in 87.5 % of the respective controls. Opposed to it CHM1 as well as ITM2A knock-down exhibit no significant differences in bone colonization and infiltration *in vivo*, compared to A673 pSIREN^{negsiRNA} cells (see Figure 51). This is quite surprising, because CHM1 significantly increases the proliferative and invasive behavior of ET cells in different other *in vitro* and *in vivo* assays. However, the author could demonstrate that CHM1 slightly decreases the expression of *PTHrP* and *TGFβ*, both important genes for osteotropism (see Figure 50), maybe indicating that CHM1 plays a special role in the regulation of the chondro-osseous phenotype of ETs. Moreover, PTHrP is also down-regulated by ITM2A at least in A673 cells (see Figure 50), which were used for the *in vivo* experiments. In contrast, DKK2 significantly enhances the mRNA levels of PTHrP as well as TGFβ compared to pSIREN^{negsiRNA}-transfected cells, as can be seen in Figure 31. These results indicate that PTHrP is an important player in respect of colonization and bone invasiveness in ETs and that decreased expression of PTHrP compensates the CHM1-mediated effect on proliferation and metastasis. Perhaps, the role of PTHrP is mediated through the enrichment of local, osteogenic factors in the bone marrow [188,224,346], which leads not only to a more suitable pre-metastatic niche, but also to an enhanced bone invasiveness.

Another possible explanation for the strong bone invasion after CHM1 and ITM2A knock-down could be a better attachment of the tumor cells to the bone surface. Attachment to the bone matrix is facilitated by the integrin αvβ3 and OPN, which are normally expressed from osteoclasts [22]. But in A673 cells, suppression of CHM1 and ITM2A significantly enhance the mRNA levels of OPN, as demonstrated by the author (see Figure 54). Moreover, suppression of ITM2A promotes integrin αvβ3 expression via the up-regulation of CXCR4 in A673 cells [345]. As mentioned before, the ability of tumor cells to express genes typical for bone-associated cells is called osteomimicry

[333]. This ability enables tumor cells on the one hand to better attach to the bone surface and on the other hand to colonize and proliferate in the bone microenvironment more easily. In addition to OPN, osteocalcin (BGLAP) is also an important player of osteomimicry, as shown for prostate cancer by Huang *et al.* [349]. *BGLAP* is the only gene that is normally expressed in osteoblasts but not in other extracellular matrix producing cells [350]. Interestingly, expression of this gene is significantly enhanced in A673 cells after CHM1 and ITM2A knock-down compared to control cells (see supplementary Figure 64). Of note, suppression of DKK2 further decreases BGLAP mRNA levels indicating that DKK2 promotes osteomimicry in ET cells, while CHM1 and ITM2A rather suppress the ability of tumor cells to express genes typically for bone-associated cells.

Interestingly, not only *in vivo* bone invasiveness is different in ET cells transfected with CHM1, DKK2 or ITM2A, but also osteolysis (see Figure 34 and Figure 51). To quantify the osteolytic lesions, the amount of osteoclasts was detected by tartrate-resistant acid phosphatase staining (TRAP staining) and the TRAP-positive cells were counted. As expected, DKK2 knock-down significantly reduces the osteolytic phenotype of ETs. Only one mouse injected with DKK2 knock-down cells developed extensive osteolytic lesions compared to four mice injected with A673 pSIREN^{negsiRNA} cells. Furthermore, the pSIREN^{DKK2}-mediated lesions were smaller and less destructive than the lesions caused by control cells, as demonstrated by the reduced number of osteoclasts up to 75.4 % (see Figure 35). Interestingly, the main part of the osteoclasts could be detected not only close to bone tissues as expected, but also on the whole outer border of the tumors. In contrast, suppression of CHM1 and ITM2A even enhances the severity of the osteolytic lesions. As shown in Figure 52, the amount of osteoclasts was increased by a half after CHM1 or ITM2A knock-down compared to A673 pSIREN^{negsiRNA} tumor samples. Interestingly, in tumors injected with A673 pSIREN^{CHM1} and pSIREN^{ITM2A}, osteoclasts were found close to the bone and the edge of the tumor comparable to samples injected with A673 pSIREN^{negsiRNA} and pSIREN^{DKK2}, but additionally all over the tumor area.

To analyze the underlying molecular mechanisms of the osteolytic behavior of ET cells, the author examined the expression levels of different genes known to be involved in osteoclastogenesis and osteolysis. These include among other things genes, which are also influenced in homing, colonization and invasion into bones, like *RUNX2*, *PTHrP* as well as *TGFβ*. As described above, only *PTHrP* seems to play a crucial role in the osteogenic phenotype of ET cells, because this gene is up-regulated after CHM1 and ITM2A knock-down at least in A673 cells and subsequently reduced after suppression

of DKK2 (see Figure 31 and Figure 50). In the context of osteoclastogenesis and osteolysis, the interaction of tumor necrosis factor ligand superfamily, member 11 (RANKL) and osteoprotegerin (OPG) is further very interesting. Thus, gene expression of *RANKL*, its antagonist *OPG* and an important osteoclast survival factor *colony-stimulating factor, macrophage-specific (M-CSF)* were examined in different ET cell lines with constitutive CHM1, DKK2 or ITM2A knock-down and respective controls. In line with the *in vivo* results, DKK2 significantly decreases mRNA expression of OPG and at the same time increases the amount of the two cytokines RANKL and M-CSF, which are essential and sufficient for osteoclastogenesis (see Figure 32). Interestingly, an increase in locally active RANKL can be further achieved directly by MMP7 [186] or indirectly by MMP1 [187]. As demonstrated, DKK2 enhances the expression of RANKL as well as of both matrix metalloproteinases (see Figure 16). Suppression of CHM1 and ITM2A exhibit a contradictorily expression pattern, since the antagonists RANKL and OPG are always influenced in the same manner (see Figure 56). For example, knock-down of CHM1 significantly enhances the expression of RANKL, MMP1 and MMP7, but also the mRNA levels of OPG. Furthermore, mRNA expression of M-CSF is enhanced in A673 cells but rather decreased in SK-N-MC cells after CHM1 and ITM2A knock-down. These results confirm the crucial role of DKK2 in ET osteolysis, but do not sufficiently explain the enhanced amount of osteolytic lesions observed after CHM1 or ITM2A down-regulation, maybe indicating that other genes are influenced in the osteolytic behavior of ETs, too.

For that reason, the author analyzed the expression of further osteolytic genes *hypoxia-inducible factor 1, alpha subunit* (*HIF1α), interleukin 6 (IL6), jagged 1 (JAG1)* and *vascular endothelial growth factor (VEGF)* in different ET cell lines after transfection with pSIREN^{CHM1}, pSIREN^{DKK2}, pSIREN^{ITM2A} and pSIREN^{negsiRNA}. Expression of the transcription factor HIF1α inhibits osteoblast differentiation and enhances the differentiation and maturation of osteoclasts, in part via VEGF and CXCR4 [188,233,234]. Furthermore, Guan *et al.* could show that VEGF increases RANKL promoter activity in ETs leading to induced bone lysis [351]. The next gene important for osteolysis is *JAG1*, a potent downstream mediator of TGFβ, which promotes osteolysis in breast cancer cells by activating the NOTCH signaling pathway leading to increased IL6 expression [235,352]. IL6 is a pro-proliferative cytokine, which promotes tumor growth [353]. As expected due to the previous results, DKK2 knock-down significantly decreases the expression of all four genes investigated (see Figure 33). In contrast, suppression of CHM1 and ITM2A clearly enhance the levels of HIF1α, IL6, JAG1 and VEGF compared to control cells. These findings clearly indicate that these four genes are crucial for the enhanced osteolysis observed *in vivo* and that

DKK2 plays an essential role in ET osteolysis via the regulation of different genes involved in the activation of osteoclasts and the release of further osteolytic genes in the bone microenvironment.

5.4. Clinical implications - importance of bone-associated genes in ETs

In addition to various *in vitro* and *in vivo* assays, the clinical implications of bone-associated genes investigated here are very interesting to completely understand the role of CHM1, DKK2 and ITM2A in ET pathogenesis. Due to the absence of applicable antibodies for CHM1 and ITM2A, only the role of DKK2 was further analyzed in the clinical context. DKK2 is an important player in ET malignancy, especially in ET metastasis, bone invasiveness and osteolysis, as demonstrated in this study using different *in vitro* and *in vivo* assays. In a pilot study of 19 ET patient samples prior to treatment, the author could further reveal, that high expression levels of DKK2 correlate with enhanced bone invasiveness and reduced overall survival (see 4.2.9). Even though no significant statement could be made due to the small number of samples, DKK2 may possibly represent a new biomarker for outcome prediction of ET patients. However, further retrospective and prospective studies are absolutely essential to obtain significant results and to make a reliable statement. The author further demonstrated, that tumor infiltration into bone tissues seems to be associated rather with cytoplasmic DKK2 localization, than with membranous localization (see Table 19). Possibly, this may indicate that DKK2-mediated bone infiltration is not primarily regulated by the activation of the Wnt/β-catenin signaling pathway, because in this case DKK2 would have to be localized on the cell membrane. This hypothesis is in line with the findings that activation of the Wnt/β-catenin pathway rather promotes maturation and activation of osteoblasts, than enhances osteoclastogenesis [34,77], although different genes associated with osteolysis (*IL6*, *JAG1*, *RUNX2* and *VEGF*) are known Wnt target genes, too [282–285]. However, DKK2 seems to influence another pathway important for bone development. As previously published, activation of the NOTCH signaling pathway promotes osteoclastogenesis and osteolysis [33,235,352], in part mediated by JAG1. Even though this pathway seems to be inactivated in ETs [354,355], Ban *et al.* demonstrated, that suppression of EWS-FLI1 reactivates the NOTCH signaling pathway via enhanced JAG1 expression. Interestingly, DKK2 significantly enhances, among many other genes important for osteoclastogenesis (for example *RANKL* and *M-CSF* [85]; see Figure 32), the expression level of JAG1 (see Figure 33) and thus seems to indirectly activate the NOTCH pathway leading to severe

osteolysis. Furthermore, *DKK2* itself seems to be a target gene of this pathway, as well [89].

With regard to the other bone-associated genes investigated (*CHM1* and *ITM2A*), no clinical studies were carried out so far, explaining why their influence on overall survival of ET patients is still unknown and thus their suitability as a biomarker for outcome prediction of ET patients. However, CHM1 may be a potential marker to distinguish ET samples from other small-round-blue-cell tumors in routine pathology of ET diagnosis, because of its high and exclusive expression in nearly all ETs (see Figure 3 and Figure 4). As previously discussed (see 5.1), DKK2 might also be a good marker gene in routine diagnosis, although the suitability of *CHM1* and *DKK2* to serve as ET marker genes has to be tested in further experiments and in particular in an adequate number of patient samples. Moreover, to precisely determine the tumor entity examination of the oncogenic fusion protein EWS-ETS on molecular level is further unavoidable.

Besides the identification of novel ET marker genes, the main clinical focus is placed on the improvement of the treatment of ET patients. Although, multimodal treatment of ET patients with localized disease has markedly improved over the past decades with the application of systemic chemotherapy in conjunction with either surgery, radiation therapy or a combination of both [46,356,357], metastatic disease – present in about 25 % of ET patients at diagnosis – is still associated with fatal outcome and can only rarely be cured by highly toxic therapies [42,45–50,358]. Hence, the development of more potent and in particular more specific drugs is an urgent need to enhance the overall survival and to reduce the toxic burden of cure [359]. To date, numerous studies have been carried out to identify novel ET-specific target genes, which are suitable for targeted therapy of this highly malignant tumor [357]. The most obvious gene in this context is the ET-specific oncogenic fusion protein EWS-FLI1, which function as a transcriptional activator to mediate oncogenic transformation of ET progenitor cells [360–362]. Thus, direct silencing of EWS-FLI1 by antisense oligonucleotides or siRNAs seems to be a useful tool in the treatment of ETs [363,364]. Although, elimination of EWS-FLI1 increases survival of ET xenograft bearing mice [365–367], therapy with antisense cDNAs or siRNAs delivered by nanoparticles is not applicable in the clinical setting so far, due to inherent bioavailability and administrative problems [70]. For this reason it is inevitably to search for other ET-specific target genes and pathways, which are exclusively expressed or even up-regulated in ETs and are involved in the pathophysiological behavior of this malignancy. The most promising candidates so far, are the IGF1 pathway, due to its activation through EWS-FLI1, and the RNA helicase A, a direct binding partner of EWS-FLI1, which suppresses growth of ETs on the one

hand via activation of CCND1 and on the other hand by inducing apoptosis (caspase 3) [70,368,369]. But also the bone-associated genes investigated are strong candidates for targeted therapy of ET patients, especially in immunotherapeutic approaches. For example, Thiel *et al.* already demonstrated that targeting *EZH2* and the bone-associated gene *CHM1* significantly inhibit ET growth in immune deficient mice after adoptively transferred T cells [370]. Moreover, none of the treated mice show any signs of graft versus host disease (GvHD), which is also important in respect to future clinical approaches. However, suppression of CHM1 clearly enhances bone invasiveness and osteolysis, as demonstrated in this doctoral thesis (see 4.3.3). Thus, it remains to be seen if this gene is also a good target gene in the presence of primary bone tumors and osteolytic metastasis. The other bone-associated genes investigated in this study, *DKK2* and *ITM2A*, have not yet been analyzed in immunotherapeutic studies. But due to the observed oncogenic potential of *DKK2 in vitro* and *in vivo*, this gene seems to be a strong candidate target gene for ET immunotherapy. DKK2 significantly promotes proliferation, invasion and tumorigenicity in ETs as well as bone invasiveness and osteolysis via the activation of different osteolytic genes, like *HIF1α*, *IL6*, *JAG1*, *M-CSF*, *PTHrP*, *RANKL* and *VEGF*. These findings predestine DKK2 to further be investigated in different studies to analyze the therapeutic potential of this bone-associated gene in ET therapy.

5.5. Future perspectives

Although the results presented in this doctoral thesis yield new and interesting insights into the function of bone-associated genes in the pathophysiological behavior of ETs, there are still some unresolved questions, which need to be answered to fully understand the role of CHM1, DKK2 as well as ITM2A in ETs.

First of all, it is important to obtain additional information about the underlying molecular mechanisms and the pathways involved in the regulation of CHM1, DKK2 and ITM2A. Even though lots of different target genes involved in metastasis, bone invasiveness and osteolysis were identified by the author, many other aspects of the oncogenic phenotype of ETs are still unknown. For example, ITM2A is overexpressed in ETs, although it suppresses proliferation, bone invasiveness and osteolysis, indicating an important role of ITM2A in another essential part of ET pathogenesis, in addition to maintaining an undifferentiated phenotype of the tumor cells. Furthermore, the author could demonstrate in this study that DKK2 is a potent Wnt agonist in ETs and additionally seems to be involved in the regulation of NOTCH signaling (see 4.2.3

and 5.4), but the pathways regulated by CHM1 and ITM2A has still not been resolved. However, Mera *et al.* postulated that CHM1 directly inhibits the STAT (signal transducer and activator of transcription) signaling pathway in HeLa, HepG2 and HUVEC cells, it is doubtful whether the influence of CHM1 on this pathway in ETs is so important due to the different phenotypes observed in ETs compared to HepG2 and HUVECs cells (see 5.3.1) [126]. With regard to ITM2A no possible signaling pathways are known, to the best of the author's knowledge, indicating that further investigations are necessary to answer this question.

Moreover, the development of proper experimental set-ups for more precise analysis of ET osteotropism and osteolysis need to be addressed in future studies. In this context, it might be interesting to analyze *in vitro* whether ET osteolysis is mainly regulated directly via an interaction between tumor cells and osteoclasts or indirectly via osteoblasts as intermediary. For this purpose, osteoclasts should be cultivated on bone slides with supernatant of ET cell lines transfected with pSIREN^{CHM1}, pSIREN^{DKK2} or pSIREN^{negsiRNA} in the presence or absence of osteoblasts using pit-formation assays [371]. To examine the influence of ITM2A on osteolysis, it will be important to work with mixed cultures consisting of osteoclasts and tumor cells, since ITM2A is a transmembrane protein and no soluble factor, like CHM1 and DKK2. Furthermore, a proper mouse model will be necessary to investigate ET osteotropism *in vivo*. As previously described no bone metastases could be detected after intra-tibial or intra-cardiac inoculation by use of the *in vivo* model in this study. Perhaps, the problem is based on the seed and soil hypothesis, which states that metastasis depends on cross-talk between tumor cells ("seed") and the microenvironment of the specific organs ("soil") [372,373]. In the animal model used, cell-cell communication might be reduced because cells of the "seed" (human tumor cells) and "soil" (murine bone marrow cells) originate from different organisms. To avoid this problem in the future, it may be helpful to generate a more human microenvironment in the bone marrow of the mice before intravenous or intracardiac injection of ET cells to improve cell-cell communication and thus enhance ET osteotropism. Therefore, suitable human cells may be injected either directly into the bone via intra-tibial injection or indirectly into the fetal liver of irradiated mice to develop a human adaptive immune system, which implicates an increase of human cells even in the bone marrow [374]. In this context, mesenchymal or hematopoietic stem cells are particularly suitable due to their characteristics, especially because it has been recognized that VEGFR1-positive hematopoietic bone marrow progenitors seems to play an essential role in preparing the pre-metastatic niche [375].

As described above, additional clinical studies are indispensable to confirm the relevance of the bone-associated genes *CHM1*, *DKK2* and *ITM2A* in ET pathology. However, a pilot study of 19 ET patients reveals a correlation of DKK2 expression and patients overall survival, additional retro- and prospective studies are necessary to confirm the findings observed. In respect to CHM1 and ITM2A, it might be interesting to get more information about the clinical implications, as well.

6. Summary

Ewing tumors (ETs) are highly malignant osteolytic bone and soft tissue sarcomas mostly affecting children and young adults and are characterized by early metastasis into lungs and bones. In this thesis, the author examined three bone-associated genes, namely *chondromodulin 1* (*CHM1*), *dickkopf 2 homolog* (*DKK2*) and *integral membrane protein 2A* (*ITM2A*), which are highly overexpressed in ETs compared to normal tissue. Using RNA interference, the author demonstrated that CHM1, DKK2 as well as ITM2A are critical for anchorage-independent colony formation, but only CHM1 and DKK2 enhance proliferation of ET cells *in vitro* and tumorigenicity *in vivo*. Analysis of the invasion potential *in vitro* and in an orthotopic xenograft mouse model revealed a strong correlation of CHM1 and DKK2 expression to ET invasiveness that may be mediated by the downstream effectors matrix metalloproteinases (MMP1 and/or MMP9). Interestingly, suppression of the pro-metastatic gene *DKK2* increases neuronal differentiation, but at the same time decreases the chondrogenic and osteogenic differentiation potential of ET cells. In contrast, knock-down of the BRICHOS-domain containing proteins CHM1 and ITM2A only influence chondrogenic differentiation capacity; however the cells exhibit a more differentiated state compared to control cells, even without any differentiation media. Further, gene expression analyses established the ability of especially DKK2 to support expression of genes such as *CXCR4*, *PTHrP*, *RUNX2* and *TGFβ*, that are associated with homing, invasion and growth of cancer cells in bone tissues as well as genes important for osteolysis, including *HIF1α*, *JAG1*, *IL6* and *VEGF*. Moreover, DKK2 promotes bone infiltration and osteolysis *in vivo* and further analyses defined DKK2 as a key factor in osteotropic malignancy. In contrast, CHM1 and ITM2A significantly reduce the osteogenic phenotype *in vivo* that may be explained by decreased expression of chondrogenic and osteogenic marker genes mediated by the BRICHOS-domain containing genes, which led to a poorer localization into bone to the principle of osteomimicry. In addition CHM1 and ITM2A decrease the expression of the osteolytic genes investigated indicating *HIF1α*, *JAG1*, *IL6, PTHrP* and *VEGF* to play an important role in bone invasion and osteolysis of ETs. These data provide strong evidence that the Wnt agonist DKK2 is a key player in ET metastasis, invasiveness and osteolysis, validating a critical role of DKK2 for malignancy and the differential phenotype of ETs. In addition, these findings might be of clinical relevance since pilot data obtained from human ET immunohistology indicate the level of DKK2 expression to be associated with tumor invasiveness and survival. Furthermore, the author demonstrated that CHM1 and

ITM2A influence malignant cell outgrowth as well as the metastatic behavior in ETs, but primarily seem to maintain the undifferentiated chondro-osseuos phenotype of ETs.

7. Zusammenfassung

Ewing Tumore (ET) sind hoch-maligne lytische Knochen- und Weichteilsarkome, welche hauptsächlich bei Kindern und jungen Erwachsenen vorkommen und deren Charakteristik die frühe Ausbildung von Metastasen in die Lunge und den Knochen ist. In dieser Arbeit wurden folgende drei Knochen-assoziierte Gene analysiert, welche in ET im Vergleich zum Normalgewebe überexprimiert sind: *Chondromodulin 1* (*CHM1*), *Dickkopf 2 Homolog* (*DKK2*) und das *integrale Membranprotein 2A* (*ITM2A*). Die Autorin konnte mit Hilfe von RNA Interferenzexperimenten zeigen, dass CHM1, DKK2 und ITM2A das kontaktunabhängige Zellwachstum begünstigen, während die Proliferation *in vitro*, sowie das Tumorwachstum *in vivo,* nur von CHM1 und DKK2 gefördert werden. Des Weiteren konnte gezeigt werden, dass das invasive Potential, sowohl *in vitro*, als auch in einem geeigneten murinen Xenograft Modell, stark von der CHM1 bzw. DKK2 Expression in den Tumorzellen abhängig ist. Dieser Effekt wird möglicherweise durch unterschiedliche Matrix Metalloproteinasen (MMP1 und/oder MMP9) vermittelt, deren Expression durch die Knochen-assoziierten Gene reguliert wird. Interessanterweise fördert eine verringerte DKK2 Expression die neuronale Differenzierung von ET Zellen, während gleichzeitig das Potential chondrogen und osteogen zu differenzieren reduziert wird. Im Vergleich dazu wird durch die verringerte Expression der BRICHOS-Domaine tragenden Proteine nur das chondrogene Differenzierungspotential beeinflusst, obwohl die Zellen nach CHM1 und ITM2A Suppression auch ohne entsprechende Differenzierungsmedia im Vergleich zu den Kontrollzellen stärker differenziert sind. Weitere Expressionsanalysen verdeutlichen vor allem die Fähigkeit von DKK2 die Expression wichtiger Gene in Bezug auf das Homingverhalten, die Invasion und das Tumorwachstum im Knochen (*CXCR4*, *PTHrP*, *RUNX2* und *TGFβ*), sowie die Knochenlyse (*HIF1α*, *JAG1*, *IL6* und *VEGF*) zu fördern. Außerdem erhöht DKK2 auch *in vivo* die Knocheninfiltration und Lyse, was auf eine essentielle Funktion dieses Gens in der Regulation dieser lytischen Tumorerkrankung schließen lässt. Im Gegensatz dazu, hemmen CHM1 und ITM2A die zerstörerische Wirkung der Tumorzellen im Knochen, was möglicherweise durch die verringerte chondrogene und osteogene Differenzierung der Zellen und der damit einhergehenden schlechteren Osteomimikry erklärt werden kann. Zusätzlich führt die Expression von CHM1 und ITM2A zu einer verringerten Expression der osteolytischen Gene *HIF1α*, *JAG1*, *IL6, PTHrP* und *VEGF*, was deren essentielle Funktion in der Tumor-vermittelten Knochenlyse bekräftigt. Anhand dieser Daten kann gezeigt werden, dass der Wnt Agonist DKK2 essentiell für die Metastasierung, Invasion und Knochenlyse des ET ist, sowie für dessen Differenzierungspotential. Zusätzlich konnte die klinische

Relevanz dieser Ergebnisse in einer Pilotstudie an humanen ET Proben verdeutlicht werden, wobei die Expressionslevel von DKK2 mit der Invasivität des Tumors sowie dem Überleben der Patienten assoziiert sind. Außerdem konnte die Autorin zeigen, dass CHM1 und ITM2A sowohl das maligne Zellwachstum, als auch das Metastasierungsverhalten von ET beeinflussen, wobei die vornehmliche Funktion die Aufrechterhaltung des undifferenzierten chondro-ossären Zustandes der Tumorzellen ist.

8. References

1 Welsch U. *Lehrbuch Histologie;* 3. Aufl. München: Elsevier, Urban & Fischer; 2010. http://opacplus.bsb-muenchen.de/search?isbn=978-3-437-44431-9

2 Lippert H. *Lehrbuch Anatomie*. 7., erw. Aufl. München [u.a.]: Elsevier, Urban & Fischer; 2006. http://opacplus.ub.uni-muenchen.de/InfoGuideClient.ubmsis/start.do?Login=igubm&Query=540="978-3-437-42362-8"

3 Hadjidakis DJ, Androulakis II. Bone remodeling. *Ann N Y Acad Sci* 2006; **1092**:385–396.

4 Watts NB. Clinical Utility of Biochemical Markers of Bone Remodeling. *Clinical Chemistry* 1999; **45**:1359–1368.

5 Javed A, Chen H, Ghori FY. Genetic and transcriptional control of bone formation. *Oral Maxillofac Surg Clin North Am* 2010; **22**:283–293, v.

6 Nijweide PJ, Burger EH, Feyen JH. Cells of bone: proliferation, differentiation, and hormonal regulation. *Physiol Rev* 1986; **66**:855–886.

7 Franceschi RT, Xiao G. Regulation of the osteoblast-specific transcription factor, Runx2: responsiveness to multiple signal transduction pathways. *J Cell Biochem* 2003; **88**:446–454.

8 Damsky CH. Extracellular matrix-integrin interactions in osteoblast function and tissue remodeling. *Bone* 1999; **25**:95–96.

9 Goldring MB, Tsuchimochi K, Ijiri K. The control of chondrogenesis. *J Cell Biochem* 2006; **97**:33–44.

10 Tuan RS. Biology of developmental and regenerative skeletogenesis. *Clin Orthop Relat Res* 2004; :S105–117.

11 Hall BK, Miyake T. All for one and one for all: condensations and the initiation of skeletal development. *Bioessays* 2000; **22**:138–147.

12 Tickle C. Molecular basis of vertebrate limb patterning. *Am J Med Genet* 2002; **112**:250–255.

13 Kmita M, Tarchini B, Zàkàny J, Logan M, Tabin CJ, Duboule D. Early developmental arrest of mammalian limbs lacking HoxA/HoxD gene function. *Nature* 2005; **435**:1113–1116.

14 Niswander L. Pattern formation: old models out on a limb. *Nat Rev Genet* 2003; **4**:133–143.

15 Yoon BS, Lyons KM. Multiple functions of BMPs in chondrogenesis. *J Cell Biochem* 2004; **93**:93–103.

16 Ng LJ, Wheatley S, Muscat GE, Conway-Campbell J, Bowles J, Wright E, *et al.* SOX9 binds DNA, activates transcription, and coexpresses with type II collagen during chondrogenesis in the mouse. *Dev Biol* 1997; **183**:108–121.

17 Lefebvre V, Behringer RR, de Crombrugghe B. L-Sox5, Sox6 and Sox9 control essential steps of the chondrocyte differentiation pathway. *Osteoarthr Cartil* 2001; **9 Suppl A**:S69–75.

18 Amano K, Hata K, Sugita A, Takigawa Y, Ono K, Wakabayashi M, *et al.* Sox9 family members negatively regulate maturation and calcification of chondrocytes through up-regulation of parathyroid hormone-related protein. *Mol Biol Cell* 2009; **20**:4541–4551.

19 Kim Y-J, Kim H-J, Im G-I. PTHrP promotes chondrogenesis and suppresses hypertrophy from both bone marrow-derived and adipose tissue-derived MSCs. *Biochem Biophys Res Commun* 2008; **373**:104–108.

20 Enomoto H, Enomoto-Iwamoto M, Iwamoto M, Nomura S, Himeno M, Kitamura Y, *et al.* Cbfa1 is a positive regulatory factor in chondrocyte maturation. *J Biol Chem* 2000; **275**:8695–8702.

21 Colnot C. Cellular and molecular interactions regulating skeletogenesis. *J Cell Biochem* 2005; **95**:688–697.

22 Reinholt FP, Hultenby K, Oldberg A, Heinegård D. Osteopontin--a possible anchor of osteoclasts to bone. *Proc Natl Acad Sci USA* 1990; **87**:4473–4475.

23 Matsuo K, Irie N. Osteoclast-osteoblast communication. *Arch Biochem Biophys* 2008; **473**:201–209.

24 Bonewald LF. Osteocytes as dynamic multifunctional cells. *Ann N Y Acad Sci* 2007; **1116**:281–290.

25 Hedgecock NL, Hadi T, Chen AA, Curtiss SB, Martin RB, Hazelwood SJ. Quantitative regional associations between remodeling, modeling, and osteocyte apoptosis and density in rabbit tibial midshafts. *Bone* 2007; **40**:627–637.

26 Verborgt O, Gibson GJ, Schaffler MB. Loss of osteocyte integrity in association with microdamage and bone remodeling after fatigue in vivo. *J Bone Miner Res* 2000; **15**:60–67.

27 Graves DT, Jiang Y, Valente AJ. The expression of monocyte chemoattractant protein-1 and other chemokines by osteoblasts. *Front Biosci* 1999; **4**:D571–580.

28 Yu X, Huang Y, Collin-Osdoby P, Osdoby P. Stromal cell-derived factor-1 (SDF-1) recruits osteoclast precursors by inducing chemotaxis, matrix metalloproteinase-9 (MMP-9) activity, and collagen transmigration. *J Bone Miner Res* 2003; **18**:1404–1418.

29 Chambers TJ. Regulation of the differentiation and function of osteoclasts. *J Pathol* 2000; **192**:4–13.

30 Boyle WJ, Simonet WS, Lacey DL. Osteoclast differentiation and activation. *Nature* 2003; **423**:337–342.

31 Zhao C, Irie N, Takada Y, Shimoda K, Miyamoto T, Nishiwaki T, *et al.* Bidirectional ephrinB2-EphB4 signaling controls bone homeostasis. *Cell Metab* 2006; **4**:111–121.

32 Kieslinger M, Folberth S, Dobreva G, Dorn T, Croci L, Erben R, *et al.* EBF2 regulates osteoblast-dependent differentiation of osteoclasts. *Dev Cell* 2005; **9**:757–767.

33 Bai S, Kopan R, Zou W, Hilton MJ, Ong C, Long F, *et al.* NOTCH1 regulates osteoclastogenesis directly in osteoclast precursors and indirectly via osteoblast lineage cells. *J Biol Chem* 2008; **283**:6509–6518.

34 Glass DA 2nd, Bialek P, Ahn JD, Starbuck M, Patel MS, Clevers H, *et al.* Canonical Wnt signaling in differentiated osteoblasts controls osteoclast differentiation. *Dev Cell* 2005; **8**:751–764.

35 Glass DA 2nd, Karsenty G. In vivo analysis of Wnt signaling in bone. *Endocrinology* 2007; **148**:2630–2634.

36 van Bezooijen RL, Roelen BAJ, Visser A, van der Wee-Pals L, de Wilt E, Karperien M, *et al.* Sclerostin is an osteocyte-expressed negative regulator of bone formation, but not a classical BMP antagonist. *J Exp Med* 2004; **199**:805–814.

37 Dorfman HD, Czerniak B. Bone cancers. *Cancer* 1995; **75**:203–210.

38 Roodman GD. Mechanisms of bone metastasis. *N Engl J Med* 2004; **350**:1655–1664.

39 UK CR. Bone cancer. 2012.http://cancerhelp.cancerresearchuk.org/type/bone-cancer/ (accessed 19 Aug2012).

40 Burchill SA. Ewing's sarcoma: diagnostic, prognostic, and therapeutic implications of molecular abnormalities. *J Clin Pathol* 2003; **56**:96–102.

41 Jedlicka P. Ewing Sarcoma, an enigmatic malignancy of likely progenitor cell origin, driven by transcription factor oncogenic fusions. *Int J Clin Exp Pathol* 2010; **3**:338–347.

42 Bernstein M, Kovar H, Paulussen M, Randall RL, Schuck A, Teot LA, *et al.* Ewing's sarcoma family of tumors: current management. *Oncologist* 2006; **11**:503–519.

43 Glass AG, Fraumeni JF Jr. Epidemiology of bone cancer in children. *J Natl Cancer Inst* 1970; **44**:187–199.

44 Riggi N, Suva M-L, Stamenkovic I. Ewing's sarcoma origin: from duel to duality. *Expert Rev Anticancer Ther* 2009; **9**:1025–1030.

45 Schleiermacher G, Peter M, Oberlin O, Philip T, Rubie H, Mechinaud F, *et al.* Increased risk of systemic relapses associated with bone marrow micrometastasis and circulating tumor cells in localized ewing tumor. *J Clin Oncol* 2003; **21**:85–91.

46 Castex M-P, Rubie H, Stevens MCG, Escribano CC, de Gauzy JS, Gomez-Brouchet A, *et al.* Extraosseous localized ewing tumors: improved outcome with anthracyclines--the French society of pediatric oncology and international society of pediatric oncology. *J Clin Oncol* 2007; **25**:1176–1182.

47 Burdach S, Jürgens H, Peters C, Nürnberger W, Mauz-Körholz C, Körholz D, *et al.* Myeloablative radiochemotherapy and hematopoietic stem-cell rescue in poor-prognosis Ewing's sarcoma. *J Clin Oncol* 1993; **11**:1482–1488.

48 Burdach S, Jürgens H. High-dose chemoradiotherapy (HDC) in the Ewing family of tumors (EFT). *Crit Rev Oncol Hematol* 2002; **41**:169–189.

49 Burdach S, Thiel U, Schöniger M, Haase R, Wawer A, Nathrath M, *et al.* Total body MRI-governed involved compartment irradiation combined with high-dose chemotherapy and stem cell rescue improves long-term survival in Ewing tumor patients with multiple primary bone metastases. *Bone Marrow Transplant* 2010; **45**:483–489.

50 Burdach S. Treatment of advanced Ewing tumors by combined radiochemotherapy and engineered cellular transplants. *Pediatr Transplant* 2004; **8 Suppl 5**:67–82.

51 Paulussen M, Ahrens S, Burdach S, Craft A, Dockhorn-Dworniczak B, Dunst J, *et al.* Primary metastatic (stage IV) Ewing tumor: survival analysis of 171 patients from the EICESS studies. European Intergroup Cooperative Ewing Sarcoma Studies. *Ann Oncol* 1998; **9**:275–281.

52 Coleman RE. Clinical features of metastatic bone disease and risk of skeletal morbidity. *Clin Cancer Res* 2006; **12**:6243s–6249s.

53 Ewing J. Classics in oncology. Diffuse endothelioma of bone. James Ewing. Proceedings of the New York Pathological Society, 1921. *CA Cancer J Clin* 1972; **22**:95–98.

54 Kovar H. Context matters: the hen or egg problem in Ewing's sarcoma. *Semin Cancer Biol* 2005; **15**:189–196.

55 Staege MS, Hutter C, Neumann I, Foja S, Hattenhorst UE, Hansen G, *et al.* DNA microarrays reveal relationship of Ewing family tumors to both endothelial and fetal neural crest-derived cells and define novel targets. *Cancer Res* 2004; **64**:8213–8221.

56 Schmidt D, Harms D, Burdach S. Malignant peripheral neuroectodermal tumours of childhood and adolescence. *Virchows Arch A Pathol Anat Histopathol* 1985; **406**:351–365.

57 Tirode F, Laud-Duval K, Prieur A, Delorme B, Charbord P, Delattre O. Mesenchymal stem cell features of Ewing tumors. *Cancer Cell* 2007; **11**:421–429.

58 Pinto A, Dickman P, Parham D. Pathobiologic markers of the ewing sarcoma family of tumors: state of the art and prediction of behaviour. *Sarcoma* 2011; **2011**:856190.

59 Takashima Y, Era T, Nakao K, Kondo S, Kasuga M, Smith AG, *et al.* Neuroepithelial cells supply an initial transient wave of MSC differentiation. *Cell* 2007; **129**:1377–1388.

60 Folpe AL, Hill CE, Parham DM, O'Shea PA, Weiss SW. Immunohistochemical detection of FLI-1 protein expression: a study of 132 round cell tumors with emphasis on CD99-positive mimics of Ewing's sarcoma/primitive neuroectodermal tumor. *Am J Surg Pathol* 2000; **24**:1657–1662.

61 Llombart-Bosch A, Machado I, Navarro S, Bertoni F, Bacchini P, Alberghini M, *et al.* Histological heterogeneity of Ewing's sarcoma/PNET: an immunohistochemical analysis of 415 genetically confirmed cases with clinical support. *Virchows Arch* 2009; **455**:397–411.

62 Mackintosh C, Madoz-Gúrpide J, Ordóñez JL, Osuna D, Herrero-Martín D. The molecular pathogenesis of Ewing's sarcoma. *Cancer Biol Ther* 2010; **9**:655–667.

63 Lessnick SL, Ladanyi M. Molecular pathogenesis of ewing sarcoma: new therapeutic and transcriptional targets. *Annu Rev Pathol* 2012; **7**:145–159.

64 Uren A, Toretsky JA. Ewing's sarcoma oncoprotein EWS-FLI1: the perfect target without a therapeutic agent. *Future Oncol* 2005; **1**:521–528.

65 Miyagawa Y, Okita H, Nakaijima H, Horiuchi Y, Sato B, Taguchi T, *et al.* Inducible expression of chimeric EWS/ETS proteins confers Ewing's family tumor-like phenotypes to human mesenchymal progenitor cells. *Mol Cell Biol* 2008; **28**:2125–2137.

66 Potikyan G, France KA, Carlson MRJ, Dong J, Nelson SF, Denny CT. Genetically defined EWS/FLI1 model system suggests mesenchymal origin of Ewing's family tumors. *Lab Invest* 2008; **88**:1291–1302.

67 Riggi N, Cironi L, Provero P, Suvà M-L, Kaloulis K, Garcia-Echeverria C, *et al.* Development of Ewing's sarcoma from primary bone marrow-derived mesenchymal progenitor cells. *Cancer Res* 2005; **65**:11459–11468.

68 Lessnick SL, Dacwag CS, Golub TR. The Ewing's sarcoma oncoprotein EWS/FLI induces a p53-dependent growth arrest in primary human fibroblasts. *Cancer Cell* 2002; **1**:393–401.

69 Neilsen PM, Pishas KI, Callen DF, Thomas DM. Targeting the p53 Pathway in Ewing Sarcoma. *Sarcoma* 2011; **2011**:746939.

70 Kelleher FC, Thomas DM. Molecular pathogenesis and targeted therapeutics in Ewing sarcoma/primitive neuroectodermal tumours. *Clin Sarcoma Res* 2012; **2**:6.

71 Niehrs C. Function and biological roles of the Dickkopf family of Wnt modulators. *Oncogene* 2006; **25**:7469–7481.

72 Krupnik VE, Sharp JD, Jiang C, Robison K, Chickering TW, Amaravadi L, *et al.* Functional and structural diversity of the human Dickkopf gene family. *Gene* 1999; **238**:301–313.

73 Glinka A, Wu W, Delius H, Monaghan AP, Blumenstock C, Niehrs C. Dickkopf-1 is a member of a new family of secreted proteins and functions in head induction. *Nature* 1998; **391**:357–362.

74 Aravind L, Koonin EV. A colipase fold in the carboxy-terminal domain of the Wnt antagonists--the Dickkopfs. *Curr Biol* 1998; **8**:R477–478.

75 van Tilbeurgh H, Bezzine S, Cambillau C, Verger R, Carrière F. Colipase: structure and interaction with pancreatic lipase. *Biochim Biophys Acta* 1999; **1441**:173–184.

76 Witte F, Dokas J, Neuendorf F, Mundlos S, Stricker S. Comprehensive expression analysis of all Wnt genes and their major secreted antagonists during mouse limb development and cartilage differentiation. *Gene Expr Patterns* 2009; **9**:215–223.

77 Tian E, Zhan F, Walker R, Rasmussen E, Ma Y, Barlogie B, *et al.* The role of the Wnt-signaling antagonist DKK1 in the development of osteolytic lesions in multiple myeloma. *N Engl J Med* 2003; **349**:2483–2494.

78 González-Sancho JM, Aguilera O, García JM, Pendás-Franco N, Peña C, Cal S, *et al.* The Wnt antagonist DICKKOPF-1 gene is a downstream target of beta-catenin/TCF and is downregulated in human colon cancer. *Oncogene* 2005; **24**:1098–1103.

79 Hoang BH, Kubo T, Healey JH, Yang R, Nathan SS, Kolb EA, *et al.* Dickkopf 3 inhibits invasion and motility of Saos-2 osteosarcoma cells by modulating the Wnt-beta-catenin pathway. *Cancer Res* 2004; **64**:2734–2739.

80 Li L, Mao J, Sun L, Liu W, Wu D. Second cysteine-rich domain of Dickkopf-2 activates canonical Wnt signaling pathway via LRP-6 independently of dishevelled. *J Biol Chem* 2002; **277**:5977–5981.

81 Brott BK, Sokol SY. Regulation of Wnt/LRP signaling by distinct domains of Dickkopf proteins. *Mol Cell Biol* 2002; **22**:6100–6110.

82 Mao B, Niehrs C. Kremen2 modulates Dickkopf2 activity during Wnt/LRP6 signaling. *Gene* 2003; **302**:179–183.

83 Mao B, Wu W, Davidson G, Marhold J, Li M, Mechler BM, *et al.* Kremen proteins are Dickkopf receptors that regulate Wnt/beta-catenin signalling. *Nature* 2002; **417**:664–667.

84 Uren A, Wolf V, Sun Y-F, Azari A, Rubin JS, Toretsky JA. Wnt/Frizzled signaling in Ewing sarcoma. *Pediatr Blood Cancer* 2004; **43**:243–249.

85 Fujita K, Janz S. Attenuation of WNT signaling by DKK-1 and -2 regulates BMP2-induced osteoblast differentiation and expression of OPG, RANKL and M-CSF. *Mol Cancer* 2007; **6**:71.

86 van der Horst G, van der Werf SM, Farih-Sips H, van Bezooijen RL, Löwik CWGM, Karperien M. Downregulation of Wnt signaling by increased expression of Dickkopf-1 and -2 is a prerequisite for late-stage osteoblast differentiation of KS483 cells. *J Bone Miner Res* 2005; **20**:1867–1877.

87 Li X, Liu P, Liu W, Maye P, Zhang J, Zhang Y, *et al.* Dkk2 has a role in terminal osteoblast differentiation and mineralized matrix formation. *Nat Genet* 2005; **37**:945–952.

88 Olivares-Navarrete R, Hyzy S, Wieland M, Boyan BD, Schwartz Z. The roles of Wnt signaling modulators Dickkopf-1 (Dkk1) and Dickkopf-2 (Dkk2) and cell maturation state in osteogenesis on microstructured titanium surfaces. *Biomaterials* 2010; **31**:2015–2024.

89 Katoh M, Katoh M. WNT antagonist, DKK2, is a Notch signaling target in intestinal stem cells: augmentation of a negative regulation system for canonical WNT signaling pathway by the Notch-DKK2 signaling loop in primates. *Int J Mol Med* 2007; **19**:197–201.

90 Sato H, Suzuki H, Toyota M, Nojima M, Maruyama R, Sasaki S, *et al.* Frequent epigenetic inactivation of DICKKOPF family genes in human gastrointestinal tumors. *Carcinogenesis* 2007; **28**:2459–2466.

91 Matsui A, Yamaguchi T, Maekawa S, Miyazaki C, Takano S, Uetake T, *et al.* DICKKOPF-4 and -2 genes are upregulated in human colorectal cancer. *Cancer Sci* 2009; **100**:1923–1930.

92 Hirata H, Hinoda Y, Nakajima K, Kawamoto K, Kikuno N, Kawakami K, *et al.* Wnt antagonist gene DKK2 is epigenetically silenced and inhibits renal cancer progression through apoptotic and cell cycle pathways. *Clin Cancer Res* 2009; **15**:5678–5687.

93 Maehata T, Taniguchi H, Yamamoto H, Nosho K, Adachi Y, Miyamoto N, *et al.* Transcriptional silencing of Dickkopf gene family by CpG island hypermethylation in human gastrointestinal cancer. *World J Gastroenterol* 2008; **14**:2702–2714.

94 Moskalev EA, Luckert K, Vorobjev IA, Mastitsky SE, Gladkikh AA, Stephan A, *et al.* Concurrent epigenetic silencing of Wnt/beta-catenin pathway inhibitor genes in B cell chronic lymphocytic leukaemia. *BMC cancer* 2012; **12**:213.

95 Rajan N, Burn J, Langtry J, Sieber-Blum M, Lord CJ, Ashworth A. Transition from cylindroma to spiradenoma in CYLD-defective tumours is associated with reduced DKK2 expression. *The Journal of Pathology* 2011; **224**:309–321.

96 Mukhopadhyay M, Gorivodsky M, Shtrom S, Grinberg A, Niehrs C, Morasso MI, *et al.* Dkk2 plays an essential role in the corneal fate of the ocular surface epithelium. *Development* 2006; **133**:2149–2154.

97 Cadigan KM, Liu YI. Wnt signaling: complexity at the surface. *J Cell Sci* 2006; **119**:395–402.

98 Tada M, Concha ML, Heisenberg CP. Non-canonical Wnt signalling and regulation of gastrulation movements. *Semin Cell Dev Biol* 2002; **13**:251–260.

99 Kohn AD, Moon RT. Wnt and calcium signaling: beta-catenin-independent pathways. *Cell Calcium* 2005; **38**:439–446.

100 Logan CY, Nusse R. The Wnt Signaling Pathway in Development and Disease. *Annual Review of Cell and Developmental Biology* 2004; **20**:781–810.

101 Clevers H, Nusse R. Wnt/β-catenin signaling and disease. *Cell* 2012; **149**:1192–1205.

102 Ross SE, Hemati N, Longo KA, Bennett CN, Lucas PC, Erickson RL, *et al.* Inhibition of adipogenesis by Wnt signaling. *Science* 2000; **289**:950–953.

103 Goodwin AM, D'Amore PA. Wnt signaling in the vasculature. *Angiogenesis* 2002; **5**:1–9.

104 Klaus A, Birchmeier W. Wnt signalling and its impact on development and cancer. *Nat Rev Cancer* 2008; **8**:387–398.

105 Giles RH, van Es JH, Clevers H. Caught up in a Wnt storm: Wnt signaling in cancer. *Biochim Biophys Acta* 2003; **1653**:1–24.

106 Polakis P. Wnt signaling and cancer. *Genes Dev* 2000; **14**:1837–1851.

107 Bienz M, Clevers H. Linking colorectal cancer to Wnt signaling. *Cell* 2000; **103**:311–320.

108 Baron R, Rawadi G. Targeting the Wnt/beta-catenin pathway to regulate bone formation in the adult skeleton. *Endocrinology* 2007; **148**:2635–2643.

109 Tetsu O, McCormick F. Beta-catenin regulates expression of cyclin D1 in colon carcinoma cells. *Nature* 1999; **398**:422–426.

110 Shtutman M, Zhurinsky J, Simcha I, Albanese C, D'Amico M, Pestell R, *et al.* The cyclin D1 gene is a target of the beta-catenin/LEF-1 pathway. *Proc Natl Acad Sci USA* 1999; **96**:5522–5527.

111 Batlle E, Henderson JT, Beghtel H, van den Born MMW, Sancho E, Huls G, *et al.* Beta-catenin and TCF mediate cell positioning in the intestinal epithelium by controlling the expression of EphB/ephrinB. *Cell* 2002; **111**:251–263.

112 He TC, Sparks AB, Rago C, Hermeking H, Zawel L, da Costa LT, *et al.* Identification of c-MYC as a target of the APC pathway. *Science* 1998; **281**:1509–1512.

113 Chien AJ, Conrad WH, Moon RT. A Wnt survival guide: from flies to human disease. *J Invest Dermatol* 2009; **129**:1614–1627.

114 Hedlund J, Johansson J, Persson B. BRICHOS - a superfamily of multidomain proteins with diverse functions. *BMC Res Notes* 2009; **2**:180.

115 Sánchez-Pulido L, Devos D, Valencia A. BRICHOS: a conserved domain in proteins associated with dementia, respiratory distress and cancer. *Trends Biochem Sci* 2002; **27**:329–332.

116 Willander H, Hermansson E, Johansson J, Presto J. BRICHOS domain associated with lung fibrosis, dementia and cancer--a chaperone that prevents amyloid fibril formation? *FEBS J* 2011; **278**:3893–3904.

117 Yanagihara I, Yamagata M, Sakai N, Shukunami C, Kurahashi H, Yamazaki M, *et al.* Genomic organization of the human chondromodulin-1 gene containing a promoter region that confers the expression of reporter gene in chondrogenic ATDC5 cells. *J Bone Miner Res* 2000; **15**:421–429.

118 Azizan A, Holaday N, Neame PJ. Post-translational processing of bovine chondromodulin-I. *J Biol Chem* 2001; **276**:23632–23638.

119 Hiraki Y, Shukunami C. Chondromodulin-I as a novel cartilage-specific growth-modulating factor. *Pediatr Nephrol* 2000; **14**:602–605.

120 Kondo J, Shibata H, Miura S, Yamakawa A, Sato K, Higuchi Y, *et al.* A functional role of the glycosylated N-terminal domain of chondromodulin-I. *J Bone Miner Metab* 2011; **29**:23–30.

121 Yoshioka M, Yuasa S, Matsumura K, Kimura K, Shiomi T, Kimura N, *et al.* Chondromodulin-I maintains cardiac valvular function by preventing angiogenesis. *Nat Med* 2006; **12**:1151–1159.

122 Hiraki Y, Inoue H, Iyama K, Kamizono A, Ochiai M, Shukunami C, *et al.* Identification of chondromodulin I as a novel endothelial cell growth inhibitor. Purification and its

localization in the avascular zone of epiphyseal cartilage. *J Biol Chem* 1997; **272**:32419–32426.

123 Shukunami C, Hiraki Y. Role of cartilage-derived anti-angiogenic factor, chondromodulin-I, during endochondral bone formation. *Osteoarthr Cartil* 2001; **9 Suppl A**:S91–101.

124 Shukunami C, Hiraki Y. Chondromodulin-I and tenomodulin: the negative control of angiogenesis in connective tissue. *Curr Pharm Des* 2007; **13**:2101–2112.

125 Klinger P, Surmann-Schmitt C, Brem M, Swoboda B, Distler JH, Carl H-D, *et al.* Chondromodulin 1 stabilizes the chondrocyte phenotype and inhibits endochondral ossification of porcine cartilage repair tissue. *Arthritis Rheum* 2011; **63**:2721–2731.

126 Mera H, Kawashima H, Yoshizawa T, Ishibashi O, Ali MM, Hayami T, *et al.* Chondromodulin-1 directly suppresses growth of human cancer cells. *BMC Cancer* 2009; **9**:166.

127 Nakamichi Y, Shukunami C, Yamada T, Aihara K, Kawano H, Sato T, *et al.* Chondromodulin I is a bone remodeling factor. *Mol Cell Biol* 2003; **23**:636–644.

128 Yukata K, Matsui Y, Shukunami C, Takimoto A, Goto T, Nishizaki Y, *et al.* Altered fracture callus formation in chondromodulin-I deficient mice. *Bone* 2008; **43**:1047–1056.

129 Hayami T, Shukunami C, Mitsui K, Endo N, Tokunaga K, Kondo J, *et al.* Specific loss of chondromodulin-I gene expression in chondrosarcoma and the suppression of tumor angiogenesis and growth by its recombinant protein in vivo. *FEBS Lett* 1999; **458**:436–440.

130 Van den Plas D, Merregaert J. In vitro studies on Itm2a reveal its involvement in early stages of the chondrogenic differentiation pathway. *Biol Cell* 2004; **96**:463–470.

131 Pittois K, Wauters J, Bossuyt P, Deleersnijder W, Merregaert J. Genomic organization and chromosomal localization of the Itm2a gene. *Mamm Genome* 1999; **10**:54–56.

132 Deleersnijder W, Hong G, Cortvrindt R, Poirier C, Tylzanowski P, Pittois K, *et al.* Isolation of markers for chondro-osteogenic differentiation using cDNA library subtraction. Molecular cloning and characterization of a gene belonging to a novel multigene family of integral membrane proteins. *J Biol Chem* 1996; **271**:19475–19482.

133 Boeuf S, Börger M, Hennig T, Winter A, Kasten P, Richter W. Enhanced ITM2A expression inhibits chondrogenic differentiation of mesenchymal stem cells. *Differentiation* 2009; **78**:108–115.

134 Kirchner J, Bevan MJ. ITM2A is induced during thymocyte selection and T cell activation and causes downregulation of CD8 when overexpressed in CD4(+)CD8(+) double positive thymocytes. *J Exp Med* 1999; **190**:217–228.

135 Tuckermann JP, Pittois K, Partridge NC, Merregaert J, Angel P. Collagenase-3 (MMP-13) and integral membrane protein 2a (Itm2a) are marker genes of chondrogenic/osteoblastic cells in bone formation: sequential temporal, and spatial expression of Itm2a, alkaline phosphatase, MMP-13, and osteocalcin in the mouse. *J Bone Miner Res* 2000; **15**:1257–1265.

136 Van den Plas D, Merregaert J. Constitutive overexpression of the integral membrane protein Itm2A enhances myogenic differentiation of C2C12 cells. *Cell Biol Int* 2004; **28**:199–207.

137 Barber TD, Barber MC, Tomescu O, Barr FG, Ruben S, Friedman TB. Identification of target genes regulated by PAX3 and PAX3-FKHR in embryogenesis and alveolar rhabdomyosarcoma. *Genomics* 2002; **79**:278–284.

138 Dohjima T, Lee NS, Li H, Ohno T, Rossi JJ. Small interfering RNAs expressed from a Pol III promoter suppress the EWS/Fli-1 transcript in an Ewing sarcoma cell line. *Mol Ther* 2003; **7**:811–816.

139 Giard DJ, Aaronson SA, Todaro GJ, Arnstein P, Kersey JH, Dosik H, *et al.* In vitro cultivation of human tumors: establishment of cell lines derived from a series of solid tumors. *J Natl Cancer Inst* 1973; **51**:1417–1423.

140 Tomeczkowski J, Yakisan E, Wieland B, Reiter A, Welte K, Sykora KW. Absence of G-CSF receptors and absent response to G-CSF in childhood Burkitt's lymphoma and B-ALL cells. *Br J Haematol* 1995; **89**:771–779.

141 Schlesinger HR, Gerson JM, Moorhead PS, Maguire H, Hummeler K. Establishment and characterization of human neuroblastoma cell lines. *Cancer Res* 1976; **36**:3094–3100.

142 McAllister RM, Gardner MB, Greene AE, Bradt C, Nichols WW, Landing BH. Cultivation in vitro of cells derived from a human osteosarcoma. *Cancer* 1971; **27**:397–402.

143 Siggelkow H, Schenck M, Rohde M, Viereck V, Tauber S, Atkinson MJ, *et al.* Prolonged culture of HOS 58 human osteosarcoma cells with 1,25-(OH)2-D3, TGF-beta, and dexamethasone reveals physiological regulation of alkaline phosphatase, dissociated osteocalcin gene expression, and protein synthesis and lack of mineralization. *J Cell Biochem* 2002; **85**:279–294.

144 Rhim JS, Park DK, Arnstein P, Huebner RJ, Weisburger EK, Nelson-Rees WA. Transformation of human cells in culture by N-methyl-N'-nitro-N-nitrosoguanidine. *Nature* 1975; **256**:751–753.

145 Rhim JS, Putman DL, Arnstein P, Huebner RJ, McAllister RM. Characterization of human cells transformed in vitro by N-methyl-N'-nitro-N-nitrosoguanidine. *Int J Cancer* 1977; **19**:505–510.

146 Fogh J, Fogh JM, Orfeo T. One hundred and twenty-seven cultured human tumor cell lines producing tumors in nude mice. *J Natl Cancer Inst* 1977; **59**:221–226.

147 Fogh J, Wright WC, Loveless JD. Absence of HeLa cell contamination in 169 cell lines derived from human tumors. *J Natl Cancer Inst* 1977; **58**:209–214.

148 Roberts WM, Douglass EC, Peiper SC, Houghton PJ, Look AT. Amplification of the gli gene in childhood sarcomas. *Cancer Res* 1989; **49**:5407–5413.

149 Oliner JD, Kinzler KW, Meltzer PS, George DL, Vogelstein B. Amplification of a gene encoding a p53-associated protein in human sarcomas. *Nature* 1992; **358**:80–83.

150 van Valen F, Winkelmann W, Jürgens H. Expression of functional Y1 receptors for neuropeptide Y in human Ewing's sarcoma cell lines. *J Cancer Res Clin Oncol* 1992; **118**:529–536.

151 Goldman JP, Blundell MP, Lopes L, Kinnon C, Di Santo JP, Thrasher AJ. Enhanced human cell engraftment in mice deficient in RAG2 and the common cytokine receptor gamma chain. *Br J Haematol* 1998; **103**:335–342.

152 Richter GHS, Plehm S, Fasan A, Rössler S, Unland R, Bennani-Baiti IM, *et al.* EZH2 is a mediator of EWS/FLI1 driven tumor growth and metastasis blocking endothelial and neuro-ectodermal differentiation. *Proc Natl Acad Sci USA* 2009; **106**:5324–5329.

153 Grunewald TGP, Diebold I, Esposito I, Plehm S, Hauer K, Thiel U, *et al.* STEAP1 Is Associated with the Invasive and Oxidative Stress Phenotype of Ewing Tumors. *Mol Cancer Res* 2012; **10**:52–65.

154 Grunewald TGP, Kammerer U, Schulze E, Schindler D, Honig A, Zimmer M, *et al.* Silencing of LASP-1 influences zyxin localization, inhibits proliferation and reduces migration in breast cancer cells. *Exp Cell Res* 2006; **312**:974–982.

155 Benelli R, Albini A. In vitro models of angiogenesis: the use of Matrigel. *Int J Biol Markers* 1999; **14**:243–246.

156 Safford KM, Hicok KC, Safford SD, Halvorsen Y-DC, Wilkison WO, Gimble JM, *et al.* Neurogenic differentiation of murine and human adipose-derived stromal cells. *Biochem Biophys Res Commun* 2002; **294**:371–379.

157 Vater C, Kasten P, Stiehler M. Culture media for the differentiation of mesenchymal stromal cells. *Acta Biomater* 2011; **7**:463–477.

158 Helson L, Das SK, Hajdu SI. Human neuroblastoma in nude mice. *Cancer Res* 1975; **35**:2594–2599.

159 Corey E, Quinn JE, Bladou F, Brown LG, Roudier MP, Brown JM, *et al.* Establishment and characterization of osseous prostate cancer models: intra-tibial injection of human prostate cancer cells. *Prostate* 2002; **52**:20–33.

160 Grunewald TGP, Ranft A, Esposito I, da Silva-Buttkus P, Aichler M, Baumhoer D, *et al.* High STEAP1 expression is associated with improved outcome of Ewing's sarcoma patients. *Ann Oncol* 2012; **23**:2185–2190.

161 Edgar R, Domrachev M, Lash AE. Gene Expression Omnibus: NCBI gene expression and hybridization array data repository. *Nucleic Acids Res* 2002; **30**:207–210.

162 Tsai C-A, Chen Y-J, Chen JJ. Testing for differentially expressed genes with microarray data. *Nucleic Acids Res* 2003; **31**:e52.

163 Sturn A, Quackenbush J, Trajanoski Z. Genesis: cluster analysis of microarray data. *Bioinformatics* 2002; **18**:207–208.

164 Tusher VG, Tibshirani R, Chu G. Significance analysis of microarrays applied to the ionizing radiation response. *Proc Natl Acad Sci USA* 2001; **98**:5116–5121.

165 Subramanian A, Tamayo P, Mootha VK, Mukherjee S, Ebert BL, Gillette MA, *et al.* Gene set enrichment analysis: a knowledge-based approach for interpreting genome-wide expression profiles. *Proc Natl Acad Sci USA* 2005; **102**:15545–15550.

166 Roth RB, Hevezi P, Lee J, Willhite D, Lechner SM, Foster AC, *et al.* Gene expression analyses reveal molecular relationships among 20 regions of the human CNS. *Neurogenetics* 2006; **7**:67–80.

167 Scotlandi K, Remondini D, Castellani G, Manara MC, Nardi F, Cantiani L, *et al.* Overcoming resistance to conventional drugs in Ewing sarcoma and identification of molecular predictors of outcome. *J Clin Oncol* 2009; **27**:2209–2216.

168 Postel-Vinay S, Véron AS, Tirode F, Pierron G, Reynaud S, Kovar H, *et al.* Common variants near TARDBP and EGR2 are associated with susceptibility to Ewing sarcoma. *Nat Genet* 2012; **44**:323–327.

169 Bhojwani D, Kang H, Menezes RX, Yang W, Sather H, Moskowitz NP, *et al.* Gene expression signatures predictive of early response and outcome in high-risk childhood acute lymphoblastic leukemia: A Children's Oncology Group Study [corrected]. *J Clin Oncol* 2008; **26**:4376–4384.

170 Van Vlierberghe P, van Grotel M, Tchinda J, Lee C, Beverloo HB, van der Spek PJ, *et al.* The recurrent SET-NUP214 fusion as a new HOXA activation mechanism in pediatric T-cell acute lymphoblastic leukemia. *Blood* 2008; **111**:4668–4680.

171 Homminga I, Pieters R, Langerak AW, de Rooi JJ, Stubbs A, Verstegen M, *et al.* Integrated transcript and genome analyses reveal NKX2-1 and MEF2C as potential oncogenes in T cell acute lymphoblastic leukemia. *Cancer Cell* 2011; **19**:484–497.

172 Kang H, Chen I-M, Wilson CS, Bedrick EJ, Harvey RC, Atlas SR, *et al.* Gene expression classifiers for relapse-free survival and minimal residual disease improve risk classification and outcome prediction in pediatric B-precursor acute lymphoblastic leukemia. *Blood* 2010; **115**:1394–1405.

173 Harvey RC, Mullighan CG, Wang X, Dobbin KK, Davidson GS, Bedrick EJ, *et al.* Identification of novel cluster groups in pediatric high-risk B-precursor acute lymphoblastic leukemia with gene expression profiling: correlation with genome-wide DNA copy number alterations, clinical characteristics, and outcome. *Blood* 2010; **116**:4874–4884.

174 Kool M, Koster J, Bunt J, Hasselt NE, Lakeman A, van Sluis P, *et al.* Integrated genomics identifies five medulloblastoma subtypes with distinct genetic profiles, pathway signatures and clinicopathological features. *PLoS ONE* 2008; **3**:e3088.

175 Łastowska M, Viprey V, Santibanez-Koref M, Wappler I, Peters H, Cullinane C, *et al.* Identification of candidate genes involved in neuroblastoma progression by combining genomic and expression microarrays with survival data. *Oncogene* 2007; **26**:7432–7444.

176 Ohtaki M, Otani K, Hiyama K, Kamei N, Satoh K, Hiyama E. A robust method for estimating gene expression states using Affymetrix microarray probe level data. *BMC Bioinformatics* 2010; **11**:183.

177 Hanahan D, Weinberg RA. Hallmarks of cancer: the next generation. *Cell* 2011; **144**:646–674.

178 van Roy F, Berx G. The cell-cell adhesion molecule E-cadherin. *Cell Mol Life Sci* 2008; **65**:3756–3788.

179 Berx G, van Roy F. Involvement of members of the cadherin superfamily in cancer. *Cold Spring Harb Perspect Biol* 2009; **1**:a003129.

180 Aruffo A, Stamenkovic I, Melnick M, Underhill CB, Seed B. CD44 is the principal cell surface receptor for hyaluronate. *Cell* 1990; **61**:1303–1313.

181 Weber GF, Ashkar S, Glimcher MJ, Cantor H. Receptor-ligand interaction between CD44 and osteopontin (Eta-1). *Science* 1996; **271**:509–512.

182 Park YS, Huh JW, Lee JH, Kim HR. shRNA against CD44 inhibits cell proliferation, invasion and migration, and promotes apoptosis of colon carcinoma cells. *Oncol Rep* 2012; **27**:339–346.

183 Roland CL, Harken AH, Sarr MG, Barnett CC Jr. ICAM-1 expression determines malignant potential of cancer. *Surgery* 2007; **141**:705–707.

184 Yang L, Froio RM, Sciuto TE, Dvorak AM, Alon R, Luscinskas FW. ICAM-1 regulates neutrophil adhesion and transcellular migration of TNF-alpha-activated vascular endothelium under flow. *Blood* 2005; **106**:584–592.

185 Rothlein R, Dustin ML, Marlin SD, Springer TA. A human intercellular adhesion molecule (ICAM-1) distinct from LFA-1. *J Immunol* 1986; **137**:1270–1274.

186 Lynch CC, Hikosaka A, Acuff HB, Martin MD, Kawai N, Singh RK, *et al.* MMP-7 promotes prostate cancer-induced osteolysis via the solubilization of RANKL. *Cancer Cell* 2005; **7**:485–496.

187 Lu X, Wang Q, Hu G, Van Poznak C, Fleisher M, Reiss M, *et al.* ADAMTS1 and MMP1 proteolytically engage EGF-like ligands in an osteolytic signaling cascade for bone metastasis. *Genes Dev* 2009; **23**:1882–1894.

188 Weilbaecher KN, Guise TA, McCauley LK. Cancer to bone: a fatal attraction. *Nat Rev Cancer* 2011; **11**:411–425.

189 Garamszegi N, Garamszegi SP, Scully SP. Matrix metalloproteinase-1 contribution to sarcoma cell invasion. *J Cell Mol Med* Published Online First: 31 July 2011. doi:10.1111/j.1582-4934.2011.01402.x

190 Jawad MU, Garamszegi N, Garamszegi SP, Correa-Medina M, Diez JA, Wen R, *et al.* Matrix metalloproteinase 1: role in sarcoma biology. *PLoS ONE* 2010; **5**:e14250.

191 Blackburn JS, Rhodes CH, Coon CI, Brinckerhoff CE. RNA interference inhibition of matrix metalloproteinase-1 prevents melanoma metastasis by reducing tumor collagenase activity and angiogenesis. *Cancer Res* 2007; **67**:10849–10858.

192 Jamora C, DasGupta R, Kocieniewski P, Fuchs E. Links between signal transduction, transcription and adhesion in epithelial bud development. *Nature* 2003; **422**:317–322.

193 ten Berge D, Koole W, Fuerer C, Fish M, Eroglu E, Nusse R. Wnt signaling mediates self-organization and axis formation in embryoid bodies. *Cell Stem Cell* 2008; **3**:508–518.

194 Wielenga VJ, Smits R, Korinek V, Smit L, Kielman M, Fodde R, *et al.* Expression of CD44 in Apc and Tcf mutant mice implies regulation by the WNT pathway. *Am J Pathol* 1999; **154**:515–523.

195 Brabletz T, Jung A, Dag S, Hlubek F, Kirchner T. beta-catenin regulates the expression of the matrix metalloproteinase-7 in human colorectal cancer. *Am J Pathol* 1999; **155**:1033–1038.

196 Crawford HC, Fingleton BM, Rudolph-Owen LA, Goss KJ, Rubinfeld B, Polakis P, *et al.* The metalloproteinase matrilysin is a target of beta-catenin transactivation in intestinal tumors. *Oncogene* 1999; **18**:2883–2891.

197 Rockman SP, Currie SA, Ciavarella M, Vincan E, Dow C, Thomas RJ, *et al.* Id2 is a target of the beta-catenin/T cell factor pathway in colon carcinoma. *J Biol Chem* 2001; **276**:45113–45119.

198 Willert J, Epping M, Pollack JR, Brown PO, Nusse R. A transcriptional response to Wnt protein in human embryonic carcinoma cells. *BMC Dev Biol* 2002; **2**:8.

199 Mann B, Gelos M, Siedow A, Hanski ML, Gratchev A, Ilyas M, *et al.* Target genes of beta-catenin-T cell-factor/lymphoid-enhancer-factor signaling in human colorectal carcinomas. *Proc Natl Acad Sci USA* 1999; **96**:1603–1608.

200 Hovanes K, Li TW, Munguia JE, Truong T, Milovanovic T, Lawrence Marsh J, *et al.* Beta-catenin-sensitive isoforms of lymphoid enhancer factor-1 are selectively expressed in colon cancer. *Nat Genet* 2001; **28**:53–57.

201 Filali M, Cheng N, Abbott D, Leontiev V, Engelhardt JF. Wnt-3A/beta-catenin signaling induces transcription from the LEF-1 promoter. *J Biol Chem* 2002; **277**:33398–33410.

202 Ashburner M, Ball CA, Blake JA, Botstein D, Butler H, Cherry JM, *et al.* Gene ontology: tool for the unification of biology. The Gene Ontology Consortium. *Nat Genet* 2000; **25**:25–29.

203 Deverman BE, Cook BL, Manson SR, Niederhoff RA, Langer EM, Rosová I, *et al.* Bcl-xL deamidation is a critical switch in the regulation of the response to DNA damage. *Cell* 2002; **111**:51–62.

204 Shimizu S, Narita M, Tsujimoto Y. Bcl-2 family proteins regulate the release of apoptogenic cytochrome c by the mitochondrial channel VDAC. *Nature* 1999; **399**:483–487.

205 Boise LH, González-García M, Postema CE, Ding L, Lindsten T, Turka LA, *et al.* bcl-x, a bcl-2-related gene that functions as a dominant regulator of apoptotic cell death. *Cell* 1993; **74**:597–608.

206 Fujise K, Zhang D, Liu J, Yeh ET. Regulation of apoptosis and cell cycle progression by MCL1. Differential role of proliferating cell nuclear antigen. *J Biol Chem* 2000; **275**:39458–39465.

207 Reeves SA, Helman LJ, Allison A, Israel MA. Molecular cloning and primary structure of human glial fibrillary acidic protein. *Proc Natl Acad Sci USA* 1989; **86**:5178–5182.

208 Choi BH, Kim RC. Expression of glial fibrillary acidic protein in immature oligodendroglia. *Science* 1984; **223**:407–409.

209 Chao MV, Bothwell MA, Ross AH, Koprowski H, Lanahan AA, Buck CR, *et al.* Gene transfer and molecular cloning of the human NGF receptor. *Science* 1986; **232**:518–521.

210 Deppmann CD, Mihalas S, Sharma N, Lonze BE, Niebur E, Ginty DD. A model for neuronal competition during development. *Science* 2008; **320**:369–373.

211 Johnson D, Lanahan A, Buck CR, Sehgal A, Morgan C, Mercer E, *et al.* Expression and structure of the human NGF receptor. *Cell* 1986; **47**:545–554.

212 Brose K, Bland KS, Wang KH, Arnott D, Henzel W, Goodman CS, *et al.* Slit proteins bind Robo receptors and have an evolutionarily conserved role in repulsive axon guidance. *Cell* 1999; **96**:795–806.

213 Itoh A, Miyabayashi T, Ohno M, Sakano S. Cloning and expressions of three mammalian homologues of Drosophila slit suggest possible roles for Slit in the formation and maintenance of the nervous system. *Brain Res Mol Brain Res* 1998; **62**:175–186.

214 Wu W, Wong K, Chen J, Jiang Z, Dupuis S, Wu JY, *et al.* Directional guidance of neuronal migration in the olfactory system by the protein Slit. *Nature* 1999; **400**:331–336.

215 Benowitz LI, Routtenberg A. GAP-43: an intrinsic determinant of neuronal development and plasticity. *Trends Neurosci* 1997; **20**:84–91.

216 Kosik KS, Orecchio LD, Bruns GA, Benowitz LI, MacDonald GP, Cox DR, *et al.* Human GAP-43: its deduced amino acid sequence and chromosomal localization in mouse and human. *Neuron* 1988; **1**:127–132.

217 Min J-K, Park H, Choi H-J, Kim Y, Pyun B-J, Agrawal V, *et al.* The WNT antagonist Dickkopf2 promotes angiogenesis in rodent and human endothelial cells. *J Clin Invest* 2011; **121**:1882–1893.

218 Shirley SK, Gilula LA, Siegal GP, Foulkes MA, Kissane JM, Askin FB. Roentgenographic-pathologic correlation of diffuse sclerosis in Ewing sarcoma of bone. *Skeletal Radiol* 1984; **12**:69–78.

219 Lefebvre V, Huang W, Harley VR, Goodfellow PN, de Crombrugghe B. SOX9 is a potent activator of the chondrocyte-specific enhancer of the pro alpha1(II) collagen gene. *Mol Cell Biol* 1997; **17**:2336–2346.

220 Long MW. Osteogenesis and bone-marrow-derived cells. *Blood Cells Mol Dis* 2001; **27**:677–690.

221 Sun Y-X, Schneider A, Jung Y, Wang J, Dai J, Wang J, *et al.* Skeletal localization and neutralization of the SDF-1(CXCL12)/CXCR4 axis blocks prostate cancer metastasis and growth in osseous sites in vivo. *J Bone Miner Res* 2005; **20**:318–329.

222 Smith MCP, Luker KE, Garbow JR, Prior JL, Jackson E, Piwnica-Worms D, *et al.* CXCR4 regulates growth of both primary and metastatic breast cancer. *Cancer Res* 2004; **64**:8604–8612.

223 Bennani-Baiti IM, Cooper A, Lawlor ER, Kauer M, Ban J, Aryee DNT, *et al.* Intercohort gene expression co-analysis reveals chemokine receptors as prognostic indicators in Ewing's sarcoma. *Clin Cancer Res* 2010; **16**:3769–3778.

224 Guise TA, Yin JJ, Taylor SD, Kumagai Y, Dallas M, Boyce BF, *et al.* Evidence for a causal role of parathyroid hormone-related protein in the pathogenesis of human breast cancer-mediated osteolysis. *J Clin Invest* 1996; **98**:1544–1549.

225 Guise TA, Mohammad KS, Clines G, Stebbins EG, Wong DH, Higgins LS, *et al.* Basic mechanisms responsible for osteolytic and osteoblastic bone metastases. *Clin Cancer Res* 2006; **12**:6213s–6216s.

226 Henderson MA, Danks JA, Slavin JL, Byrnes GB, Choong PFM, Spillane JB, *et al.* Parathyroid hormone-related protein localization in breast cancers predict improved prognosis. *Cancer Res* 2006; **66**:2250–2256.

227 Li J, Karaplis AC, Huang DC, Siegel PM, Camirand A, Yang XF, *et al.* PTHrP drives breast tumor initiation, progression, and metastasis in mice and is a potential therapy target. *J Clin Invest* 2011; **121**:4655–4669.

228 Pratap J, Imbalzano KM, Underwood JM, Cohet N, Gokul K, Akech J, *et al.* Ectopic runx2 expression in mammary epithelial cells disrupts formation of normal acini structure: implications for breast cancer progression. *Cancer Res* 2009; **69**:6807–6814.

229 Javed A, Barnes GL, Pratap J, Antkowiak T, Gerstenfeld LC, van Wijnen AJ, *et al.* Impaired intranuclear trafficking of Runx2 (AML3/CBFA1) transcription factors in breast cancer cells inhibits osteolysis in vivo. *Proc Natl Acad Sci USA* 2005; **102**:1454–1459.

230 Yin JJ, Selander K, Chirgwin JM, Dallas M, Grubbs BG, Wieser R, *et al.* TGF-beta signaling blockade inhibits PTHrP secretion by breast cancer cells and bone metastases development. *J Clin Invest* 1999; **103**:197–206.

231 Ikushima H, Miyazono K. TGFbeta signalling: a complex web in cancer progression. *Nat Rev Cancer* 2010; **10**:415–424.

232 Taylor R, Knowles HJ, Athanasou NA. Ewing sarcoma cells express RANKL and support osteoclastogenesis. *J Pathol* 2011; **225**:195–202.

233 Dunn LK, Mohammad KS, Fournier PGJ, McKenna CR, Davis HW, Niewolna M, *et al.* Hypoxia and TGF-beta drive breast cancer bone metastases through parallel signaling pathways in tumor cells and the bone microenvironment. *PLoS ONE* 2009; **4**:e6896.

234 Hiraga T, Kizaka-Kondoh S, Hirota K, Hiraoka M, Yoneda T. Hypoxia and hypoxia-inducible factor-1 expression enhance osteolytic bone metastases of breast cancer. *Cancer Res* 2007; **67**:4157–4163.

235 Sethi N, Dai X, Winter CG, Kang Y. Tumor-derived JAGGED1 promotes osteolytic bone metastasis of breast cancer by engaging notch signaling in bone cells. *Cancer Cell* 2011; **19**:192–205.

236 mediatum - digital collection management. http://nbn-resolving.de/urn/resolver.pl?urn:nbn:de:bvb:91-diss-20110113-981233-1-3 (accessed 25 Jul2012).

237 Zhou S, Schuetz JD, Bunting KD, Colapietro AM, Sampath J, Morris JJ, *et al.* The ABC transporter Bcrp1/ABCG2 is expressed in a wide variety of stem cells and is a molecular determinant of the side-population phenotype. *Nat Med* 2001; **7**:1028–1034.

238 Mitsui K, Tokuzawa Y, Itoh H, Segawa K, Murakami M, Takahashi K, *et al.* The homeoprotein Nanog is required for maintenance of pluripotency in mouse epiblast and ES cells. *Cell* 2003; **113**:631–642.

239 Katoh Y, Katoh M. Comparative genomics on PROM1 gene encoding stem cell marker CD133. *Int J Mol Med* 2007; **19**:967–970.

240 Aoyama T, Okamoto T, Nagayama S, Nishijo K, Ishibe T, Yasura K, *et al.* Methylation in the core-promoter region of the chondromodulin-I gene determines the cell-specific expression by regulating the binding of transcriptional activator Sp3. *J Biol Chem* 2004; **279**:28789–28797.

241 Carrillo J, García-Aragoncillo E, Azorín D, Agra N, Sastre A, González-Mediero I, *et al.* Cholecystokinin down-regulation by RNA interference impairs Ewing tumor growth. *Clin Cancer Res* 2007; **13**:2429–2440.

242 Wai DH, Schaefer K-L, Schramm A, Korsching E, Van Valen F, Ozaki T, *et al.* Expression analysis of pediatric solid tumor cell lines using oligonucleotide microarrays. *Int J Oncol* 2002; **20**:441–451.

243 Riggi N, Suvà M-L, Suvà D, Cironi L, Provero P, Tercier S, *et al.* EWS-FLI-1 expression triggers a Ewing's sarcoma initiation program in primary human mesenchymal stem cells. *Cancer Res* 2008; **68**:2176–2185.

244 Burdach S, Plehm S, Unland R, Dirksen U, Borkhardt A, Staege MS, *et al.* Epigenetic maintenance of stemness and malignancy in peripheral neuroectodermal tumors by EZH2. *Cell Cycle* 2009; **8**:1991–1996.

245 Aoyama T, Okamoto T, Kohno Y, Fukiage K, Otsuka S, Furu M, *et al.* Cell-specific epigenetic regulation of ChM-I gene expression: crosstalk between DNA methylation and histone acetylation. *Biochem Biophys Res Commun* 2008; **365**:124–130.

246 Aoyama T, Okamoto T, Fukiage K, Otsuka S, Furu M, Ito K, *et al.* Histone modifiers, YY1 and p300, regulate the expression of cartilage-specific gene, chondromodulin-I, in mesenchymal stem cells. *J Biol Chem* 2010; **285**:29842–29850.

247 Miyagawa Y, Okita H, Itagaki M, Toyoda M, Katagiri YU, Fujimoto J, *et al.* EWS/ETS regulates the expression of the Dickkopf family in Ewing family tumor cells. *PLoS ONE* 2009; **4**:e4634.

248 Navarro D, Agra N, Pestaña A, Alonso J, González-Sancho JM. The EWS/FLI1 oncogenic protein inhibits expression of the Wnt inhibitor DICKKOPF-1 gene and antagonizes beta-catenin/TCF-mediated transcription. *Carcinogenesis* 2010; **31**:394–401.

249 Gage PJ, Qian M, Wu D, Rosenberg KI. The canonical Wnt signaling antagonist DKK2 is an essential effector of PITX2 function during normal eye development. *Developmental Biology* 2008; **317**:310–324.

250 Kumar S, Duester G. Retinoic acid signaling in perioptic mesenchyme represses Wnt signaling via induction of Pitx2 and Dkk2. *Developmental Biology* 2010; **340**:67–74.

251 Michl P, Knobel B, Downward J. CUTL1 is phosphorylated by protein kinase A, modulating its effects on cell proliferation and motility. *J Biol Chem* 2006; **281**:15138–15144.

252 Schulte TW, Toretsky JA, Ress E, Helman L, Neckers LM. Expression of PAX3 in Ewing's Sarcoma Family of Tumors. *Biochemical and Molecular Medicine* 1997; **60**:121–126.

253 Ducy P, Zhang R, Geoffroy V, Ridall AL, Karsenty G. Osf2/Cbfa1: a transcriptional activator of osteoblast differentiation. *Cell* 1997; **89**:747–754.

254 Shultz LD, Ishikawa F, Greiner DL. Humanized mice in translational biomedical research. *Nat Rev Immunol* 2007; **7**:118–130.

255 Nanni P, Nicoletti G, Landuzzi L, Croci S, Murgo A, Palladini A, *et al.* High metastatic efficiency of human sarcoma cells in Rag2/gammac double knockout mice provides a powerful test system for antimetastatic targeted therapy. *Eur J Cancer* 2010; **46**:659–668.

256 Hillen F, Griffioen A. Tumour vascularization: sprouting angiogenesis and beyond. *Cancer and Metastasis Reviews* 2007; **26**:489–502.

257 Carmeliet P, Jain RK. Angiogenesis in cancer and other diseases. *Nature* 2000; **407**:249–257.

258 Jain RK, Carmeliet P. SnapShot: Tumor Angiogenesis. *Cell* 2012; **149**:1408–1408.e1.

259 Inoue H, Kondo J, Koike T, Shukunami C, Hiraki Y. Identification of an autocrine chondrocyte colony-stimulating factor: chondromodulin-I stimulates the colony formation of growth plate chondrocytes in agarose culture. *Biochem Biophys Res Commun* 1997; **241**:395–400.

260 Shukunami C, Hiraki Y. Expression of cartilage-specific functional matrix chondromodulin-I mRNA in rabbit growth plate chondrocytes and its responsiveness to growth stimuli in vitro. *Biochem Biophys Res Commun* 1998; **249**:885–890.

261 Mori Y, Hiraki Y, Shukunami C, Kakudo S, Shiokawa M, Kagoshima M, *et al.* Stimulation of osteoblast proliferation by the cartilage-derived growth promoting factors chondromodulin-I and -II. *FEBS Lett* 1997; **406**:310–314.

262 Vormoor J, Baersch G, Decker S, Hotfilder M, Schäfer KL, Pelken L, *et al.* Establishment of an in vivo model for pediatric Ewing tumors by transplantation into NOD/scid mice. *Pediatr Res* 2001; **49**:332–341.

263 Manara MC, Landuzzi L, Nanni P, Nicoletti G, Zambelli D, Lollini PL, *et al.* Preclinical In vivo Study of New Insulin-Like Growth Factor-I Receptor–Specific Inhibitor in Ewing's Sarcoma. *Clin Cancer Res* 2007; **13**:1322–1330.

264 Rocchi A, Manara MC, Sciandra M, Zambelli D, Nardi F, Nicoletti G, *et al.* CD99 inhibits neural differentiation of human Ewing sarcoma cells and thereby contributes to oncogenesis. *J Clin Invest* 2010; **120**:668–680.

265 Scotlandi K, Benini S, Manara MC, Serra M, Nanni P, Lollini PL, *et al.* Murine model for skeletal metastases of Ewing's sarcoma. *J Orthop Res* 2000; **18**:959–966.

266 Bucan V, Mandel K, Bertram C, Lazaridis A, Reimers K, Park-Simon T-W, *et al.* LEF-1 regulates proliferation and MMP-7 transcription in breast cancer cells. *Genes to cells: devoted to molecular & cellular mechanisms* Published Online First: 12 June 2012. doi:10.1111/j.1365-2443.2012.01613.x

267 Mori S, Chang JT, Andrechek ER, Matsumura N, Baba T, Yao G, *et al.* An Anchorage-Independent Cell Growth Signature Identifies Tumors with Metastatic Potential. *Oncogene* 2009; **28**:2796–2805.

268 Jiang Y, Cui L, Yie TA, Rom WN, Cheng H, Tchou-Wong KM. Inhibition of anchorage-independent growth and lung metastasis of A549 lung carcinoma cells by IkappaBbeta. *Oncogene* 2001; **20**:2254–2263.

269 Derksen PWB, Liu X, Saridin F, van der Gulden H, Zevenhoven J, Evers B, *et al.* Somatic inactivation of E-cadherin and p53 in mice leads to metastatic lobular mammary carcinoma through induction of anoikis resistance and angiogenesis. *Cancer Cell* 2006; **10**:437–449.

270 Guadamillas MC, Cerezo A, Del Pozo MA. Overcoming anoikis--pathways to anchorage-independent growth in cancer. *J Cell Sci* 2011; **124**:3189–3197.

271 Junxia W, Ping G, Yuan H, Lijun Z, Jihong R, Fang L, *et al.* Double strand RNA-guided endogeneous E-cadherin up-regulation induces the apoptosis and inhibits proliferation of breast carcinoma cells in vitro and in vivo. *Cancer Sci* 2010; **101**:1790–1796.

272 Onder TT, Gupta PB, Mani SA, Yang J, Lander ES, Weinberg RA. Loss of E-cadherin promotes metastasis via multiple downstream transcriptional pathways. *Cancer Res* 2008; **68**:3645–3654.

273 Jeanes A, Gottardi CJ, Yap AS. Cadherins and cancer: how does cadherin dysfunction promote tumor progression? *Oncogene* 2008; **27**:6920–6929.

274 Anborgh PH, Mutrie JC, Tuck AB, Chambers AF. Role of the metastasis-promoting protein osteopontin in the tumour microenvironment. *J Cell Mol Med* 2010; **14**:2037–2044.

275 Fuchs B, Inwards CY, Janknecht R. Upregulation of the matrix metalloproteinase-1 gene by the Ewing's sarcoma associated EWS-ER81 and EWS-Fli-1 oncoproteins, c-Jun and p300. *FEBS Lett* 2003; **553**:104–108.

276 Bin Hafeez B, Adhami VM, Asim M, Siddiqui IA, Bhat KM, Zhong W, *et al.* Targeted knockdown of Notch1 inhibits invasion of human prostate cancer cells concomitant with inhibition of matrix metalloproteinase-9 and urokinase plasminogen activator. *Clin Cancer Res* 2009; **15**:452–459.

277 Mitra RS, Goto M, Lee JS, Maldonado D, Taylor JMG, Pan Q, *et al.* Rap1GAP promotes invasion via induction of matrix metalloproteinase 9 secretion, which is associated with poor survival in low N-stage squamous cell carcinoma. *Cancer Res* 2008; **68**:3959–3969.

278 Wang X, Lu H, Urvalek AM, Li T, Yu L, Lamar J, *et al.* KLF8 promotes human breast cancer cell invasion and metastasis by transcriptional activation of MMP9. *Oncogene* 2011; **30**:1901–1911.

279 Wiercinska E, Naber HPH, Pardali E, van der Pluijm G, van Dam H, ten Dijke P. The TGF-β/Smad pathway induces breast cancer cell invasion through the up-regulation of matrix metalloproteinase 2 and 9 in a spheroid invasion model system. *Breast Cancer Res Treat* 2011; **128**:657–666.

280 Shchors K, Nozawa H, Xu J, Rostker F, Swigart-Brown L, Evan G, *et al.* Increased invasiveness of MMP-9-deficient tumors in two mouse models of neuroendocrine tumorigenesis. *Oncogene* Published Online First: 5 March 2012. doi:10.1038/onc.2012.60

281 Braet F, Wisse E. Structural and functional aspects of liver sinusoidal endothelial cell fenestrae: a review. *Comp Hepatol* 2002; **1**:1.

282 Longo KA, Kennell JA, Ochocinska MJ, Ross SE, Wright WS, MacDougald OA. Wnt signaling protects 3T3-L1 preadipocytes from apoptosis through induction of insulin-like growth factors. *J Biol Chem* 2002; **277**:38239–38244.

283 Rodilla V, Villanueva A, Obrador-Hevia A, Robert-Moreno A, Fernández-Majada V, Grilli A, *et al.* Jagged1 is the pathological link between Wnt and Notch pathways in colorectal cancer. *Proc Natl Acad Sci USA* 2009; **106**:6315–6320.

284 Dong Y-F, Soung DY, Schwarz EM, O'Keefe RJ, Drissi H. Wnt induction of chondrocyte hypertrophy through the Runx2 transcription factor. *J Cell Physiol* 2006; **208**:77–86.

285 Zhang X, Gaspard JP, Chung DC. Regulation of vascular endothelial growth factor by the Wnt and K-ras pathways in colonic neoplasia. *Cancer Res* 2001; **61**:6050–6054.

286 Mao J, Wang J, Liu B, Pan W, Farr GH 3rd, Flynn C, *et al.* Low-density lipoprotein receptor-related protein-5 binds to Axin and regulates the canonical Wnt signaling pathway. *Mol Cell* 2001; **7**:801–809.

287 Mao B, Wu W, Li Y, Hoppe D, Stannek P, Glinka A, *et al.* LDL-receptor-related protein 6 is a receptor for Dickkopf proteins. *Nature* 2001; **411**:321–325.

288 Wu W, Glinka A, Delius H, Niehrs C. Mutual antagonism between dickkopf1 and dickkopf2 regulates Wnt/beta-catenin signalling. *Curr Biol* 2000; **10**:1611–1614.

289 Wang K, Zhang Y, Li X, Chen L, Wang H, Wu J, *et al.* Characterization of the Kremen-binding site on Dkk1 and elucidation of the role of Kremen in Dkk-mediated Wnt antagonism. *J Biol Chem* 2008; **283**:23371–23375.

290 Glass DA 2nd, Karsenty G. Molecular bases of the regulation of bone remodeling by the canonical Wnt signaling pathway. *Curr Top Dev Biol* 2006; **73**:43–84.

291 Yeo AT, Porco JA Jr, Gilmore TD. Bcl-XL, but not Bcl-2, can protect human B-lymphoma cell lines from parthenolide-induced apoptosis. *Cancer Lett* 2012; **318**:53–60.

292 Bouillet P, Strasser A. BH3-only proteins — evolutionarily conserved proapoptotic Bcl-2 family members essential for initiating programmed cell death. *J Cell Sci* 2002; **115**:1567–1574.

293 Huang DC, Strasser A. BH3-Only proteins-essential initiators of apoptotic cell death. *Cell* 2000; **103**:839–842.

294 Inuzuka H, Shaik S, Onoyama I, Gao D, Tseng A, Maser RS, *et al.* SCF(FBW7) regulates cellular apoptosis by targeting MCL1 for ubiquitylation and destruction. *Nature* 2011; **471**:104–109.

295 Mott JL, Kobayashi S, Bronk SF, Gores GJ. mir-29 regulates Mcl-1 protein expression and apoptosis. *Oncogene* 2007; **26**:6133–6140.

296 Chen L, Willis SN, Wei A, Smith BJ, Fletcher JI, Hinds MG, *et al.* Differential targeting of prosurvival Bcl-2 proteins by their BH3-only ligands allows complementary apoptotic function. *Mol Cell* 2005; **17**:393–403.

297 Willis SN, Chen L, Dewson G, Wei A, Naik E, Fletcher JI, *et al.* Proapoptotic Bak is sequestered by Mcl-1 and Bcl-xL, but not Bcl-2, until displaced by BH3-only proteins. *Genes Dev* 2005; **19**:1294–1305.

298 Weng C, Li Y, Xu D, Shi Y, Tang H. Specific cleavage of Mcl-1 by caspase-3 in tumor necrosis factor-related apoptosis-inducing ligand (TRAIL)-induced apoptosis in Jurkat leukemia T cells. *J Biol Chem* 2005; **280**:10491–10500.

299 Oh H, Ryu J-H, Jeon J, Yang S, Chun C-H, Park H, *et al.* Misexpression of Dickkopf-1 in endothelial cells, but not in chondrocytes or hypertrophic chondrocytes, causes defects in endochondral ossification. *J Bone Miner Res* 2012; **27**:1335–1344.

300 Jung IL, Kang HJ, Kim KC, Kim IG. Knockdown of the Dickkopf 3 gene induces apoptosis in a lung adenocarcinoma. *Int J Mol Med* 2010; **26**:33–38.

301 Nakamura REI, Hunter DD, Yi H, Brunken WJ, Hackam AS. Identification of two novel activities of the Wnt signaling regulator Dickkopf 3 and characterization of its expression in the mouse retina. *BMC Cell Biol* 2007; **8**:52.

302 Herishanu Y, Gibellini F, Njuguna N, Hazan-Halevy I, Farooqui M, Bern S, *et al.* Activation of CD44, a receptor for extracellular matrix components, protects chronic lymphocytic leukemia cells from spontaneous and drug induced apoptosis through MCL-1. *Leuk Lymphoma* 2011; **52**:1758–1769.

303 Hauptschein RS, Sloan KE, Torella C, Moezzifard R, Giel-Moloney M, Zehetmeier C, *et al.* Functional Proteomic Screen Identifies a Modulating Role for CD44 in Death Receptor–Mediated Apoptosis. *Cancer Res* 2005; **65**:1887–1896.

304 Henke C, Bitterman P, Roongta U, Ingbar D, Polunovsky V. Induction of fibroblast apoptosis by anti-CD44 antibody: implications for the treatment of fibroproliferative lung disease. *Am J Pathol* 1996; **149**:1639–1650.

305 Cao Y, Liu X, Zhang W, Deng X, Zhang H, Liu Y, *et al.* TGF-beta repression of Id2 induces apoptosis in gut epithelial cells. *Oncogene* 2009; **28**:1089–1098.

306 Gandhirajan RK, Staib PA, Minke K, Gehrke I, Plickert G, Schlösser A, *et al.* Small molecule inhibitors of Wnt/beta-catenin/lef-1 signaling induces apoptosis in chronic lymphocytic leukemia cells in vitro and in vivo. *Neoplasia* 2010; **12**:326–335.

307 Gutierrez A Jr, Tschumper RC, Wu X, Shanafelt TD, Eckel-Passow J, Huddleston PM 3rd, *et al.* LEF-1 is a prosurvival factor in chronic lymphocytic leukemia and is expressed in the preleukemic state of monoclonal B-cell lymphocytosis. *Blood* 2010; **116**:2975–2983.

308 Zhou F, Zhang L, van Laar T, van Dam H, Ten Dijke P. GSK3β inactivation induces apoptosis of leukemia cells by repressing the function of c-Myb. *Mol Biol Cell* 2011; **22**:3533–3540.

309 Kasahara Y, Tuder RM, Taraseviciene-Stewart L, Le Cras TD, Abman S, Hirth PK, *et al.* Inhibition of VEGF receptors causes lung cell apoptosis and emphysema. *J Clin Invest* 2000; **106**:1311–1319.

310 Li Y, Zhang F, Nagai N, Tang Z, Zhang S, Scotney P, *et al.* VEGF-B inhibits apoptosis via VEGFR-1-mediated suppression of the expression of BH3-only protein genes in mice and rats. *J Clin Invest* 2008; **118**:913–923.

311 Tao Z, Chen B, Tan X, Zhao Y, Wang L, Zhu T, *et al.* Coexpression of VEGF and angiopoietin-1 promotes angiogenesis and cardiomyocyte proliferation reduces apoptosis in porcine myocardial infarction (MI) heart. *Proc Natl Acad Sci USA* 2011; **108**:2064–2069.

312 Kang H-G, Jenabi JM, Zhang J, Keshelava N, Shimada H, May WA, *et al.* E-cadherin cell-cell adhesion in ewing tumor cells mediates suppression of anoikis through activation of the ErbB4 tyrosine kinase. *Cancer Res* 2007; **67**:3094–3105.

313 Torres VA, Tapia JC, Rodriguez DA, Lladser A, Arredondo C, Leyton L, *et al.* E-cadherin is required for caveolin-1-mediated down-regulation of the inhibitor of apoptosis protein survivin via reduced beta-catenin-Tcf/Lef-dependent transcription. *Mol Cell Biol* 2007; **27**:7703–7717.

314 Eng LF, Ghirnikar RS, Lee YL. Glial fibrillary acidic protein: GFAP-thirty-one years (1969-2000). *Neurochem Res* 2000; **25**:1439–1451.

315 Lee R, Kermani P, Teng KK, Hempstead BL. Regulation of cell survival by secreted proneurotrophins. *Science* 2001; **294**:1945–1948.

316 Huang P, Kishida S, Cao D, Murakami-Tonami Y, Mu P, Nakaguro M, *et al.* The neuronal differentiation factor NeuroD1 downregulates the neuronal repellent factor Slit2 expression and promotes cell motility and tumor formation of neuroblastoma. *Cancer Res* 2011; **71**:2938–2948.

317 Yu J, Cao Q, Yu J, Wu L, Dallol A, Li J, *et al.* The neuronal repellent SLIT2 is a target for repression by EZH2 in prostate cancer. *Oncogene* 2010; **29**:5370–5380.

318 Wang C, Liu Z, Woo C-W, Li Z, Wang L, Wei JS, *et al.* EZH2 Mediates epigenetic silencing of neuroblastoma suppressor genes CASZ1, CLU, RUNX3, and NGFR. *Cancer Res* 2012; **72**:315–324.

319 Li X, McGee-Lawrence ME, Decker M, Westendorf JJ. The Ewing's sarcoma fusion protein, EWS-FLI, binds Runx2 and blocks osteoblast differentiation. *J Cell Biochem* 2010; **111**:933–943.

320 Endo Y, Beauchamp E, Woods D, Taylor WG, Toretsky JA, Uren A, *et al.* Wnt-3a and Dickkopf-1 stimulate neurite outgrowth in Ewing tumor cells via a Frizzled3- and c-Jun N-terminal kinase-dependent mechanism. *Mol Cell Biol* 2008; **28**:2368–2379.

321 Bergers G, Benjamin LE. Tumorigenesis and the angiogenic switch. *Nat Rev Cancer* 2003; **3**:401–410.

322 Smadja DM, d' Audigier C, Weiswald L-B, Badoual C, Dangles-Marie V, Mauge L, *et al.* The Wnt antagonist Dickkopf-1 increases endothelial progenitor cell angiogenic potential. *Arterioscler Thromb Vasc Biol* 2010; **30**:2544–2552.

323 Untergasser G, Steurer M, Zimmermann M, Hermann M, Kern J, Amberger A, *et al.* The Dickkopf-homolog 3 is expressed in tumor endothelial cells and supports capillary formation. *Int J Cancer* 2008; **122**:1539–1547.

324 Pendás-Franco N, García JM, Peña C, Valle N, Pálmer HG, Heinäniemi M, *et al.* DICKKOPF-4 is induced by TCF/beta-catenin and upregulated in human colon cancer, promotes tumour cell invasion and angiogenesis and is repressed by 1alpha,25-dihydroxyvitamin D3. *Oncogene* 2008; **27**:4467–4477.

325 Blackburn JS, Brinckerhoff CE. Matrix metalloproteinase-1 and thrombin differentially activate gene expression in endothelial cells via PAR-1 and promote angiogenesis. *Am J Pathol* 2008; **173**:1736–1746.

326 Hiraki Y, Tanaka H, Inoue H, Kondo J, Kamizono A, Suzuki F. Molecular cloning of a new class of cartilage-specific matrix, chondromodulin-I, which stimulates growth of cultured chondrocytes. *Biochem Biophys Res Commun* 1991; **175**:971–977.

327 Tsuda M, Takahashi S, Takahashi Y, Asahara H. Transcriptional co-activators CREB-binding protein and p300 regulate chondrocyte-specific gene expression via association with Sox9. *J Biol Chem* 2003; **278**:27224–27229.

328 Huang W, Lu N, Eberspaecher H, De Crombrugghe B. A new long form of c-Maf cooperates with Sox9 to activate the type II collagen gene. *J Biol Chem* 2002; **277**:50668–50675.

329 Schmid TM, Linsenmayer TF. Immunohistochemical localization of short chain cartilage collagen (type X) in avian tissues. *J Cell Biol* 1985; **100**:598–605.

330 Shen G. The role of type X collagen in facilitating and regulating endochondral ossification of articular cartilage. *Orthod Craniofac Res* 2005; **8**:11–17.

331 Kern B, Shen J, Starbuck M, Karsenty G. Cbfa1 contributes to the osteoblast-specific expression of type I collagen genes. *J Biol Chem* 2001; **276**:7101–7107.

332 Sugawara M, Kato N, Tsuchiya T, Motoyama T. RUNX2 expression in developing human bones and various bone tumors. *Pathol Int* 2011; **61**:565–571.

333 Rucci N, Teti A. Osteomimicry: how tumor cells try to deceive the bone. *Front Biosci (Schol Ed)* 2010; **2**:907–915.

334 Doyle LA, Yang W, Abruzzo LV, Krogmann T, Gao Y, Rishi AK, *et al.* A multidrug resistance transporter from human MCF-7 breast cancer cells. *Proc Natl Acad Sci USA* 1998; **95**:15665–15670.

335 Yin AH, Miraglia S, Zanjani ED, Almeida-Porada G, Ogawa M, Leary AG, *et al.* AC133, a novel marker for human hematopoietic stem and progenitor cells. *Blood* 1997; **90**:5002–5012.

336 Miraglia S, Godfrey W, Yin AH, Atkins K, Warnke R, Holden JT, *et al.* A novel five-transmembrane hematopoietic stem cell antigen: isolation, characterization, and molecular cloning. *Blood* 1997; **90**:5013–5021.

337 Bellahcène A, Maloujahmoum N, Fisher LW, Pastorino H, Tagliabue E, Ménard S, *et al.* Expression of bone sialoprotein in human lung cancer. *Calcif Tissue Int* 1997; **61**:183–188.

338 Bäuerle T, Adwan H, Kiessling F, Hilbig H, Armbruster FP, Berger MR. Characterization of a rat model with site-specific bone metastasis induced by MDA-MB-231 breast cancer cells and its application to the effects of an antibody against bone sialoprotein. *Int J Cancer* 2005; **115**:177–186.

339 Lau WM, Weber KL, Doucet M, Chou Y-T, Brady K, Kowalski J, *et al.* Identification of prospective factors promoting osteotropism in breast cancer: a potential role for CITED2. *Int J Cancer* 2010; **126**:876–884.

340 Sackstein R, Merzaban JS, Cain DW, Dagia NM, Spencer JA, Lin CP, *et al.* Ex vivo glycan engineering of CD44 programs human multipotent mesenchymal stromal cell trafficking to bone. *Nat Med* 2008; **14**:181–187.

341 Thankamony SP, Sackstein R. Enforced hematopoietic cell E- and L-selectin ligand (HCELL) expression primes transendothelial migration of human mesenchymal stem cells. *Proc Natl Acad Sci USA* 2011; **108**:2258–2263.

342 Son J, Lee J-H, Kim H-N, Ha H, Lee ZH. cAMP-response-element-binding protein positively regulates breast cancer metastasis and subsequent bone destruction. *Biochem Biophys Res Commun* 2010; **398**:309–314.

343 De S, Chen J, Narizhneva NV, Heston W, Brainard J, Sage EH, *et al.* Molecular pathway for cancer metastasis to bone. *J Biol Chem* 2003; **278**:39044–39050.

344 Kakonen S-M, Selander KS, Chirgwin JM, Yin JJ, Burns S, Rankin WA, *et al.* Transforming growth factor-beta stimulates parathyroid hormone-related protein and osteolytic metastases via Smad and mitogen-activated protein kinase signaling pathways. *J Biol Chem* 2002; **277**:24571–24578.

345 Parmo-Cabañas M, Bartolomé RA, Wright N, Hidalgo A, Drager AM, Teixidó J. Integrin alpha4beta1 involvement in stromal cell-derived factor-1alpha-promoted myeloma cell

transendothelial migration and adhesion: role of cAMP and the actin cytoskeleton in adhesion. *Exp Cell Res* 2004; **294**:571–580.

346 Li X, Loberg R, Liao J, Ying C, Snyder LA, Pienta KJ, *et al.* A destructive cascade mediated by CCL2 facilitates prostate cancer growth in bone. *Cancer Res* 2009; **69**:1685–1692.

347 Chou Y-T, Wang H, Chen Y, Danielpour D, Yang Y-C. Cited2 modulates TGF-beta-mediated upregulation of MMP9. *Oncogene* 2006; **25**:5547–5560.

348 González I, Vicent S, de Alava E, Lecanda F. EWS/FLI-1 oncoprotein subtypes impose different requirements for transformation and metastatic activity in a murine model. *J Mol Med* 2007; **85**:1015–1029.

349 Huang W-C, Xie Z, Konaka H, Sodek J, Zhau HE, Chung LWK. Human Osteocalcin and Bone Sialoprotein Mediating Osteomimicry of Prostate Cancer Cells: Role of cAMP-Dependent Protein Kinase A Signaling Pathway. *Cancer Res* 2005; **65**:2303–2313.

350 Ducy P, Karsenty G. Two distinct osteoblast-specific cis-acting elements control expression of a mouse osteocalcin gene. *Mol Cell Biol* 1995; **15**:1858–1869.

351 Guan H, Zhou Z, Cao Y, Duan X, Kleinerman ES. VEGF165 promotes the osteolytic bone destruction of ewing's sarcoma tumors by upregulating RANKL. *Oncol Res* 2009; **18**:117–125.

352 Tao J, Erez A, Lee B. One NOTCH Further: Jagged 1 in Bone Metastasis. *Cancer Cell* 2011; **19**:159–161.

353 Ara T, Song L, Shimada H, Keshelava N, Russell HV, Metelitsa LS, *et al.* Interleukin-6 in the bone marrow microenvironment promotes the growth and survival of neuroblastoma cells. *Cancer Res* 2009; **69**:329–337.

354 Ban J, Bennani-Baiti IM, Kauer M, Schaefer K-L, Poremba C, Jug G, *et al.* EWS-FLI1 suppresses NOTCH-activated p53 in Ewing's sarcoma. *Cancer Res* 2008; **68**:7100–7109.

355 Bennani-Baiti IM, Aryee DN, Ban J, Machado I, Kauer M, Mühlbacher K, *et al.* Notch signalling is off and is uncoupled from HES1 expression in Ewing's sarcoma. *J Pathol* 2011; **225**:353–363.

356 Lissat A, Chao MM, Kontny U. Targeted therapy in ewing sarcoma. *ISRN Oncol* 2012; **2012**:609439.

357 Kovar H, Alonso J, Aman P, Aryee DNT, Ban J, Burchill SA, *et al.* The First European Interdisciplinary Ewing Sarcoma Research Summit. *Front Oncol* 2012; **2**. doi:10.3389/fonc.2012.00054

358 Thiel U, Wawer A, Wolf P, Badoglio M, Santucci A, Klingebiel T, *et al.* No improvement of survival with reduced- versus high-intensity conditioning for allogeneic stem cell transplants in Ewing tumor patients. *Ann Oncol* 2011; **22**:1614–1621.

359 Kovar H, Aryee D, Zoubek A. The Ewing family of tumors and the search for the Achilles' heel. *Curr Opin Oncol* 1999; **11**:275–284.

360 Lessnick SL, Braun BS, Denny CT, May WA. Multiple domains mediate transformation by the Ewing's sarcoma EWS/FLI-1 fusion gene. *Oncogene* 1995; **10**:423–431.

361 May WA, Gishizky ML, Lessnick SL, Lunsford LB, Lewis BC, Delattre O, *et al.* Ewing sarcoma 11;22 translocation produces a chimeric transcription factor that requires the DNA-binding domain encoded by FLI1 for transformation. *Proc Natl Acad Sci USA* 1993; **90**:5752–5756.

362 May WA, Lessnick SL, Braun BS, Klemsz M, Lewis BC, Lunsford LB, *et al.* The Ewing's sarcoma EWS/FLI-1 fusion gene encodes a more potent transcriptional activator and is a more powerful transforming gene than FLI-1. *Mol Cell Biol* 1993; **13**:7393–7398.

363 Hühn R, Staege MS, Hesse M, Liebig B, Burdach SEG. Cleavage of the Ewing tumour-specific EWSR1-FLI1 mRNA by hammerhead ribozymes. *Anticancer Res* 2009; **29**:1901–1908.

364 Maksimenko A, Malvy C. Oncogene-targeted antisense oligonucleotides for the treatment of Ewing sarcoma. *Expert Opin Ther Targets* 2005; **9**:825–830.

365 Hu-Lieskovan S, Heidel JD, Bartlett DW, Davis ME, Triche TJ. Sequence-specific knockdown of EWS-FLI1 by targeted, nonviral delivery of small interfering RNA inhibits tumor growth in a murine model of metastatic Ewing's sarcoma. *Cancer Res* 2005; **65**:8984–8992.

366 Tanaka K, Iwakuma T, Harimaya K, Sato H, Iwamoto Y. EWS-Fli1 antisense oligodeoxynucleotide inhibits proliferation of human Ewing's sarcoma and primitive neuroectodermal tumor cells. *J Clin Invest* 1997; **99**:239–247.

367 Lambert G, Bertrand JR, Fattal E, Subra F, Pinto-Alphandary H, Malvy C, *et al.* EWS fli-1 antisense nanocapsules inhibits ewing sarcoma-related tumor in mice. *Biochem Biophys Res Commun* 2000; **279**:401–406.

368 Erkizan HV, Kong Y, Merchant M, Schlottmann S, Barber-Rotenberg JS, Yuan L, *et al.* A small molecule blocking oncogenic protein EWS-FLI1 interaction with RNA helicase A inhibits growth of Ewing's sarcoma. *Nat Med* 2009; **15**:750–756.

369 Scotlandi K, Picci P. Targeting insulin-like growth factor 1 receptor in sarcomas. *Curr Opin Oncol* 2008; **20**:419–427.

370 Thiel U, Pirson S, Müller-Spahn C, Conrad H, Busch DH, Bernhard H, *et al.* Specific recognition and inhibition of Ewing tumour growth by antigen-specific allo-restricted cytotoxic T cells. *Br J Cancer* 2011; **104**:948–956.

371 Takahashi N, Udagawa N, Kobayashi Y, Suda T. Generation of osteoclasts in vitro, and assay of osteoclast activity. *Methods Mol Med* 2007; **135**:285–301.

372 Fidler IJ. The pathogenesis of cancer metastasis: the "seed and soil" hypothesis revisited. *Nat Rev Cancer* 2003; **3**:453–458.

373 Mathot L, Stenninger J. Behavior of seeds and soil in the mechanism of metastasis: a deeper understanding. *Cancer Sci* 2012; **103**:626–631.

374 Traggiai E, Chicha L, Mazzucchelli L, Bronz L, Piffaretti J-C, Lanzavecchia A, *et al.* Development of a human adaptive immune system in cord blood cell-transplanted mice. *Science* 2004; **304**:104–107.

375 Kaplan RN, Riba RD, Zacharoulis S, Bramley AH, Vincent L, Costa C, *et al.* VEGFR1-positive haematopoietic bone marrow progenitors initiate the pre-metastatic niche. *Nature* 2005; **438**:820–827.

9. Publications

Parts of this doctoral thesis have already been published or submitted:

Hauer, K, Calzada-Wack, J, Steiger, K, Grunewald, TGP, Baumhoer, D, Plehm, S, Buch, T, Prazeres da Costa, O, Esposito, I, Burdach, S, Richter, GHS (2012). *DKK2 mediates osteolysis, invasiveness and metastatic spread in Ewing sarcoma*. Cancer Res (under second review).

Grunewald, TGP, Diebold, I, Esposito, I, Plehm, S, **Hauer, K**, Thiel, U, da Silva-Buttkus, P, Neff, F, Unland, R, Müller-Tidow, C, Zobywalski, C, Lohrig, K, Lewandrowski, U, Sickmann, A, Prazeres da Costa, O, Görlach, A, Cossarizza, A, Butt, E, Richter, GHS, Burdach, S (2012). *STEAP1 Is Associated with the Invasive and Oxidative Stress Phenotype of Ewing Tumors.* Mol Cancer Res 10: 52-65.

10. Appendices

10.1. Supplemental figures

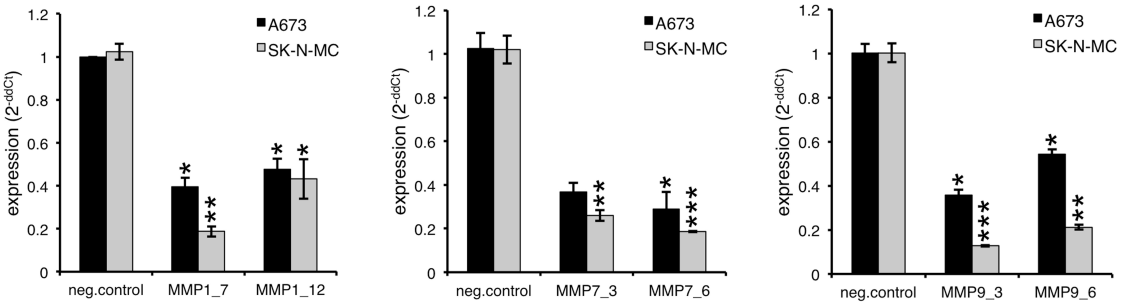

Figure 58: Expression of MMPs after transient transfection with specific siRNAs
Left panel: MMP1 expression levels 48 h after transient transfection with MMP1_7, MMP1_12 and control siRNA in A673 and SK-N-MC cells using qRT-PCR. **Middle panel**: Transient transfection of two ET cell lines with specific MMP7 siRNAs (MMP7_3 and MMP7_6) and corresponding control. MMP7 expression levels after 48 h were shown using qRT-PCR. **Right panel**: Expression of MMP9 levels 48 h after transient transfection with MMP9_3, MMP9_6 or control siRNA using qRT-PCR. Data are mean ± SEM of one or two independent experiments; t-test (*p < 0.05; **p < 0.005; ***p < 0.0005; NTC: non template control).

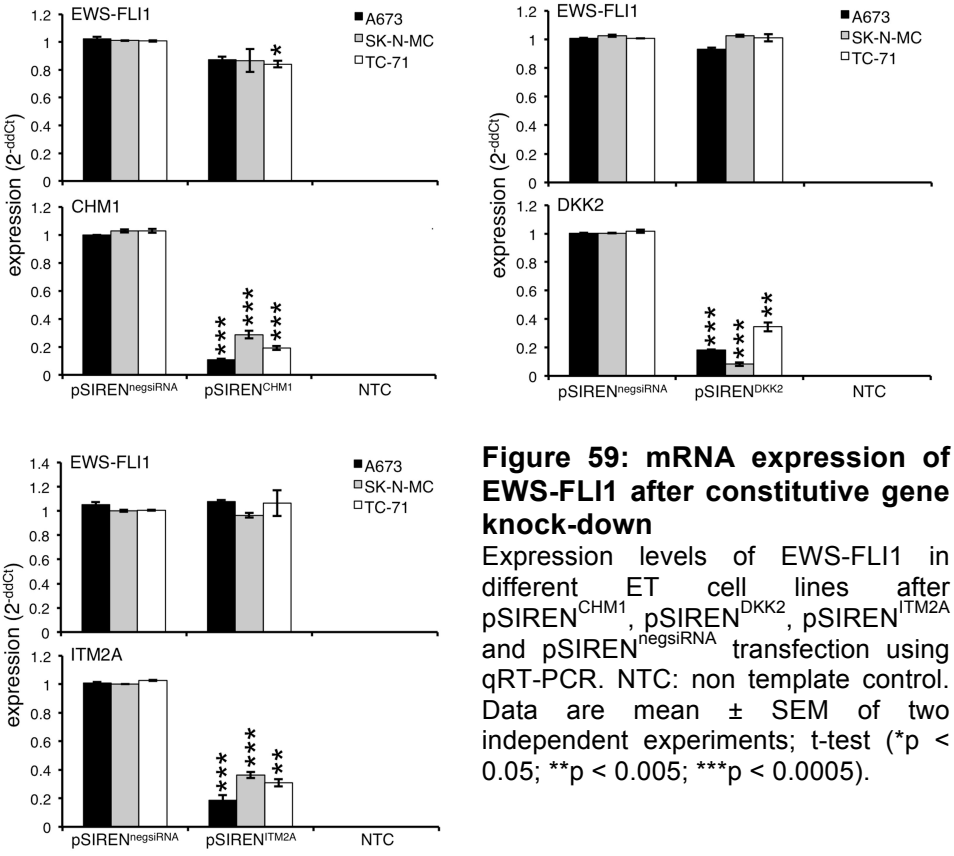

Figure 59: mRNA expression of EWS-FLI1 after constitutive gene knock-down
Expression levels of EWS-FLI1 in different ET cell lines after pSIREN^{CHM1}, pSIREN^{DKK2}, pSIREN^{ITM2A} and pSIREN^{negsiRNA} transfection using qRT-PCR. NTC: non template control. Data are mean ± SEM of two independent experiments; t-test (*p < 0.05; **p < 0.005; ***p < 0.0005).

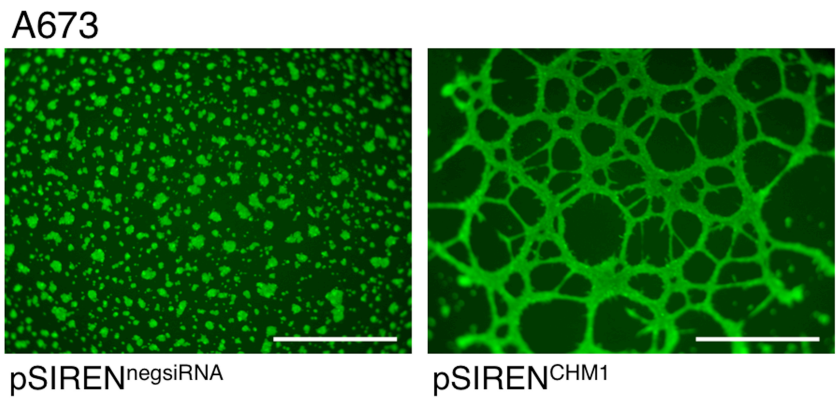

Figure 60: CHM1 suppressed endothelial differentiation potential in A673 cells
Tube formation assay with constitutively pSIREN^{negsiRNA}- and pSIREN^{CHM1}-transfected A673 cells (scale bar 0.5 mm).

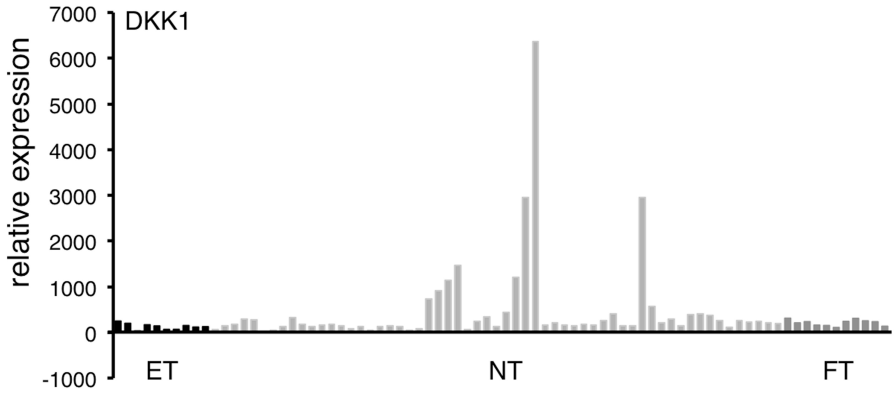

Figure 61: Expression of DKK1 in ETs compared to NBA
Microarray data that show the expression profile of DKK1 on mRNA level in primary ET samples (black bars) compared to normal body tissue (NT; light grey bars) and fetal tissue (FT; dark grey bars) [55].

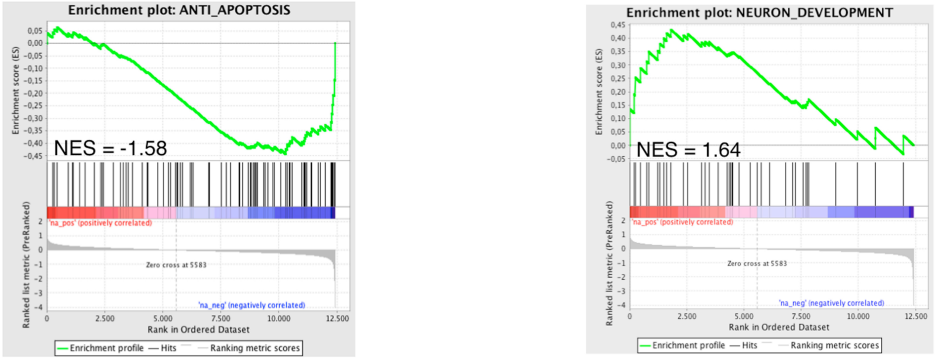

Figure 62: Enrichment plot of two representative gene sets after DKK2 knock-down
Enrichment plot of one representative down-regulated (**left**) and up-regulated (**right**) gene set after constitutive suppressed DKK2 RNA expression using the GSEA tool.

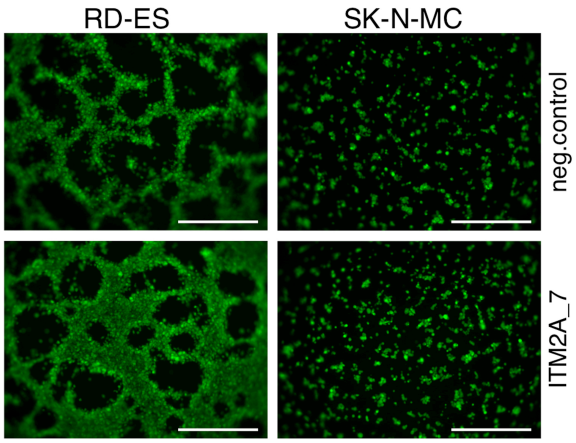

Figure 63: Tube formation assay with transiently ITM2A-transfected ET cells
Tube formation assay with transiently ITM2A-transfected RD-ES and SK-N-MC cells and respective controls (scale bar 0.5 mm).

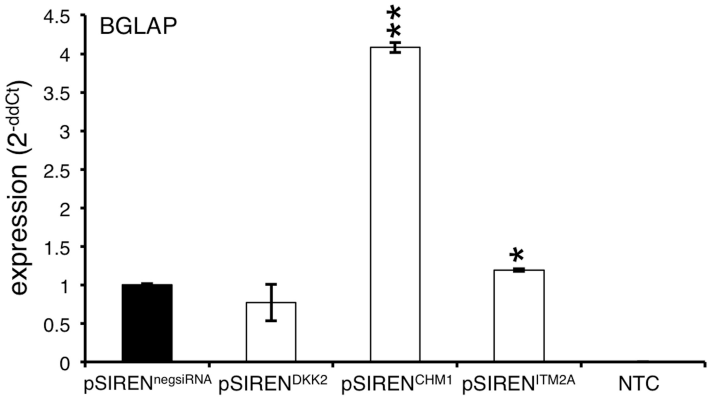

Figure 64: Expression of BGLAP in A673 cells after knock-down of CHM1, DKK2 or ITM2A
Expression levels of BGLAP (gamma-carboxyglutamic acid protein, bone; osteocalcin) in A673 cells after pSIREN^{CHM1}, pSIREN^{DKK2}, pSIREN^{ITM2A} and pSIREN^{negsiRNA} transfection using qRT-PCR. NTC: non template control. Data are mean ± SEM of two independent experiments; t-test (*$p < 0.05$; **$p < 0.005$).

10.2. List of figures

10.3. List of tables

10.4. List of abbreviations

aa	amino acids
ABCG2	atp-binding cassette, subfamily g, member 2
ACTB	β-actin
AKT	v-akt murine thymoma viral oncogene homolog 1
ALP	alkaline phosphatase
APC	APC gene
APC	allophycocyanin
APS	ammonium persulfate
BAX	bcl2-associated x protein
BCL2L1	bcl2-like 1
BCL2L11	bcl2-like 11
BCP	1-bromo-3-chloropropane
BGLAP	gamma-carboxyglutamic acid protein, bone; osteocalcin
BHA	butylated hydroxyanisole
BID	bh3-interacting domain death agonist
BMP	bone morphogenic protein
bp	base pairs
BrdU	bromodeoxyuridine
CA11	carbonic anhydrase XI
CAV1	caveolin 1
CCL2	chemokine, cc motif, ligand 2
CCND1	cycline D1
CD	Cluster of differentiation
CDH1	E-cadherin
cDNA	complementary DNA
CHM1	chondromodulin 1
CH-SP	chondrosurfactant protein
CITED2	cbp/p300-interacting transactivator, with glu/asp-rich c-terminal domain, 2
CK1α (CSNK1A1)	casein kinase 1, alpha-1
COL1A1	collagen, type 1, alpha 1
COL2A1	collagen, type 2, alpha 1
COL10A1	collagen, type 10, alpha 1
CREB1	cAMP response element-binding protein 1
CRC	colorectal cancer
CUTL1	cut-like 1
CXCL12	chemokine, cxc motif, ligand 12
CXCR4	chemokine, cxc motif, receptor 4
Cys	cysteine

C2C12	undifferentiated myoblast cell
DKK2 (DKK1-4)	dickkopf, xenopus, homolog of, 2 (1-4)
DMSO	Dimetylsulfoxide
DNA	desoxyribonucleic acid
dNTP	deoxyribonucleotide triphosphate
ds	double stranded
Dvl	dishevelled 1
EBF2	early B-cell factor 2
EDTA	ethane-1,2-diyldinitrilo tetraacetic acid
ELISA	Enzyme Linked Immunoabsorbent Assay
EPHB2/4	ephrin receptor EphB2/4
ERBB4	v-erb-b2 avian erythroblastic leukemia viral oncogene homolog 4
ERG	v-ets avian erythroblastosis virus e26 oncogene homolog
ERK	extracellular signal-regulated kinase
ES cell	embryonic stem cell
ESFT	Ewing sarcoma family of Tumors
ET	Ewing tumor
EtBr	ethidium bromide
ETS transcription factor	e-twenty six transcription factor (leukemia virus E26)
EWS	Ewing's sarcoma oncogene
FACS	fluorescence activated cell sorting
FAM	6-carboxy-fluorescein
FBS	fetal bovine serum
FGF	fibroblast growth factor
FITC	Fluoresceinisothiocyanat
FLI1	friend leukemia integration
for (primer)	Forward
FSC	forward scatter
Fz	frizzled
GAP43	growth associated protein 43
GAPDH	glyceraldehyde 3-phosphate dehydrogenase
gDNA	genomic DNA
GFAP	glial fibrillary acidic protein
GKN1+2	gastrokine 1+2
GSK3β	glycogen synthase kinase 3-beta
H3	histone 3
H&E	hematoxylin & eosin
HCELL	hematopoetic cell E-selectin/L-selectin ligand glycoform of CD44

HCl	hydrogen chloride
HeLa	human uterine cervical adenocarcinoma
HepG2	human hepatocellular carcinoma
HIF1α	hypoxia-inducible factor 1, alpha subunit
HOXA/D	homeobox A/D
HPRT	hypoxanthine-guanine phosphoribosyltransferase
HRP	horse radish peroxidase
HT-29	colorectal adenocarcinoma HT-29
HUVECs	human umbilical vein endothelial cells
ICAM1	intercellular adhesion molecule 1
ID2	inhibitor of dna binding 2
IFITM1	interferon induced transmembrane protein 1
IFN	Interferon
IGF1	insulin-like growth factor 1
IGF1R	insulin-like growth factor 1 receptor
IgG	immunoglobulin G
IHC	Immunohistochemistry
IL6/11	interleukin 6/11
ISG15 (G1P2)	ubiquitin-like modifier ISG15 (clone IFI-15K)
ITM2A	integrale membrane protein 2A
JAG1	jagged 1
JUN	jun proto-oncogene
Kb	kilo bases
kDa	kilo dalton
KRM1/2	kremen 1/2
LECT1 (CHM1)	leukocyte cell-derived chemotaxin 1
LEF1	lymphoid enhancer-binding factor 1
LRP6	low density lipoprotein receptor-related protein 6
LSEC	liver sinusoidal endothelial cells
LTR	long terminal repeats
c-MAF	c-musculo-aponeurotic fibrosarcoma
MAPK	mitogen-activated protein kinase
MCL1	myeloid cell leukemia sequence 1
M-CSF	colony-stimulating factor 1, macrophage-specific
miRNA	microRNA
MMP	matrix metalloproteinase
mRNA	messenger RNA
MSC	mesenchymal stem cell
c-MYC	v-myc avian myelocytomatosis viral oncogene homolog
Na_2HPO_4	disodium hydrogen phosphate

NaCl	sodium chloride
NaH_2PO_4	monosodium phosphate
NANOG	homeobox transcription factor nanog
NaOH	sodium hydroxide
NBA	normal body atlas
NF-κB	nuclear factor kappa-B
NGFR	nerve growth factor receptor
NK cell	natural killer cell
NOTCH	notch, drosophila, homolog of, 1
NT	normal tissue
NTC	non-template control
OPG (TNFRSF11B)	tumor necrosis factor receptor superfamily, member 11b
OPN (SPP1)	secreted phosphoprotein 1, osteopontin
OUMS-27	human chondrosarcom OUMS-27
PAX3	paired box gene 3
PBS	phosphate buffered saline
PCP	planar cell polarity pathway
PCR	polymerase chain reaction
PE	H-phycoerythrin
PFA	paraformaldehyde
PI	propidium iodide
PITX2	paired-like homeodomain transcription factor 2
PNET	peripheral primitive neuroectodermal tumor
PROM1	prominin 1
proSP-C	pulmonary surfactant protein C precursor
PTHrP	parathyroid hormone-like hormone
PVDF	polyvinylidene fluoride
p300	E1A-binding protein 300 kD
RANK (TNFRSF11A)	tumor necrosis factor receptor superfamily, member 11A
RANKL (TNFSF11)	tumor necrosis factor ligand superfamily, member 11
RCC	renal cell carcinoma
qRT-PCR	quantitative real time PCR
rev (primer)	reverse
RT	reverse transcriptase or room temperature
RUNX2	runt-related transcription factor 2
SAM	significance analysis of microarrays
s.c.	sub-cutaneous
SDS	sodium dodecyl sulfate
SDS-PAGE	SDS polyacrylamide gel electrophoresis
Ser	serine

sFRP	secreted frizzled-related protein
sgy	soggy
shRNA	small hairpin RNA
siRNA	short interfering RNA
SLIT2	slit, drosophila, homolog of, 2
SOX9	sry-box 9
SPARC	secreted protein, acidic, cysteine-rich
Sp3	transcription factor sp3
Ss	single stranded
SSC	sideward scatter
STAT	signal transducer and activator of transcription
TAE	Tris-acetate-EDTA
TBST	Tris-Buffered Saline Tween-20
TCF	transcription factor
TEMED	N,N,N′,N′-Tetramethylethan-1,2-diamin
TGFβ	transforming growth factor, beta-1
Thr	threonine
TNMD	tenomodulin
TRAP	tartrate-resistant acid phosphatase
βTrCP	beta-transducin repeat-containing protein
TSS	transcriptional start site
VC	vector control
VDAC	voltage-dependent anion channel
VEGFR1	vascular endothelial growth factor receptor 1
WIF	Wnt inhibitory factor
WNT2A/2C/5A	wingless-type MMTV integration site family, member 2A/2C/5A
YY1	transcription factor YY1

11. Acknowledgements

Ich möchte mich an dieser Stelle bei allen bedanken, die zum Gelingen dieser Doktorarbeit beigetragen haben.

Mein besonderer Dank gilt:

Herrn Prof. Dr. Stefan Burdach und Herrn Dr. Günther Richter für die Möglichkeit meine Dissertation an diesem interessanten und anspruchsvollen Thema am Forschungszentrum für krebskranke Kinder der TU München durchführen zu können, für das mir entgegengebrachte Vertrauen sowie für ihre Unterstützung und Begleitung der Arbeit, die größtenteils von der Wilhelm Sander Stiftung (2009.901.1) und dem Bundesministerium für Bildung und Forschung (FK 01GM0870 und 01GM1104B) finanziert wurde.

Herrn Prof. Dr. Martin Hrabé de Angelis für die Betreuung meiner Doktorarbeit, sowie Herrn Prof. Dr. Siegfried Scherer für die Übernahme des Prüfungsvorsitzes und für die Organisation des Prüfungsverfahrens.

Frau Prof. Dr. Irene Esposito, Frau Dr. Julia Calzada-Wack und Frau Dr. Katja Steiger vom Institut für Pathologie am Helmholtz Zentrum München für die sorgfältige und schnelle Durchführung der zahlreichen histologischen Untersuchungen und die interessanten Diskussionen.

Frau Olivia Prazeres da Costa vom Institut für medizinische Mikrobiologie, Immunologie und Hygiene der TU München für die Durchführung der aufschlussreichen Microarray Analysen, sowie allen weiteren Kooperationspartnern für die engagierte und zuverlässige Kooperation und die Bereitstellung von Zelllinien (Dr. Jan Smida und PD Dr. Michaela Nathrath), Gewebeproben (Dr. Daniel Baumhoer) und Mäusen (Dr. Mamoru Ito).

Meinen liebgewonnenen Arbeitskollegen für die Einarbeitung, Unterstützung und die schöne Zeit, besonders Dr. Uwe Thiel und Dr. Thomas Grünewald für die kritische und hilfreiche Durchsicht dieser Arbeit sowie für den Zuspruch und Rückhalt.

Meinen Freunden die mir immer den nötigen Rückhalt und Ausgleich gegeben haben.

Und nicht zuletzt meiner Familie - meinen Eltern, meiner Schwester und meinem Verlobten Christopher - die immer an mich geglaubt und mich in allen Bereichen unterstützt und gestützt haben und ohne die diese Arbeit nicht möglich gewesen wäre.
DANKE!